



McVeigh, Ashley (2016) The conversion of lignin to alkylphenolic monomers using heterogeneous catalysis. PhD thesis.

<http://theses.gla.ac.uk/7136/>

Copyright and moral rights for this thesis are retained by the author

A copy can be downloaded for personal non-commercial research or study, without prior permission or charge

This thesis cannot be reproduced or quoted extensively from without first obtaining permission in writing from the Author

The content must not be changed in any way or sold commercially in any format or medium without the formal permission of the Author

When referring to this work, full bibliographic details including the author, title, awarding institution and date of the thesis must be given



University  
of Glasgow

**The Conversion of Lignin to Alkylphenolic Monomers  
using Heterogeneous Catalysis**

**Ashley McVeigh**

**Supervisor: Professor S.D. Jackson**

**School of Chemistry**

**College of Science and Engineering**

**University of Glasgow**

**February 2016**

*'If we knew what it was we were doing, it would not be called research...'*

# Abstract

Lignin is the most recalcitrant part of woody biomass yet is one of the few natural aromatic resources available in abundance. There is huge potential for this material to be used as a key feedstock in future applications however a conversion route to fine chemicals must first be established. In this thesis, a methodology to take raw wood sawdust and convert its lignin component to value added products whilst avoiding a pyrolysis route has been reported.

During biofuel processing, lignin is subjected to a number of pretreatment steps in order to separate it from the lignocellulosic material and it is during these steps that modification of the lignin can occur. The aim of this project was to selectively cleave the dominant  $\beta$ -O-4 linkage using heterogeneous catalysis to form functional aromatic monomers. It was found to be imperative that an appropriate pretreatment was firstly identified in order to avoid depletion of this dominant alkyl-aryl ether bond where, for example, the lignin isolated using an ammonia pretreatment from poplar wood gave an uncondensed structure in comparison to the condensed lignin produced using an organosolv pretreatment. We have shown that lignin can be effectively depolymerised to low molecular weight compounds when the starting material is rich in  $\beta$ -O-4 bonds and we were able to verify this finding using a Pt/Al<sub>2</sub>O<sub>3</sub> catalyst under hydrodeoxygenation/hydrogenolysis conditions. Organosolv lignin from Poplar sawdust was found to have a low  $\beta$ -O-4 content (9.2 %) and subsequently gave limited conversion to fine chemicals (9.0 %) in comparison to the ammonia lignin with a high  $\beta$ -O-4 content (28.9 %) which gave much higher conversion to monomeric product (16.4 %). Further work using lignins isolated using different pretreatment methods supported this conclusion. Whilst GPC was used to give an overview of the initial cracking to breakdown products, GC-MS analysis enabled us to successfully identify 21 monomeric products.

Optimisation work using a Pt/Al<sub>2</sub>O<sub>3</sub> catalyst with the ammonia lignin was carried out in order to minimise char production and maximize the yield of the fine chemical products to varying success. Experimental conditions were altered in terms of the solvent used and its composition, reaction temperatures, pressures, time and stirring rates, as well as changing the pH and active metal. It was found that the use of 100 % methanol under the standard conditions yielded the highest amount of monomeric product (43.5 %), whilst the use of 100 % water alternatively gave the highest char production (47.1 %). This knowledge obtained during the initial lignin conversion study was then used to tackle a sulfur-

containing lignin known as Kraft lignin. This lignin is readily available as a by-product of the dominant pulping technique adopted by the paper and pulp industry but due to the nature of the technique used to isolate the lignin, the Kraft lignin often incorporates sulfur onto its structure. Such impurities could prove detrimental to the catalytic depolymerisation reaction via catalyst poisoning but it was found that the Kraft lignin behaved in a similar manner to the other condensed lignins under the standard conditions in terms of the total monomeric yield obtained. The Kraft lignin produced 9.2 % of alkylphenolic product in comparison to 7.4 % produced from the standard reaction with soda lignin. It was also noted that the optimised conditions found for the benchmark ammonia lignin did not depolymerise the Kraft lignin to the same extent where, for example, using 100 % methanol with the Kraft lignin hindered the reaction and gave an overall monomeric yield of 5.6 %. This highlighted the fact that whilst one set of conditions may be efficient for the conversion of one type of lignin, this may not be the case for another.

This work was followed by an isotopic labelling study to investigate the reaction mechanism which indicated an inverse kinetic isotope effect and that the depolymerisation reaction occurred in two steps. These two steps involved an initial cracking step of the entire lignin molecule to fragmented lignin pieces followed by conversion to monomeric product. Some post-catalyst analysis was also carried out using XRD, BET, TPO and Raman analysis in order to analyse the catalyst surface. The work showed that during the reaction, the lignin deposited onto the catalyst surface and formed a carbonaceous layer which was graphitic in nature. Some samples were found to be more ordered in nature but no obvious trend with respect to the type of lignin used was established.

# Acknowledgements

It would have been impossible to get through my PhD without the help and much needed support of so many lovely people along the way.

I would firstly like to thank my supervisor, Professor David Jackson for giving me this opportunity, and for always being patient and able to answer my questions, no matter how small or silly... Albeit, with a few raises of the eyebrow or looks over the glasses to keep me on my toes! Thank you for everything.

A big thank you to my second supervisor, Dr Mike Jarvis for his guidance and fountain of knowledge - All the best with your retirement!

To Florent Bouxin, I owe so much of this project to your expertise and patience. Thank you for sticking it out with me! I really appreciate all of your help and wish you all the luck in the world with your future adventures. I couldn't have done this without you.

I would like to say a huge thank you to all of the technical support staff at Glasgow University who were always on hand when I needed a favour or advice. To Ron Spence, thank you for all of your assistance over the years. To Andy Monaghan who always took the time to help me no matter how busy he was, your chat and advice got me through so many slow times at the start and I can't tell you how much that meant to me at the time – I made it! And finally to Michael Beglan, what a guy! Thank you for all of your help and kindness over the years, for always offering your support no matter how big or small a task and most of all, for being a great friend to me.

To Team Catalysis, old and new, what a great bunch of people! I just want to say a massive thank you for making my past four years so special. My PhD was totally made by the friends I met along the way and I can't thank you enough for that. Good luck with everything!

To Clement, my whole PhD experience completely changed when I met you. Thank you for putting up with the moods and for listening to every strop, for always being ready to help me no matter what and for being the best support (and boyfriend!) a girl could ask for.

And finally to my family and friends who have always been there to support me through the good and the bad times, ready to answer the phone or just to say good luck and let me know that they are there - I hope I've made you proud.

# Declaration

The work contained in this thesis, submitted for the degree of Doctor of Philosophy, is my original work, except where due reference is made to other authors. No material within this thesis has been previously submitted for a degree at this or any other university.

## Table of Contents

1	Introduction.....	1
1.1	Fossil Fuel vs. Biofuel.....	1
1.2	Lignocellulose as a Potential Renewable Resource .....	2
1.3	Paper and Pulp Industry .....	6
1.3.1	Kraft Pulping Process.....	7
1.3.2	Organosolv Pulping Process .....	8
1.3.3	Ammonia Fibre Expansion (AFEX) Process .....	8
1.3.4	Soda Pulping Process .....	8
1.4	The Role of Heterogeneous Catalysis in Lignin Conversion.....	9
1.5	Overview of Lignin Valorisation .....	11
1.5.1	Pyrolysis Studies of Lignin .....	11
1.5.2	Model Compound Conversion Studies .....	13
1.5.3	Lignin Conversion Studies.....	20
1.6	Project Aims.....	22
2	Experimental Methods.....	23
2.1	Lignin Sources and Preparation Methods .....	23
2.1.1	Kraft Lignin.....	23
2.1.2	Other Lignins Used .....	23
2.2	Catalyst Preparation .....	25
2.2.1	1 wt. % Platinum/alumina Catalyst.....	25
2.2.2	1 wt. % Rhodium/alumina Catalyst .....	25
2.2.3	1 wt. % Iridium/alumina Catalyst .....	25
2.3	Reactor Studies.....	26
2.3.1	Reactor Set-up.....	26
2.3.2	Reaction Procedure .....	26
2.4	Analysis Methods.....	27
2.4.1	Surface Area and Pore Volume Determination.....	27
2.4.2	X-Ray Diffraction (XRD) Analysis .....	28
2.4.3	Thermo-gravimetric Analysis (TGA) .....	29
2.4.4	Raman Spectroscopy.....	29
2.4.5	CHN .....	29
2.4.6	Thioacidolysis .....	29
2.4.7	UV-Visible Spectrophotometer.....	29

	2.4.8 Gel Permeation Chromatography (GPC) .....	30
	2.4.9 Gas Chromatography – Mass Spectrometry (GC-MS) .....	33
	2.4.10 Quantification of the Heavy Fraction.....	44
3	Results and Discussion .....	45
	3.1 Characterisation and Catalytic Depolymerisation Activity of Six Lignins using 1 % Pt/alumina.....	45
	3.1.1 Characterisation of Six Lignins.....	45
	3.1.2 Non-Catalytic and Catalytic Standard Reaction Testing of Six Lignins....	53
	3.1.3 Summary of the Catalytic Standard Reaction Testing of Six Lignins .....	74
	3.2 Optimisation of the Ammonia Lignin .....	80
	3.2.1 Reproducibility and Recycling of the Standard Catalytic Reaction.....	80
	3.2.2 Further Non-Catalytic Reaction Testing .....	84
	3.2.3 Optimisation of the Standard Reaction Parameter Conditions .....	90
	3.2.4 Summary of the Optimisation of Ammonia Lignin .....	121
	3.3 Characterisation and Catalytic Depolymerisation Activity of Kraft Lignin using 1 % Pt/alumina.....	127
	3.3.1 Characterisation of the Kraft Lignin .....	127
	3.3.2 Non-Catalytic and Catalytic Standard Reaction Testing .....	135
	3.3.3 Summary of the Catalytic Standard Reaction Testing of Kraft Lignin....	156
	3.4 Isotopic Labelling Studies of Lignin .....	161
	3.4.1 Ammonia Lignin Deuterium Studies .....	161
	3.4.2 Kraft Lignin Deuterium Studies.....	186
	3.4.3 Summary of the Isotopic Labelling Studies of Lignin.....	190
	3.5 Post-Reaction Catalyst Characterisation .....	192
	3.5.1 Analysis of the Post-Reaction Catalyst Samples from the Standard Reactions with the Seven Lignins .....	192
	3.5.2 Analysis of the Post-Reaction Catalyst Samples from the Optimisation Studies .....	202
	3.5.3 Analysis of the Post-Reaction Catalyst Samples from the Isotopic Labelling Studies.....	207
	3.5.4 Summary of the Post-Reaction Catalyst Characterisation .....	209
4	Project Conclusions .....	211
5	Recommendations for Future Work .....	214
6	References.....	216
7	Glossary .....	223

## List of Figures

Figure 1: Illustration of lignocellulose comprising of cellulose, hemicellulose and lignin ...	2
Figure 2: Representation of the lignin structure.....	3
Figure 3: The three main lignin alcohol precursors .....	4
Figure 4: Examples of uncondensed linkages found in the lignin structure .....	4
Figure 5: Examples of condensed linkages found in the lignin structure .....	4
Figure 6: Examples of condensed linkages found in the lignin structure .....	5
Figure 7: Bond dissociation enthalpy values of common lignin linkages .....	12
Figure 8: Examples of monomeric lignin model compounds .....	14
Figure 9: Proposed reaction scheme for guaiacol conversion.....	16
Figure 10: Model compounds mimicking the $\beta$ -O-4 (A), 5-5 (B), and phenylcoumaran (C) linkages found in lignin.....	17
Figure 11: Products formed from the cleavage of the $\beta$ -O-4 linkage .....	18
Figure 12: Reaction network for conversion of guaiacol using Pt supported on magnesia or alumina.....	19
Figure 13: Schematic diagram of Parr autoclave reactor .....	26
Figure 14: GPC polystyrene calibration curve.....	31
Figure 15: Illustration of GPC integration .....	32
Figure 16: Guaiacol and 2,6-dimethoxyphenol respectively and their TMS derivatives ....	33
Figure 17: 2-methoxy-4-propylphenol and 2,6-dimethoxy-4-methylphenol and their TMS derivatives .....	34
Figure 18: Guaiacol calibration curve.....	35
Figure 19: 2,6-dimethoxyphenol calibration curve .....	35
Figure 20: 2-methoxy-4-propylphenol calibration curve.....	36
Figure 21: 2,6-dimethoxy-4-methylphenol calibration curve .....	36
Figure 22: Mass spectrometry data for guaiacol .....	38
Figure 23: Mass spectrometry data for 2,6-dimethoxyphenol .....	38
Figure 24: Mass spectrometry data for 2-methoxy-4-propylphenol .....	39
Figure 25: Mass spectrometry data for 2,6-dimethoxy-4-methylphenol .....	39
Figure 26: Basic alkylphenolic monomer unit .....	40
Figure 27: GPC profiles of six lignins .....	49
Figure 28: TPR of six lignins .....	51
Figure 29: Example of mass spectra data obtained from TPR of lignin including m/z 16, 18, 28 and 44.....	52
Figure 30: GPC profile of ammonia lignin vs. with and without 1 wt. % Pt/alumina catalyst reactions .....	56
Figure 31: Ammonia lignin blank vs. standard reaction with 1 wt. % Pt/alumina .....	57
Figure 32: GPC profile of organosolv lignin vs. with and without 1 wt. % Pt/alumina catalyst reactions .....	59
Figure 33: Organosolv lignin blank vs. standard reaction with 1 wt. % Pt/alumina.....	60
Figure 34: GPC profile of alkali lignin vs. with and without 1 wt. % Pt/alumina catalyst reactions .....	63
Figure 35: Alkali lignin blank vs. standard reaction with 1 wt. % Pt/alumina .....	64
Figure 36: Proposed reaction mechanism of wheat straw lignins.....	65

Figure 37: GPC profile of AFEX lignin with and without 1 wt. % Pt/alumina catalyst reactions .....	67
Figure 38: AFEX lignin blank vs. standard reaction with 1 wt. % Pt/alumina.....	68
Figure 39: AFEX vs. Fr-AFEX lignin reaction with 1 wt. % Pt/alumina.....	70
Figure 40: GPC profile of AFEX lignin vs. with and without 1 wt. % Pt/alumina catalyst reactions .....	72
Figure 41: Soda lignin blank vs. standard reaction with 1 wt. % Pt/alumina .....	73
Figure 42: Catalytic depolymerisation products of five lignins.....	76
Figure 43: Inter-chain condensation pathway of lignin .....	78
Figure 44: Reproducibility testing of the Pt/alumina catalyst and ammonia lignin.....	82
Figure 45: Recyclability testing of the Pt/alumina catalyst with ammonia lignin .....	83
Figure 46: Thermal transformation sequence of aluminium hydroxides .....	85
Figure 47: The effect of ammonia depolymerisation using the alumina support .....	87
Figure 48: The effect on ammonia depolymerisation without hydrogen.....	89
Figure 49: The effect of ammonia depolymerisation on altering the stirring speed .....	91
Figure 50: The effect of ammonia depolymerisation on reaction time .....	93
Figure 51: The effect of ammonia depolymerisation at 523 K and 573 K .....	96
Figure 52: The effect of ammonia depolymerisation with increasing hydrogen pressure ...	98
Figure 53: Solubilisation of ammonia lignin in methanol-water at room temperature.....	100
Figure 54: The effect of ammonia depolymerisation with changing solvent composition	103
Figure 55: Adsorption behaviour of substituted phenols onto the catalyst surface .....	104
Figure 56: The effect of ammonia depolymerisation with alternative solvents.....	106
Figure 57: The effect of ammonia depolymerisation using different pH environments....	109
Figure 58: Product selectivities using different pH conditions.....	110
Figure 59: The effect of ammonia depolymerisation using different masses of catalyst...	113
Figure 60: The effect of ammonia depolymerisation using different masses of lignin .....	115
Figure 61: The effect of ammonia depolymerisation using alternative precious metals ...	118
Figure 62: Product selectivity between the three alumina-supported catalysts .....	119
Figure 63: Alternative mechanism to cleave the alkyl chain .....	124
Figure 64: Possible dealkylation mechanisms .....	125
Figure 65: Possible mechanism showing allyl cationic polymerisation .....	126
Figure 66: GPC profile of Kraft lignin.....	130
Figure 67: TPR of Kraft lignin.....	132
Figure 68: Mass spectra data obtained from TPR of Kraft lignin.....	133
Figure 69: TPO of Kraft lignin showing derivative weight loss and SO <sub>2</sub> evolution.....	134
Figure 70: Depolymerisation effect of the catalyst and gas used with Kraft lignin.....	137
Figure 71: Reproducibility testing of the Pt/alumina catalyst and Kraft lignin .....	139
Figure 72: Reproducibility testing of the Pt/alumina catalyst and Kraft lignin .....	141
Figure 73: Depolymerisation effect of using a 4 h reaction time with Kraft lignin.....	144
Figure 74: Depolymerisation effect of using 30 barg hydrogen pressure with Kraft lignin .....	146
Figure 75: Depolymerisation effect of using 100 % MeOH with Kraft lignin .....	149
Figure 76: Depolymerisation effect of using IPA/water with Kraft lignin .....	151
Figure 77: Depolymerisation effect of using 0.2 g of catalyst with Kraft lignin .....	153
Figure 78: Effect of using 1 wt. % Rh/alumina catalyst with Kraft lignin .....	155

Figure 79: Catalytic depolymerisation products of Kraft lignin compared to the other lignins used .....	157
Figure 80: Effect of methanol on the depolymerisation of ammonia lignin .....	163
Figure 81: Fully hydrogenated vs. fully deuterated standard reaction with ammonia lignin .....	165
Figure 82: Depolymerisation products of ammonia lignin with respect to alkyl chain length .....	168
Figure 83: Energy diagram for C-H and C-D bond breakage .....	169
Figure 84: Secondary KIE example .....	172
Figure 85: Monomeric product formation from the cracked lignin fragments .....	174
Figure 86: Added deuterium atoms onto G2 product.....	182
Figure 87: Added deuterium atoms onto S2 product .....	183
Figure 88: H/D exchange on the aromatic ring .....	185
Figure 89: Deuterium exchange onto the alumina support via hydration depending on the reaction solvent used .....	186
Figure 90: Fully hydrogenated vs. fully deuterated standard reaction with Kraft lignin...	187
Figure 91: TPO of spent Pt/alumina catalyst after standard reaction with the poplar lignins showing derivative weight loss (black and red) and m/z 44 evolution (blue).....	194
Figure 92: TPO of spent Pt/alumina catalyst after standard reaction with the wheat straw lignins showing derivative weight loss (various colours) and m/z 44 evolution (blue).....	195
Figure 93: TPO of spent Pt/alumina catalyst after standard reaction with the Kraft lignin showing derivative weight loss (black) and m/z 44 evolution (blue) .....	196
Figure 94: XRD diffraction patterns of the catalyst pre-reaction compared to the post-reaction samples .....	199
Figure 95: Raman spectra obtained for the post-reaction catalyst used in the standard reaction with the ammonia and alkali lignin .....	201
Figure 96: Derivative weight loss profiles of the spent Pt/alumina catalysts after recyclability testing with the ammonia and Kraft lignin.....	204
Figure 97: Derivative weight loss profiles of the spent Pt/alumina catalysts after solvent optimisation testing using the ammonia lignin .....	206
Figure 98: Derivative weight loss profiles of the spent Pt/alumina catalysts after the isotopic labelling testing using the ammonia and Kraft lignins.....	208

## List of Tables

Table 1: Typical distribution of linkages found in lignin obtained from different wood sources.....	6
Table 2: Catalyst reduction conditions.....	27
Table 3: Summary of calibration data.....	37
Table 4: Summary of products structures and names .....	41
Table 5: Structures of the identified GC-MS products .....	42
Table 6: Elemental analysis of six lignins.....	45
Table 7: Lignin $\beta$ -O-4 linkage percentages and monomer ratios.....	46
Table 8: GPC data for six lignins.....	48
Table 9: TPR weight loss percentage of six lignins.....	53
Table 10: GPC data of ammonia reactions with 1 wt. % Pt/alumina.....	54
Table 11: GPC data of organosolv reactions with 1 wt. % Pt/alumina.....	58
Table 12: GPC data of alkali reactions with 1 wt. % Pt/alumina.....	61
Table 13: GPC data of AFEX reactions with 1 wt. % Pt/alumina.....	66
Table 14: GPC data of soda reactions with 1 wt. % Pt/alumina .....	71
Table 15: Identification and quantification of reaction products from five lignin samples.....	75
Table 16: Thioacidolysis and catalytic product ratios of six lignins.....	77
Table 17: Char production of six lignins.....	78
Table 18: Effect of char production with the presence of Pt/alumina.....	85
Table 19: Effect of changing the stirring speed on char production .....	90
Table 20: Effect of changing reaction time with char production .....	92
Table 21: Cleavage of linkages at 523 K and 573 K.....	95
Table 22: Natural logarithm of hydrogen pressure and monomeric yield .....	99
Table 23: The effect of increasing hydrogen pressure on char production.....	99
Table 24: The effect of changing solvent composition on char production.....	102
Table 25: The effect of using alternative solvents on char production .....	105
Table 26: The effect of changing pH on char production .....	108
Table 27: The effect of changing the catalyst mass on char production.....	112
Table 28: The effect of changing the lignin mass on char production.....	114
Table 29: The effect of changing catalyst on char production.....	116
Table 30: Effect on monomer yield from using Pt and Rh metal .....	117
Table 31: Optimised conditions for each parameter change.....	121
Table 32: Summary of optimisation results using the ammonia lignin .....	122
Table 33: Elemental analysis of Kraft lignin .....	127
Table 34: $\beta$ -O-4 linkage percentage and monomer ratio of Kraft lignin .....	128
Table 35: GPC data for Kraft lignin.....	129
Table 36: Effect of using a catalyst or hydrogen gas on char production.....	136
Table 37: Summary of the optimised conditions for ammonia lignin .....	142
Table 38: Summary of results using Kraft lignin.....	159
Table 39: Summary of results using Kraft lignin (continued) .....	160
Table 40: Summary of isotopic labelling results.....	171
Table 41: KIE values for each monomeric product across each standard deuterium reaction .....	176

Table 42: KIE values for each monomeric product across each standard deuterium reaction (continued) .....	177
Table 43: Summary of the H/D exchange onto the monomer products for each reaction.	179
Table 44: Summary of the H/D exchange onto the monomer products for each reaction (continued) .....	180
Table 45: Product selectivities obtained between the protonated and deuterated standard reactions .....	188
Table 46: Comparison of the H/D exchange for the ammonia and Kraft lignins .....	190
Table 47: Weight loss observed for each catalyst used in the standard reaction of each lignin .....	197
Table 48: Surface area and pore volume data for each catalyst used in the standard reaction of each lignin.....	198
Table 49: D:G ratios determined from the raman analysis for each catalyst used in the standard reaction of each lignin .....	200
Table 50: Characterisation of the recycled catalysts used with the ammonia and Kraft lignins.....	205
Table 51: Characterisation of the solvent optimisation catalysts used with the ammonia lignin .....	207
Table 52: Characterisation of the isotopic labelling catalysts used with the ammonia and Kraft lignins .....	209

## List of Equations

Equation 1: The BET equation.....	28
Equation 2: Calculating the $V_m$ value for the BET equation .....	28
Equation 3: Surface area equation.....	28
Equation 4: Surface area per unit equation .....	28
Equation 5: The Scherrer equation.....	29
Equation 6: Calculating the baseline deviation .....	31
Equation 7: Calculating the intensity correction.....	31
Equation 8: Calculating the molecular weight of a GPC sample.....	32
Equation 9: Calculating the molecular number of a GPC sample .....	32
Equation 10: Calculating the polydispersity of a GPC sample .....	32
Equation 11: Calculating the coefficient value for each reference compound .....	34
Equation 12: GC-MS product quantification calculation.....	44
Equation 13: Calculating the actual mass of product using GC-MS .....	44
Equation 14: Quantification of the heavy fraction.....	44
Equation 15: The Arrhenius equation .....	94
Equation 16: Energy of bond vibrational levels.....	169
Equation 17: Energy of a bond assuming zero-point vibrational state .....	169
Equation 18: Fundamental vibrational frequency equation .....	170
Equation 19: Calculating $\mu$ for Equation 18 .....	170
Equation 20: The Arrhenius equation for both the hydrogen and deuterium systems.....	170
Equation 21: Calculating the isotope effect .....	170
Equation 22: Activation energy calculation incorporating Equation 17 .....	170

# 1 Introduction

## 1.1 Fossil Fuel vs. Biofuel

With escalating global demand and a rapid decline in the availability of fossil fuels, it is becoming increasingly important that we research alternative, sustainable resources for the production of both fuels and chemicals. Oil is the world's primary fuel source with 33 % of global primary energy consumption [2]. World demand in 2015 was approximately 94 million barrels per day which was set to rise substantially with increasing population and income growth [2, 3]. Transport fuels account for around 60 % of this total alone and while the transport industries continue to expand, growth in developing countries is also vastly increasing and putting a heavier strain on fuel availability [3]. This heavy reliance on fossil fuels coupled with environmental concerns has stimulated the utilisation of alternative greener resources, as well as the development of current technologies to lower their carbon footprint. This will therefore require a key balance between the necessities of developing a process that is not only sustainable, but one that is also environmentally friendly and as a result, chemical and petroleum industries are now turning their attention towards biomass conversion.

Biomass is generally inexpensive and globally accessible so the available feedstocks should be sufficient enough to replace a significant proportion of the non-renewable raw materials required by industry should an efficient conversion method be established. Plant biomass sources are diverse and include wood and its waste processing products, herbaceous and sea plants, and various waste agricultural waste products [4]. Industrial processes mainly use coniferous wood but there are also copious amounts of low-quality deciduous wood and substandard wood available, including overripe wood or wood affected by pests or fire which is viewed as unusable and therefore waste [4]. Furthermore, timber cutting and wood processing technologies produce various wood wastes which are currently not used to their full potential. Although it is possible for all kinds of biomass to be converted to a variety of chemicals and fuels, the use of edible crops for this purpose cannot be justified. In order to prevent competition for land and resources, it is recommended that the use of second-generation biomass is used exclusively, with lignocellulose being recognised as a potential replacement feedstock.

## 1.2 Lignocellulose as a Potential Renewable Resource

Lignocellulosic matter is the cheapest, most abundant carbon-based source on the planet [5]. In China alone, there is a wealth of biomass resource with approximately 0.73 billion tons of agricultural residue per annum which is the equivalent to 12,000 trillion kJ of energy [6]. Forestry worldwide covers 9 % of the Earth's surface (or 30 % of the land area) and has the potential to be fully exploited as a rich sustainable feedstock for future biorefinery technologies. The lignocellulosic material itself is composed of three polymers: cellulose, hemicellulose and lignin as illustrated in Figure 1 [7].

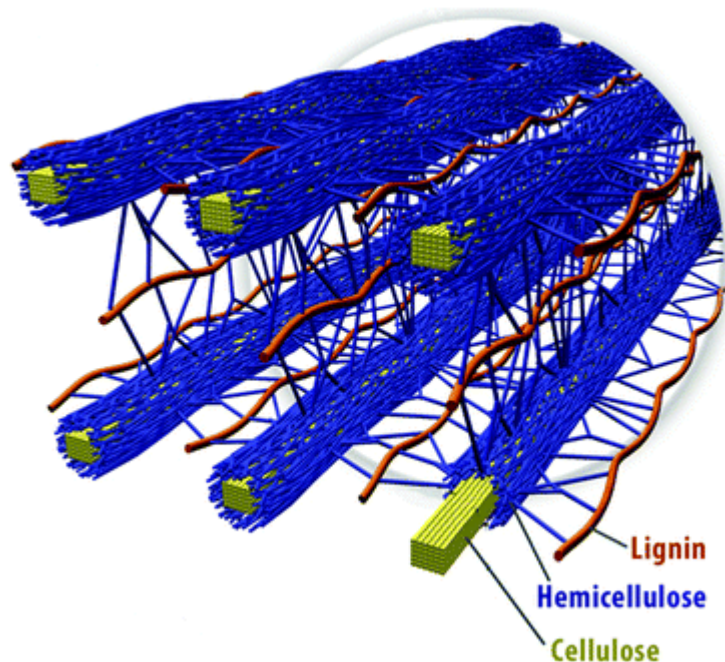


Figure 1: Illustration of lignocellulose comprising of cellulose, hemicellulose and lignin

Cellulose ( $C_6H_{10}O_6$ )<sub>n</sub> is a linear anhydroglucose polymer that represents approximately 30-50 % of the overall mass of lignocellulosic material. Cellulosic materials have crystalline structures separated by less ordered, amorphous regions. These differences in structure have an impact on the effectiveness of chemical reactions that could be used in possible industrial applications. Where the crystalline region is highly resistant to chemical attack, the amorphous regions could have potential for chemical degradation. Hemicellulose ( $C_5H_8O_5$ )<sub>n</sub> is a highly branched amorphous polymer that is much easier to chemically breakdown than cellulose. It is the second biggest component of lignocellulosic matter taking up 20-30 % of the total dry matter and although cellulose and hemicellulose are promising raw materials for carbohydrate-based chemistry, it is the third component of

lignocellulose that carries the most potential for hydrocarbon chemistry due to its unique composition. Lignin ( $C_9H_{10}O_2(OCH_3)_n$ ) is essentially the glue that provides the overall rigidity to the structure of plants and trees. It is found in the spaces between cellulose and hemicelluloses in the plants matrix and this association with the other components allows for protection against biological and mechanical degradation. Lignin consists of a three-dimensional amorphous polymer which contains a mixture of oxygenated polyaromatics substituted with randomly cross-linked methoxy and phenol units [8]. Comprising of 15-30 % of the total lignocellulosic dry matter, lignin is the largest non-carbohydrate fraction in lignocellulose [8]. There is no exact structure available for lignin as it has been shown to vary in different species of plants (see Figure 2 for a representation) but the main structure and linkages of lignin have been reviewed by Chakar and Ragauskas [9] who found that the polymer consisted primarily of three basic monomer units, namely coniferyl, sinapyl, and coumaryl alcohols (see Figure 3). These units are connected by ether labile bonds ( $\beta$ -O-4) or condensed bonds ( $\beta$ -5, 5-5, 4-O-5,  $\beta$ -1, and  $\beta$ - $\beta$ ) as shown in Figure 4, Figure 5 and Figure 6. It should be noted that literature will sometimes not name the  $\alpha$ -O-4 bond as a main linkage due to the fact that it is present in the dibenzodioxocin structure which already contains the 5-5 and  $\beta$ -O-4 linkages.

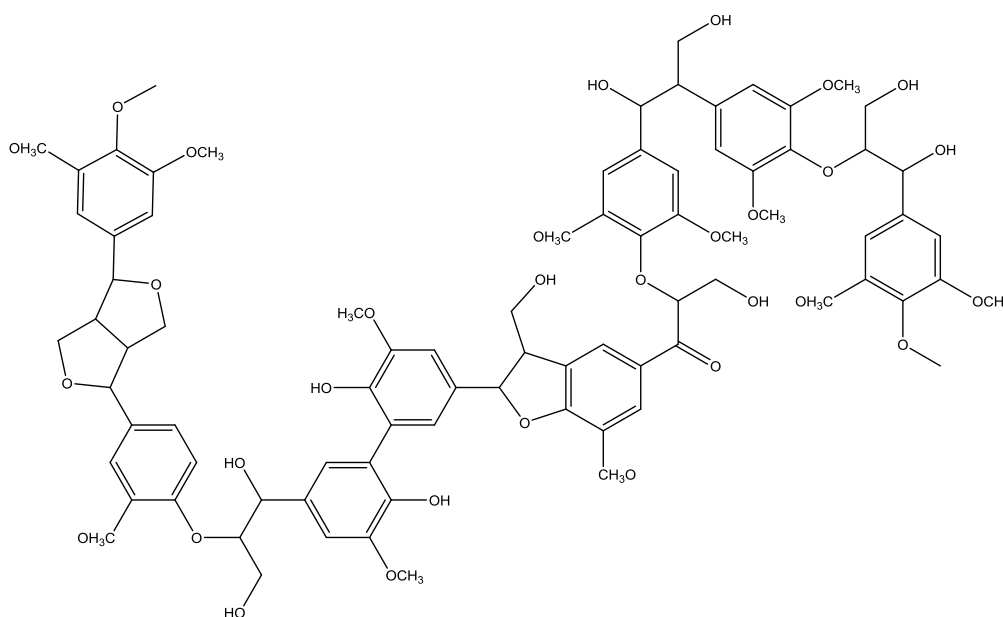


Figure 2: Representation of the lignin structure

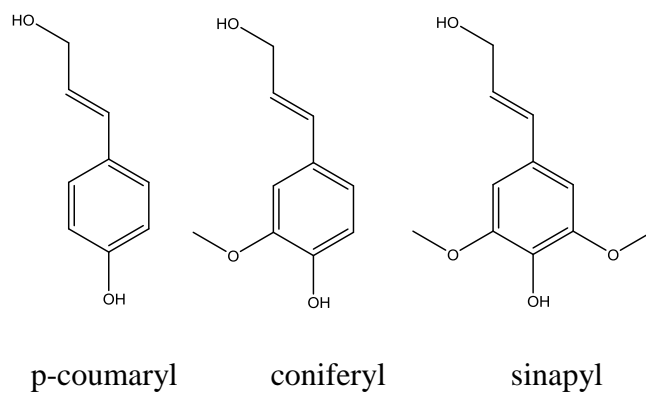


Figure 3: The three main lignin alcohol precursors

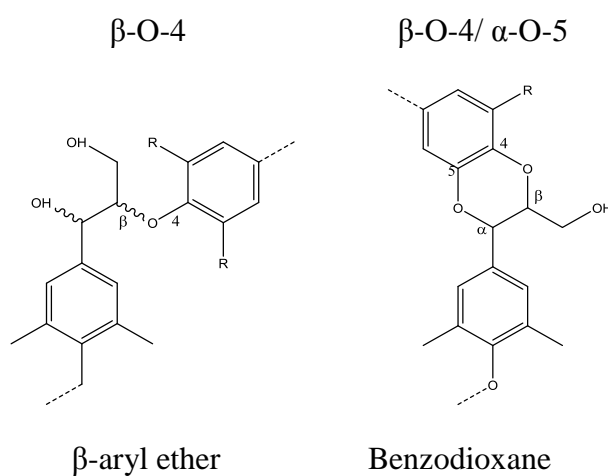


Figure 4: Examples of uncondensed linkages found in the lignin structure

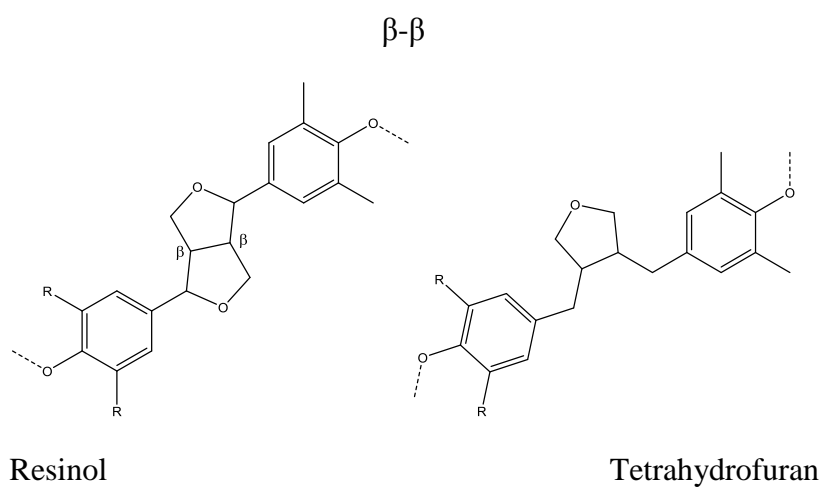
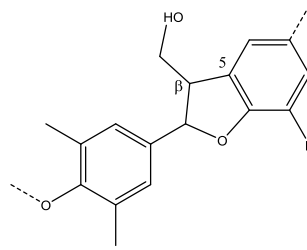


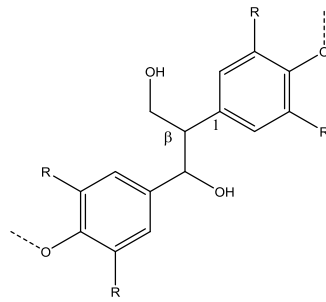
Figure 5: Examples of condensed linkages found in the lignin structure

$\beta$ -5

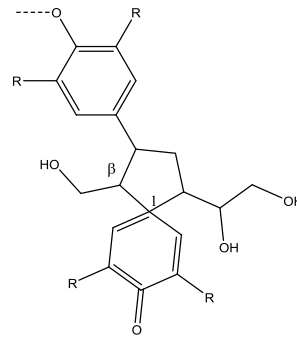


Phenylcoumaran

$\beta$ -1

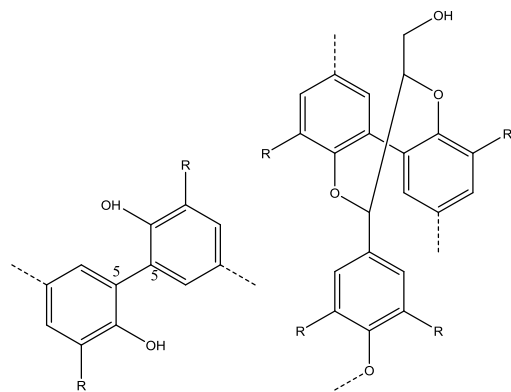


Diarylpropane



Spirodienone

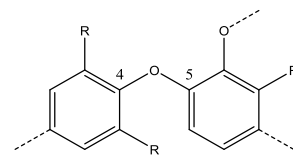
5-5



Biphenyl

Dibenzodioxocin

4-O-5



Diphenyl ether

Figure 6: Examples of condensed linkages found in the lignin structure

As illustrated in Table 1 (adapted from Lapierre et al [10]), the dominant linkage in lignin is the  $\beta$ -O-4 bond which is created via the radical polymerisation of the monolignol precursors during formation of the lignin polymer. During the initial step of polymerisation (dimerisation), all linkages are produced but the 4-O-5 and 5-5 are found to reform to other linkages due to their instability at this stage. During the second stage, cross-coupling between monomer-oligomer and oligomer-oligomer units occurs. Initially, only monomer-oligomer units will couple to produce  $\beta$ -O-4 and  $\beta$ -5 linkages but when the monomer unit supply is exhausted, the oligomer units will start to couple with themselves to produce 5-5 and 4-O-5 linkage type. This results in a lower abundance of the 4-O-5 and 5-5 as shown in Table 1:

Table 1: Typical distribution of linkages found in lignin obtained from different wood sources

Wood Source	$\beta$ -O-4	$\beta$ -1	$\beta$ - $\beta$	$\beta$ -5	4-O-5	5-5
<b>Poplar</b>	57.8	2.1	2.1	1.8	0.7	0.7
<b>Spruce</b>	31.5	2.1	0.4	2.5	0.5	2.7
<b>Pine</b>	11.3	1.9	0.3	1.2	0.2	0.6
<b>Birch</b>	15.4	47.0	24.5	6.8	3.4	2.5

### 1.3 Paper and Pulp Industry

Although carbohydrates constitute the majority of the lignocellulosic material, lignin is nevertheless an integral component. In contrast to the carbohydrate-based polymers which are easily converted to their primary monomers, lignin is structurally very complex and difficult to depolymerise. In fact, depolymerisation is such a challenging task for industrial processes, such as the paper and pulp industry, that many take the chemical degradation route instead. Furthermore, the different separation techniques used to isolate the lignin from the lignocellulose can also lead to very different lignin streams which differ with regards to their composition [11]. The paper and pulp industry produces approximately 50 million tonnes of residual lignin per year worldwide in the form of a by-product, of which only 2 % is commercially used at present [9]. Although the lignin streams are currently

utilised in the paper mills as a source of heat and energy, it is typically viewed as industrial waste with little or no commercial value beyond this application. With the upgrading of lignin streams to chemicals being considered significantly harder than that of cellulose and hemicellulose, the potential added value available with lignin is vast. To exploit lignin to its full potential, one of the key challenges of lignin conversion lies with successfully recovering the lignin from the process streams of the paper and pulp industry effectively. During the pre-treatment stages, the wood is subjected to a chemical pulping process in order to remove enough lignin to separate the cellulosic fibres from one another to give a suitable pulp for the manufacture of paper and other related products. This process is known as the delignification stage and several techniques relevant to this thesis have been described in the following sections.

### **1.3.1 Kraft Pulping Process**

The Kraft pulping process is the most dominant global process at present, producing approximately 80 % of the world's paper pulp via this process [11, 12]. Its popularity as a process stems from its ability to produce an excellent quality of pulp and its flexibility with regards to the raw material used. A conventional Kraft cook will involve chemically degrading the wood chips in an aqueous environment of sodium hydroxide (NaOH) and sodium sulfide (NaSH), also known as white liquor, in a large pressure vessel called a digester to separate the hemicellulose and lignin fractions from the cellulose. The white liquor and wood are subjected to pH values of 13-14 and temperatures of 413-452 K for various periods of time depending on the degree of delignification required. During this treatment, the liquor reacts with the lignin in the wood forming smaller water/alkali soluble fragments. Fragmentation continues by cleaving inter unit linkages and generating phenolic hydroxyl groups which make the lignin more soluble in the cooking liquor. Delignification occurs in three phases, known as the initial, bulk and residual phases, where different degrees of delignification are observed. The initial phase is carried out at temperatures of around 423 K which is then increased to 452 K for the bulk phase. The bulk phase is where most of the lignin is removed. The final residual stage begins when roughly 90 % of the lignin has been removed but the selectivity of this final phase is poor and further delignification can result in the degradation of carbohydrates and a decrease in pulp strength. The poor selectivity levels in the final phase could be a result of poor reactivity between the remaining lignin residue and the pulping chemicals, but there is also the possibility that the lignin is actually resistant to chemical attack due to connections to the carbohydrate fraction found in cellulose. The Kraft pulping conditions are capable of

typically removing 85-93 % lignin and 56-71 % hemicelluloses [13] and any remaining lignin can be removed using additional bleaching techniques with  $\text{Cl}_2\text{O}$ . It should also be noted that a number of other reactions will also occur during the Kraft cook that are not for the benefit of separation. These reactions typically lead to structural changes in the separated lignin and include excessive rupture of  $\beta$ -O-4 linkages, particularly in softwood lignin.

### **1.3.2 Organosolv Pulping Process**

Although Kraft pulping is the dominant process, it is plagued with problems such as air pollution caused by the release of sulfur compounds, or by water pollution as a result of using chlorine bleaching compounds. An alternative process known as the organosolv process involves using organic solvents to extract and solubilise lignin from the woody starting material. The application is becoming increasingly popular for the producing of ethanol biofuel from lignin which is able to give a high purity product that is essentially free from sulfur and ash. This product is also less condensed and has a narrower molecular weight distribution than lignin extracted using the Kraft process [14]. The organosolv process treats the lignocellulose with organic solvents at temperatures ranging from 422-493 K, which causes the breakdown of lignin to soluble fragments which can then be extracted.

### **1.3.3 Ammonia Fibre Expansion (AFEX) Process**

Ammonia fibre expansion is also a promising method for pretreating biomass, where liquid ammonia is added under moderate pressures (10-25 barg) and temperatures of 343-473 K with a rapid pressure release at the end to separate the lignocellulosic components. The AFEX treatment can also depolymerise the lignin itself via rupture of the linkages but it is able to minimise degradation of the sugars found in biomass which is important for further processing. Like other pretreatment methods which use ammonia, the ammonia can be recovered and recycled and although the process has several advantages compared to other ammonia methods, it is a more complicated process to implement at a commercial level with high operating costs which are not economically viable from an industrial perspective.

### **1.3.4 Soda Pulping Process**

Soda pulping accounts for approximately 5 % of the world pulp production and is generally used with annual plants which require less severe pulping conditions than woods [11]. The soda pulping process is cheaper than other pulping processes and is sulfur-free, and the recovery of the lignin from the effluent streams is based on precipitation and

liquid/solid separation, followed by drying. Soda lignins are available in Asia, however they are often of low and variable quality due to contamination issues from the raw material [15]. The soda process was adapted to include the use of sodium sulfide and was found to give a stronger pulp; this was renamed the Kraft process as shown previously.

#### **1.4 The Role of Heterogeneous Catalysis in Lignin Conversion**

In order for lignin to be utilised to its full potential, development of the catalytic technology to perform the required depolymerisation step is required. If it was possible to selectively rupture C-C and C-O bonds within the lignin polymer, there would be enormous potential for the formation of monomeric aromatic compounds. Depending on what bond cleavage is carried out, the depolymerisation of lignin could lead towards aromatic platform molecules such as BTX (benzene, toluene and xylenes) or phenolics, as well as various functionalised molecules. These monomers could then be used as platform molecules to undergo transformations to value-added products using existing technology and subsequently incorporated into current petrochemical or pharmaceutical processes.

Around 90 % of all current chemical processes, in particular for the production of bulk and speciality chemicals, are catalytic. Despite the extensive use and success of heterogeneous catalysts in these existing chemical and petroleum plants, heterogeneous catalysis technology in biorefineries is lacking and there is therefore a great need for research and development in this area. Lignin conversion has received less attention compared to that given for cellulose with regards to its utility, mainly because lignin is known as a difficult molecule to break down due to its complex structure. There are various advantages of using heterogeneous catalysts but the main benefit in relation to industry is that a catalyst can be easily separated and recycled from the reactants and products. Heterogeneous catalysts can also withstand high temperatures and pressures and remain stable and intact compared with homogeneous or biological catalysts.

With lignin's potential comes an array of disadvantages due to its complex nature. In short, lignin by nature acts as a form of protection for the carbohydrate components of lignocellulose so it is therefore very recalcitrant against chemical attack. It also has a highly functionalised structure with several kinds of linkages of various bond strengths, which can vary depending on the plant species and pretreatment method used to isolate the lignin from lignocellulose. With a complex structure, its conversion will therefore yield an equally complex product mixture with a wide range of possible products. Dissolution of lignin is also known to be problematic and its structure contains too much oxygen for

effective fuel or chemical applications, with some O-containing molecules being capable of readily polymerising to cause fuel instability and poor performance. The chance of repolymerisation to heavy molecular weight material is also highly likely under the required reaction conditions needed to depolymerise the molecule.

A one step approach which carries considerable potential for the conversion of lignin to value-added products is catalytic hydrodeoxygenation (HDO). During HDO reactions, the oxygen from the feed is converted to H<sub>2</sub>O which has the additional benefit of being environmentally friendly. HDO will also allow for the removal of this excess oxygen whilst yielding a molecule with high energy density and good combustion properties. The presence of sulfur in Kraft lignin is also a concern for the catalytic processing due to sulfur being considered a catalyst poison. The Kraft lignin will typically contain 1-3 % sulfur after the cook and this is thought to be present as sulfate ions, elemental sulfur and/or as organically bound sulfur [16]. The nature and extent of sulfur poisoning is not fully established but a combined methodology of hydrodeoxygenation (HDO) with hydrodesulfurisation (HDS) used simultaneously during the hydrotreatment of the lignin molecule should prove effective when attempting to minimise the effects of sulfur.

Catalyst deactivation via sulfur poisoning will be an important challenge during this project. As previously stated, there will typically be 1-3 % of unidentified sulfur compounds in the Kraft lignin sample which could potentially poison and deactivate the catalyst thus rendering the reaction useless. Catalyst deactivation involves a loss of catalyst activity and/or selectivity over time and is a continuing concern for industrial catalytic processes due to excessive costs for catalyst replacement and process shutdown. Catalyst poisoning in general terms can be described as a feed-stream impurity that impairs catalyst performance via competitive adsorption of the active sites [17]. Sulfur may cause significant deactivation even at very low concentrations due to the formation of metal-S-bonds. Five main mechanisms of sulfur poisoning have been detailed by Bartholomew [18]:

- Sulfur physically blocks active sites on the catalyst thus preventing subsequent adsorption of reactants
- Due to its strong chemical bond, sulfur is capable of modifying neighbouring metal atoms thereby affecting their ability to adsorb and/or dissociate reactant molecules

- The stable metal-adsorbate bonds can lead to non-selective side reactions and reconstruction of the metal surface which can alter the surface chemistry and chemical properties of the catalyst
- The adsorbed poison can form a barrier between adsorbed reactants preventing them from accessing each other
- Sulfur can inhibit or slow the surface diffusion of adsorbed reactants

## **1.5 Overview of Lignin Valorisation**

When this project was undertaken, there was a real lack of literature available with respect to lignin conversion using heterogeneous catalysis. Instead, reviews on biomass conversion focused on the utilisation of cellulose with very little regard for lignin. Little literature was available on the conversion of the entire lignin molecule, especially under similar reaction conditions, and a majority alternatively concentrated on work using model compounds which mimicked parts the lignins structure. Attention towards conventional hydrotreating catalysts was originally given but this has moved towards the use of alternative catalysts such as noble metals in recent years and although full conversion to specific target molecules has yet to come, a better handling of the lignin molecule is evident with a decrease in undesired material and an increase in aromatic monomers with various functional groups to a reasonable yield. Collectively, this published work provides a better understanding of the reaction behaviour of lignin under a variety of reaction conditions and highlights that although the work on lignin conversion is moving forward at a better rate, there is still a definite need for this research to continue to enable its use in future applications.

### **1.5.1 Pyrolysis Studies of Lignin**

Degradation of lignin can be achieved using thermochemical treatments which can include the use of catalysts, solvents and other promoters. Pyrolysis has been studied as a means of producing lower molecular weight compounds and is known to simultaneously occur during other thermal processes such as hydrogenation. It is therefore important to have an understanding of how lignin thermally decomposes. Pyrolysis of lignin involves the thermal treatment of the molecule in the absence of oxygen, with or without a catalyst, where the reaction products typically include solid char, liquid oil and gases. The type of products obtained and their yields will depend upon the lignin structure and isolation methods, where softwoods produce guaiacyl units and hardwood lignins produce both

guaiacyl and syringyl units. More specifically, products from lignin pyrolysis can typically be divided into gaseous hydrocarbons together with carbon dioxide and carbon monoxide, volatile liquids (water, methanol, acetone, acetaldehyde) and monophenols (phenol, guaiacol, catechol) and other more functionalised phenolic compounds [19].

Lignin degradation involves a substantial weight loss (~40 %) regardless of origin at temperature intervals of 473-873 K, with maximum material loss occurring around 673 K [20]. The wide temperature range is a result of having so many functional groups within the lignin structure, each with their own thermal stability. As already stated, the  $\beta$ -O-4 bond is the dominant linkage and it can be cleaved at relatively low temperatures, whilst the  $\beta$ -ether linkages are known to have different cleavage mechanisms depending on the side-chain structure. Bond enthalpy energies for the linkages associated with lignin have been given in Figure 7.

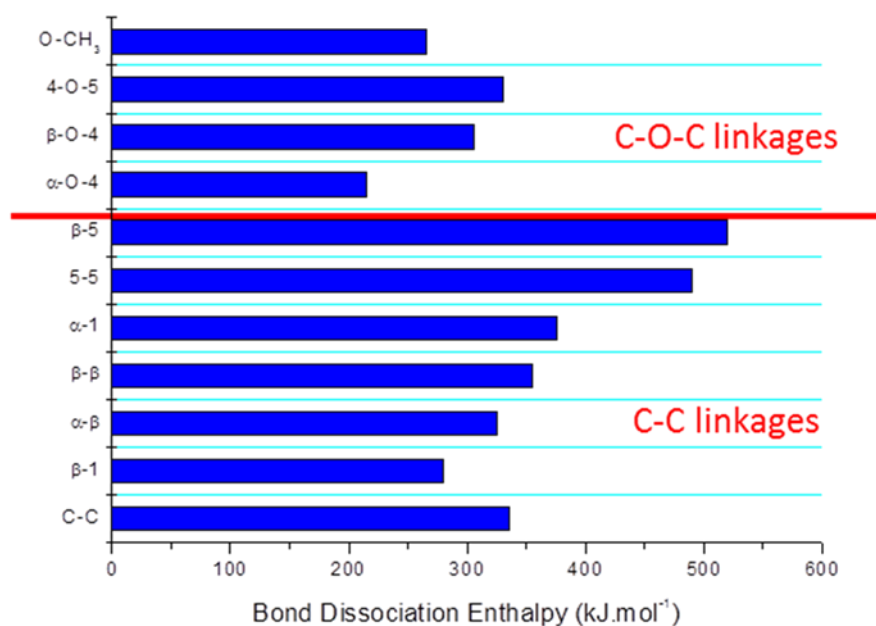


Figure 7: Bond dissociation enthalpy values of common lignin linkages

In terms of reaction conditions, low heating rates tend to favour the formation of oxygen-containing compounds, whilst fast heating rates tend to give hydrocarbons and alkyl-phenol molecules which would be more desirable for the purposes of this project. Although the pyrolysis of lignin does look to favour higher temperatures, remnants always remain. This material was found to be chemically modified to form a stable structure that could not

be easily decomposed [21]. This carbonated structure is commonly known as char and is found to stick to catalysts used during catalytic reactions thus raising issues with catalyst deactivation.

Brodin et al ran experiments using step-wise pyrolysis from 473-1173 K using Kraft lignins from softwood and hardwood sources to give an indication of the difference in mass loss as a result of pretreatment changes [21]. The authors found that all samples released guaiacol or syringol at temperatures of 473-573 K but differences were observed at higher temperatures. At 673 K, the hardwood lignins released a substantial amount of phenol with a maximum release at 773 K, in comparison to the softwood lignins which exhibited a maximum release at 773 K and 873 K, with a small loss at 673 K. Phenolic and cresol compounds were also identified at 973 K for the softwood lignin only. These studies recognised that Kraft lignin could be degraded using simple thermal treatment alone without the aid of catalysis and although it is clear that the general trend of degradation was similar, the yield of particular products at specific temperatures was found to vary depending on the type of lignin used in the study. This work therefore highlights a lack in product selectivity which could potentially be overcome with the use of catalysts.

### **1.5.2 Model Compound Conversion Studies**

As well as using the lignin molecule itself, the use of model compounds are also employed in order to simplify the reaction due to lignin being a highly functionalised molecule. It is common for studies to use compounds that mimic parts of the lignin structure, where these model compounds contain linkages and functional groups that are typical of those found in lignin. The study of their reactivity enables the researcher to gain perspective into possible reactivity's of the lignin polymer itself, with the added benefit of greatly simplifying product analysis. Figure 8 shows examples of monomeric model compounds frequently used including phenol (1), cresole (2), anisole (3), and more commonly guaiacol (4):

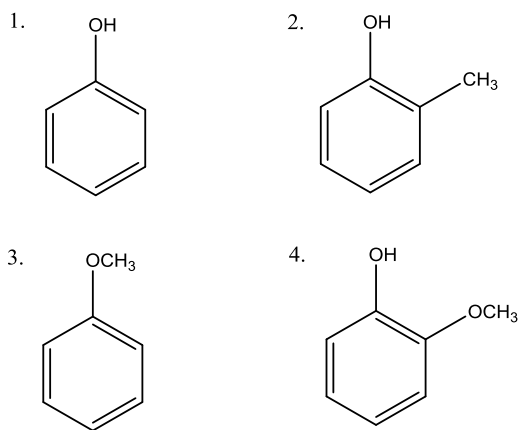


Figure 8: Examples of monomeric lignin model compounds

The most common industrial hydrotreating catalysts for HDO and HDS applications are CoMo and NiMo supported on alumina. These hydrotreating catalysts were originally developed for the removal of nitrogen and sulfur to avoid poisoning of the oil feeds, but they were found to also be effective for the removal of oxygen from the highly oxygenated biomass molecules without hydrogenation of the aromatic rings. The metal oxide form of Co or Ni species must be activated prior to its use and conversion from metal oxide to its metal sulfided state is often used to maximise its catalyst activity. The presence of Co or Ni does not increase the number of vacant sites but any vacancies associated with Co or Ni are considerably more active than the Mo thus giving a ‘promoted’ effect on the activity of the catalyst. The use of alumina as a catalyst support can be credited to its properties such as high surface area and relatively low cost, but it has been recognised that alumina is not an inert carrier and that it is possible for the promoter (Ni or Co) to react with the support resulting in undesirable metal aluminates ( $\text{CoAl}_2\text{O}_4$  or  $\text{NiAl}_2\text{O}_4$ ) depending on the conditions of preparation. Alumina is also active for coke formation [22, 23] and is unstable in large amounts of water [24], so alternative support options have been investigated. Duchet et al showed that both cobalt and nickel on carbon supports were highly active catalysts, although cobalt proved to be the more active of the two [25]. Due to carbon being an inert material, it had the advantage over alumina of fully converting the metal to its sulfided form but an important drawback for employing the use of carbon as a support is its low surface area. Vissers et al over two studies established two possible applications to overcome this issue [26, 27]. The first involved the application of carbon black composite material that formed a binding type material at high temperatures. They showed promising results but required oxidation treatments to increase their heterogeneity.

The second modification involved covering the alumina surface with a thin layer of carbon to combine the favourable benefit of both supports. The authors found a threefold increase in activity in comparison to Co/Al<sub>2</sub>O<sub>3</sub> due to the carbon forming an effective shield to eliminate the metal-alumina interaction. Literature using silica as an alternative support generally reports lower catalyst activity in comparison to using an alumina support as a result of poor Mo dispersion [28]. However the use of mixing silica and alumina supports has been proven useful as it gives a good compromise with better dispersion and reducing properties which therefore increase its sulphiding abilities [29].

In terms of using these catalysts with model compounds, Laurent and Delmon [30] showed during their studies using guaiacol over CoMo and NiMo sulfided catalysts that the main products were catechol and phenol with additional traces of benzene and cyclohexane being identified during longer reaction times. They proposed that phenol was not a primary product but that it was produced as a function of time in very low quantities directly from guaiacol. They agreed that the initial reaction involved the rupture of the O-methyl bond of the methoxy group leading to catechol production. They carried out comparison experiments using alumina support alone against sulfided bimetallic CoMo and NiMo catalyst and found that the latter gave much higher catalytic activity. They found that NiMo catalyst had a better activity for the conversion of guaiacol than the CoMo catalyst, but they also showed that the CoMo catalyst gave better selectivity which suggested that side reactions were more important with NiMo. The decrease in the catalytic activity was thought to be attributed to a blockage of the active sites via the formation of coke or deposits of heavy products on the catalyst surface.

Bui et al [31, 32] produced literature on the promoting effect of cobalt and support types on molybdenum sulfide catalysts, giving a more detailed reaction scheme for guaiacol conversion (see Figure 9 [31]). They suggested that the formation of anisole in trace amounts implied that the C-OH bond was the most difficult to rupture and the production of methanol confirmed that both demethylation (DME) and demethoxylation (DMO) reactions took place but the DMO route was favoured by the CoMo catalyst. Methylated products were produced due to the acid sites on the support surface, as well as the formation of heavier products via condensation reactions. They concluded that Co facilitated the C-OMe rupture and that the addition of Co greatly enhanced the hydrodeoxygenation (HDO) performance of the catalyst. These guaiacol studies also enabled the researchers to investigate the intermediate reaction of phenol which would be representative of actual lignin conversion studies which will undoubtedly involve

simultaneous intermediate reactions. They found that the phenol followed one of two routes; a direct deoxygenation route (DDO) to form benzene or a consecutive route including hydrogenation (HYD) with subsequent elimination of oxygen. Thus it is possible for the formation of benzene by direct cleavage of the C-O bond in phenol, while cyclohexane and cyclohexene could also be formed from hydrogenation of the aromatic cycle and elimination of water. This highlights the difficulty of lignin studies producing an array of products via many reaction pathways, even when using a ‘simple’ model compound in comparison to the entire lignin polymer.

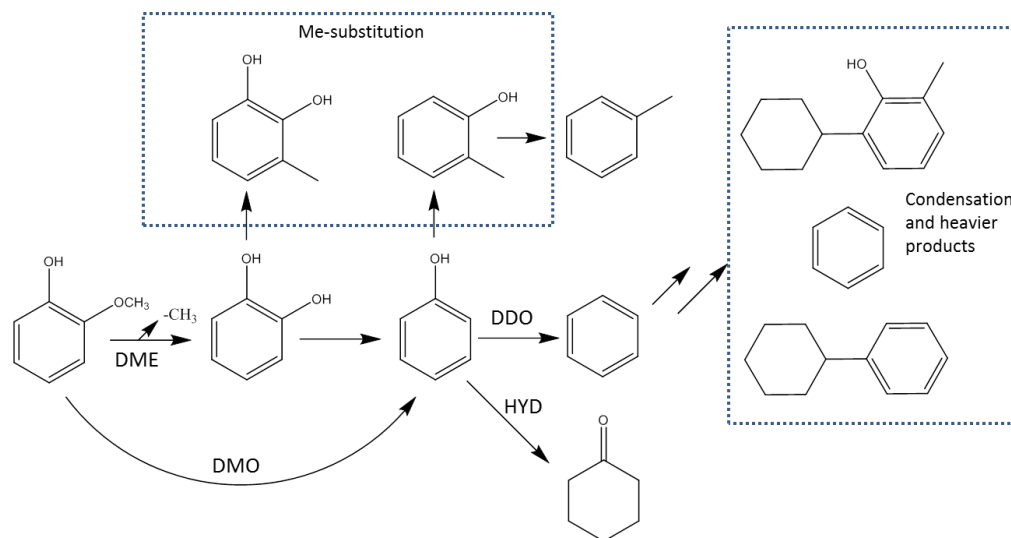


Figure 9: Proposed reaction scheme for guaiacol conversion

Jongerius et al carried out experiments in an attempt to unify results that they felt were lacking direct comparison due to differing experimental conditions in all other available literature [33]. They used monomeric model compounds over a sulfided CoMo/Al<sub>2</sub>O<sub>3</sub> catalyst under identical HDO conditions. They obtained high selectivities for many of the compounds and found that phenol made up the majority part of the reaction mixture, as well as producing trace amounts of benzene and toluene. The presence of these trace compounds suggested to the researchers that full deoxygenation had not taken place and the formation of several different products in each reaction suggested that HDO, O-demethylation and hydrogenation pathways occurred simultaneously. It was also suggested that it was the substrate that determined which pathway was favoured but phenolics were formed regardless. In comparison to previous studies, no cyclohexanes were found. It was assumed that demethylation and HDO reactions took place in the initial stages of the reaction and they noted a considerable difference in the reactivity of methylated and non-

methylated compounds, where conversion and selectivity favoured deoxygenated products of the methylated substrates. Less ring methylation products were found for methylated substrates suggesting that the presence of a methyl group on the ring was sterically less favourable. This was due to methyl groups making the ring more difficult to approach thus inhibiting hydrogenation reactions because the molecule was unable to adsorb flat onto the catalyst surface in the presence of methyl groups. In terms of studies using guaiacol as a lignin compound, Jongerius et al were in agreement with the previous reports [31, 32]. They also carried out experiments to study the effect of the catalyst system on linkages typically present in the lignin polymer. They chose model compounds to represent both the  $\beta$ -O-4 and phenylcoumaran ether linkages, as well as the 5-5 aryl-aryl linkage (see Figure 10), and they confirmed that the  $\beta$ -O-4 bond could be cleaved under HDO conditions. 33 % of aromatics were recovered for GC analysis, including phenol, guaiacol and syringol-type products as shown in Figure 11. They demonstrated that the 5-5 bond could not be cleaved and this was in agreement with previous literature that found 5-5 (as well as aromatic structures) posed more of a problem to rupture due to their stability [34]. Other observations were made on similar compounds which showed that only one hydroxyl group was removed via HDO and that this led to the formation of dibenzofuran, but its formation was thought to be via a separate pathway which competed with HDO. HDO reactions on the compound mimicking phenylcoumaran showed high selectivity for 2-ethyl-phenol. In summary, although the experiment resulted in low conversion, it was evident that it was possible to cleave the alkyl-oxygen bond using CoMo/ Al<sub>2</sub>O<sub>3</sub> which proved promising for the cleavage of the other ether linkages found in lignin.

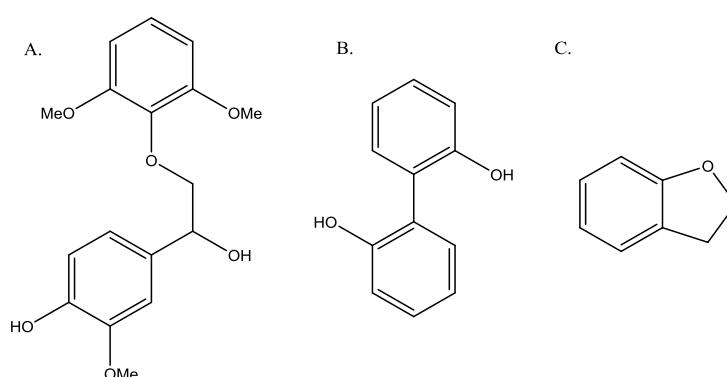


Figure 10: Model compounds mimicking the  $\beta$ -O-4 (A), 5-5 (B), and phenylcoumaran (C) linkages found in lignin

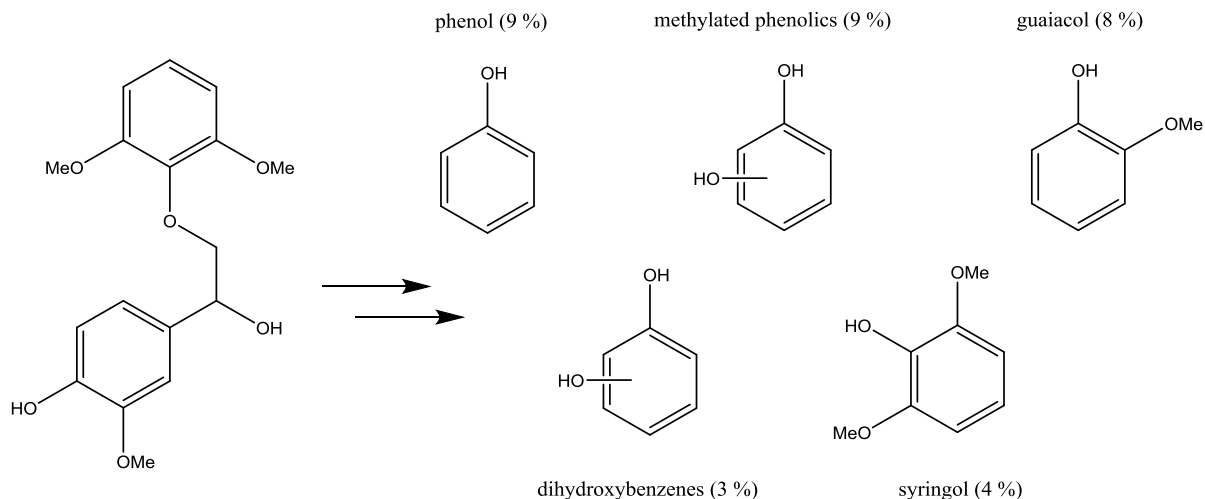


Figure 11: Products formed from the cleavage of the  $\beta$ -O-4 linkage

The drawbacks of using conventional hydrotreating catalysts include the support issues as discussed, but they also require severe conditions and have issues maintaining their sulfided state throughout the reaction. Gutierrez et al reported full conversion of guaiacol to predominately benzene at 573 K using a sulfided CoMo/Al<sub>2</sub>O<sub>3</sub> catalyst but it was found that the sulfur leached during reaction resulting in contamination of the products [35]. As an alternative, noble metal catalysts offer interesting lignin catalytic reactions without the need for their sulfided forms

Gutierrez et al continued their work by comparing their CoMo/Al<sub>2</sub>O<sub>3</sub> findings to those obtained using zirconia supported noble metals [35]. They found that guaiacol also underwent full or almost complete conversion producing mainly benzene, with small amounts of cyclohexanol present. The non-catalytic and support only equivalent reactions gave much lower conversions (13 and 27 % respectively) and cyclohexanol was the main product which showed that the reaction pathway could be altered to desirable products with the inclusion of a noble metal. Rh and RhPd showed particular high selectivity towards deoxygenation reactions.

Studies with Pt/carbon catalysts have shown high activity and durability in the hydrogenation of phenol with hydrogenation of the aromatic ring followed by subsequent hydrogenolysis of the C-O bond of cyclohexanols [36]. Although hydrogenation of the ring was not favourable, this study showed that the catalyst was capable of reacting with the complex molecule. The catalyst also had the benefit of being reusable – it could be easily separated from the reaction mixture and remained active for a total of 3 reactions at high

pressures of 40 barg and at a temperature of ~553 K. Further studies using a similar platinum catalyst on carbon, as well as palladium and bimetallic Pt-Pd catalysts for comparative purposes, illustrated the deoxygenation of benzofuran where it was shown that there was no direct removal of oxygen but that it took place after the dehydrogenation of the heterocyclic ring [37].

Alternative research showed that the conversion of guaiacol catalysed by Pt/MgO gave predominately phenol and some anisole [38]. Benzene was not a primary product and was found to be the result of a secondary HDO reaction from phenol or anisole. A series of experiments were run in comparison to previous work using Pt/Al<sub>2</sub>O<sub>3</sub> [39] and Figure 12 [38] shows the conversion of guaiacol to the identified products, where dashed arrows indicate transalkylation reactions and solid arrows represent hydrogenation/dehydrogenation/HDO reactions. HDO was evident for both catalysts with the production of phenol from guaiacol via cleavage of the C-O bond and removal of the oxygen to form water or methanol. Regardless of support, this showed that Pt was HDO active but hydrogenolysis reactions also occurred due to the production of anisole which exhibited C-O bond cleavage without the removal of oxygen. It was also observed that the different support options altered the formation of catechol and that the Pt/Al<sub>2</sub>O<sub>3</sub> catalyst could facilitate transalkylation reactions that the MgO support was incapable of. Again, coke formation on the used catalyst was also an issue for the alumina support whereas it was not as evident for the magnesia alternative, highlighting the need to explore support options when carrying out a catalytic study.

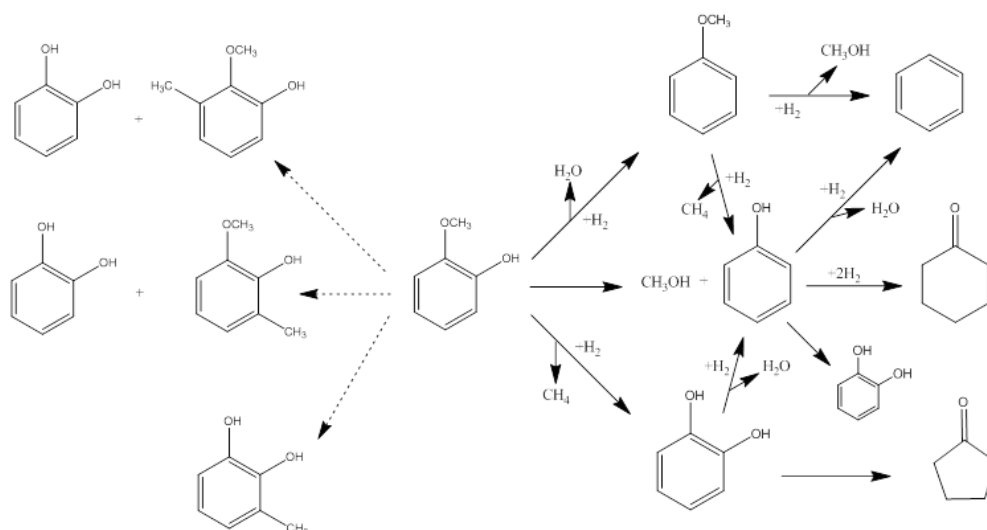


Figure 12: Reaction network for conversion of guaiacol using Pt supported on magnesia or alumina

### 1.5.3 Lignin Conversion Studies

With respect to studies using the entire lignin molecule, hydrotreatment of lignin was considered among the most suitable conversion methods for the depolymerisation of lignin [40], where the method uses thermal means to first rupture the bonds in lignin to form free radical fragments which could then be stabilised using hydrogen derived from the reaction atmosphere or hydrogen-donor solvents. Superior to pyrolysis methods, high-pressure direct liquefaction can be used to produce bio-oil that has a high calorific value and contains a range of molecules such as vanillin, phenols and aldehydes [41]. Typical products after depolymerisation and extraction are gas (mainly CO<sub>2</sub>), small organic compounds, aromatic monomers, oligomers and condensed residue [42]. The monomeric fraction is composed of oxygenated compounds which have the potential to be valorised after extraction or separated using distillation or flash chromatography. The oligomer rich fraction is a little more difficult to process as it is principally made up of dimers and trimers with oxygen functions but there is potential for it to be converted to fuel additives using hydroprocessing technology. Supercritical fluids have also been used, for example Gosselink et al used a mixture of supercritical CO<sub>2</sub>/acetone/water (573-643 K and 100 barg) to convert organosolv lignin from hardwood and wheat straw to phenolic oil and aromatic monomers, with conversions of 10-12 % [43]. Promoters such as NaOH can be also be added to the reaction medium to aid conversion [44], whilst solvents such as phenol can be employed as capping agents [45]. Valorisation of birch lignin to monomeric phenols using a hydrogenolysis route with Ni-based catalysts has shown >90 % selectivity to propylguaiacol and propylsyringol and a total lignin conversion of 50 % [46]. Alcohols such as methanol and ethanol were also deemed as suitable solvents for lignin conversion due to their capping and solubilisation abilities.

It is now common for lignin conversion to take place in the liquid phase because lignin and the derived aromatic products are known to have a low vapour pressure and high polarity. The original catalyst materials designed for processing low oxygen content feeds are now no longer useful in these oxygen-rich environments so the catalysts requirements therefore have to change in terms of increasing their stability. Liquid-phase conversion takes place during a process known as aqueous-phase reforming (APR) and offers an interesting pathway for the breakdown of lignin. APR using lignin and Pt/ $\gamma$ -Al<sub>2</sub>O<sub>3</sub> catalyst at 498 K and a pressure of 29 barg showed the production of monomer units but the system still suffered from recondensation issues [47]. In order to overcome this familiar issue with lignin, studies involving solvent optimisation took place to give more efficient processes

with higher product yields. Zakzeski et al also aimed to address the problem of lignin condensation by using a liquid-phase reforming (LPR) step which involved incorporating a water-ethanol mix into the reaction to aid lignin solubilisation and increase monomer yields [48]. Lignin solubilisation prior to reaction seems like a logical step due to its use in pretreatment steps to aid delignification and its ability to reduce starting molecular weight of lignin due to cleavage of the ether linkages [48]. Their 2D NMR data showed a specific reduction in the number of  $\beta$ - $\beta$ , phenylcoumaran, and  $\beta$ -O-4 linkages present in the structure after solubilisation and enhanced product yields were noted as a result of the inclusion of ethanol-water solvent. More importantly, no char formation occurred. They reported that LPR of Kraft lignin generated 17.6 % of aromatic monomeric compounds against 6.2 % for the equivalent HDO reaction. It was found that guaiacol was the main product using a LPR route whilst an HDO approach yielded more alkylated phenolics compounds. Although the LPR gave a better overall yield, the higher added value of the HDO products (alkylphenolic compounds) could hold more potential.

As previously discussed, there are limitations to using alumina supports in these types of conditions but there are also possible problems using platinum on the support surface. There was no evidence of sintering in the work carried out by Jongerius et al [49], but it has been noted elsewhere that large parts of the metal surface area can suffer from blockages due to the formation of carbonaceous materials [50]. Jongerius et al studied the stability of Pt/ $\gamma$ -Al<sub>2</sub>O<sub>3</sub> under LPR conditions and found that the transformation of the support to boehmite and Pt sintering was reduced dramatically in the presence of lignin-derived molecules, which they believed adsorbed onto the alumina via its oxygen functionalities thus providing stability [49]. It was thought that although the catalyst wasn't stable at the conditions required to solubilise lignin, and they felt that this could be overcome by increasing the lignin concentration used during reaction. Work has continued in the LPR area with favourable results but the authors rightly stated that although good work is being carried out using one-step conversion routes, none of these processes are actually able to produce oxygen-free, or even low-oxygen content monomeric products. They suspected that a two-step strategy would allow for a general depolymerisation step to occur, followed by a second conversion step which would upgrade the fragmented product mixture. They considered ways of using an HDO step to upgrade the depolymerisation products to low-oxygen products using the bio-oil extracted from the depolymerisation products as a feed. They were able to produce 9 % monomeric yields, of which 24 % of the products obtained were oxygen-free. They believed that the results greatly depended on the

lignin source and that increased temperatures (623 K) could see complete conversion when using a two-step process.

What these studies all have in common is the fact that there is a clear increase in the amount of data now available on the whole lignin compound and that it is possible to generate interesting, useful results. It is clear that there is a direct link between the lignin source and conditions used with the resultant product distributions and yields. A major problem identified throughout this project was the fact that little literature comparing a variety of lignins over the same conditions was available and that a fair comparison could not be made across the different reaction conditions employed. In order for this work to move forward, lignin sources of a high purity must be established, followed by optimisation work using the same conditions to maximise reaction efficiency and ensure that the lignin feedstock is used to its full potential.

## **1.6 Project Aims**

The primary aim of this thesis was to study the depolymerisation of Kraft lignin to functional aromatic monomers using heterogeneous catalysis. In order to tackle the sulfur-containing lignin, it was decided that initial groundwork on sulfur-free lignins would be carried out in order to build a sense of how the lignin behaved under catalytic conditions without the complication of sulfur.

## 2 Experimental Methods

In this section, all experimental techniques used in this thesis will be introduced. Firstly, the different types of lignin used and the catalysts utilised in this work will be explained. The laboratory setups which allowed for the various reactor studies to be carried out will also be described in detail and the analysis methods that were either internally or externally conducted will also be included.

### 2.1 Lignin Sources and Preparation Methods

#### 2.1.1 Kraft Lignin

In order to achieve the main objective of the project, a commercial Kraft lignin was purchased from Sigma Aldrich. This lignin was obtained from Norway Spruce and was quoted by Sigma as having 3 % sulfur in an unknown form. Typical Kraft processes use a mixture of sodium hydroxide and sodium sulfide at elevated temperatures to treat wood chips during the pulping process for the manufacture of paper and other related products. The actual conditions used to isolate this lignin are unknown.

#### 2.1.2 Other Lignins Used

In order to build a profile on how different lignins react under catalytic conditions, a variety of other lignin samples were also used. All other lignins, except the Kraft and Soda lignins, were isolated by Dr Florent Bouxin at the University of Glasgow and are summarised briefly below. The details of each treatment are well described elsewhere [1, 51, 52].

##### 2.1.2.1 Soda Lignin

One other lignin was sourced commercially, namely the Protobind 1000 lignin from Green Value, Switzerland. This lignin was isolated from wheat straw using the Soda process. This alkaline pulping process typically involves treating wood shavings with sodium hydroxide under elevated temperatures. The actual conditions used to give the lignin used here are unknown.

##### 2.1.2.2 Ammonia Fibre Expanded (AFEX) Lignin

Ammonia fibre expanded wheat straw was obtained from Professor Bruce Dale, Michigan State University, and was extracted under reflux with 0.5 N sodium hydroxide in ethanol-water (6/4 : v/v). The mixture was then filtered and washed with ethanol-water (6/4). The filtrate was neutralised to pH 6, then the hemicellulose fraction was precipitated using

ethanol and subsequently removed by centrifugation. The supernatant was concentrated and acidified to pH 2 which allowed for the precipitated AFEX lignin to be recovered.

### **2.1.2.3 Fermented AFEX (Fr-AFEX) Lignin**

It was of added interest to the project to determine the difference in monomer production from lignin extracted from saccharification residues compared to lignin extracted from fermentation residues. In order to prepare a fermentation residue, a one-pot saccharification/fermentation step was performed on the AFEX pre-treated wheat straw. Firstly, the saccharification step reacted 200 g of the AFEX wheat straw at 323 K for 68 h with a magnetic stirring rate of 1200 rpm. This was carried out in a citrate buffer solution (pH 4.7) with 60 mL of Celluclast 1.5 L (20 FPU/g) and 30 mL of Novozym 188 (40 CBU/g). 12 g of peptone, 2.5 g of  $(\text{NH}_4)_2\text{SO}_4$ , 2.5 g  $\text{K}_2\text{HPO}_4$ , 1.25 g of  $\text{MgSO}_4$  and 1.25 g of  $\text{MnSO}_4$  was then added after the saccharification step.

For the fermentation step, 10 mg of  $\text{K}_2\text{CO}_3$  and 10 mg of  $\text{CaCO}_3$  was dissolved in 100 mL of water which contained 1 % yeast extract. This solution was boiled for 10 min then cooled to 318 K before adding dry Baker's Yeast. The hydrated yeast was then added to the saccharified slurry and kept under anaerobic conditions for 48 h. The residue was then centrifuged, washed with deionised water and freeze dried. The residue was then treated the same way as the AFEX lignin to obtain the isolated Fr-AFEX lignin sample.

### **2.1.2.4 Acid Organosolv (Org) Lignin**

The acid organosolv lignin from poplar wood was prepared in a stainless steel reactor using ethanol-water (6/4 : v/v) which contained sulfuric acid (1.25 % w/w of poplar). The reaction was carried out at 453 K for 1 h. After cooling, the mixture was filtered, acidified to pH 2 then diluted in three volumes of water. The precipitated organosolv lignin was recovered after centrifugation, washed with deionised water and freeze dried.

### **2.1.2.5 Ammonia (Amm) Lignin**

The ammonia lignin was prepared by percolating aqueous ammonia (15 % w/v) through poplar sawdust at 453 K, 20 barg pressure, with a  $3 \text{ mL}\cdot\text{min}^{-1}$  flow rate and a total liquid to solid ratio of 10:1. This liquor was concentrated and acidified to pH 2 with HCl then recovered using a centrifuge. The lignin was purified using a mild organosolv process where the lignin was solubilised in ethanol-water-0.1 N  $\text{H}_2\text{SO}_4$  under reflux for 2 h. The ethanol-soluble lignin was separated from the residue by centrifugation then precipitated in

three volumes of water and acidified to pH 2 using HCl. The lignin was washed in deionised water and freeze dried.

#### **2.1.2.6 Alkali (Alk) Lignin**

The alkali lignin was extracted from wheat straw under reflux for 4 h using ethanol-water (6/4 : v/v) which contained sodium hydroxide (5 % w/w loading). This produced an alkali liquor which was neutralised to pH 6, mixed with three volumes of ethanol to precipitate the hemicellulose fraction, then concentrated and acidified to pH 2. The precipitated lignin sample was then recovered using centrifugation.

### **2.2 Catalyst Preparation**

Three precious metal catalysts supported on alumina were used in this project. The platinum/alumina was commercially purchased, whilst the other two were prepared in house.

#### **2.2.1 1 wt. % Platinum/alumina Catalyst**

The main catalyst used throughout this work was a commercial 1 wt. % Pt/alumina catalyst supplied by Johnson Matthey (reference number 1074). Powder XRD showed that no metal was observed due to the low metal loading but the support phase was found to be theta-alumina when compared against the XRD Powder Diffraction Database [53]. The platinum dispersion, as measured by carbon monoxide chemisorption, was 56 %, while the catalyst had a BET surface area of  $119 \text{ m}^2.\text{g}^{-1}$ , a pore volume of  $0.49 \text{ cm}^3.\text{g}^{-1}$  and an average pore diameter of 11 nm.

#### **2.2.2 1 wt. % Rhodium/alumina Catalyst**

This catalyst was prepared by Dr Claire Gillan using an impregnation method at the University of Glasgow. Full details on the preparation of this catalyst and its characterisation can be found elsewhere [54]. XRD analysis was unable to identify the metal but found that the alumina support used was a mix between a theta and delta phase. BET analysis gave a surface area of  $102 \text{ m}^2.\text{g}^{-1}$  and a pore volume of  $0.51 \text{ cm}^3.\text{g}^{-1}$ , whilst the rhodium dispersion was quoted as being 121 % from CO chemisorption.

#### **2.2.3 1 wt. % Iridium/alumina Catalyst**

This catalyst was prepared by Miss Stephy Wilson at the University of Glasgow using an incipient wetness technique [55]. No metal oxide was visible using XRD but the support

phase was found to be mixture of theta and delta alumina. The surface area of the catalyst was calculated to be  $106 \text{ m}^2 \cdot \text{g}^{-1}$  with a pore volume of  $0.45 \text{ cm}^3 \cdot \text{g}^{-1}$ .

## 2.3 Reactor Studies

### 2.3.1 Reactor Set-up

The catalytic reactions were conducted in a 300 mL 316 stainless steel Parr batch autoclave reactor equipped with a digital temperature controller ( $\pm 1 \text{ K}$ ). Figure 13 gives a schematic diagram of the reactor where, A is the gas inlet, B is the heater, C is the 300 mL reactor vessel, D is the magnetic stirrer, E is the pressure gauge, F is the gas outlet and G represents the temperature and stirrer controller. The reactant mix within the reactor was stirred using a Parr magnetic driven stirrer and the pressure was achieved using an external gas cylinder and high pressure gauge.

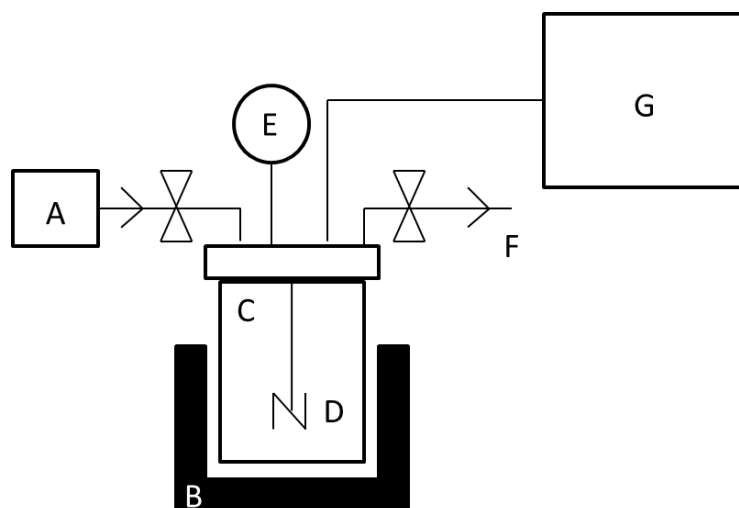


Figure 13: Schematic diagram of Parr autoclave reactor

### 2.3.2 Reaction Procedure

Prior to reaction, all catalysts were pre-reduced on the glass-line apparatus. Typically, 0.5 g of catalyst (sieved to 250-425  $\mu\text{m}$ ) was transferred to a glass reactor tube and purged with argon ( $30 \text{ mL} \cdot \text{min}^{-1}$ ) for 10 min. The catalyst was then reduced as stated in Table 2 in 2 %  $\text{H}_2/\text{N}_2$ . After the reduction step, the catalyst was cooled to room temperature in flowing argon then passivated in 2 %  $\text{O}_2/\text{Ar}$  for 1 h.

Table 2: Catalyst reduction conditions

<b>Catalyst</b>	<b>Ramp Rate</b> (°C.min <sup>-1</sup> )	<b>Final Temperature</b> (°C)	<b>Dwell Time</b> (h)
<b>1 % Pt/alumina</b>	10	250	2
<b>1% Rh/alumina</b>	10	300	1
<b>1 % Ir/alumina</b>	10	300	1

During a typical standard experiment, 0.5 g of lignin was added to the autoclave along with 0.1 g of catalyst and 100 mL methanol-water mix (50/50 : v/v). The reactor was purged with hydrogen and pressurised to 20 barg. The reaction was heated to 573 K  $\pm$  1 K under a mechanical stirring rate of 1000 rpm and stopped after 2.5 h. All reactions used these conditions as standard unless otherwise stated. The optimisation and deuterium reactions altered one or more of the parameters stated here but this will be highlighted as required.

The reaction mixture was filtered using a glass filter (po. 3) to remove the catalyst and insoluble products. Any remaining high molecular weight material was solubilised in acetone and made up to 200 mL. This acetone fraction will now be referred to as the 'heavy fraction'. The methanol-water soluble fraction (now known as the 'light fraction') was centrifuged to isolate finely dispersed solids and made up to 200 mL. A 15 mL aliquot of this light fraction was mixed with 0.2 mL of 10 g.L<sup>-1</sup> hexadecane (C16) internal standard and acidified to pH 3 using HCl. The products were then extracted with dichloromethane/dioxane (8/2 : v/v) three times. The solvent was removed using a rotary evaporator and the remaining products were then solubilised in 2 mL dichloromethane (DCM) ready for further analysis (see 2.4.9).

## 2.4 Analysis Methods

### 2.4.1 Surface Area and Pore Volume Determination

The total surface area and pore volume of the catalysts used were measured using Brunauer, Emmett and Teller (BET) analysis using a Micromeritics Gemini III 2375 Surface Area Analyser at 77 K and approximately 40 mg of sample per run. Samples were weighed in a glass tube and left overnight at 383 K under a nitrogen purge prior to analysis.

The BET equation can be expressed as Equation 1, where P is the pressure of the adsorbate gas, P<sub>0</sub> is the saturated pressure of the adsorbate gas, V is the volume of adsorbed gas, V<sub>m</sub> is the volume of monolayer adsorbed gas, and C is the BET constant ( $C = e^{((q_1 - q_l)/RT)}$ ).

$$\frac{P}{V(P_0 - P)} = \frac{1}{V_m C} + \frac{(C - 1)P}{V_m C P_0}$$

Equation 1: The BET equation

The graph plot of  $[P / V (P_0 - P)]$  vs.  $[P / P_0]$  gives a straight line with a slope of  $[(C - 1) / V_m C]$  and an intercept of  $[1 / V_m C]$ . The V<sub>m</sub> value can be determined using the following equation, where I and J are the intercept and slope values respectively:

$$V_m = 1 / (I + J)$$

Equation 2: Calculating the V<sub>m</sub> value for the BET equation

The surface area of the catalyst can then be calculated using Equation 3, where N is Avogadro's number ( $6.022 \times 10^{23}$ ), M<sub>v</sub> is the molar volume of adsorbed gas, and σ is the adsorption cross-section of the adsorbed gas molecule (N<sub>2</sub> gas).

$$S_{\text{Total}} = V_m N \sigma / M_v$$

Equation 3: Surface area equation

The surface area per unit weight of catalyst can then be calculated using Equation 4, where m is the mass of catalyst used:

$$S = S_{\text{Total}} / m$$

Equation 4: Surface area per unit equation

#### 2.4.2 X-Ray Diffraction (XRD) Analysis

Diffraction patterns were measured using a Siemens D5000 x-ray diffractometer (40 Kv, 40 mA, monochromatised), using a CuK alpha source (1.5418 Å). Samples were scanned between 5-85 ° 2θ, with a scanning rate of 2 s/step and a step size of 0.02 °. Crushed catalyst was placed in the sample holder and levelled off ready for analysis.

The Scherrer equation can be used to calculate crystal size from XRD diffraction patterns if the metal particles are visible. Equation 5 displays the Scherrer equation where d is the average crystal size, K is the Scherrer constant (typically 0.9), λ is the wavelength of the x-

ray source (1.5418 Å),  $\beta$  is the full width at half maximum (°), and  $\theta$  is the diffraction angle (°):

$$d = K \lambda / \beta \cos \theta$$

Equation 5: The Scherrer equation

### 2.4.3 Thermo-gravimetric Analysis (TGA)

Thermo-gravimetric analysis was carried out using a combined TGA/DSC SDT Q600 thermal analyser coupled to an ESS mass spectrometer for evolved gas analysis. A sample loading of 10-15 mg was used and samples were typically heated from 303 K to 1273 K using a ramp rate of 1 K.min<sup>-1</sup> under Ar, O<sub>2</sub>/Ar or H<sub>2</sub>/Ar conditions, with a flow rate of 100 mL.min<sup>-1</sup>. For mass spectrometric analysis, various mass fragments were followed such as 16 (CH<sub>4</sub>), 18 (H<sub>2</sub>O), 28 (CO), and 44 (CO<sub>2</sub>). All TGA work was kindly carried out by Mr Andy Monaghan at The University of Glasgow.

### 2.4.4 Raman Spectroscopy

Raman spectra of post-reaction catalyst samples were collected using a Horiba Jobin Yvon LabRAM High Resolution spectrometer. A Helium Cadmium IK3201R-F 325 nm UV laser was used as the excitation source. The laser light was focused on to the sample for 10 s using a 15x UV objective lens and a grating of 1200. The scattered light was collected in a back scattering configuration and detected using a nitrogen cooled charge-coupled detector CCD. The spectral range examined was in the region of 500 to 3000 cm<sup>-1</sup>.

### 2.4.5 CHN

CHN analysis was performed by combustion using a CE-440 elemental analyser. All CHN analysis was carried out by Mrs Kim Wilson at The University of Glasgow.

### 2.4.6 Thioacidolysis

Thioacidolysis was used to determine the monomer content of each of the lignins shown in this thesis. All thioacidolysis work was carried out by Dr Bouxin at the University of Glasgow, details of which can be found in literature [52].

### 2.4.7 UV-Visible Spectrophotometer

The ammonia lignin was added to various methanol-water concentrations using the same lignin to solvent ratio used during the Parr reactions (0.5 g of lignin in 100 ml of solvent). The methanol concentration was increased from 0 to 100 %, with the remaining volume

being made up with deionised water. The samples were manually mixed and left to dissolve at room temperature for 30 minutes. The absorbance measurements of each sample were taken at a wavelength of 280 nm using a U-1500 Hitachi UV-Visible spectrophotometer.

UV-visible spectra were also collected in order to determine the presence or absence of BTX products in the post-product methanol-water mix from the ammonia lignin standard reaction. 15 ml of the light fraction was taken and an extraction was carried out in hexane. Absorbance measurements were taken from this extracts using a UV-160A Shimadzu UV-Visible spectrophotometer in the range of 200-400 nm.

#### **2.4.8 Gel Permeation Chromatography (GPC)**

In order to determine the molecular weight distribution of each lignin sample, 5 mg of lignin was acetylated in 0.5 mL of pyridine and 0.5 mL of acetic anhydride overnight. For the analysis of the catalytic products, equal volumes of both the light and heavy fraction (1 mL of each) were mixed together in order to give an overall representation of the product weight distribution. The solvents were evaporated to dryness then 0.5 mL of pyridine and 0.5 mL of acetic anhydride was added to solubilise and acetylate the products overnight. The solvents were then removed under N<sub>2</sub> blowing and 2 mL of tetrahydrofuran (THF) was added to solubilise the products prior to injection. GPC analysis was performed on a Gilson pump system equipped with a UV detector (280 nm). A set of PS/DVB columns (5 m, 300x7.5 mm, 50 and 500 Å, Polymer Lab) set at 303 K was used with an injection volume of 100 µL and a THF eluent flow rate of 1 ml.min<sup>-1</sup>. ChromPerfect software managed the data.

##### **2.4.8.1 GPC Calibration Work**

For calibration purposes, polystyrene standards (PS) were prepared and run by Dr Bouxin (see Figure 14) and gave a line equation of  $y = -0.031x^3 + 1.2581x^2 - 17.264x + 83.146$ . The PS standards ranged from 474 to 28000 g.mol<sup>-1</sup> and were diluted in THF to a concentration of 0.5 g.L<sup>-1</sup>.

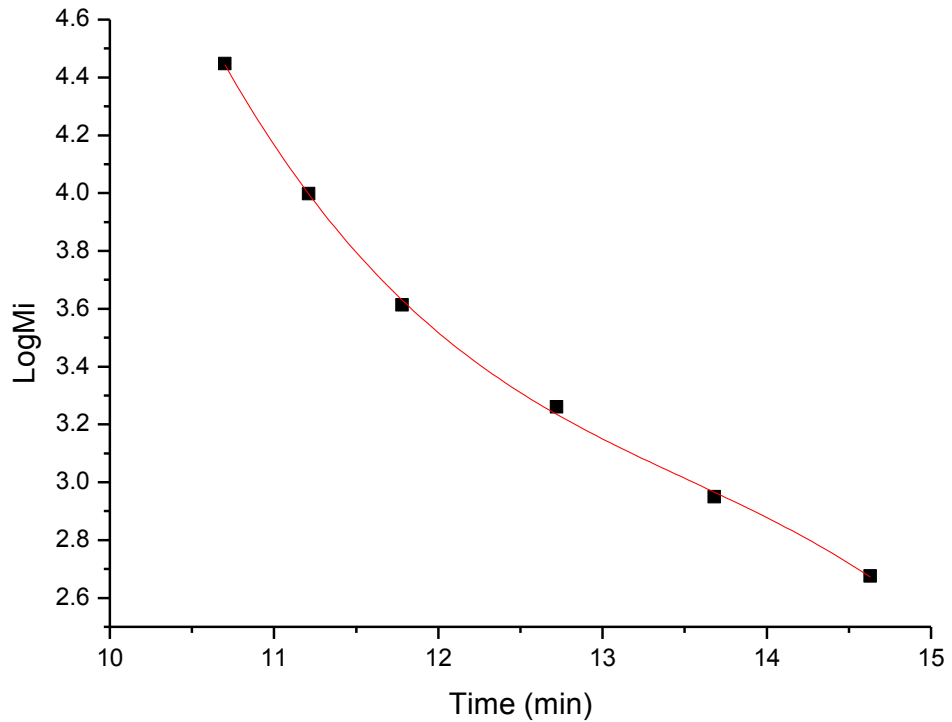


Figure 14: GPC polystyrene calibration curve

In order to calculate the molecular weight of any given sample, a number of steps and equations were required. Firstly, only the time of interest was exported from the software (i.e. 10-18 min). The baseline deviation of the GPC data was then established using Equation 6, where  $p$  is the corrected baseline,  $h$  is intensity and  $t$  is time.

$$p = \frac{\Delta h}{\Delta t}$$

Equation 6: Calculating the baseline deviation

Using this value, the corrected intensity ( $h^I$ ) could then be calculated using Equation 7, where  $h_i$  is the first intensity value at  $t = 10$  min, and  $t_i$  is the first time value in the data set.

$$h^I = (h - h_i) - p \cdot (t - t_i)$$

Equation 7: Calculating the intensity correction

The corrected intensity was plotted against the samples molecular weight distribution at each retention time ( $M_i$ ) to give an indication of the overall distribution. In order to

calculate  $M_i$  for each data segment, the line equation calculated in Figure 14 was used, where  $x = \text{time}$  and  $y = \log M_i$ . The antilog of this value was then taken to give  $M_i$ . The average integration between the baseline ( $M_i = M_{RT1}$ ) and the curve ( $A_i$ ) was then taken for the surrounding data points as illustrated in Figure 15.  $A_i$  could then be multiplied by  $M_i$ , and also divided by  $M_i$ , for all data points. Finally, the sum for all  $A_i$ ,  $A_i/M_i$ , and  $A_i * M_i$  values was taken. The ways in which the molecular weight ( $M_w$ ), molecular number ( $M_n$ ) and polydispersity ( $I_p$ ) were calculated are shown below [56, 57]:

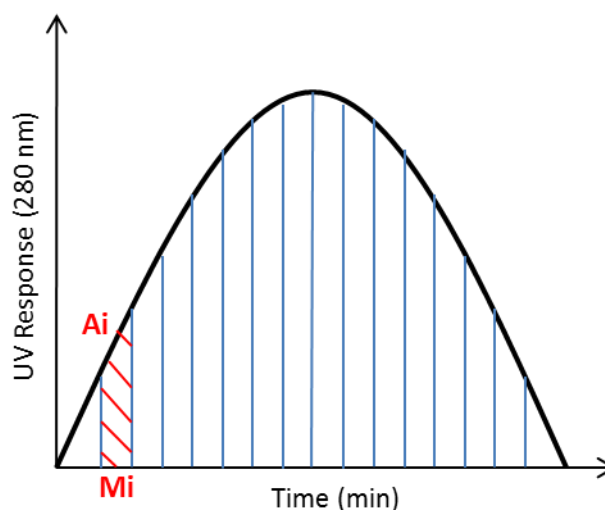


Figure 15: Illustration of GPC integration

$$M_w = \frac{\sum(A_i * M_i)}{\sum A_i}$$

Equation 8: Calculating the molecular weight of a GPC sample

$$M_n = \frac{\sum A_i}{\sum \left(\frac{A_i}{M_i}\right)}$$

Equation 9: Calculating the molecular number of a GPC sample

$$I_p = \frac{M_w}{M_n}$$

Equation 10: Calculating the polydispersity of a GPC sample

## 2.4.9 Gas Chromatography – Mass Spectrometry (GC-MS)

All GC-MS data was collected using the light fraction that was previously prepared and solubilised in 2 mL DCM (see section 2.3.2). A 10  $\mu\text{L}$  aliquot of this prepared sample was added to 30  $\mu\text{L}$  pyridine and 70  $\mu\text{L}$  trimethylsilyl (TMS). This was then left for at least 2 h prior to injection. Chemical composition was determined using a Shimadzu GC-MS-QP2010S coupled to a Shimadzu GC-2010 equipped with a ZB-5MS capillary column (30 m x 0.25 mm x 0.25  $\mu\text{m}$ ) with He as a carrier. The column was initially kept at 333 K for 2 min then heated at a rate of 1  $\text{K}\cdot\text{min}^{-1}$  to 533 K, where it was held for 10 min. 1  $\mu\text{L}$  of sample was injected using split mode (50:1) and an injection temperature of 523 K.

### 2.4.9.1 GC-MS Calibration Work

Quantification of the products was measured on the total ion chromatogram (TIC), and based on reference compounds and the C16 internal standard. Due to the amount of products produced and their limited commercial availability, four standards were run in order to calculate a response factor. Varying concentrations (0.1, 0.5, 1, 5 and 10  $\text{g}\cdot\text{L}^{-1}$ ) were prepared for each reference compound, using the C16 internal standard (10  $\text{g}\cdot\text{L}^{-1}$ ). The reference samples were then run on the GC-MS using the same conditions described previously. Note that TMS was used to derivatise the hydroxyl groups present on the molecule. The reference compounds and their derivatised version can be found below, where the guaiacol and 2,6-dimethoxyphenol are illustrated in Figure 16 and 2-methoxy-4-propylphenol and 2,6-dimethoxy-4-methylphenol are represented in Figure 17:

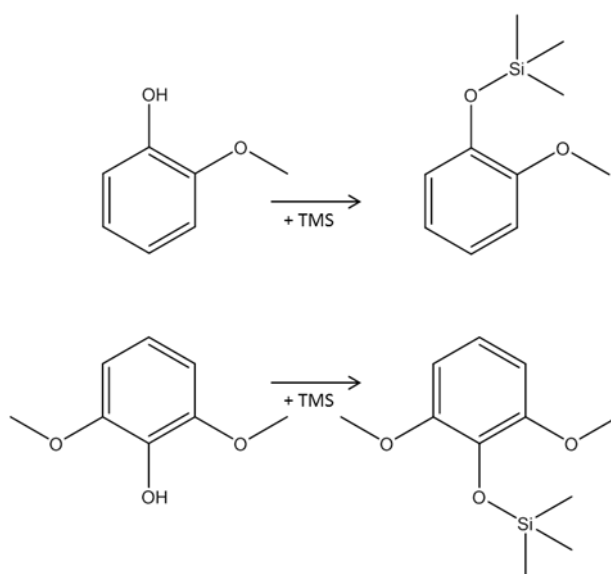


Figure 16: Guaiacol and 2,6-dimethoxyphenol respectively and their TMS derivatives

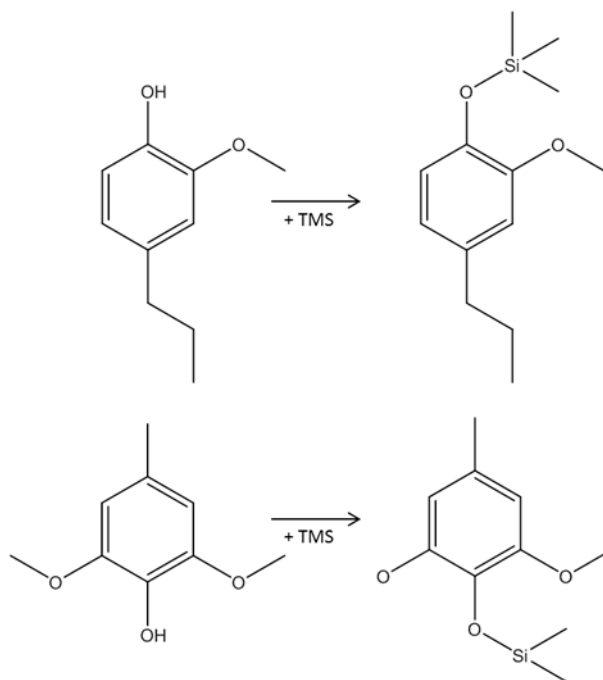


Figure 17: 2-methoxy-4-propylphenol and 2,6-dimethoxy-4-methylphenol and their TMS derivatives

The following equation was used to calculate the response factor ( $\alpha$ ):

$$\alpha = \frac{\text{Intensity of reference}}{\text{Intensity of internal standard}} \times \frac{\text{Mass of internal standard}}{\text{Mass of reference}}$$

Equation 11: Calculating the coefficient value for each reference compound

Using Equation 11, it was possible to obtain a linear relationship of intensity against mass for each reference compound and therefore calculate the resultant gradient which is equal to the response factor ( $\alpha$ ). This relationship can be seen in the below figures for each reference compound used:

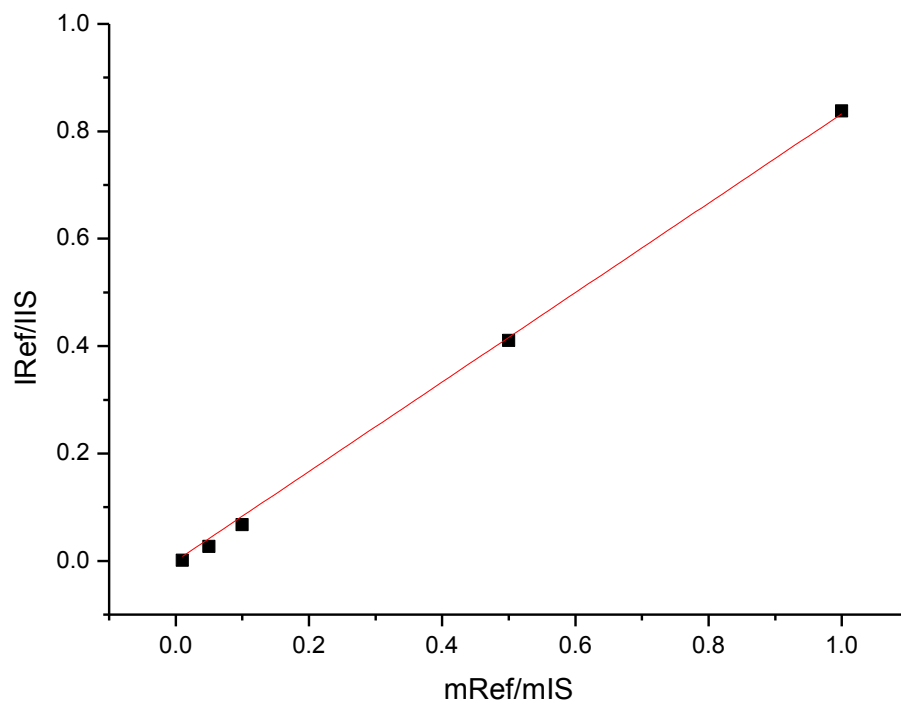


Figure 18: Guaiacol calibration curve

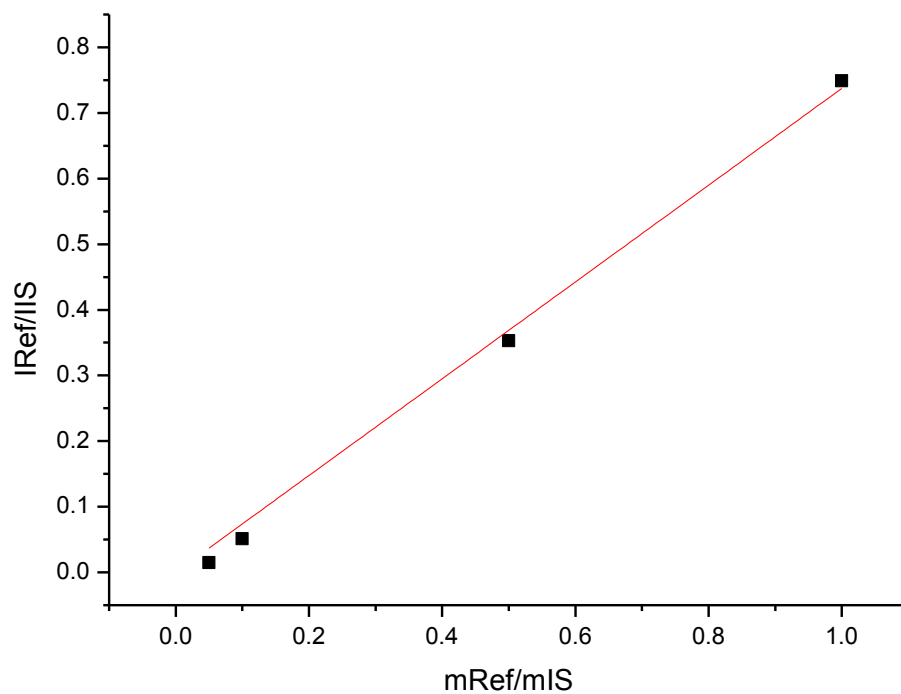


Figure 19: 2,6-dimethoxyphenol calibration curve

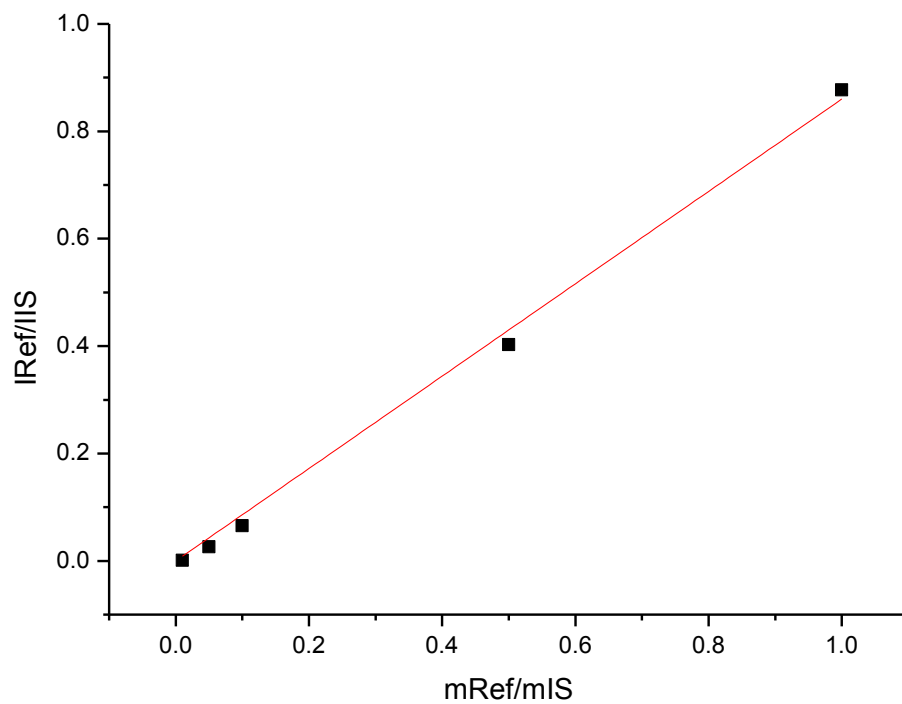


Figure 20: 2-methoxy-4-propylphenol calibration curve

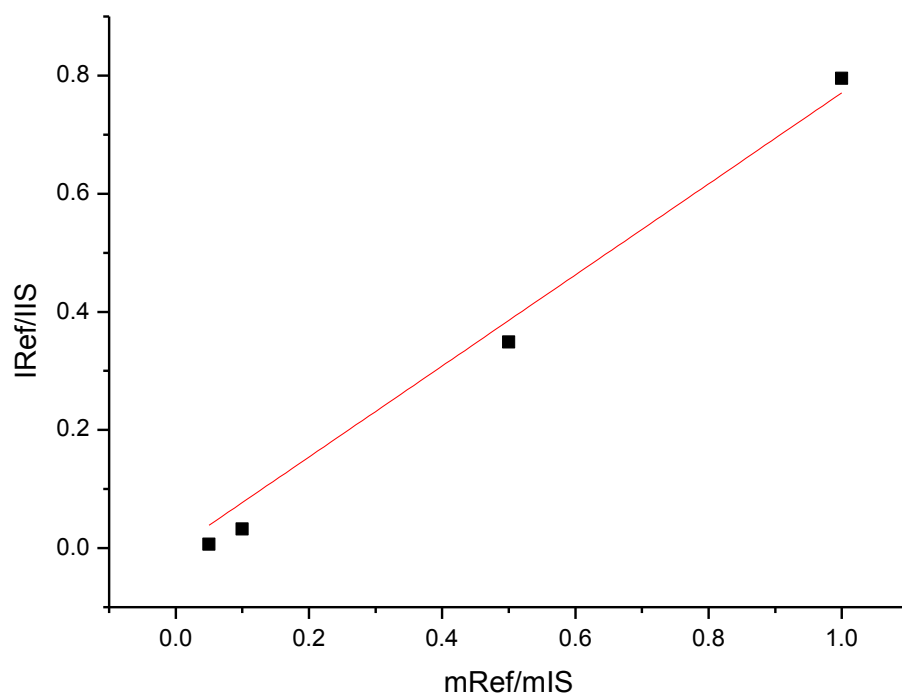


Figure 21: 2,6-dimethoxy-4-methylphenol calibration curve

This data has been summarised in Table 3:

Table 3: Summary of calibration data

<b>Reference Compound</b>	<b>Type of Unit</b>	<b>Response Factor (<math>\alpha</math>)</b>
<b>Guaiacol</b>	Guaiacyl (G)	0.833
<b>2,6-dimethoxyphenol</b>	Syringyl (S)	0.737
<b>2-methoxy-4-propylphenol</b>	Guaiacyl (G)	0.860
<b>2,6-dimethoxy-4-methylphenol</b>	Syringyl (S)	0.771

From the data presented in Table 3, there was an obvious trend between the type of monomer unit, with respect to S or G, and the resultant response factor. We could therefore assume the response factor for each of the other identified products based on their structure, with respect to H, G or S. The response factors for all other S, G and H units were deemed to be approximately 0.75, 0.85 and 0.95 respectively.

#### **2.4.9.2 GC-MS Product Identification**

In terms of the peaks collected through GC-MS analysis of the light fraction, 21 monomeric aromatic products were successfully identified through mass fragment data analysis for each peak based on the reference data and knowledge of the lignin structure. It was found that the reactions produced a range of alkylphenolic products with various functional groups. The absence of ring hydrogenation was confirmed through collaborative 2D NMR work [1] which showed an abundance of cross peaks in the aromatic region and no cyclohexanols were detected using GC-MS analysis. The presence of BTX molecules was also investigated but none could be found using UV-vis spectrophotometry or GC-FID analysis.

Mass data was collected for each reference compound and is shown below. Note that all samples were treated with TMS so the proton from any hydroxyl groups on the product molecule was replaced with a  $[-\text{Si}(\text{CH}_3)_3]$  group, with a molecular weight of  $73 \text{ g}\cdot\text{mol}^{-1}$ . This therefore added an additional mass of 72 onto the total product mass.

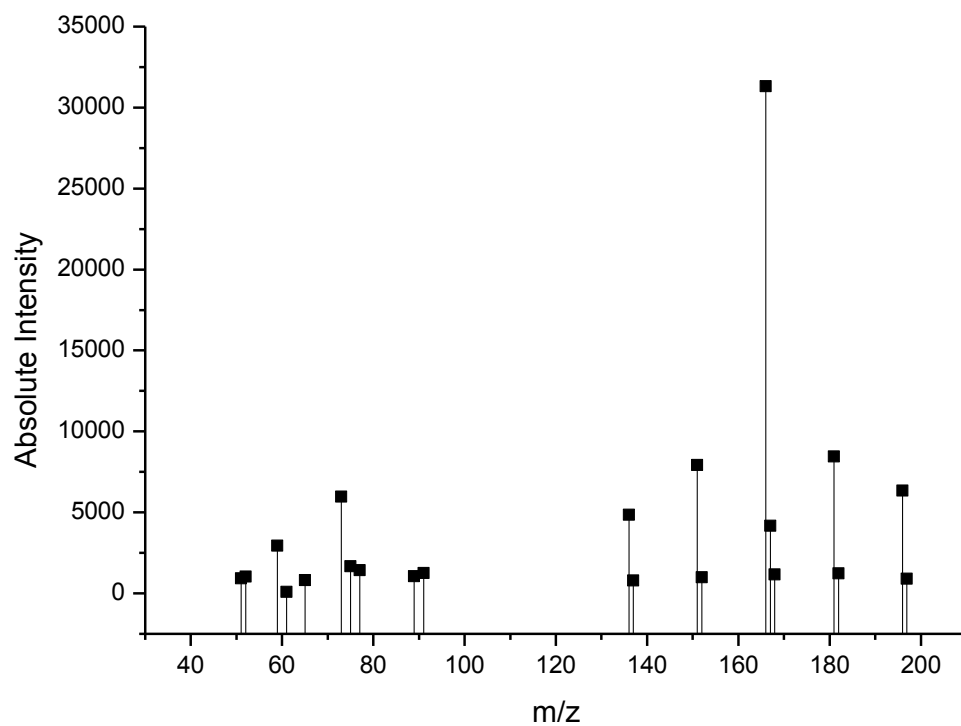


Figure 22: Mass spectrometry data for guaiacol

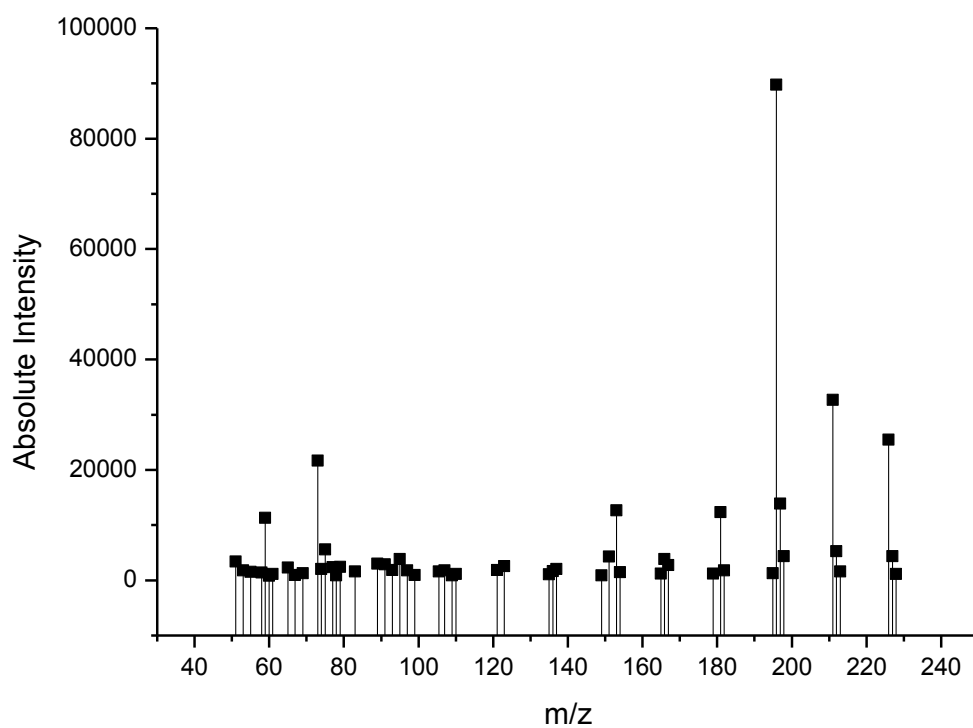


Figure 23: Mass spectrometry data for 2,6-dimethoxyphenol

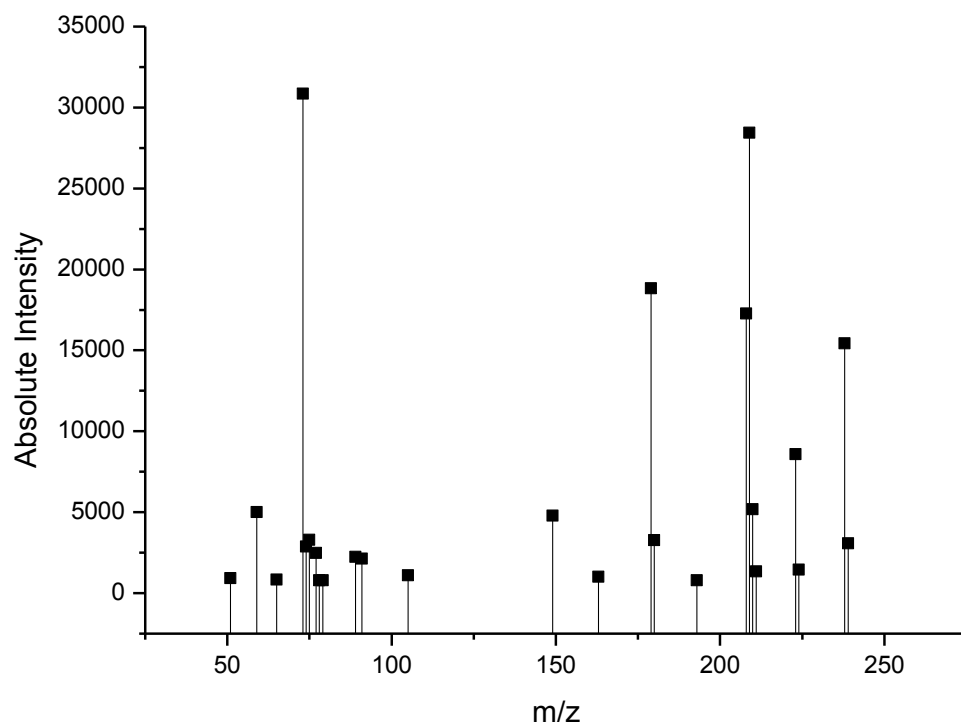


Figure 24: Mass spectrometry data for 2-methoxy-4-propylphenol

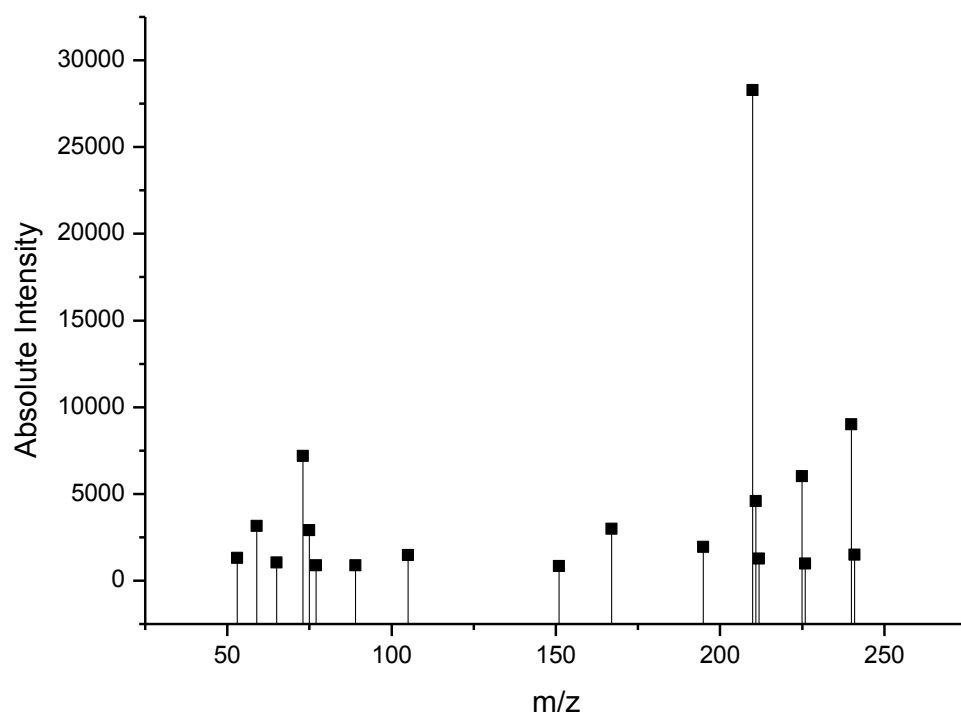


Figure 25: Mass spectrometry data for 2,6-dimethoxy-4-methylphenol

For convenience purposes, appropriate terminology was adopted for each of the identified products. Figure 26 shows the basic alkyl phenol unit produced, where p-hydroxyphenylpropane (H) units have  $R_1 = R_2 = H$ ; guaiacylpropane (G) units have  $R_1 = OMe$ ,  $R_2 = H$ ; and syringylpropane (S) units have  $R_1 = OMe$ ,  $R_2 = OMe$ . The alkyl chain ( $R_3$ ) was also numbered in relation to the number of carbons present, where 3(i) represents a 1-propenyl chain, 3 represents a propyl chain, 2 represents a ethyl chain, 1 represents a methyl chain, and 0 represents no alkyl chain. Some products maintained a hydroxyl or methoxy group at the end of the alkyl chain and these were annotated as '3(OH)' or '3(OMe)' respectively, whilst some G units generated catechol-type structures (e.g. G(OH)). Table 4 provides a summary of each product is in relation to their structure which is illustrated in Table 5.

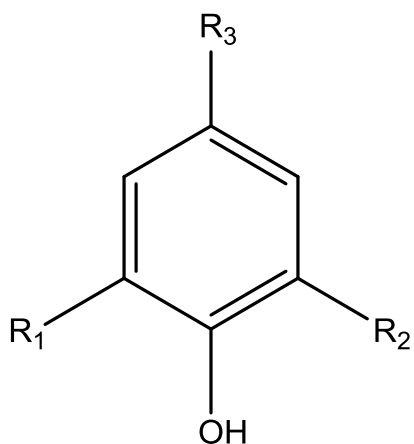
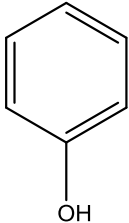
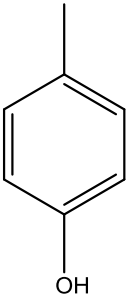
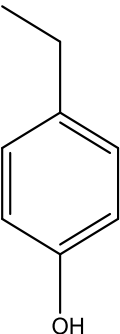
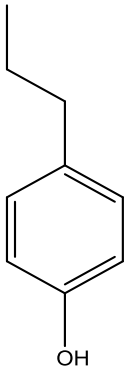
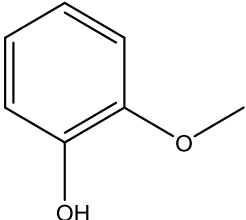
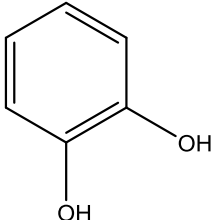
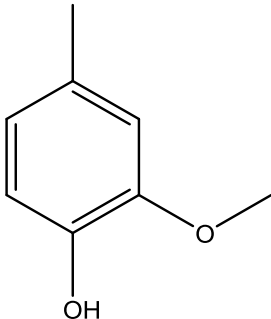
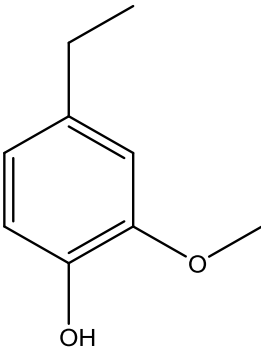
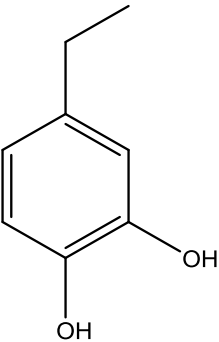
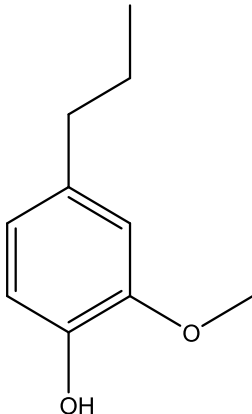
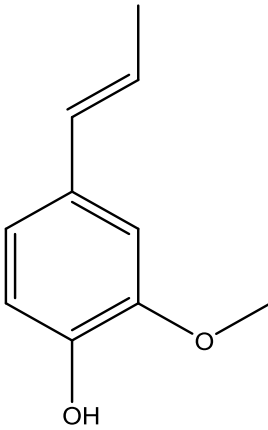
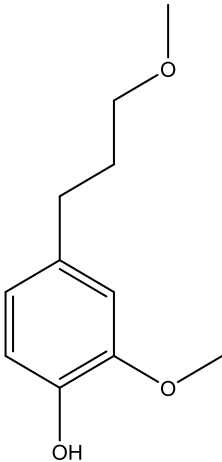


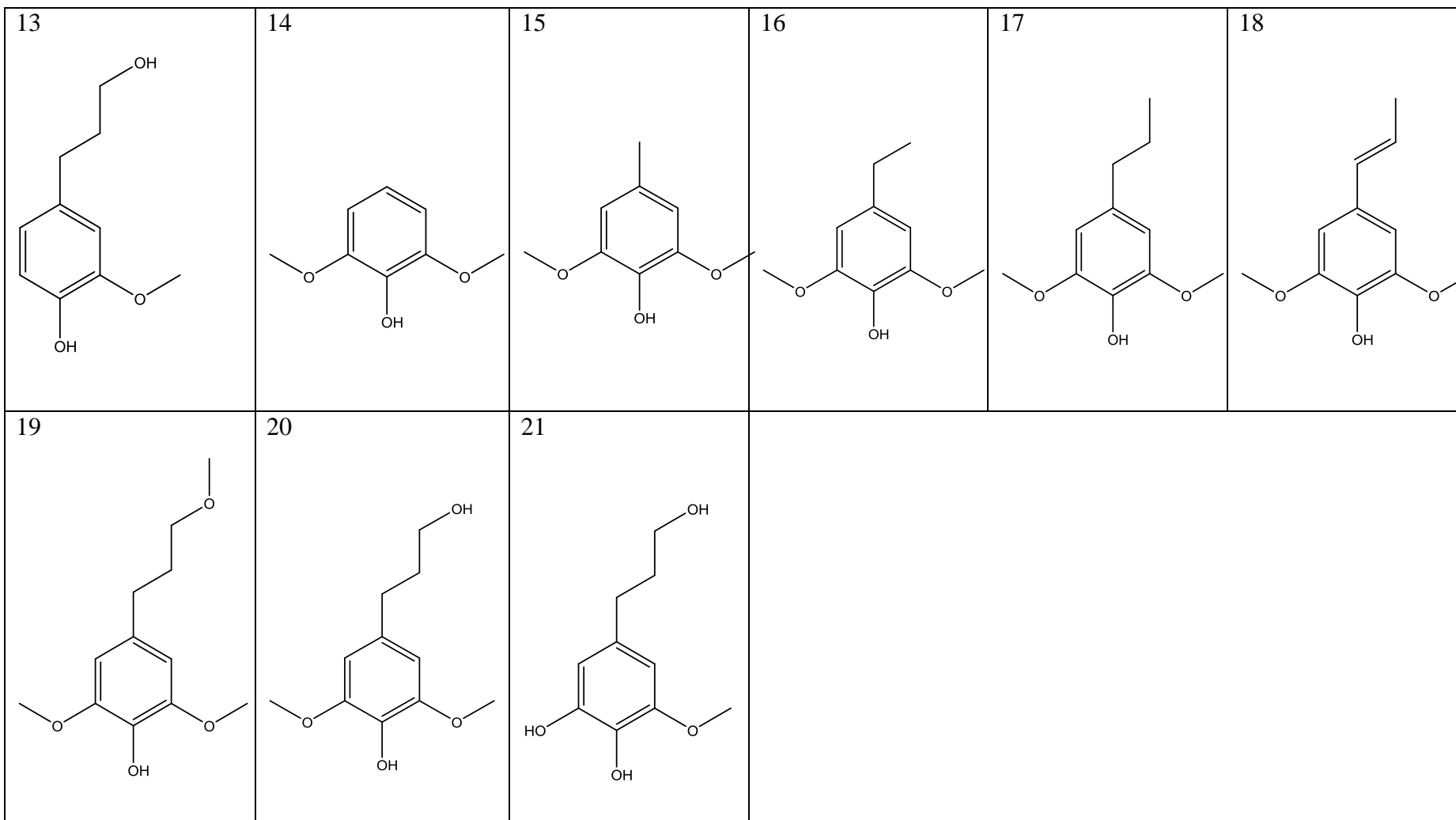
Figure 26: Basic alkylphenolic monomer unit

Table 4: Summary of products structures and names

Number	Abbreviation	R <sub>1</sub> / R <sub>2</sub> / R <sub>3</sub> Group	Product Name
1	H0	R <sub>1</sub> =R <sub>2</sub> =R <sub>3</sub> =H	phenol
2	H1	R <sub>1</sub> =R <sub>2</sub> =H; R <sub>3</sub> =CH <sub>3</sub>	methylphenol ( <i>p</i> -cresol)
3	H2	R <sub>1</sub> =R <sub>2</sub> =H; R <sub>3</sub> =CH <sub>2</sub> CH <sub>3</sub>	ethylphenol
4	H3	R <sub>1</sub> =R <sub>2</sub> =H; R <sub>3</sub> =CH <sub>2</sub> CH <sub>2</sub> CH <sub>3</sub>	propylphenol
5	G0	R <sub>1</sub> =R <sub>3</sub> =H; R <sub>2</sub> =OCH <sub>3</sub>	2-methoxyphenol (guaiacol)
6	G(OH)0	R <sub>1</sub> =R <sub>3</sub> =H; R <sub>2</sub> =OH	1,2-dihydroxybenzene (catechol)
7	G1	R <sub>1</sub> =H; R <sub>2</sub> =OCH <sub>3</sub> ; R <sub>3</sub> =CH <sub>3</sub>	2-methoxy-4-methylphenol
8	G2	R <sub>1</sub> =H; R <sub>2</sub> =OCH <sub>3</sub> ; R <sub>3</sub> =CH <sub>2</sub> CH <sub>3</sub>	4-ethyl-2-methoxyphenol
9	G(OH)2	R <sub>1</sub> =H; R <sub>2</sub> =OH; R <sub>3</sub> =CH <sub>2</sub> CH <sub>3</sub>	4-ethylbenzene-1,2-diol
10	G3	R <sub>1</sub> =H; R <sub>2</sub> =OCH <sub>3</sub> ; R <sub>3</sub> =CH <sub>2</sub> CH <sub>2</sub> CH <sub>3</sub>	2-methoxy-4-propylphenol
11	G3(i)	R <sub>1</sub> =H; R <sub>2</sub> =OCH <sub>3</sub> ; R <sub>3</sub> =CH=CHCH <sub>3</sub>	2-methoxy-4-propenylphenol
12	G3(OMe)	R <sub>1</sub> =H; R <sub>2</sub> =OCH <sub>3</sub> ; R <sub>3</sub> =CH <sub>2</sub> CH <sub>2</sub> CH <sub>2</sub> OCH <sub>3</sub>	2-methoxy-4-(3-methoxypropyl)phenol
13	G3(OH)	R <sub>1</sub> =H; R <sub>2</sub> =OCH <sub>3</sub> ; R <sub>3</sub> =CH <sub>2</sub> CH <sub>2</sub> CH <sub>2</sub> OH	4-(3-hydroxypropyl)-2-methoxyphenol
14	S0	R <sub>1</sub> =R <sub>2</sub> =OCH <sub>3</sub> ; R <sub>3</sub> =H	2,6-dimethoxyphenol (syringol)
15	S1	R <sub>1</sub> =R <sub>2</sub> =OCH <sub>3</sub> ; R <sub>3</sub> =CH <sub>3</sub>	2,6-dimethoxy-4-methylphenol
16	S2	R <sub>1</sub> =R <sub>2</sub> =OCH <sub>3</sub> ; R <sub>3</sub> =CH <sub>2</sub> CH <sub>3</sub>	4-ethyl-2,6-dimethoxyphenol
17	S3	R <sub>1</sub> =R <sub>2</sub> =OCH <sub>3</sub> ; R <sub>3</sub> =CH <sub>2</sub> CH <sub>2</sub> CH <sub>3</sub>	2,6-dimethoxy-4-propylphenol
18	S3(i)	R <sub>1</sub> =R <sub>2</sub> =OCH <sub>3</sub> ; R <sub>3</sub> =CH=CHCH <sub>3</sub>	2,6-dimethoxy-4-propenylphenol
19	S3(OMe)	R <sub>1</sub> =R <sub>2</sub> =OCH <sub>3</sub> ; R <sub>3</sub> =CH <sub>2</sub> CH <sub>2</sub> CH <sub>2</sub> OCH <sub>3</sub>	2,6-dimethoxy-4-(3-methoxypropyl)phenol
20	S3(OH)	R <sub>1</sub> =R <sub>2</sub> =OCH <sub>3</sub> ; R <sub>3</sub> =CH <sub>2</sub> CH <sub>2</sub> CH <sub>2</sub> OH	4-(3-hydroxypropyl)-2,6-dimethoxyphenol
21	S(OH)3(OH)	R <sub>1</sub> =OH; R <sub>2</sub> =OCH <sub>3</sub> ; R <sub>3</sub> =CH <sub>2</sub> CH <sub>2</sub> CH <sub>2</sub> OH	5-(3-hydroxypropyl)-3-methoxybenzene-1,2-diol

Table 5: Structures of the identified GC-MS products

1  <chem>Oc1ccccc1</chem>	2  <chem>Cc1ccc(O)cc1</chem>	3  <chem>CCc1ccc(O)cc1</chem>	4  <chem>CCCc1ccc(O)cc1</chem>	5  <chem>COc1cccc(O)c1</chem>	6  <chem>Oc1cc(O)ccc1</chem>
7  <chem>Cc1cc(OC)c(O)cc1</chem>	8  <chem>CCc1cc(OC)c(O)cc1</chem>	9  <chem>CCc1cc(O)c(O)cc1</chem>	10  <chem>CCCc1cc(OC)c(O)cc1</chem>	11  <chem>CC=Cc1cc(OC)c(O)cc1</chem>	12  <chem>CCOCc1cc(OC)c(O)cc1</chem>



### 2.4.9.3 GC-MS Product Quantification

To quantify the resultant peaks, the peaks were first integrated to establish their peak area. This was then compared to the internal standard peak to give a relative quantity. By rearranging Equation 11 to give Equation 12, it was possible to calculate the mass of product represented by that peak.

$$\text{Mass of product} = \frac{\text{Intensity of product}}{\text{Intensity of internal standard}} \times \frac{\text{Mass of internal standard}}{\alpha}$$

Equation 12: GC-MS product quantification calculation

Other factors then had to be taken into account to calculate the actual mass of product. This has been shown in Equation 13, where the 15 mL aliquot and 200 mL light fraction was factored into the calculation, as well as the mass of lignin used in the reaction (500 mg). This was then multiplied by 100 so that the actual product mass could be quoted as gram of product per 100 g of lignin.

$$\text{Actual mass of product (g/100 g)} = \left( \frac{\text{mass of product from Equation 13}/(15 \times 200)}{500} \right) \times 100$$

Equation 13: Calculating the actual mass of product using GC-MS

### 2.4.10 Quantification of the Heavy Fraction

The analysis of the heavy fraction proved difficult due to its composition, and identification or quantification was not possible using GC-MS. In order to crudely weigh the heavy products, namely the char, a 3 ml sample was taken from the 200 ml volumetric flask of the heavy fraction (see 2.3.2) into a pre-weighed vial and the solvent was removed to dryness under N<sub>2</sub> blowing. The vial was then left in a desiccator overnight and weighed again to give the product weight in 3 ml. This was then multiplied out to give the char weight in g/100g as shown below:

$$\frac{\text{product weight in 3 ml}}{3 \text{ ml of sample}} \times 200 = \frac{\text{product weight in 200 ml}}{0.5 \text{ g of lignin}} \times 100 = \text{g/100g}$$

Equation 14: Quantification of the heavy fraction

## 3 Results and Discussion

### 3.1 Characterisation and Catalytic Depolymerisation Activity of Six Lignins using 1 % Pt/alumina

This section will discuss the results obtained using a 1 wt. % Pt/alumina catalyst and six different lignin samples under ‘typical’ hydrogenolysis/hydrodeoxygenation conditions described in section 2.3.2. The lignins were characterised prior to reaction then reacted over the Pt/alumina catalyst, with the subsequent reaction mixture being analysed using the methods described previously.

#### 3.1.1 Characterisation of Six Lignins

All of the lignins used in this section, namely the ammonia and organosolv lignins from poplar wood and the alkaline, AFEX, Fr-AFEX and soda lignins from wheat straw, were characterised using CHN and thioacidolysis analysis, gel permeation chromatography (GPC), and temperature-programmed reduction (TPR) methods prior to reaction testing.

##### 3.1.1.1 CHN Analysis

The elemental composition of each lignin was determined and found to be typical values of lignins used elsewhere [48]. These are reported in Table 6:

Table 6: Elemental analysis of six lignins

	C %	H %	N %	O %*	Chemical Formula	O/C Ratio	H/C Ratio
<b>Ammonia</b>	60.2	6.0	1.8	31.9	C <sub>5</sub> H <sub>6</sub> O <sub>2</sub>	0.40	1.20
<b>Organosolv</b>	63.6	6.1	-	30.4	C <sub>5</sub> H <sub>6</sub> O <sub>2</sub>	0.36	1.15
<b>Alkaline</b>	60.2	5.9	1.4	32.5	C <sub>5</sub> H <sub>6</sub> O <sub>2</sub>	0.41	1.18
<b>AFEX</b>	59.5	6.4	2.1	31.9	C <sub>5</sub> H <sub>6</sub> O <sub>2</sub>	0.41	1.31
<b>Fr-AFEX</b>	61.2	6.5	2.9	29.4	C <sub>5</sub> H <sub>6</sub> O <sub>2</sub>	0.35	1.27
<b>Soda</b>	61.3	5.6	0.9	32.2	C <sub>5</sub> H <sub>6</sub> O <sub>2</sub>	0.39	1.10

(\* the oxygen content was calculated as a difference)

The elemental compositions shown in Table 6 indicates that each lignin had a fairly similar elemental composition but the O/C and H/C ratios helped make a more thorough comparison between the six samples. It is clear from the O/C ratio values presented that the ammonia, alkaline and AFEX lignins contain more oxygen. This would suggest that these lignins contain more alkyl-aryl bonds in comparison to the organosolv, Fr-AFEX and soda

lignin. Additionally, the O/C ratio can also reflect the S/G ratio found in the lignin sample, where a sample with more S units will give a higher O/C ratio. For example, this would imply that the ammonia lignin will contain more S units in comparison to the organosolv lignin from the same wood source. The H/C ratios were also higher for the ammonia and AFEX lignins in particular. The presence of nitrogen is attributed to the incorporation of the ammonia used during the pre-treatment steps into the lignin's structure.

### 3.1.1.2 Thioacidolysis Analysis

The uncondensed fraction (i.e. percentage of  $\beta$ -O-4 bonds) and the ratio of each monomer unit (S, G and H) were estimated from the total monomer yield generated from the thioacidolysis experiments. This work was carried out by Dr Bouxin and is reported in Table 7:

Table 7: Lignin  $\beta$ -O-4 linkage percentages and monomer ratios

	$\beta$ -O-4 %	S:G:H Ratio
<b>Ammonia</b>	28.9 (0.3)*	0.65:0.35:0
<b>Organosolv</b>	9.2 (0.2)	0.57:0.43:0
<b>Alkaline</b>	17.7 (0.8)	0.48:0.48:0.04
<b>AFEX</b>	16.8 (0.4)	0.49:0.46:0.05
<b>Fr-AFEX</b>	17.0 (0.5)	0.48:0.49:0.03
<b>Soda</b>	2.8 (0.3)	0.51:0.49:0

(\* standard deviation is in brackets)

The linkage percentages ( $\beta$ -O-4,  $\beta$ - $\beta$  and  $\beta$ -5) were also calculated using 2D-NMR [58], and despite slight differences in the measurements taken, the lignins were found to give the same order with respect to the uncondensed fractions [1]. The poplar ammonia lignin was found to have the highest  $\beta$ -O-4 content (28.9 %) compared to the soda lignin from wheat straw which gave only 2.8%. These figures relate well to those values obtained in section 3.1.1.1. It is thought that this difference comes from both the plant feedstock and the pre-treatment used to isolate the lignin. It can be assumed that harsher pre-treatments, such as the soda alkaline environment, aids condensation of the plant material as opposed to the mild alkaline organosolv extraction used with the AFEX lignin which retained 16.8 % of its uncondensed fraction. The organosolv conditions used with the poplar wood resulted in a more condensed structure due to the higher temperatures (453 K) and acidic environment, hence the lower value of 9.2 %. Although similar temperatures were used during the ammonia percolation pre-treatment, the use of aqueous ammonia limited

condensation due to it being a weaker base than the typical sodium hydroxide. Table 7 also exhibits the monomer ratios present in each of the samples. It is clearly evident that the poplar ammonia lignin had the highest relative percentage of syringyl units in relation to the other types of lignin analysed. This data correlates well with the uncondensed fraction value obtained, where a high abundance of syringyl units can be related to an uncondensed lignin starting material due to the additional methoxy group linked to the C5 in the syringyl structure.

### 3.1.1.3 GPC Analysis

Figure 27 shows the separation of the polymer based on the molecular size as a function of time, where the heavier molecules eluted first followed by the smaller molecules. The molecular weight, number and polydispersity values were also calculated and these can be found in Table 8. This table gives the molecular weight ( $M_w$ ) value, which depends not only on the number of polymer molecules but on the size or weight of each polymer molecule in the lignin, and the molecular number ( $M_n$ ), which does not specify between sizes (i.e. high and low molecular weight products are counted as 1:1) but takes the total weight of the polymer divided by the number of polymer molecules. The polydispersity ( $I_p$ ) number is also given and this indicates how uniform a polymer is, where 1 would indicate a more uniform polymer with similar sized molecules.

The GPC analysis of the alkaline, AFEX, Fr-AFEX and soda lignins from wheat straw all exhibited fairly similar molecular distribution profiles as exhibited in Figure 27. They each centred at ~12 min which was attributed to the higher molecular weight compounds, but they showed slight variation at ~13.5 min. The two AFEX lignins displayed some differences in their molecular weight distributions, where the Fr-AFEX lignin was higher. This is likely due to the fact that more of the lignin was isolated after efficient fermentation of the sugars during the pre-treatment stages. In the case of the poplar lignins, differences between the two samples were more apparent in the GPC profiles. As with the wheat straw lignins, the poplar lignins exhibit a higher molecular weight fraction centred at ~12 min, however there was a much more significant change in the lower molecular weight profile. It is likely that the high temperature organosolv pre-treatment led to the partial cleavage of the alkyl-aryl ether linkage which thereby reduced the molecular weight of the lignin and caused the high UV response shown in Figure 27. However the higher molecular weight of the ammonia lignin suggested that its pre-treatment medium allowed for no significant cleavage of the alkyl-aryl bonds. This conclusion could also be said for the wheat straw lignins, where the soda lignin gave a higher response in the region of ~13.5 min. It can

therefore be assumed that the soda pre-treatment was much harsher than the AFEX or alkaline conditions, and therefore caused more structural changes to the starting material [59].

Table 8: GPC data for six lignins

	<b>Molecular Weight (Mw)</b>	<b>Molecular Number (Mn)</b>	<b>Polydispersity (Ip)</b>
<b>Ammonia</b>	3884	1588	2.45
<b>Organosolv</b>	3221	1229	2.62
<b>Alkali</b>	2673	964	2.77
<b>AFEX</b>	2672	1066	2.51
<b>Fr-AFEX</b>	4340	1287	3.37
<b>Soda</b>	2926	1063	2.75



#### 3.1.1.4 Temperature-Programmed Reduction (TPR) Analysis

In order to establish how the lignin samples might react in a reductive medium, each lignin was subjected to TPR. Figure 28 shows that there was a broad thermal breakdown range between 473-773 K, with four main areas of decomposition. This is because the various oxygen functional groups in lignin have different thermal stabilities, with the cleavage of weaker bonds occurring at lower temperatures and the breakage of stronger bonds occurring at higher temperatures. Figure 28 shows that the first step occurred <373 K and this corresponded to the loss of water. The dehydration of the lignin structure can result in pyrolysis products with unsaturated side chains, such as styrene derivatives, eugenol, isoeugenol and vanillin. Aryl ether linkages are also relatively easy to break and if the  $\beta$ -O-4 content from section 3.1.1.2 is taken into account, it is clear that the more uncondensed samples (ammonia, alkaline, Fr-AFEX and AFEX lignins) showed a breakdown at lower temperatures (<573 K) because there were more functional groups available to cleave. The main thermal process occurred between 573-673 K, with the formation of aromatic hydrocarbons, phenolics, hydroxyphenolics and guaiacyl/ syringyl-type compounds with phenolic -OH groups [60, 61]. Non-condensable gases were also formed, the main of which were CO, CO<sub>2</sub> and CH<sub>4</sub> as shown in Figure 29. Pyrolysis studies have shown that CO<sub>2</sub> is released from the carboxyl groups, CO from the weakly bound oxygen groups such as aldehyde groups, and H<sub>2</sub> from the aliphatic and methoxy groups [62]. It was also evident from Figure 29 that water was released throughout the main breakdown area. This evolved water was from the cleavage of -OH functional groups which are linked to the  $\beta$  or  $\gamma$  carbons on the aliphatic side chains [63]. The sample only lost between 55-67 % of its original mass (depending on the sample) as shown in Table 9 due to condensation reactions which occurred from the cleavage of aryl-ether bonds. Cleavage of the stronger bonds occurs at higher temperatures and this results in highly unstable radicals which go on to form products with increased stability [64], commonly known as char. Although the general trend of degradation across each sample was similar, the specific temperature for each bond cleavage and the resultant products varies between lignin types [65], where softwood lignins will give mainly guaiacols and hardwood lignins will give both guaiacol and syringol-type products.

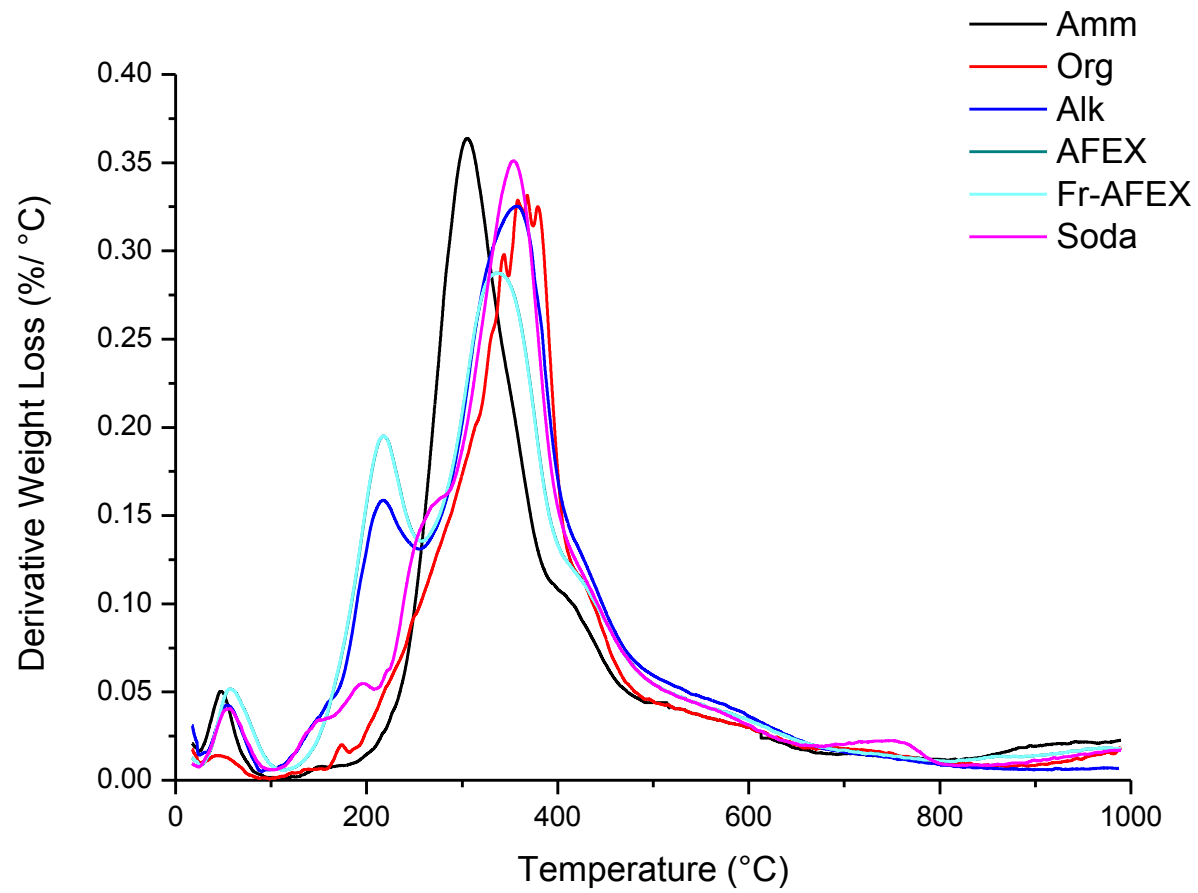


Figure 28: TPR of six lignins

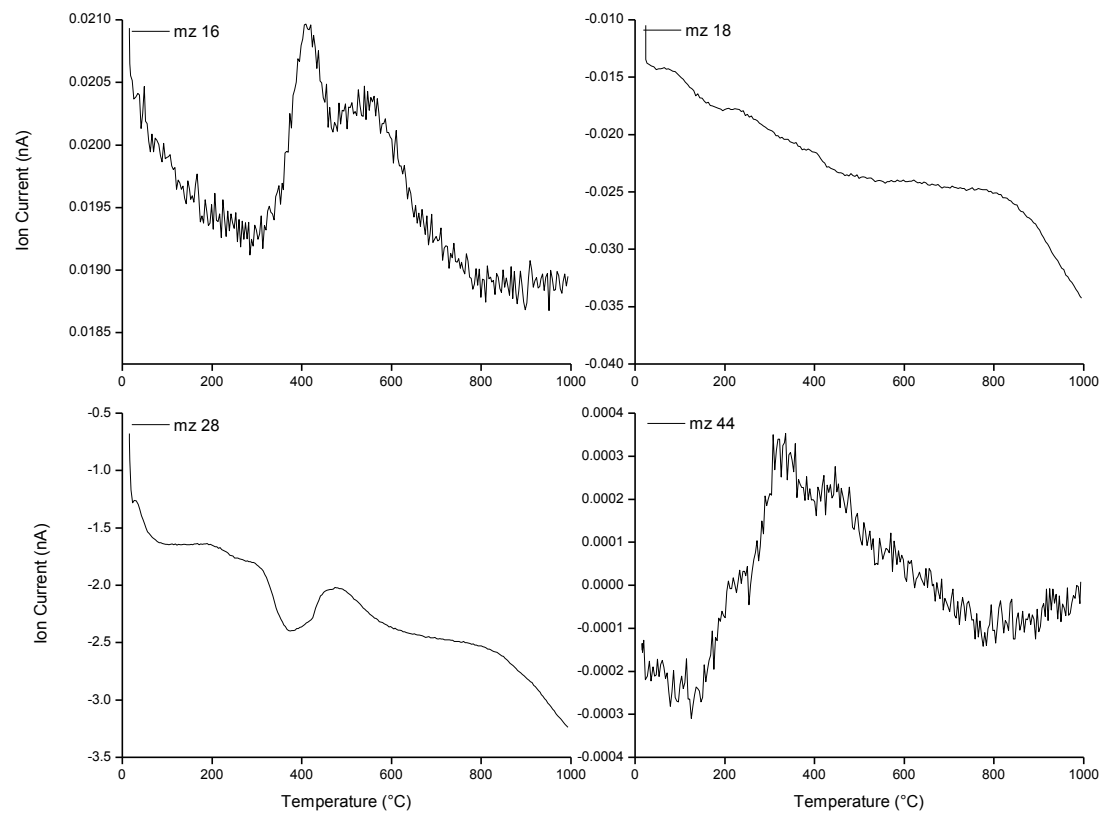


Figure 29: Example of mass spectra data obtained from TPR of lignin including m/z 16, 18, 28 and 44

Table 9: TPR weight loss percentage of six lignins

<b>Weight Loss (%)</b>	
<b>Ammonia</b>	56.1
<b>Organosolv</b>	55.3
<b>Alkaline</b>	68.5
<b>AFEX</b>	63.5
<b>Fr-AFEX</b>	67.0
<b>Soda</b>	66.9

### 3.1.2 Non-Catalytic and Catalytic Standard Reaction Testing of Six Lignins

This section will show work with and without the use of the 1 wt. % Pt/alumina catalyst for each of the six lignins. Before reacting the lignins in the presence of a catalyst, it was important to first establish what effects the solvent and hydrogen pressure had on the lignin depolymerisation reaction in the absence of the Pt/alumina catalyst. These lignin reactions were carried out under 20 barg hydrogen pressure with methanol-water as the solvent in the absence of a catalyst. Direct comparisons were then made against the depolymerisation products obtained under the standard conditions using the Pt/alumina catalyst, as depicted in section 2.3.2. Although GPC analysis gave an overview of the mass distribution, quantitative GC-MS analysis was also performed. This allowed for 21 monomeric aromatic structures to be identified (see Table 4, section 2.4.9.2). GPC profiles followed by GC-MS product distribution plots have been shown for each of the six lignins.

This work is based on: F.P. Bouxin\*, A. McVeigh\*, F. Tran, N.J. Westwood, M.C. Jarvis, and S.D. Jackson, *Catalytic depolymerisation of isolated lignins to fine chemicals using a Pt/ alumina catalyst: Part 1 - Impact of the lignin structure*. Green Chemsitry, 2015. 17: p. 1235-1242.

\*both authors contributed to this published work

#### 3.1.2.1 Ammonia Lignin

Figure 30 compares the GPC profiles of the starting ammonia lignin to the acetylated products obtained after reaction, with and without the Pt/alumina catalyst. It is evident from these plots that there was a clear shift to lower molecular weights from ~11.5 min to ~14 min. There was no significant difference between the two reactions but Table 10 shows that there was enhanced depolymerisation when the catalyst was added to the

reaction. Table 10 shows that the molecular weight of the catalytic products was 1042 Da which is 26.8 % of that calculated for the ammonia lignin (3884 Da). This is in comparison to the blank run which produced products with a molecular weight of 1304 Da which is slightly higher in size. Moreover, the polydispersity of the ammonia lignin decreased from 2.45 to 1.96 and 1.75 for the blank and catalytic run respectively. This indicated that the lignin fragment size was much more uniform than the starting lignin after both reactions.

Table 10: GPC data of ammonia reactions with 1 wt. % Pt/alumina

	<b>Ammonia Lignin</b>	<b>No Catalyst</b>	<b>With Catalyst</b>
<b>Molecular Weight (Mw)</b>	3884	1304	1042
<b>Molecular Number (Mn)</b>	1588	666	594
<b>Polydispersity (Ip)</b>	2.45	1.96	1.75

GC-MS quantification of the monomers showed significant differences across the 21 identified products. As shown in Figure 31, the reaction without catalyst for the ammonia lignin from poplar wood showed the lowest overall yield of 6.8 % and generated mainly phenol (H0), guaiacol (G0) and syringol (S0) with selectivities of 45, 7 and 24 % respectively. In the presence of the Pt/alumina catalyst, the overall yield increased by more than four times to 16.4 %. Unlike the blank run which promoted dealkylation, the products obtained in the catalytic run were able to maintain the alkyl chain with various functional groups attached to the terminal gamma carbon. The ammonia lignin was found to contain the most uncondensed linkages (see Table 7, section 3.1.1.2) so the production of these types of products imply that C-O-C bond cleavage was more achievable and more selective with the inclusion of the catalyst. Although there was no obvious selectivity towards one particular product, phenol (14 %), syringol (11 %), propylsyringol (S3) (16 %) and propenylsyringol (S3i) (10 %) were the main products obtained which meant that there was a selectivity towards S-units. In fact, by implementing the use of the catalyst, the selectivity towards S-units increased from 37 % to 60 %, and phenol decreased from 45 % to 14 %. This selectivity made sense when the original S:G:H ratios were taken into account (see Table 7, section 3.1.1.2) because S-units were found to be the main monomer unit (65 %) in this particular lignin.

In addition, UV analysis was also carried out on the ammonia lignin lights fraction at this point to determine the presence or absence of BTX-type molecules as described in section 2.4.7. Absorption bands at 215 and 280 nm were found which are typical of a lignin structure [66] but no bands associated with BTX molecules were observed. From these results, it was deemed that BTX production was not likely and would require further investigation.

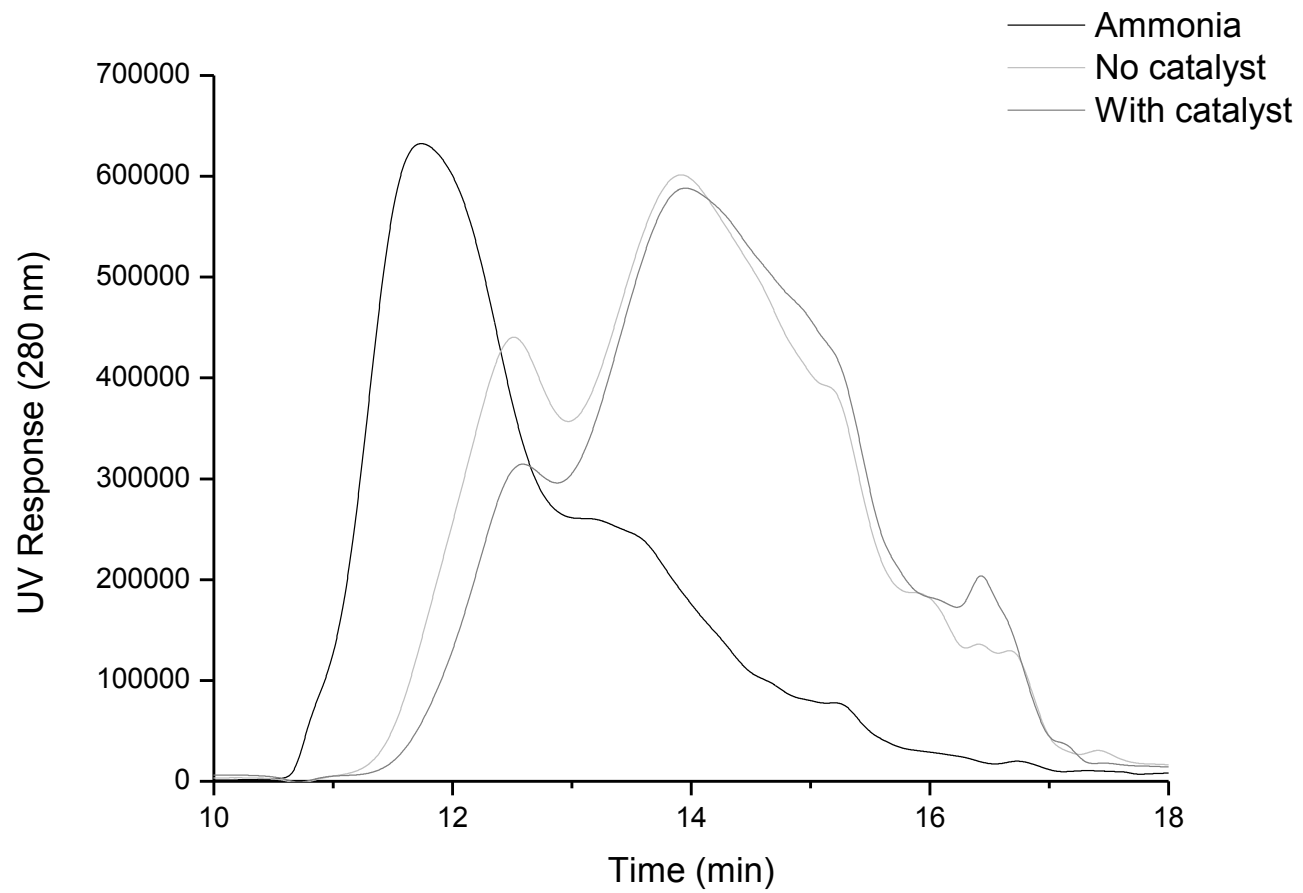


Figure 30: GPC profile of ammonia lignin vs. with and without 1 wt. % Pt/alumina catalyst reactions

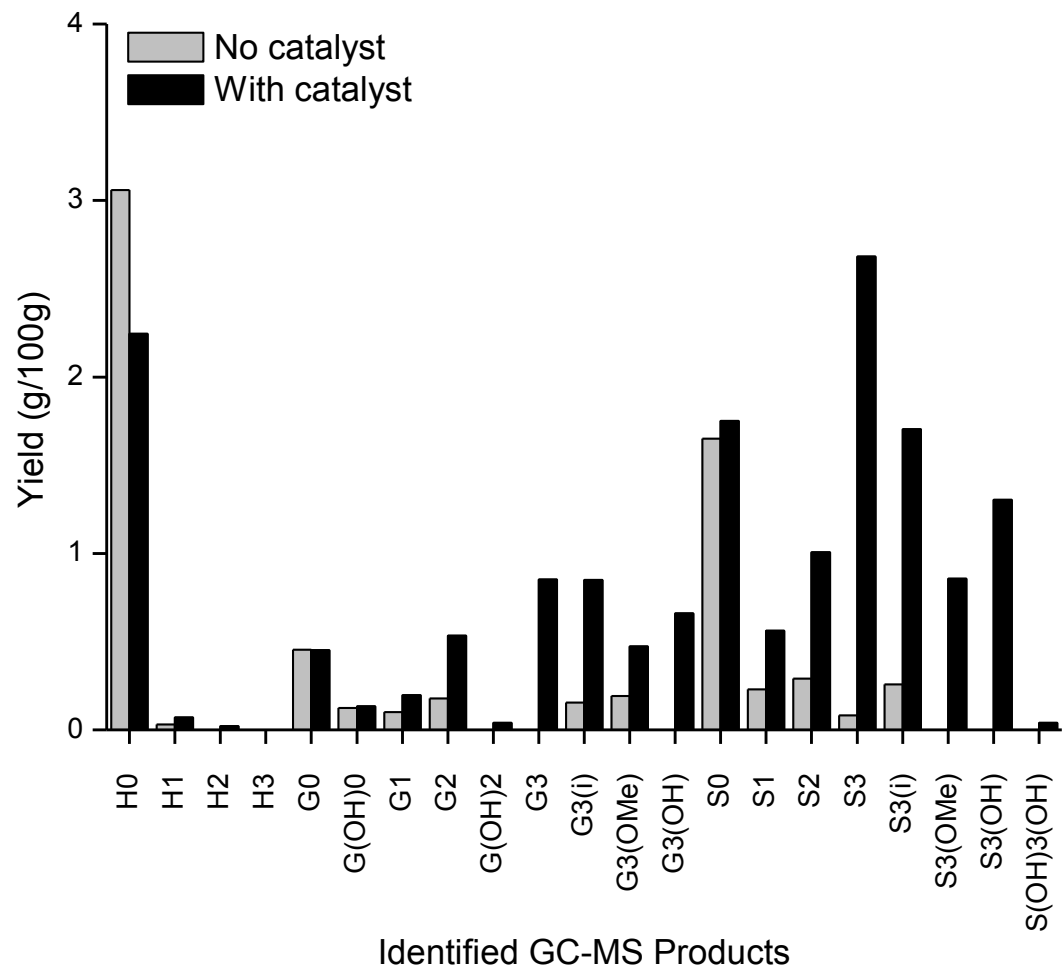


Figure 31: Ammonia lignin blank vs. standard reaction with 1 wt. % Pt/alumina

### 3.1.2.2 Organosolv Lignin

When the organosolv lignin was reacted in the presence and absence of the Pt/alumina catalyst, the resultant GPC plots were fairly similar in appearance. Figure 32 shows a shift to lower molecular weights from ~12-14 min to 14 min for both profiles. Table 11 shows that there was increased level of depolymerisation when the catalyst was added to the reaction, where 41.9 % of the original Mw remained after the blank reaction in comparison to 31.5 % after the catalytic reaction. There was also a decrease in the Ip value, from 2.6 to 1.9 and 1.6 indicating that the presence of the catalyst formed a less complex polymer.

Table 11: GPC data of organosolv reactions with 1 wt. % Pt/alumina

	Organosolv Lignin	No Catalyst	With Catalyst
<b>Molecular Weight (Mw)</b>	3221	1350	1015
<b>Molecular Number (Mn)</b>	1229	707	637
<b>Polydispersity (Ip)</b>	2.62	1.91	1.59

Figure 33 displays the GC-MS monomeric product distribution for both reactions, with and without catalyst, using organosolv lignin from poplar wood. It is clear from this graph that the blank reaction yielded a slightly lower overall level of products (6 %) in comparison to the catalytic reaction (9 %). The main products for the blank reaction were selective towards phenol (40 %), guaiacol (11 %) and syringol (23 %), in comparison to the catalytic reaction which also selectively favoured the production of phenol (27 %) and syringol (11 %), as well as propylsyringol (13 %). The presence of the catalyst produced similar products to those obtained in the blank run but in higher quantities. This suggested that the catalytic reaction also favoured dealkylation with this particular lignin but other reaction pathways were made available to produce other types of products with added functionality. It is also likely that this reaction favoured products with smaller alkyl chains because the starting lignin was more condensed and contained a low proportion of  $\beta$ -O-4 bonds (see Table 7, section 3.1.1.2). The amount of propylphenolic compounds can be directly correlated with the frequency of  $\beta$ -O-4 linkages because there is no other way to form these types of monomers.

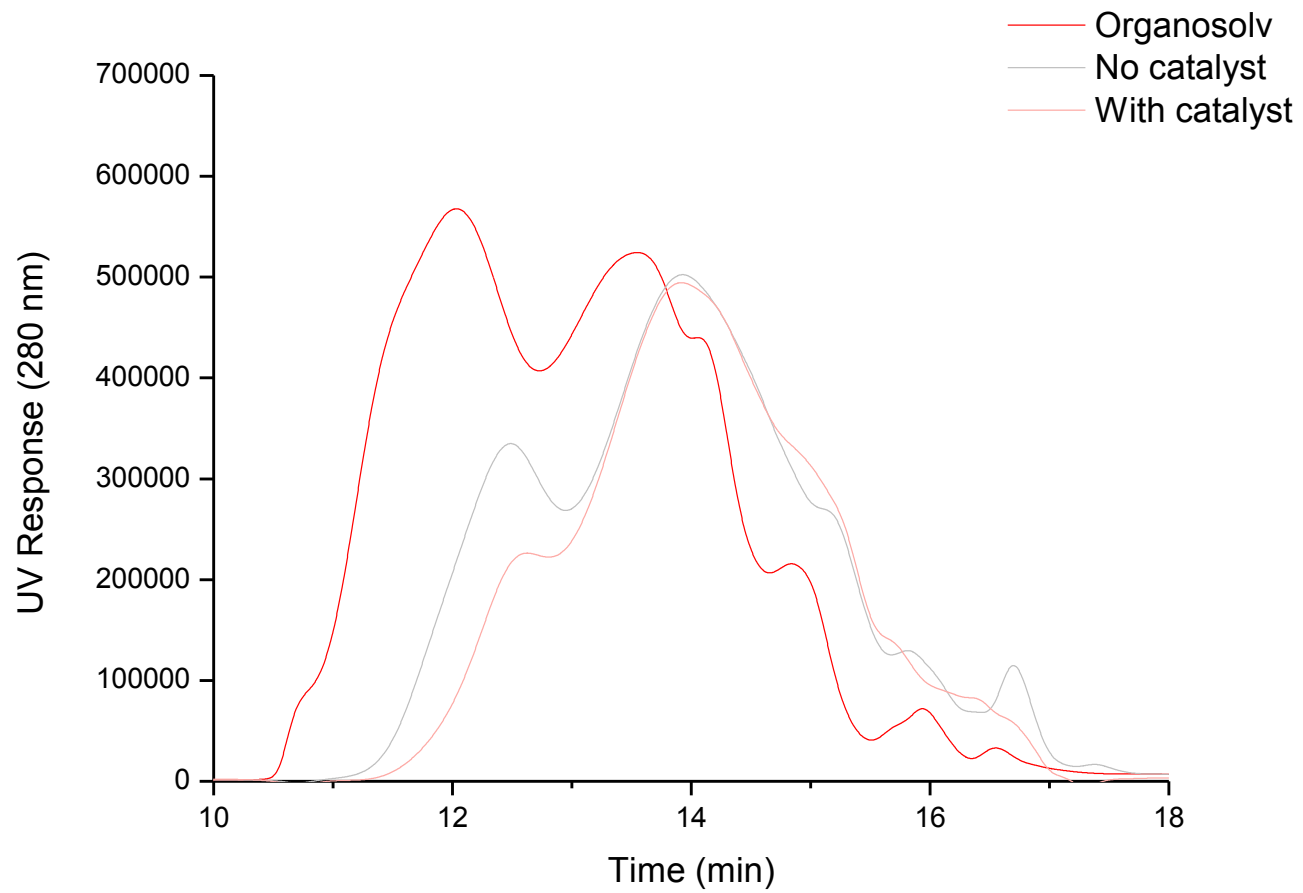


Figure 32: GPC profile of organosolv lignin vs. with and without 1 wt. % Pt/alumina catalyst reactions

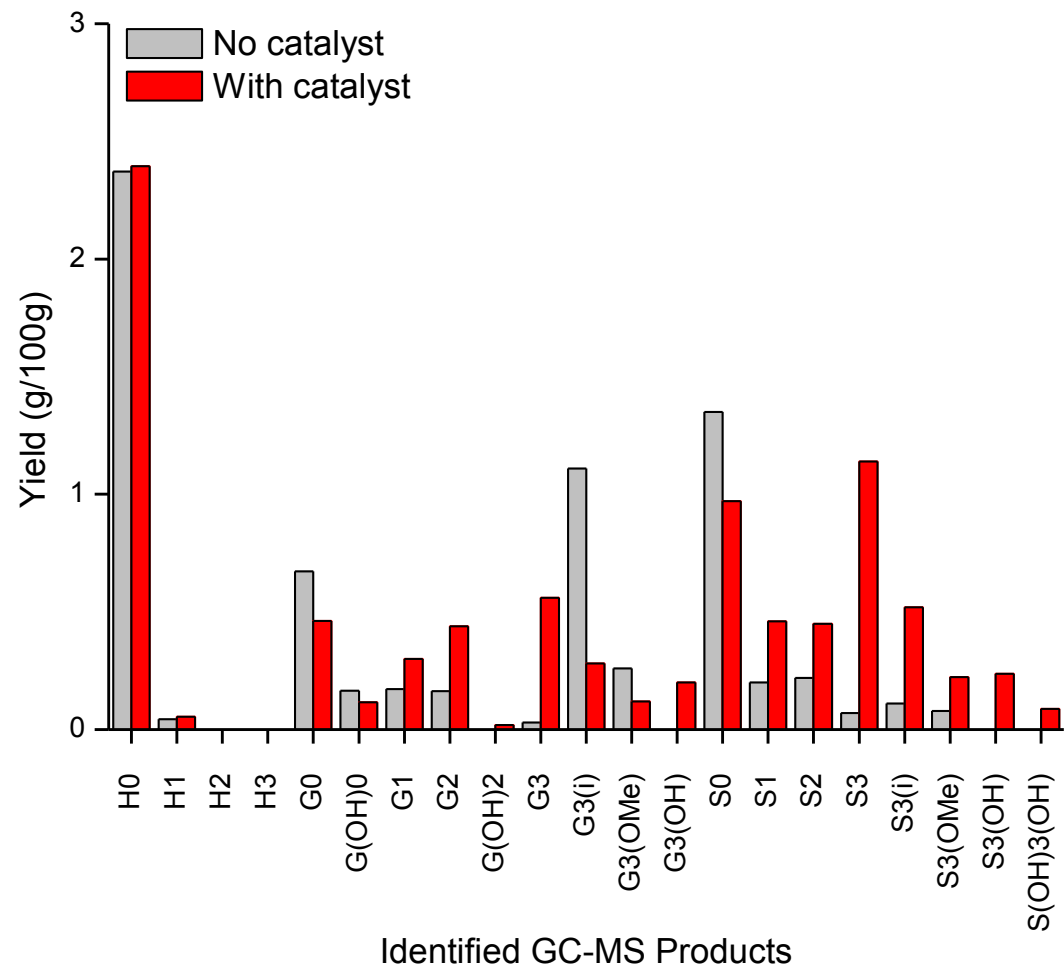


Figure 33: Organosolv lignin blank vs. standard reaction with 1 wt. % Pt/alumina

### 3.1.2.3 Alkali Lignin

The presence of the Pt/alumina catalyst made little difference to the appearance of the GPC profiles shown in Figure 34 but both reactions did show a shift of the acetylated products to lower molecular weights. Table 12 shows the molecular weight, number and polydispersity values calculated for each of the product distributions. Interestingly, the blank run gave a slightly lower molecular weight value (1148 Da) than the catalytic run (1314 Da). This meant that 49.1 % of the starting weight remained after the catalytic reaction in comparison to 42.9 % when no catalyst was added to the reaction. This was also reflected in the polydispersity values obtained.

Table 12: GPC data of alkali reactions with 1 wt. % Pt/alumina

	Alkali Lignin	No Catalyst	With Catalyst
<b>Molecular Weight</b> (Mw)	2673	1148	1314
<b>Molecular Number</b> (Mn)	964	632	669
<b>Polydispersity</b> (Ip)	2.77	1.82	1.96

Compared to the previous lignins from poplar wood, the blank run with the alkali lignin from wheat straw generated mainly ethylguaiacol (G2) (1.7 g/100g) and gave a similar, wide distribution across many other products as shown in Figure 35. The blank run gave a total overall yield of 7.1 %. The addition of the catalyst did not make a significant difference to the overall yield (8.3 %) but there was a change in the amount of each monomer unit obtained. Again, the ethylguaiacol was favoured with the yield increasing to 2.59 g/100g. When the catalyst was included, the units with no carbon alkyl chain were not favoured and the monomers which maintained the alkyl chain were produced in higher quantities. The larger products which maintained the ethyl and propyl chain were attainable because the starting material contained 17.7 % of alkyl-aryl bonds and the reaction selectively favoured ethylguaiacol due to the fact that wheat lignins are rich in ferulic acid [1]. As shown in Figure 36, ferulic acid can readily undergo decarboxylation to ethylguaiacol via the hydrogenation of 4-vinylguaiacol (this product was not identified in this work). The total molar quantity of the catalytic run was therefore higher than that calculated for the blank experiment which explained why the GPC data gave a lower Mw

value for the blank run. Furthermore, the yields obtained for ethylguaiacol, ethylphenol (H2) and phenol looked to be in proportion to each other which would suggest that demethoxylation was followed by dealkylation (see Figure 36).

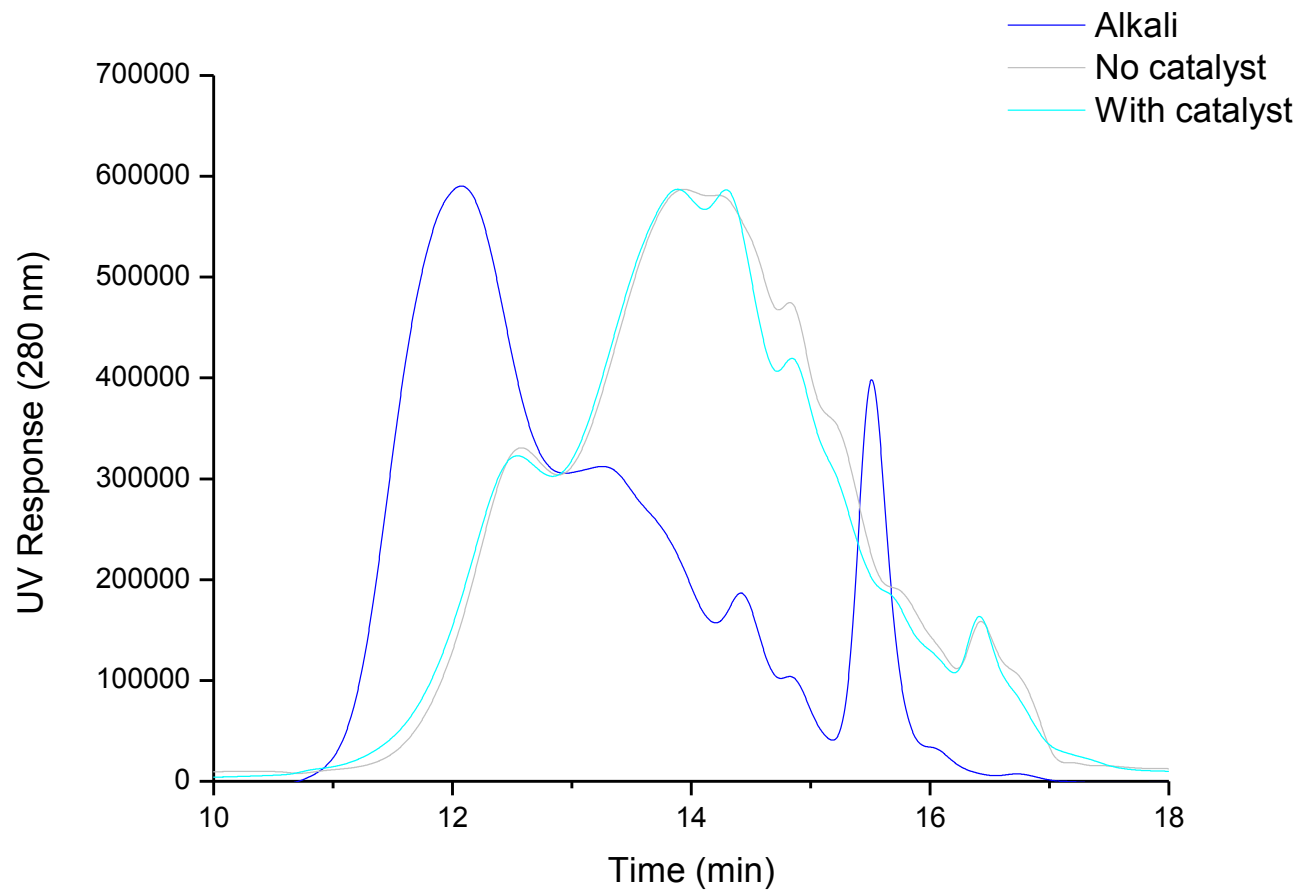


Figure 34: GPC profile of alkali lignin vs. with and without 1 wt. % Pt/alumina catalyst reactions

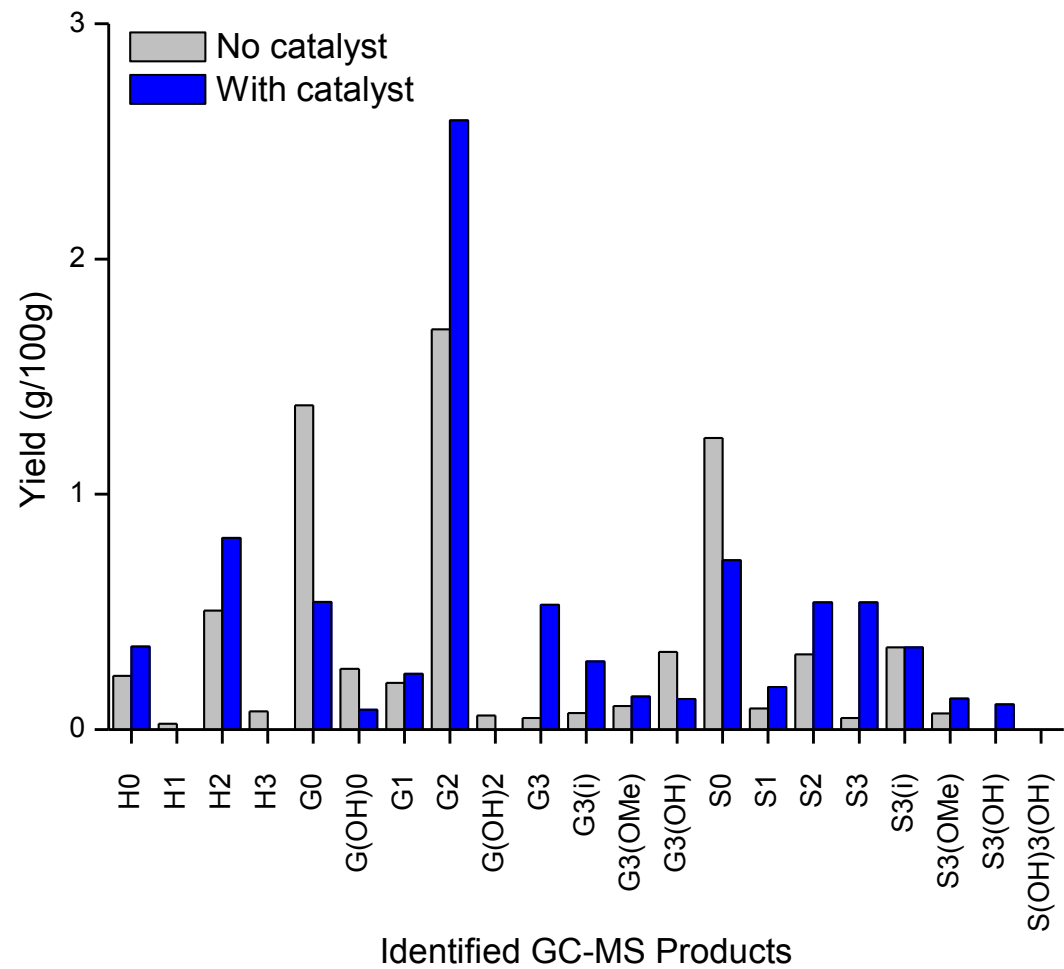


Figure 35: Alkali lignin blank vs. standard reaction with 1 wt. % Pt/alumina

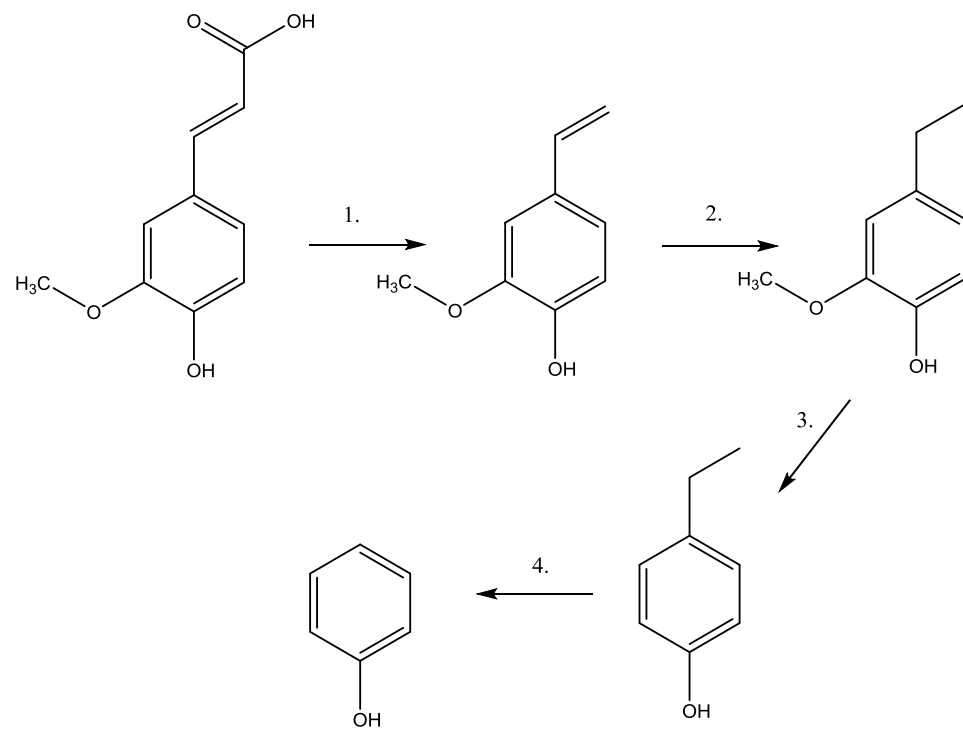


Figure 36: Proposed reaction mechanism of wheat straw lignins

### 3.1.2.4 AFEX Lignin

Similar to the alkali lignin GPC results discussed previously, the GPC profiles for each reaction shown in Figure 37 displayed little difference in their appearance but gave a lower Mw value for the blank run. The starting AFEX lignin was reduced from 2672 to 1143 Da (42.8 %) without catalyst and to only 1325 Da (49.6 %) with the catalyst present. In line with the molecular weight values, the Ip values also showed that the blank run gave more uniform fragments (1.86) in comparison to the catalytic run (2.09) and the starting material (2.51).

Table 13: GPC data of AFEX reactions with 1 wt. % Pt/alumina

	AFEX Lignin	No Catalyst	With Catalyst
<b>Molecular Weight (Mw)</b>	2672	1143	1325
<b>Molecular Number (Mn)</b>	1066	614	633
<b>Polydispersity (Ip)</b>	2.51	1.86	2.09

This wheat straw lignin also favoured the production of ethylguaiacol in both reactions as shown in Figure 38. The blank run selectively formed ethylguaiacol, guaiacol and syringol, with little other products being formed. This gave the blank run a total overall yield of 4.5 % run in comparison to the catalytic run which more than doubled in its total overall yield (9.8 %). The formation of ethylguaiacol doubled in quantity when the catalyst was employed. There was also an increase in most other products, except for guaiacol which almost halved in quantity. The rise in phenol could be attributed to the demethoxylation of the guaiacol, however phenol could also have been produced following the same mechanism as suggested with the alkali lignin, where ethylguaiacol goes to form ethylphenol then phenol. Although there was no high selectivity towards one product other than ethylguaiacol, there was a clear increase of selectivity towards three-carbon alkyl chained products being formed when the catalyst was included in the reaction. There was a large increase in the selectivity towards three-chain alkylated products from 15 % to 40 % in the catalytic run.

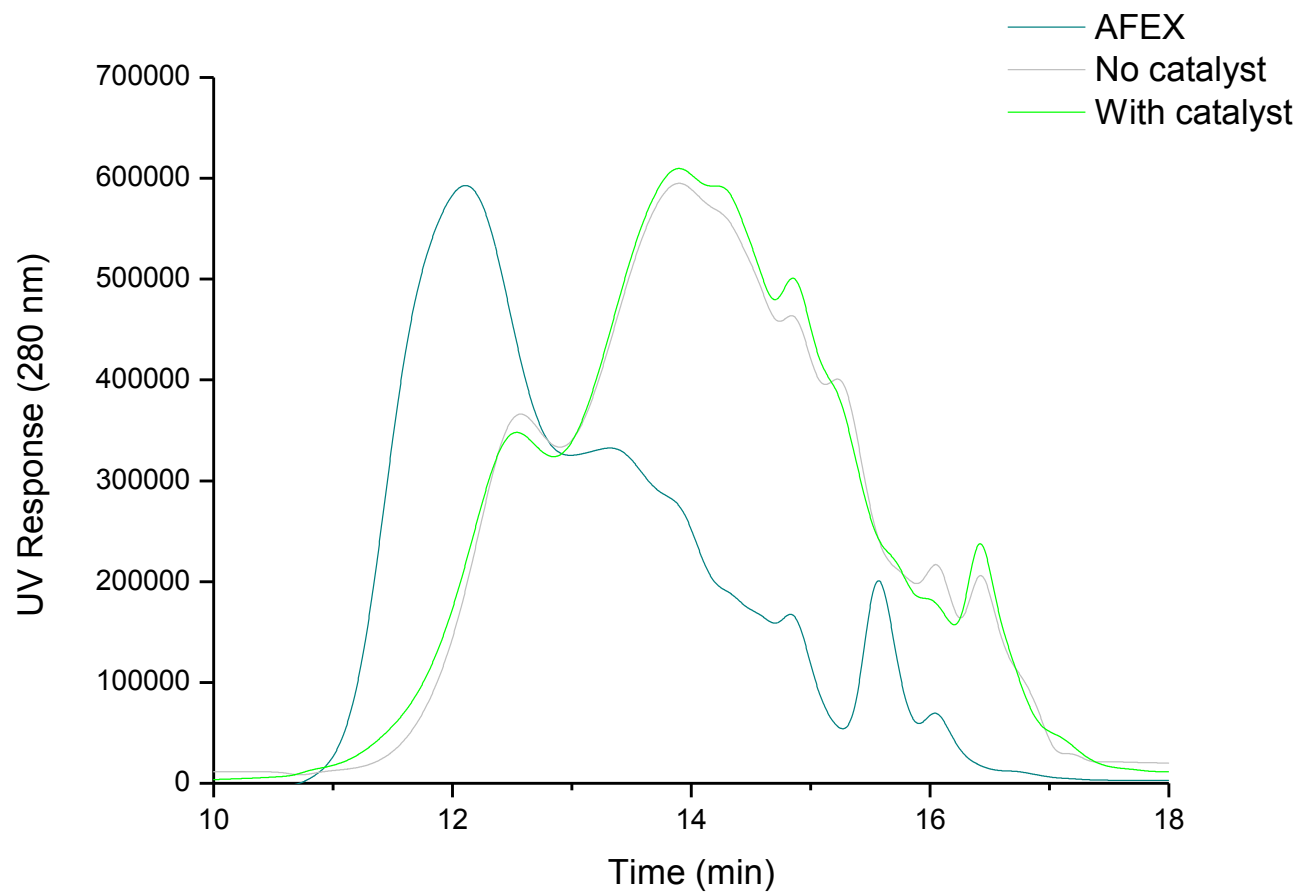


Figure 37: GPC profile of AFEX lignin with and without 1 wt. % Pt/alumina catalyst reactions

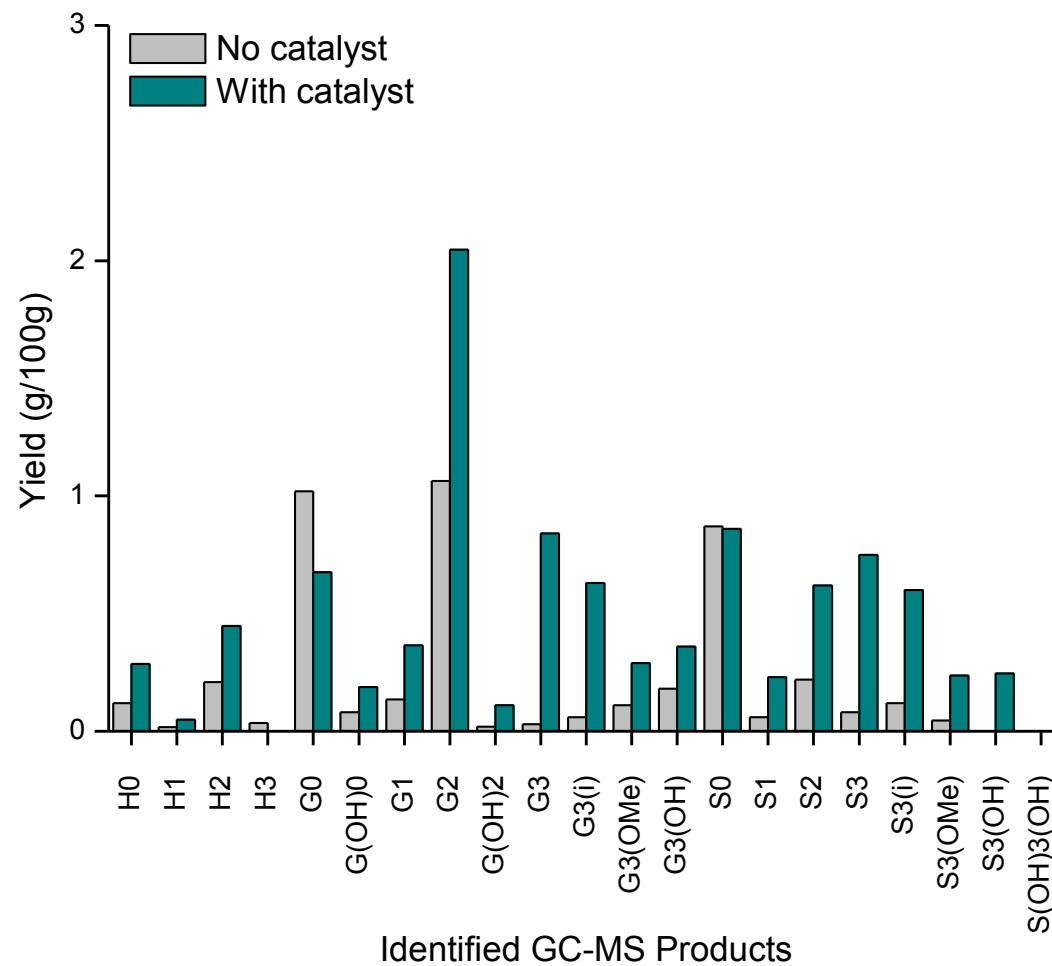


Figure 38: AFEX lignin blank vs. standard reaction with 1 wt. % Pt/alumina

#### **3.1.2.4.1 Fermented AFEX Lignin**

As explained previously, the project was also interested in the catalytic potential of AFEX lignin from fermentation residues. Here the fermented AFEX lignin was subjected to the same catalytic conditions as those used for the AFEX lignin to give a direct comparison between the two product distributions obtained. GPC analysis of the acetylated products after the catalytic reaction gave a molecular weight value of 1305 Da and a polydispersity of 1.86 which is similar to the values obtained for the AFEX lignin products. The catalytic products identified using GC-MS were compared to those produced using the AFEX lignin and are given in Figure 39. The Fr-AFEX lignin gave a higher yield (13.8 %) than that produced by the AFEX lignin (9.8 %). The range of products obtained for the Fr-AFEX lignin was similar but they were found in higher quantities. This increase could be attributed to residual sodium hydroxide found in the Fr-AFEX after the pre-treatment step which could have assisted depolymerisation. What is important to take from these results is the fact that the second fermentation step made little difference to the quality of the lignin and that a good yield was obtainable either way. This is of use to industry because the production of ethanol produces a lignin-rich residue which is currently unused and by showing that this unexploited resource has the potential to be used to the same extent as the saccharification residue, this eliminates the need to add a further step to purify the lignin in any way prior to a catalytic step.

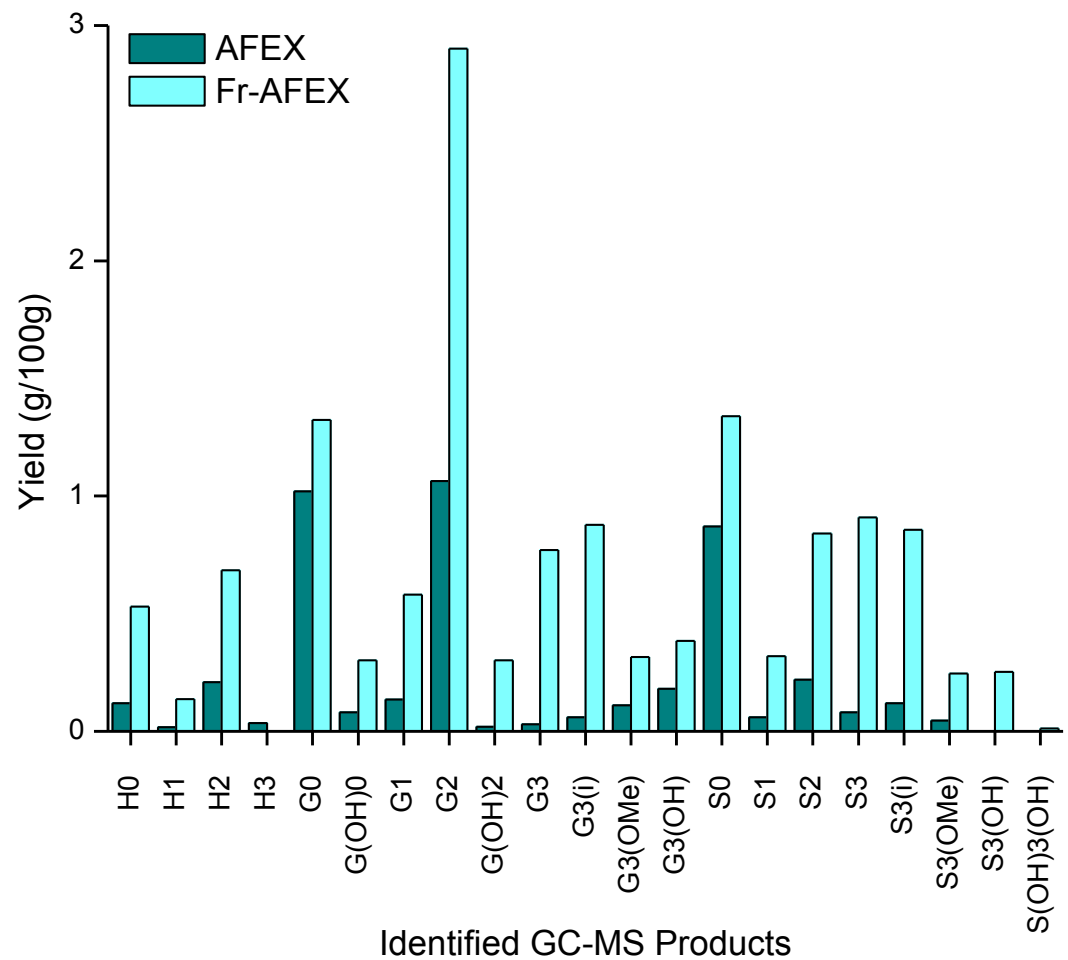


Figure 39: AFEX vs. Fr-AFEX lignin reaction with 1 wt. % Pt/alumina

### 3.1.2.5 Soda Lignin

The final GPC profile (Figure 41) shows a clear shift from 12 min to 14 min for both reactions, thus indicating a shift to lower molecular monomeric products. The profiles obtained were very similar regardless of the catalyst's presence which suggested that, from this data alone, that the catalyst made little difference to the reaction. Table 14 verified this suggestion because the Mw values obtained were also in the same region, 1227 Da and 1270 Da respectively. These values show that the soda lignin was able to convert to ~42% of its original weight in both environments.

Table 14: GPC data of soda reactions with 1 wt. % Pt/alumina

	Soda Lignin	No Catalyst	With Catalyst
<b>Molecular Weight (Mw)</b>	2926	1227	1270
<b>Molecular Number (Mn)</b>	1063	652	645
<b>Polydispersity (Ip)</b>	2.75	1.88	1.97

Figure 41 displays the difference in product distribution between the blank and catalytic run for the soda lignin from wheat straw. It is clear from this data that the overall yield of products did not drastically change after the addition of the catalyst, with the total yields being 7.8 % and 7.4 % respectively. The main products obtained did however change. The blank run mainly generated syringol, guaiacol and ethylguaiacol like the other wheat straw lignins, whilst the catalytic run produced syringol, phenol and ethylguaiacol. The starting material was the most condensed of the six lignins shown here, with only 2.8 % of  $\beta$ -O-4 linkages being found, so the fact that products with no alkyl chain were observed was not surprising. It is possible that the catalyst also improved the level of demethoxylation so the amount of phenol increased as a result.

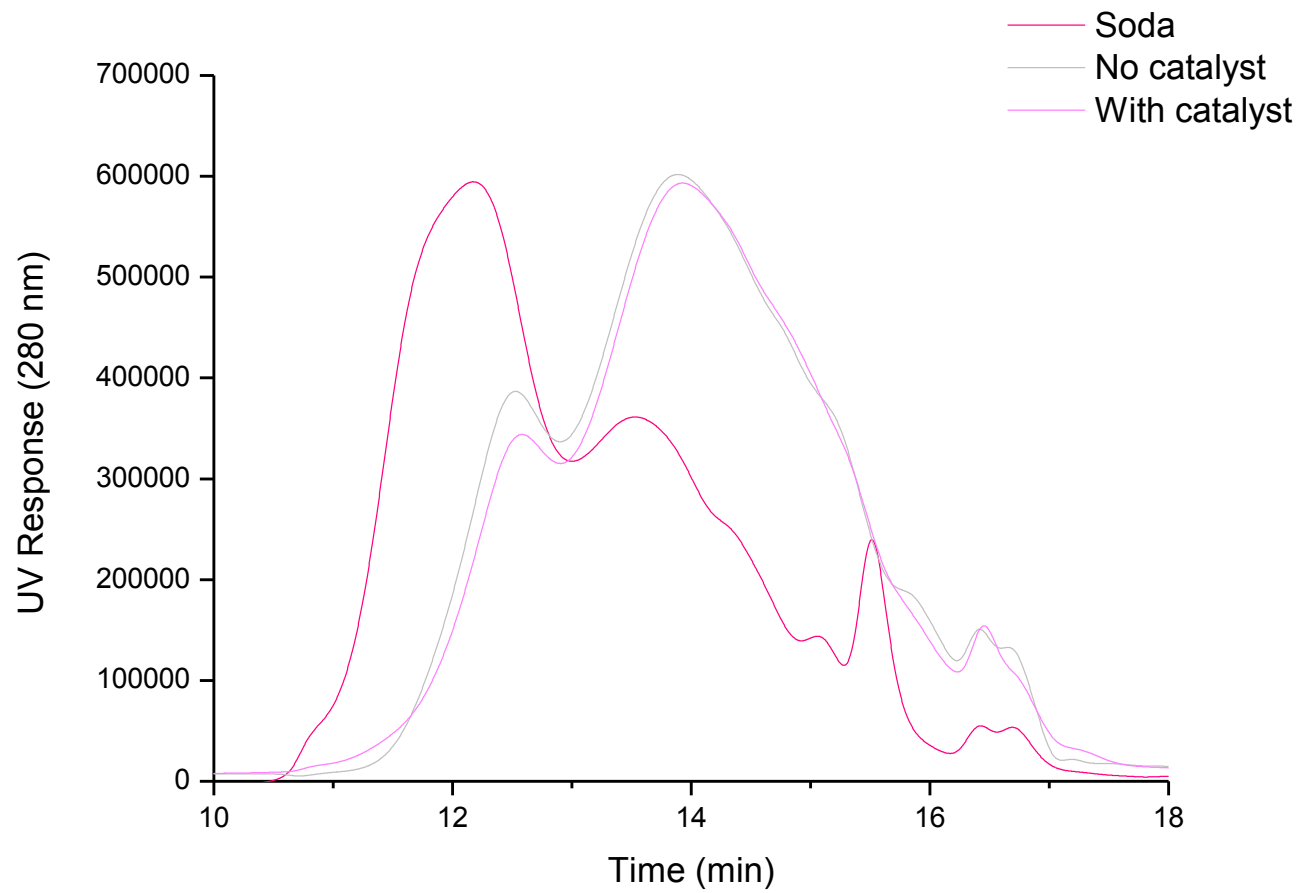


Figure 40: GPC profile of AFEX lignin vs. with and without 1 wt. % Pt/alumina catalyst reactions

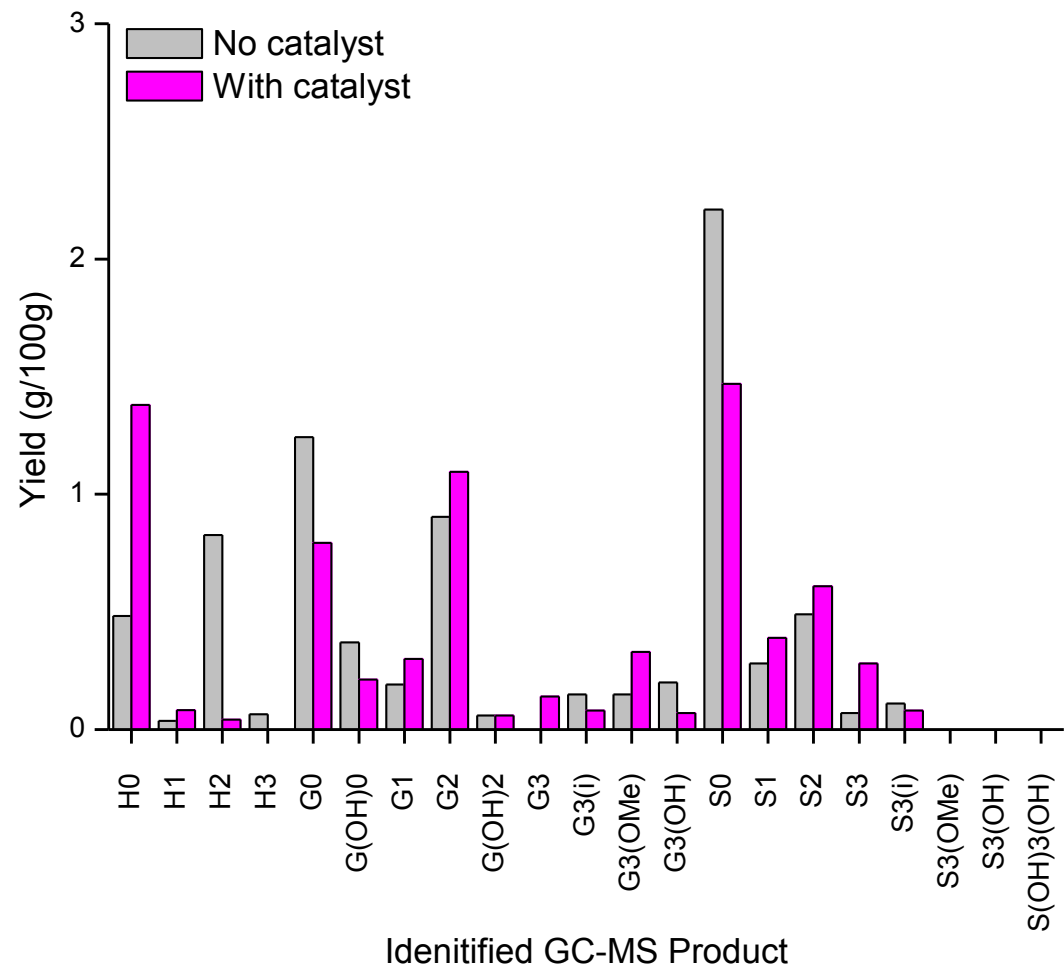


Figure 41: Soda lignin blank vs. standard reaction with 1 wt. % Pt/alumina

### 3.1.3 Summary of the Catalytic Standard Reaction Testing of Six Lignins

Below, Table 14 provides a summary of all of the products obtained in both the blank and catalytic reaction for the five main lignins, namely the ammonia and organosolv lignins from Poplar wood and the alkaline, AFEX and soda lignins from wheat straw. With regards to the catalytic reaction, it is clear from Table 14 that the ammonia lignin achieved the highest overall yield (16.4 %) which was more than double that obtained for the soda lignin (7.4 %). The blank runs showed that guaiacol and syringol production was favourable with all five lignins. The high pressure, temperature and solvent present in the blank run likely resulted in a pyrolysis/solvolytic-type reaction where light and heavy aromatics were formed which went on to polymerise and form char. It is also possible that guaiacol and syringol were generated from the condensed parts of the lignin structure itself. Interestingly, the alkali and AFEX lignins (and the soda blank run to some extent) observed the same trend for both the blank and catalytic reactions where the ethylguaiacol formed ethylphenol via C-O cleavage of the methoxy group, followed by the production of phenol via dealkylation. No obvious trends were seen with the poplar lignins. The catalytic results suggested that the presence of the noble metal catalyst suppressed recondensation to heavy molecular weights and enhanced depolymerisation to give better overall yields and more functionalised alkylphenolics. The reaction could have taken place via fragmentation of the lignin polymer followed by hydrogenolysis of the fragmented species, with the methanol-water solvent acting as a hydrogen donor.

Table 15: Identification and quantification of reaction products from five lignin samples

Product No.	Monomer Unit	Amm Blank	Amm w/ Catalyst	Org Blank	Org w/ Catalyst	Alk Blank	Alk w/ Catalyst	AFEX Blank	AFEX w/ Catalyst	Soda Blank	Soda w/ Catalyst
1	H0	3.06	2.24	2.37	2.39	0.23	0.35	0.12	0.29	0.48	1.38
2	H1	0.03	0.07	0.04	0.05	0.02	0.00	0.02	0.05	0.04	0.08
3	H2	0.00	0.02	0.00	0.00	0.51	0.82	0.21	0.45	0.83	0.04
4	H3	0.00	0.00	0.00	0.00	0.08	0.00	0.04	0.00	0.07	0.00
5	G0	0.45	0.45	0.67	0.46	1.38	0.54	1.02	0.68	1.24	0.79
6	G(OH)0	0.12	0.13	0.16	0.12	0.26	0.08	0.08	0.19	0.37	0.21
7	G1	0.10	0.20	0.17	0.30	0.20	0.24	0.13	0.37	0.19	0.30
8	G2	0.18	0.53	0.16	0.44	1.70	2.59	1.06	2.05	0.90	1.10
9	G(OH)2	0.00	0.04	0.00	0.02	0.06	0.00	0.02	0.11	0.06	0.07
10	G3	0.00	0.85	0.03	0.56	0.05	0.53	0.03	0.84	0.00	0.14
11	G3(i)	0.15	0.85	1.11	0.28	0.07	0.29	0.06	0.63	0.15	0.08
12	G3(OMe)	0.19	0.47	0.26	0.12	0.10	0.14	0.11	0.29	0.15	0.33
13	G3(OH)	0.00	0.66	0.00	0.20	0.33	0.13	0.18	0.36	0.20	0.07
14	S0	1.65	1.75	1.35	0.97	1.24	0.72	0.87	0.86	2.21	1.47
15	S1	0.23	0.56	0.20	0.46	0.09	0.18	0.06	0.23	0.28	0.39
16	S2	0.29	1.01	0.22	0.45	0.32	0.54	0.22	0.62	0.49	0.61
17	S3	0.08	2.68	0.07	1.14	0.05	0.54	0.08	0.75	0.07	0.28
18	S3(i)	0.26	1.70	0.11	0.52	0.35	0.35	0.12	0.60	0.11	0.08
19	S3(OMe)	0.00	0.86	0.08	0.22	0.07	0.13	0.05	0.24	0.00	0.00
20	S3(OH)	0.00	1.30	0.00	0.24	0.00	0.11	0.00	0.25	0.00	0.00
21	S(OH)3(OH)	0.00	0.04	0.00	0.09	0.00	0.00	0.00	0.00	0.00	0.00
	<b>Total (g/100g)</b>	<b>6.79</b>	<b>16.41</b>	<b>6.00</b>	<b>9.03</b>	<b>7.11</b>	<b>8.28</b>	<b>4.48</b>	<b>9.84</b>	<b>7.84</b>	<b>7.42</b>

The distribution of products obtained after the catalytic reaction varied significantly with respect to the starting material as shown in Figure 42. Guaiacol and syringol accounted for 54 % of the molar fraction of depolymerised products from soda lignin, whilst they only accounted for 29, 30, 27 and 21 % of the total molar quantity of alkali, organosolv, AFEX and ammonia lignin respectively. In comparison, the relative proportion of propylphenolics increased from 17 to 64 % of the overall total from soda to ammonia lignin as illustrated below:

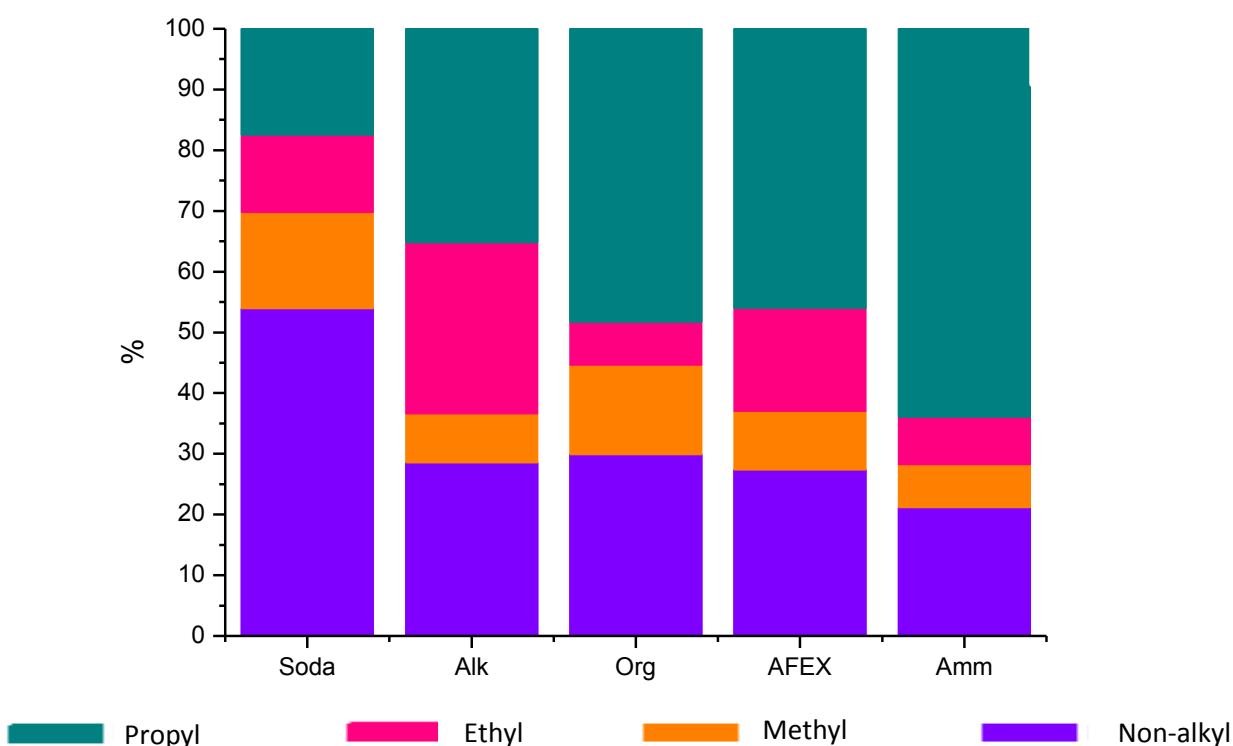


Figure 42: Catalytic depolymerisation products of five lignins

(Note that this figure has been corrected with respect to the high ethylguaiacol and phenol content in the wheat straw lignins.)

When the ratio of starting S/G units from the thioacidolysis results (Table 7, section 3.1.1.2) of each lignin was considered, the hardwood lignins from poplar wood were found to give higher values due to their high syringyl content in comparison to the wheat straw lignins which had similar syringyl and guaiacyl content hence the lower ratio value. These values in relation to the catalytic depolymerisation products with 3-carbon side chains generally gave an excellent correlation as shown in Table 16. This suggested that both the

guaiacyl and syringyl units underwent the same type of complex reactions at a similar rate to form the same types of depolymerisation products. The difference in values was found to be more significant for the condensed soda lignin which suggested that, in this case, the thioacidolysis technique was more effective for depolymerisation than the catalytic step because the thioacidolysis was more selective towards the uncondensed fraction of the lignin and it decreased the condensation effect [1]. Table 16 also shows the S/G ratio obtained when no catalyst was used and there is a marked difference in the values given. Without catalyst, the reaction using syringyl-rich hardwood lignins (ammonia and organosolv) produced more G-units in comparison to the catalytic reactions which produced more S-units, whilst the wheat straw lignins gave similar values to those calculated for the catalytic reactions. The alkali monomer yields were similar for both the non- and catalytic reactions so this is reflected by the similar ratio value. The others, especially the soda lignin non-catalytic value, are likely a result of condensation reactions which have occurred simultaneously during the depolymerisation steps.

Table 16: Thioacidolysis and catalytic product ratios of six lignins

	<b>Thioacidolysis</b>	<b>Catalytic Product</b>	<b>Non-catalytic</b>
	<b>S/G Ratio</b>	<b>S/G Ratio</b>	<b>Product S/G</b>
<b>Ammonia</b>	1.86	1.99	0.91
<b>Organosolv</b>	1.33	1.61	0.61
<b>Alkali</b>	1.00	0.87	0.79
<b>AFEX</b>	1.07	0.74	0.60
<b>Fr-AFEX</b>	0.98	0.75	-
<b>Soda</b>	1.04	0.55	0.32

Further condensation of the lignin during the catalytic step is one of the greatest issues associated with its conversion abilities. Depolymerisation of the lignin is one of the key aims of this project but the generation of unstable products seems unavoidable. Whilst this work aimed to depolymerise through a combined HDO/hydrogenolysis step with fast stabilisation of products through hydrogenation, the results showed that condensation reactions were still a major issue, particularly without catalyst and with the more condensed soda lignin as shown in Table 17.

Table 17: Char production of six lignins

	<b>Non-catalytic Reaction (g/100g)</b>	<b>Catalytic Reaction (g/100g)</b>
<b>Ammonia</b>	56.67	28.67
<b>Organosolv</b>	-	14.00
<b>Alkali</b>	29.87	22.93
<b>AFEX</b>	30.67	26.80
<b>Fr-AFEX</b>	-	30.40
<b>Soda</b>	37.60	33.60

(- indicates that no sample was available for analysis)

A common pathway to these highly condensed products is through inter-chain condensation of an electron rich carbon after heterolytic bond cleavage of the benzylic C-O linkage. This mechanism is shown in Figure 43 below [67]:

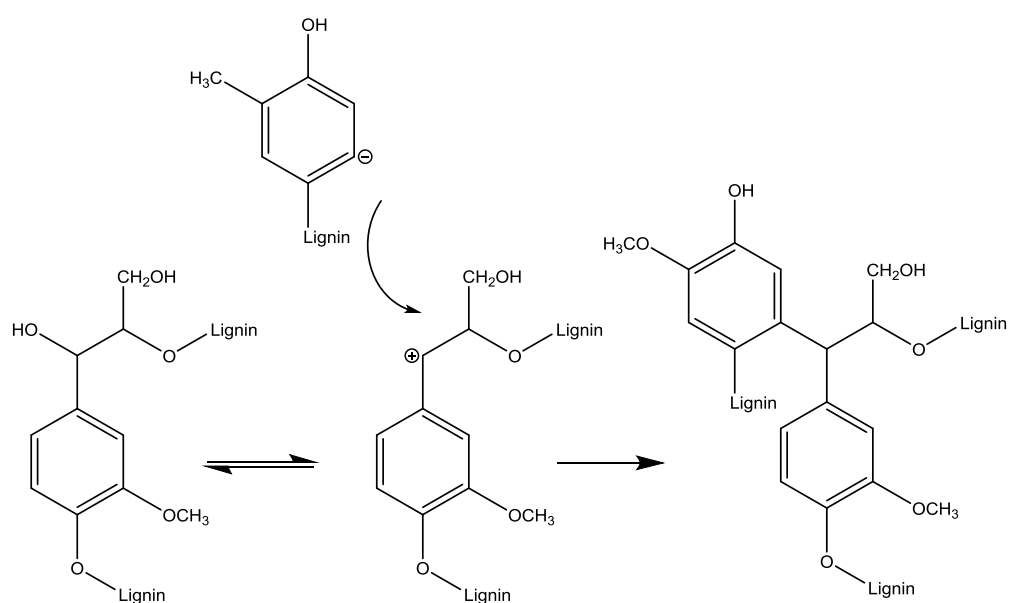


Figure 43: Inter-chain condensation pathway of lignin

Additionally, although all material was soluble in the methanol-water solution or acetone, there was a ~20 % weight loss observed in the catalyst TPO data (this will be discussed later, see section 3.5) which implied that there was char formation on the catalyst surface for all six lignin reactions. Minimal char formation is preferred for effective catalytic depolymerisation because the catalyst can undergo deactivation due to char deposits on the

surface [68]. The acidic character of the alumina support could also have been an influencing factor in the product distribution obtained here because the acidic support is well known to be associated with high coking abilities during HDO due to the acid surface sites [23]. Other work also found that the alumina support itself can show catalytic activity [30] but this will be discussed more fully in section 3.2.2.1.

The results presented here show that the starting structure of lignin greatly affected the type and yield of the resultant monomeric aromatic products. The catalytic conversion of lignin to fine chemicals was found to be the most promising when the starting lignin was uncondensed in nature, like the ammonia lignin. This was likely the case with the ammonia lignin because the percolation pre-treatment continuously removed the lignin from the reaction vessel as it became soluble so it therefore limited the amount of depolymerisation reactions which could go on to form unstable intermediates and cause condensation. However using this type of isolation technique in reality would be problematic due to its high cost which will obviously affect and dominate industrial decisions. There therefore must be a balance between the cost efficiency and the potential to generate higher-values products from the isolated lignins.

With this knowledge, further optimisation of the catalytic conversion process must be carried out in order to prevent or limit condensation reactions from occurring. It could be suggested that conversion of highly uncondensed lignins, such as the ammonia or AFEX lignins, will require more gentle and carefully optimised conditions to achieve selective cleavage of the C-O bonds to generate high yields of fine aromatic chemicals, whilst the more condensed lignins such as the soda or organosolv lignins will require harsher conditions and possibly different types of catalysts to crack the material efficiently.

## 3.2 Optimisation of the Ammonia Lignin

This section will focus on optimising the reaction conditions using the ammonia lignin as a benchmark lignin. Here the conditions were altered for each parameter to observe what effect each had on the depolymerisation activity, monomer yield and char production found in the heavy fraction. The char production was based on the residue formed in the heavy fraction (see section 2.4.10), which was thought to be composed of condensed material. This has been quoted as g/100g. All reaction conditions were carried out under the standard parameters stated in section 2.3.2, unless otherwise indicated. When the reaction reached the desired reaction temperature, the reactor pressure was found to increase based on the conditions used (e.g. the vapour pressure of the solvent used) and these values can be found in Table 32 given in the section's summary section. Following the reaction, the autoclave was cooled to room temperature and the residual pressure was found to reduce back to the starting pressure in all experiments unless otherwise stated. The alkylphenolic products for each reaction were analysed using GPC and GC-MS, where all products have been grouped together to give simpler distribution plots and compared against the standard ammonia lignin run shown in section 3.1.2.1. All data has been summarised in Table 32.

### 3.2.1 Reproducibility and Recycling of the Standard Catalytic Reaction

The standard run using the ammonia lignin with Pt/alumina catalyst presented in section 3.1.2.1 was repeated to ensure its reproducibility as illustrated in Figure 44. Deviation in the amount of each product formed was found when compared to the original run, particularly with the alkylated products (G3, G3(i), G3+, S3, S3(i) and S3+), but the overall yields were fairly similar compared to the standard run. The standard run gave an overall yield of 16.4 % in comparison to 14.4 % obtained for reproduced run. The char yield was calculated from the heavy fraction obtained after reaction and was found to be 28.7 and 28.2 g/100g. In relation to the starting S/G ratio of the ammonia lignin (1.86), the catalytic product S/G ratio, with respect to the 3-chained guaiacol and syringol products, was 2.05. This was similar to that obtained for the original standard run (1.99) as shown previously.

In order to test the recyclability and stability of the catalyst, the catalyst was isolated and collected at the end of the standard reaction, dried then placed into the clean Parr autoclave with fresh ammonia lignin. The catalyst was still active for the depolymerisation reaction but gave a lower overall yield of 8.3 %. In general, each product was found in lower quantities as illustrated in Figure 45 and there was no obvious change in selectivity in

terms of the products formed. The S/G ratio, with respect to the 3-chained G- and S-units, was however found to decrease from 2.05 to 1.08. This result showed that more G units were produced in relation to the S units for the reproduced run. This was similar to that observed with the non-catalytic runs with the softwood lignins, where the G units increased when no catalyst was employed during reaction and gave a ratio value of 0.91. After each reaction, the spent catalyst was black in colour which suggested that coke deposits had formed on the surface so it is therefore likely that the additional reaction caused a larger build-up of carbonaceous material. It is possible that this effect could have blocked the active sites to some extent and altered the reaction pathway to one which was similar to the non-catalytic reactions, where condensation of the lignin was also more favourable. However, the standard (retest) reaction produced 28.7 g/100g of residue in the heavy fraction whilst the reaction using the recycled catalyst gave a similar amount (26.9 g/100g). This therefore suggested that the char production was not promoted as a result of using the recycled catalyst.

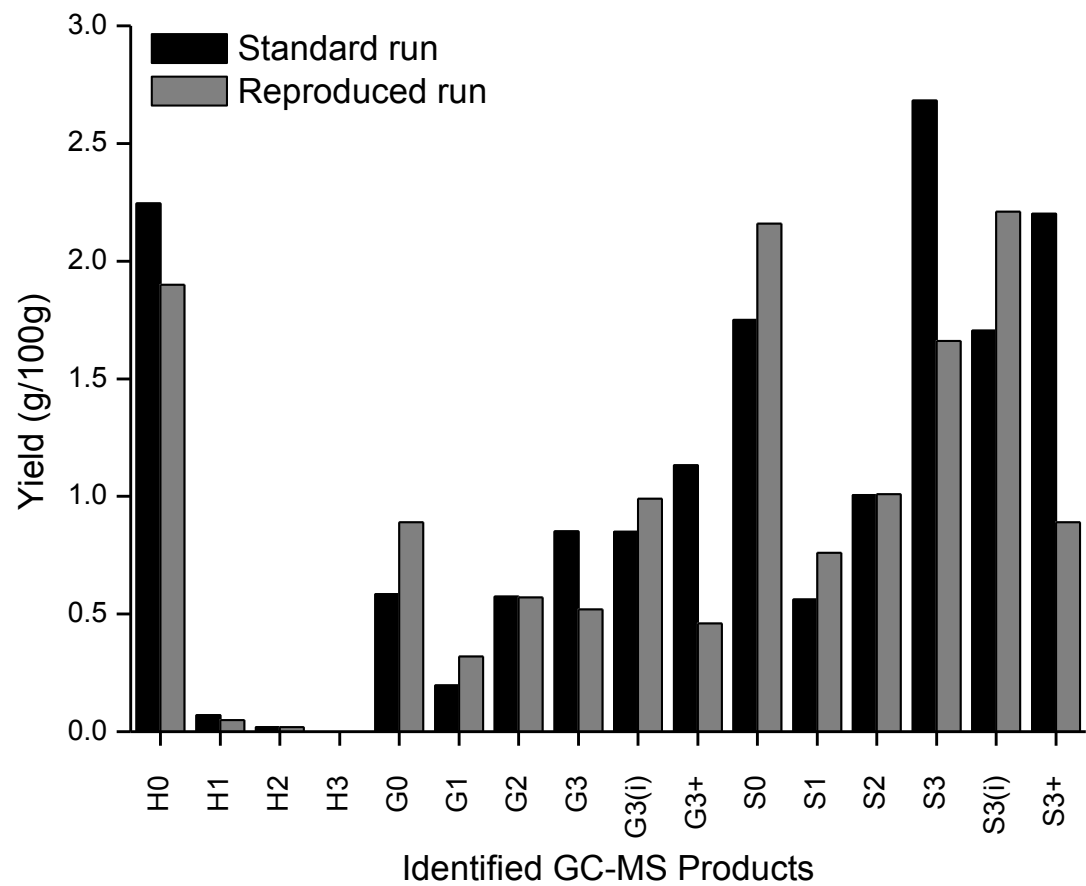


Figure 44: Reproducibility testing of the Pt/alumina catalyst and ammonia lignin

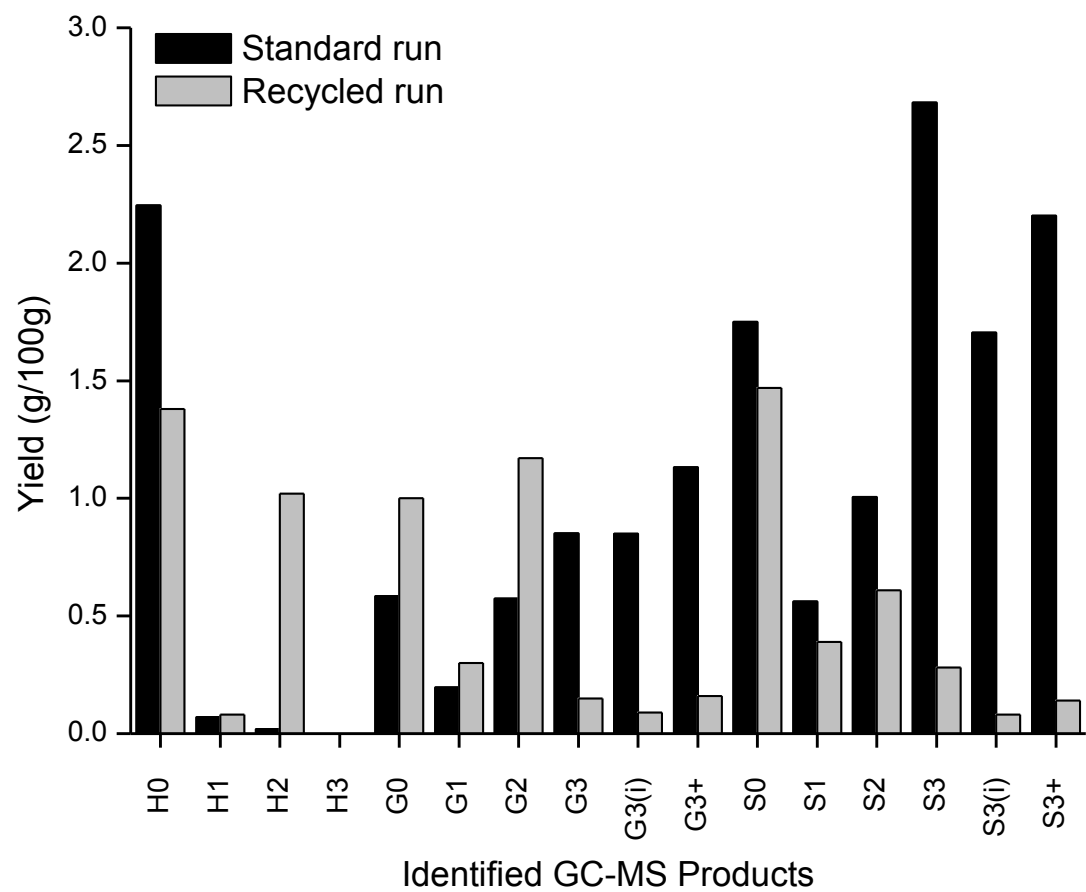


Figure 45: Recyclability testing of the Pt/alumina catalyst with ammonia lignin

### 3.2.2 Further Non-Catalytic Reaction Testing

Previously, the differences between products obtained under the standard conditions in the presence and absence of the Pt/alumina catalyst with the ammonia lignin were discussed. In the absence of catalyst, 6.8 % of product was yielded in comparison to the catalytic run which gave a yield of 16.4 %. This change in yield suggested that some depolymerisation was achievable without the aid of a catalyst. It was therefore essential to carry out further experiments to note what effect the alumina support and hydrogen gas had on the depolymerisation activity.

#### 3.2.2.1 Effect of Alumina Support

The alumina support was tested in the absence of the platinum metal to determine its stability and whether it had any catalytic activity. As discussed previously in section 3.1.3, alumina supports are known for their coking tendencies due to their acidic nature and ability to hydrate in water environments. Holleman and Wiberg investigated the stability of  $\gamma$ -alumina under aqueous phase reforming conditions using hot water and found that  $\gamma$ -alumina underwent phase transition to hydrated boehmite at 473 K and above, resulting in a lower surface area [69]. This occurred because  $\gamma$ -,  $\delta$ -, and  $\theta$ -alumina supports are prepared from dehydrated boehmite minerals so they are able to revert back to their hydrated form under hydrothermal conditions [70] as shown in Figure 46 [71]. The authors did however note that the presence of metal particles resulted in a significant decrease in the rate of boehmite formation, even with a low platinum metal loading of 1 wt. %. Furthermore, research has shown that the presence of oxygenates can enhance the stability of the support material by blocking the surface of the support with carbonaceous material thus preventing hydrolysis of the alumina [50]. Ravenelle et al suggested that the type of oxygen functionality did not influence the stabilisation of the support and that the different oxygenated molecules eventually formed the same surface oxygen species. It was also put forward that hydrolysis was prevented due to the oxygen functionalities coordinated with the unsaturated alumina sites thus preventing the water molecules from accessing the sites [44]. Additionally, the use of ethanol was proven to slow down the formation of boehmite crystals to some extent as well [44, 50].

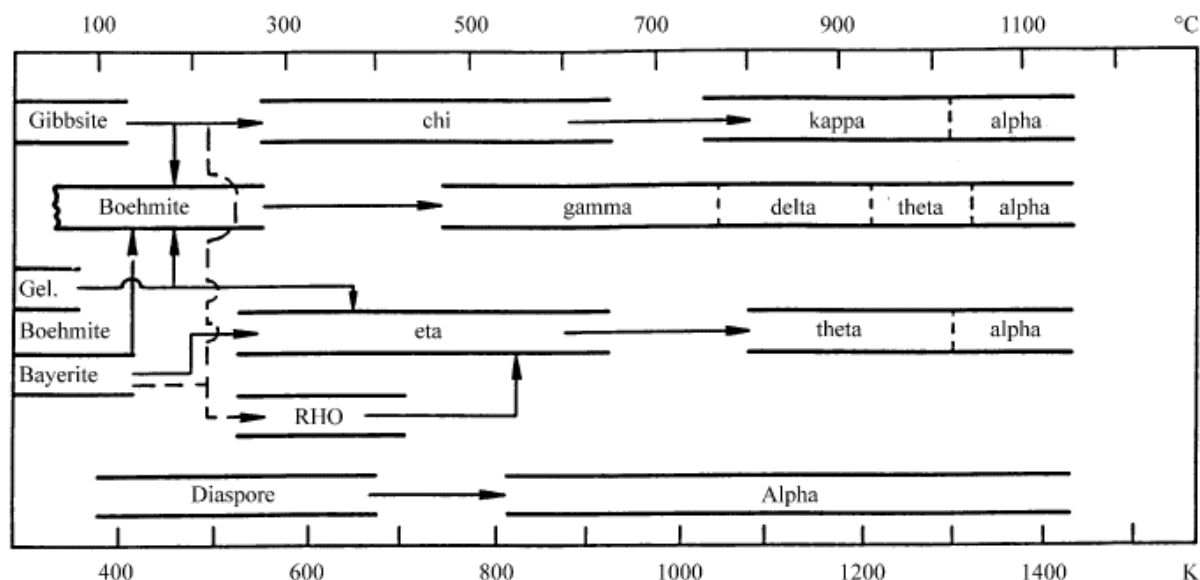


Figure 46: Thermal transformation sequence of aluminium hydroxides

Post-analysis of the alumina using XRD showed that the XRD diffraction pattern of the support post-reaction did not differ from that obtained prior to reaction. No boehmite peaks were observed and the support remained in the theta phase which suggested that hydration had not taken place during the reaction. There was also no significant change in the support surface area after reaction. Table 18 shows that the char production was lower when the alumina support was added to the reaction medium but it was not as effective as the metal catalyst. This result demonstrated the importance of the metallic function in not only increasing the overall monomeric yield, but in suppressing the condensation mechanism further than the support.

Table 18: Effect of char production with the presence of Pt/alumina

<b>Reaction</b>	<b>Weight (g/100g)</b>
<b>Standard reaction in H<sub>2</sub></b>	28.67
<b>Alumina support in H<sub>2</sub></b>	35.73
<b>No catalyst in H<sub>2</sub></b>	56.67

The GC-MS results shown in Figure 47 reveal that the alumina support had some catalytic activity and altered the depolymerisation reaction in comparison to the run without

catalyst. The overall yield of monomeric products obtained using the alumina support was slightly higher than the run without catalyst at 9.2 %, where there was generally more of each product produced except phenol. The S/G ratio with respect to 3-chained guaiacyl and syringyl units was found to be 1.62 which was fairly similar to the starting lignin S/G ratio of 1.86.

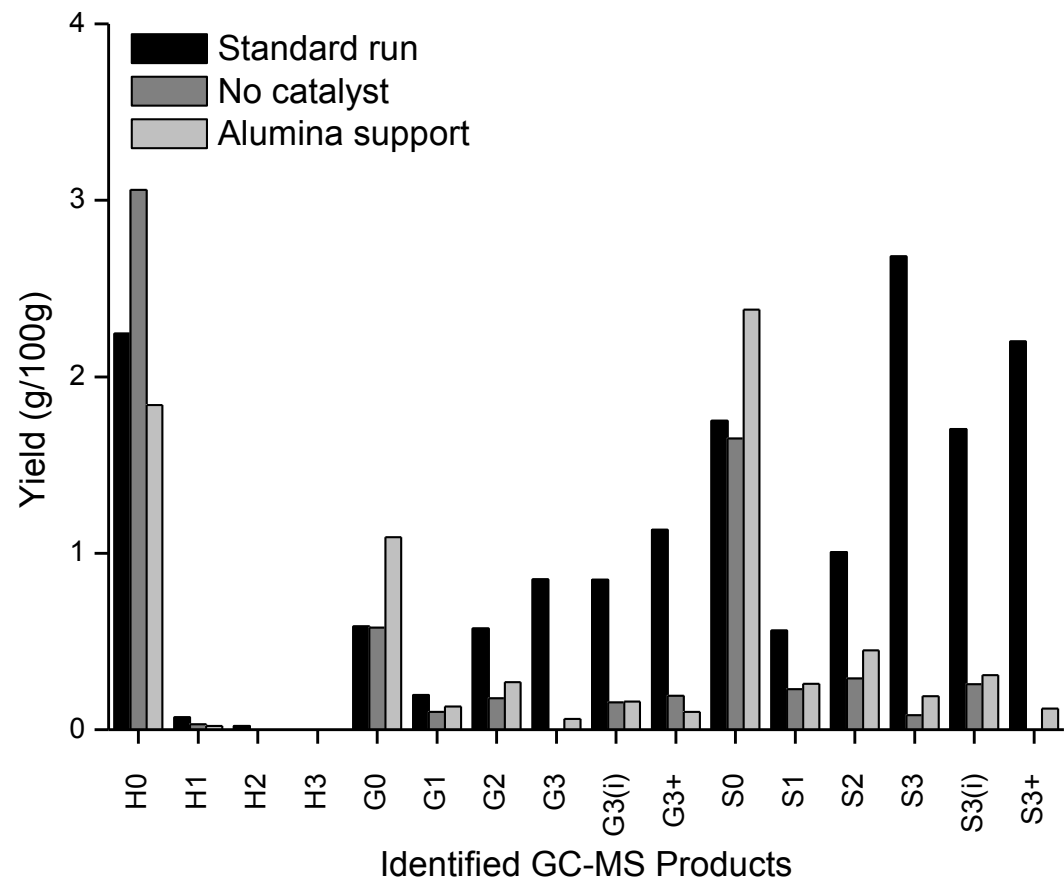


Figure 47: The effect of ammonia depolymerisation using the alumina support

### 3.2.2.2 Effect of Hydrogen

The reaction was altered to note the effect of hydrogen by replacing it with helium at 4 barg. Aqueous-phase reforming (APR) using Pt/alumina catalysts for the production of hydrogen and alkanes from biomass model compounds has been explored [72], but more recently APR has been used for the conversion of actual lignin samples [47]. These lignin studies showed that at temperatures of 498 K and helium pressures of 29 barg, they were able to achieve conversions of 9.8-14.6 % across four different types of lignins. In comparison, the reactions shown here (Figure 48), albeit at lower pressures than the literature, gave a much lower overall yield of products. The yields for the reaction with and without catalyst in helium were 5.4 % and 4.8 % respectively, where the catalyst aided the production of alkylated products and the experiment without catalyst favoured guaiacol and syringol production. Interestingly, the amount of phenol produced was similar for both experiments. In general, across all experiments in this chapter, phenol production plateaued at ~2.5 g/100g which suggested that an equilibrium had taken place. The use of phenol as a capping agent has also been explored so it is possible that some of the phenol product was also used in this way [73].

The char production was found to be lower when no catalyst was used in helium (35.3 g/100g) than it was when no catalyst was used in hydrogen (56.7 g/100g, see Table 18). This result was to be expected due to the increased product formation in hydrogen which causes simultaneous char formation. It is clear from these results that the presence of hydrogen (and pressure) is necessary to drive the reaction and give better overall yields.

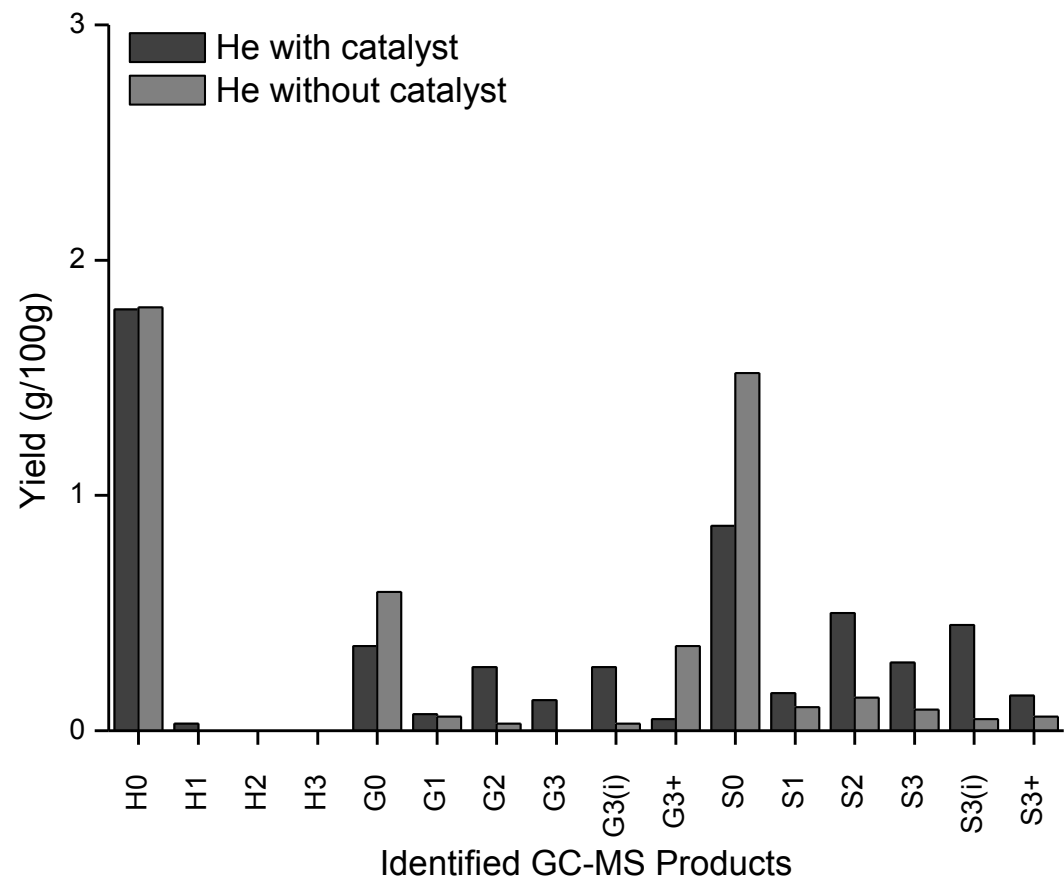


Figure 48: The effect on ammonia depolymerisation without hydrogen

### 3.2.3 Optimisation of the Standard Reaction Parameter Conditions

This section will present and discuss the results found when the parameters of the standard reaction were altered in terms of stirring speed, reaction time, temperature, pressure, solvent composition, pH, and the mass of catalyst or lignin used. Alternative precious metal catalysts on alumina were also investigated to see how the depolymerisation activity changed in relation to the active metal used.

#### 3.2.3.1 Effect of Stirring Speed

The stirring speed was altered to ensure that the reactions were run under kinetic control. Figure 49 shows an increase in monomer formation with increasing stirring speed from 500 to 1000 rpm, with a similar conversion value obtained at 1500 rpm. The experiments carried out at 500, 1000 and 1500 rpm gave yields of 6.7, 16.4 and 15.9 %. The larger change in monomer yield between 500 and 1000 rpm would suggest that the reaction was diffusion controlled at this point, whereas little difference between 1000 and 1500 rpm would suggest that the reaction then became kinetically controlled. Although an increase of the desirable monomer aromatics occurred, a consequence of this was an increase in the simultaneous condensation reactions to heavier unwanted molecules. This relates well to Table 19 which shows that the char formation increased with increasing speed from 23.3 to 33.3 g/100g. From these results, this would imply that 1000 rpm was the optimum stirring speed.

Table 19: Effect of changing the stirring speed on char production

<b>Stirring Speed (rpm)</b>	<b>Weight (g/100g)</b>
<b>500</b>	23.33
<b>1000</b>	28.67
<b>1500</b>	33.33

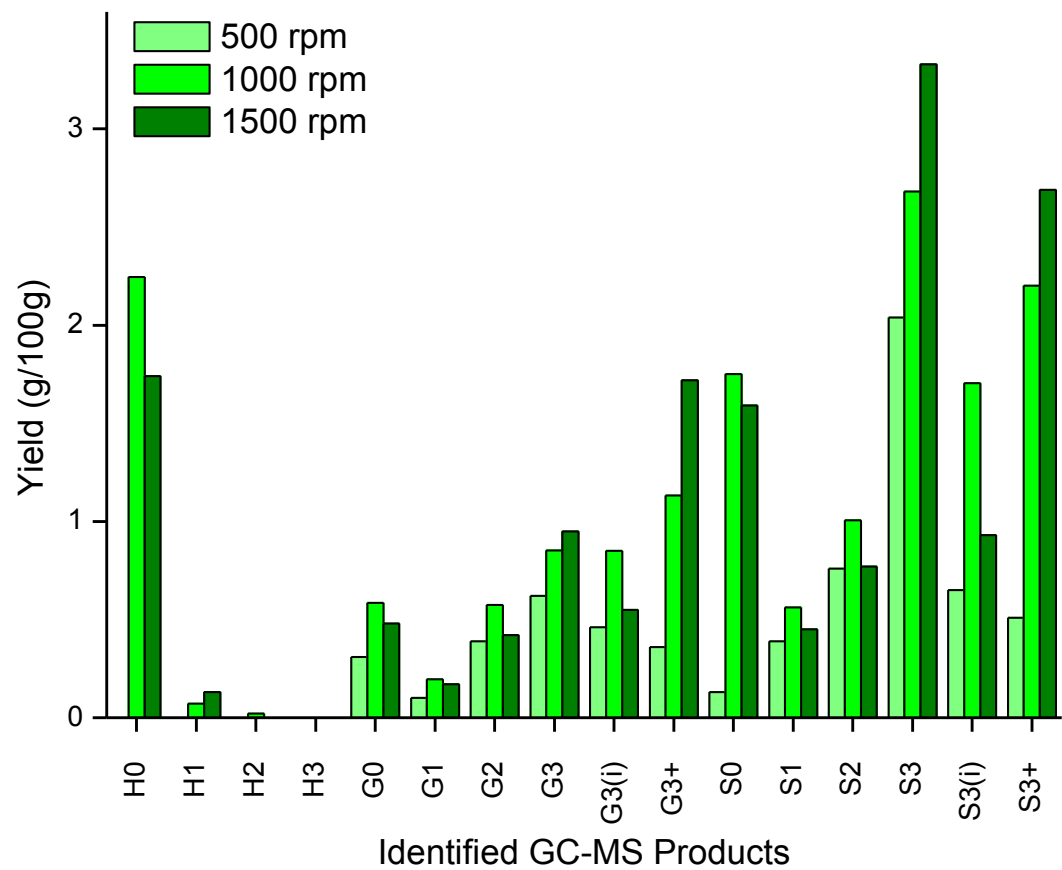


Figure 49: The effect of ammonia depolymerisation on altering the stirring speed

### 3.2.3.2 Effect of Reaction Time

Here, the reaction time of the reaction was altered from 1 to 6 h (plus 30 min for each reaction) to investigate how it affected the depolymerisation reaction. The maximum product yield was observed at 4 h and the effect of residence time is illustrated in Figure 50. This shows that the monomer yield first increased with increasing residence time from 1 to 4 h (12.5, 16.4 and 20.1 % respectively) but a further increase to 6 h saw a decrease in monomer production to 18.6 %. During the reaction, simultaneous cracking and condensation reactions will have occurred and after a certain amount of time, the cleavage of the more easily cleaved bonds (ether bonds or carbonyl groups) will have been cracked as much as possible. Once these depolymerisation steps were complete, further residence times likely favoured condensation of the intermediates. Table 20 shows that char formation systematically decreased with increasing time which suggests that longer reaction times were able to break stronger bonds. Furthermore, the residual pressure for the 6 h run after reaction at room temperature was noted to be 25 barg. This was 5 barg higher than all other reactions which suggested the formation of additional gaseous products which was not seen with the any other reactions in this chapter.

Table 20: Effect of changing reaction time with char production

<b>Reaction Time (hour)</b>	<b>Weight (g/100g)</b>
<b>1</b>	29.33
<b>2</b>	28.67
<b>4</b>	23.73
<b>6</b>	22.27

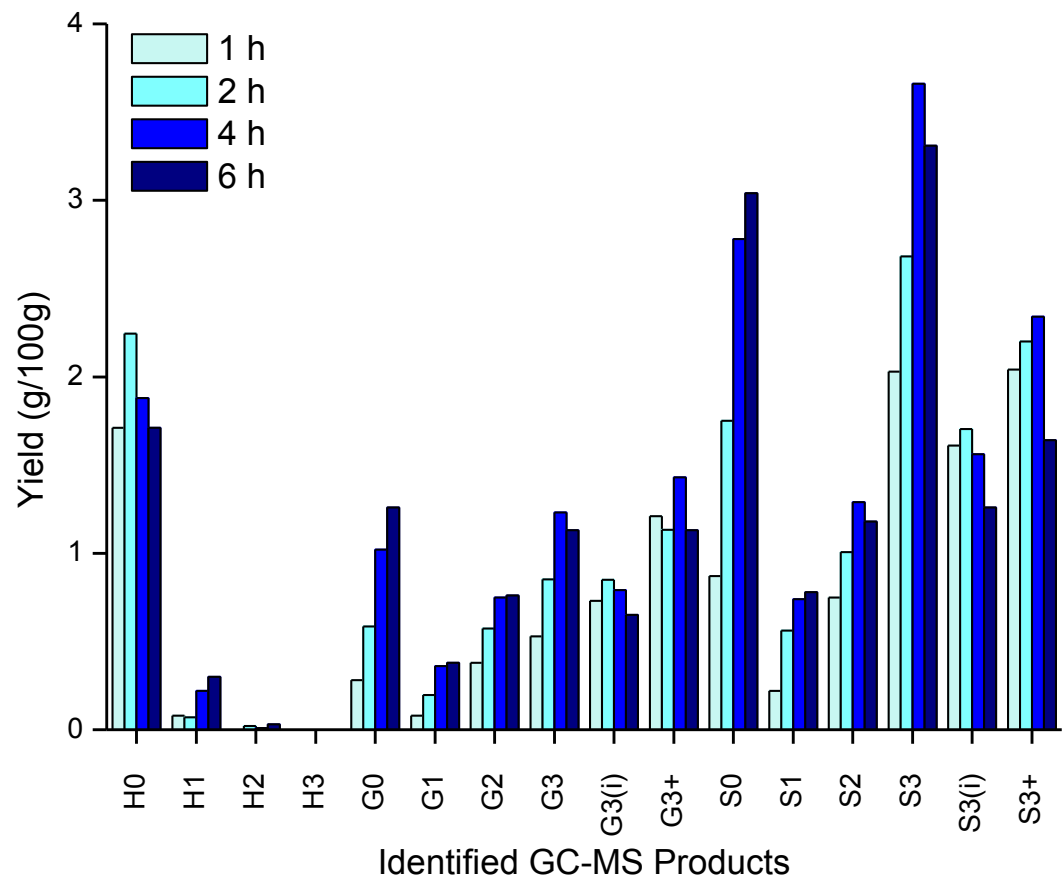


Figure 50: The effect of ammonia depolymerisation on reaction time

### 3.2.3.3 Effect of Temperature

In keeping with the Arrhenius equation (see Equation 15), it was expected that a rise in temperature would promote lignin depolymerisation, however literature has shown that an increase in temperature from 473 K to 553 K can reduce the yield of products obtained using hydrothermal liquefaction with ethanol [41]. A similar trend was also found elsewhere where the yield of products decreased with increasing temperature from 498 K to 573 K in ethanol-water [74]. The authors concluded that depolymerisation was more dominant at lower temperatures (<523 K) whilst the repolymerisation reaction became predominant at higher temperatures. However the results that we obtained and present below are in keeping with depolymerisation and cleavage of the weaker bonds being promoted with an increase in temperature (see Figure 51). Table 21 displays 2D-NMR results obtained through collaborative work. These results showed that there was a depletion of bonds in the post-reaction mix at both temperatures. Although the reaction at 523 K did convert the lignin molecule efficiently, the reaction at 573 K saw nearly a complete reduction in the  $\beta$ -O-4 linkages present suggesting that hydrogenolysis/HDO was more effective at the higher temperature. This may have occurred because lignin depolymerisation is endothermic and hence thermodynamically favourable at higher temperatures [75], but increasing the reaction temperature will have increased lignin solubility thus improving the monomer yield by further prompting the hydrogenolysis reaction [76]. With regards to ring hydrogenation, it was suggested in the literature that low temperatures favoured a ring hydrogenation pathway due to a higher hydrogen surface coverage in comparison to high temperatures which shifted selectivity towards deoxygenation [77], whilst hydrolysis studies elsewhere stated that the hydrolytic process did not alter the lignins aromaticity at all [78]. The latter statement was observed in this work where no loss of aromaticity was found at either temperature as outlined in our recent publication [1].

$$k = Ae^{-E_a/RT},$$

Equation 15: The Arrhenius equation

Table 21: Cleavage of linkages at 523 K and 573 K

	$\beta$ -O-4 (%)	$\beta$ - $\beta$ (%)	$\beta$ -5 (%)
<b>Ammonia Lignin</b>	15.25	3.11	0.83
<b>Reaction at 523 K</b>	2.52	1.62	0.38
<b>Reaction at 573 K</b>	0.10	0.47	0.05

Figure 51 shows the difference in the product distribution obtained between the two reaction temperatures. At 523 K, 10.1 % of alkylphenolic product was achievable in comparison to the standard run at 573 K which produced 16.4 % of products. There was no significant change observed in the general selectivities over the two temperatures but the reaction at 523 K compared to 573 K did selectively produce more phenol (23 % vs. 14 %) and slightly higher amounts of the G3+ (11 % vs. 7 %) and S3+ (21 % vs. 13 %) in relation to the other products. The phenol production was again seen to plateau at ~2.3 g/100g, and the G3+ and S3+ yield remained similar at both temperatures which suggested that its production and conversion had increased.

No increase in temperature from 573 K was carried out due to insufficient sample volume and negative literature feedback. It was shown by Mahmood et al that an increase in temperature from 573 to 623 K lowered the monomeric yield. The authors showed that an increase from 573 to 623 K greatly reduced the yield of monomeric product obtained and gave a marked increase in the condensed fraction [78]. They explained that this change in reaction selectivity was due to the presence of prominent dehydration and crosslinking reactions, similar to the condensation reaction example given in the previous chapter (see section 3.1.3). This result also relates well to the TGA data presented in section 3.1.1.4, where the lignin was found to condense at elevated temperatures.

With complete  $\beta$ -O-4 cleavage it could be expected that the yield should have increased more dramatically but it is likely that recombination to condensed structures was an issue, especially at higher temperatures, so this had a negative effect on the monomer yield. This observation would indicate that other parameters such as solvent and pressure have a larger impact on the lignins ability to depolymerise effectively. There is clearly a competition between the cracking of the lignin structure and how fast it reforms to unwanted condensed structures so it is therefore necessary to investigate ways in which this can be reduced through capping mechanisms.

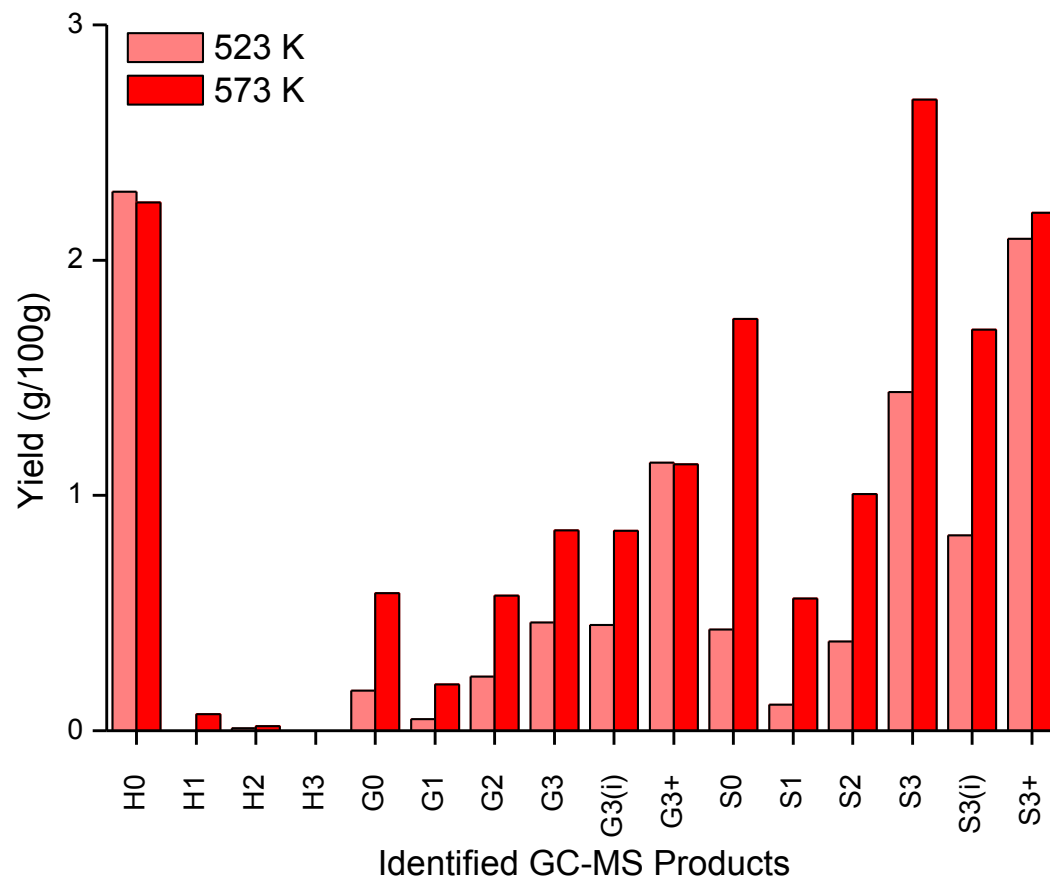


Figure 51: The effect of ammonia depolymerisation at 523 K and 573 K

#### **3.2.3.4 Effect of Hydrogen Pressure**

The effect of hydrogen pressure was studied to see how it affected the depolymerisation reaction (see Figure 52) and char production (see Table 23). In the literature, higher p-cresol conversion with increasing hydrogen pressure was reported and attributed to an increase in hydrogen availability [77]. In Figure 52 there is a clear increase in the yield of each product with increasing hydrogen pressure. The yields obtained for 0, 10, 20 and 30 barg hydrogen pressure were 5.7, 11.8, 16.4 and 18.9 % respectively.

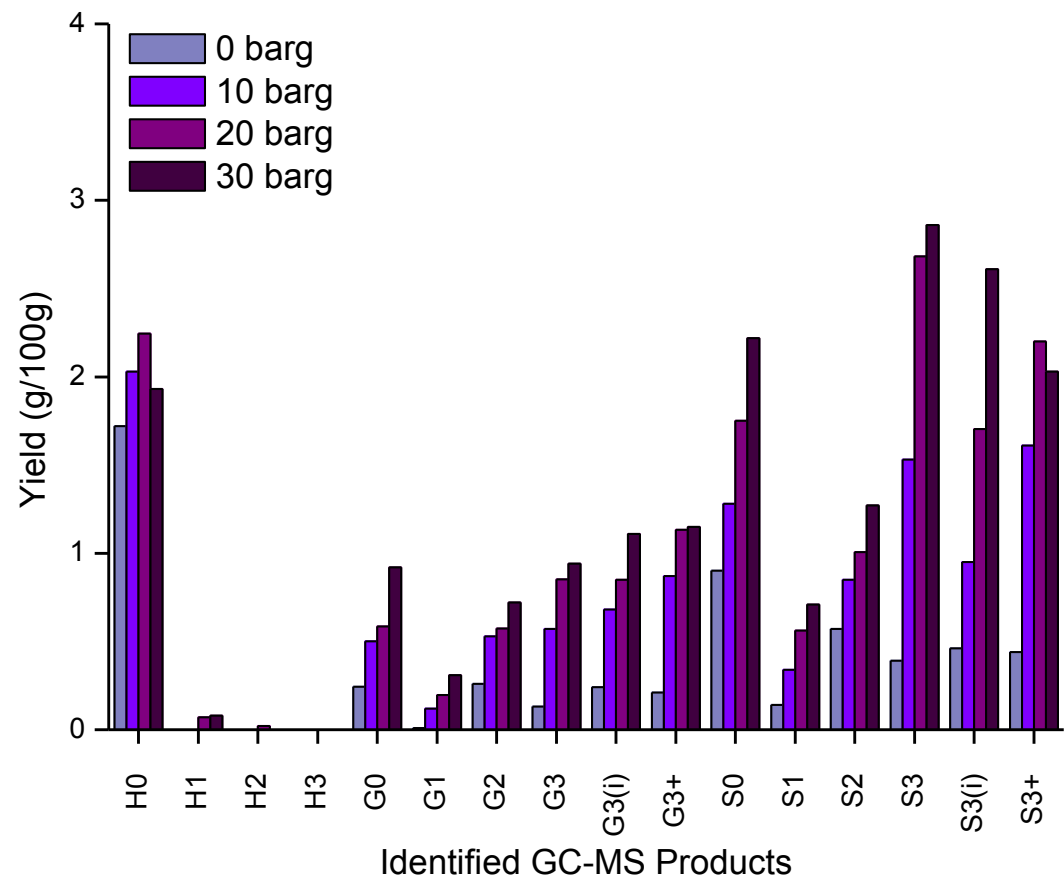


Figure 52: The effect of ammonia depolymerisation with increasing hydrogen pressure

Assuming that all reaction parameters were the same with the exception of hydrogen pressure, an estimated order of reaction with respect to hydrogen pressure could be calculated, where the rate was substituted for the alkylphenolic yield of product. The natural logs of the yields and each corresponding pressure are tabulated in Table 22:

Table 22: Natural logarithm of hydrogen pressure and monomeric yield

<b>ln (pressure)</b>	<b>ln (monomeric yield)</b>
0	1.7
2.3	2.5
3.0	2.8
3.4	2.9

From the table above it is clear that there is a change in the monomeric product with increasing hydrogen pressure and when plotted, this gives an order of 0.4 with respect to hydrogen pressure. This implies a typical dissociative adsorption of hydrogen on the platinum with it being the less strongly bound reactant. The total yield of char products found in the heavy fraction (see Table 23) also decreased with increasing pressure which suggested that the higher pressure conditions also suppressed repolymerisation of the monomers.

Table 23: The effect of increasing hydrogen pressure on char production

<b>Hydrogen Pressure (barg)</b>	<b>Weight (g/100g)</b>
<b>0</b>	41.87
<b>10</b>	34.27
<b>20</b>	28.67
<b>30</b>	23.33

### 3.2.3.5 Effect of Solvent Composition

Low monomer yields and condensation problems are strongly associated with poor solubility of the lignin in the aqueous solution so increasing the organic solvent proportion

should hold obvious advantages [44]. The use of alcohols during depolymerisation reactions can be used to aid solubilisation by generally increasing dissolution of the lignin and/or by acting as a capping-agent [48]. Literature reports that protonic polar solvents (alcohols) exhibit a larger dissolving capability than non-polar solvents like cyclohexane, and that solvents with more hydroxyl groups are also better for lignin dissolution [46]. The use of methanol-water for the valorisation of lignin has therefore been explored in this project where typical experiments were carried out using 50:50 v/v mix. This section aims to determine which solvent composition provided the best environment to obtain maximum monomer yields.

Firstly, the ammonia lignin was added to various compositions of methanol-water at room temperature to determine its initial solubility. As shown in Figure 53, the lignin solubility increased with increasing methanol content as expected. Research has shown that cleavage of the lignin ether linkages occurs during this solubilisation process either by shortening the polymer chain or by increasing its polarity [48]. An increase in organic solvent should therefore also lead to increased monomer production as a direct result.

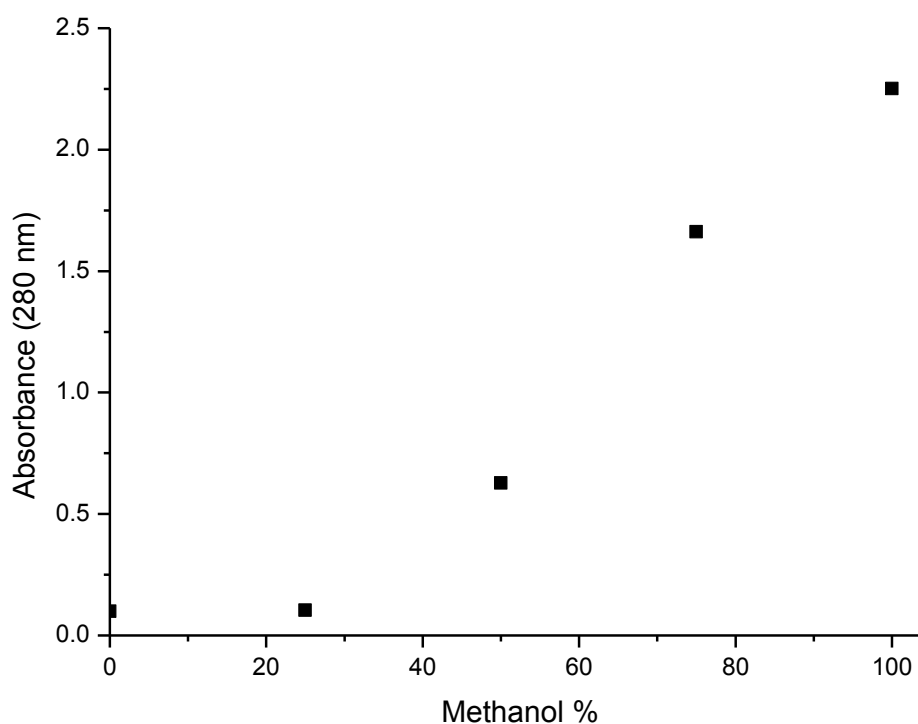


Figure 53: Solubilisation of ammonia lignin in methanol-water at room temperature

With increasing temperature, it was expected that the lignin would dissolve into aqueous solution at a faster rate as shown by Zakzeski et al [48]. The reaction temperature of 573 K used here will bring the methanol component of the solvent mix to its supercritical point (513 K, 79 barg). In general, when a gas and liquid mixture are heated, thermal expansion causes the liquid to become less dense and the gas to become denser. At the critical point, these two densities become equal and they lose their distinction. The advantages of using supercritical reaction media in lignin conversion include faster mass and heat transfer, liquid-like density and dissolving power, and gas-like diffusivity and viscosity [79]. Lignin has been shown to depolymerise in aqueous conditions under subcritical or supercritical conditions at relatively low temperatures (553-673 K), at 200-250 barg pressure with varying reaction times and lignin-water ratios [80]. At conditions close to or at water's critical point (647 K, 221 barg), the use of water holds advantages such as high solubility of organic substances, low viscosity, good thermal stability, and high concentration of  $H^+$  and  $OH^-$  at subcritical conditions [80]. Supercritical water is also known to aid reactions such as hydrolysis [81] but the principal disadvantages of using it include the high temperatures and pressures required to reach water's supercritical conditions which are not ideal from an economic point of view, as well as the increased probability of yielding significant amounts of char from the severe reaction conditions [82]. Other work has proposed the use of water mixed with other solvents and has shown that phenol, catechol, guaiacol, and methoxy phenols are formed from the hydrolysis of ether linkages, which can be further hydrolysed at the methoxy groups [80]. The benzene ring has also proven to be stable in these conditions [80]. A reaction medium of water mixed with organic solvent holds advantages such as increased lignin solubility and the prevention of cross-linking reactions [83, 84]. Research has been carried out using water-acetone [43], water-phenol [82] and water-ethanol [85] mixtures with varying success.

Figure 54 shows the effect of changing the solvent composition of the methanol-water from 100 % water to 100 % methanol. The use of 100 % water was observed to be less effective than the methanol-water co-solvent for higher overall product yields. The conditions used here were not severe enough to cause the water to reach its supercritical point so it is likely that lignin solubility was an issue when 100 % water was used, as illustrated in Figure 53. This also had an effect on the char production which was found to be 47.1 g/100g and one of the highest values of char produced from any parameter change. However, when the methanol concentration was increased from 0 to 100 %, the product yields increased from 11.2 to 43.5 % and the char formation decreased from 47.1 to 5.6 g/100g. The highest yield of 43.5 % was obtained at a concentration of 100 % methanol

which also gave the highest selectivity towards one particular product, namely the S3(OH) product (38 %), in comparison to all other runs. Song et al also observed that pure methanol gave better yields and a slight change in product selectivity compared to a mixture of water and methanol [46].

These results suggested that by using 100 % methanol, or a methanol-water mixture, it inhibited condensation whilst the absence of methanol resulted in the formation of recalcitrant residues. This could be because the addition of methanol helped dissolve not only the lignin but its degraded intermediates as well, thus reducing the char residue. The use of methanol could also lead to the stabilisation of free radicals generated during the depolymerisation by acting as a capping-agent [74].

Table 24: The effect of changing solvent composition on char production

<b>Methanol %</b>	<b>Weight (g/100g)</b>
<b>0</b>	47.07
<b>25</b>	38.93
<b>50</b>	28.67
<b>75</b>	5.60
<b>100</b>	5.60

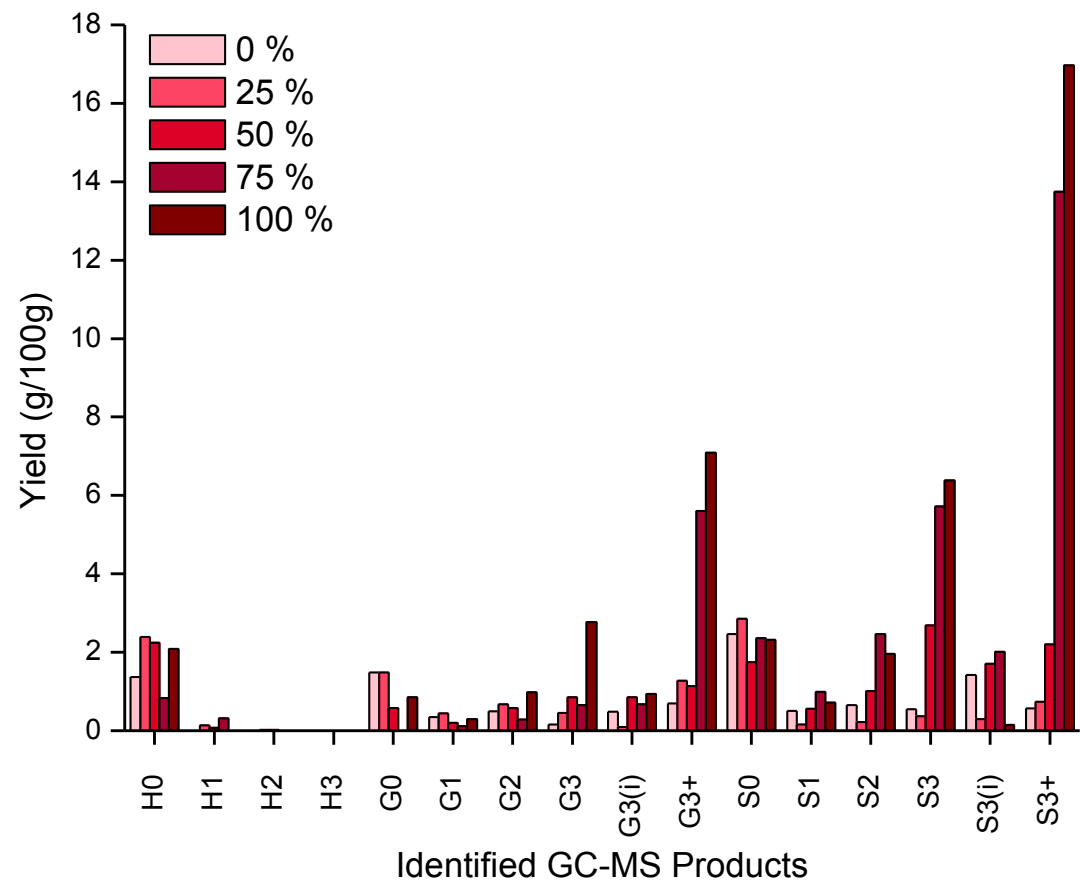


Figure 54: The effect of ammonia depolymerisation with changing solvent composition

The absence of ring hydrogenation in this study could be due to the solvent used during reaction. Product selectivities are known to be dependent on how the aromatic ring adsorbs onto the supported noble metal catalyst surface and the polarity of the solvent used is also thought to affect this. It was reported by Wen et al that phenolic compounds can adsorb onto the surface via a vertical or co-planar orientation. The vertical orientation occurs when the product is adsorbed via the hydroxyl group and this facilitates the removal of oxygen. If the product undergoes planar adsorption, the aromatic ring will saturate and cause ring hydrogenation. It has also been stated that when polar solvents are used, the vertical orientation of the hydroxyl group is favoured, whereas non-polar solvents cause co-planar adsorption and therefore ring hydrogenation [77]. This is demonstrated in Figure 55 [74]. Additionally, the presence of a methyl group on the ring is also sterically unfavourable so the aromatic molecule is therefore unable to adsorb flat onto the catalyst surface and hydrogenate [33].

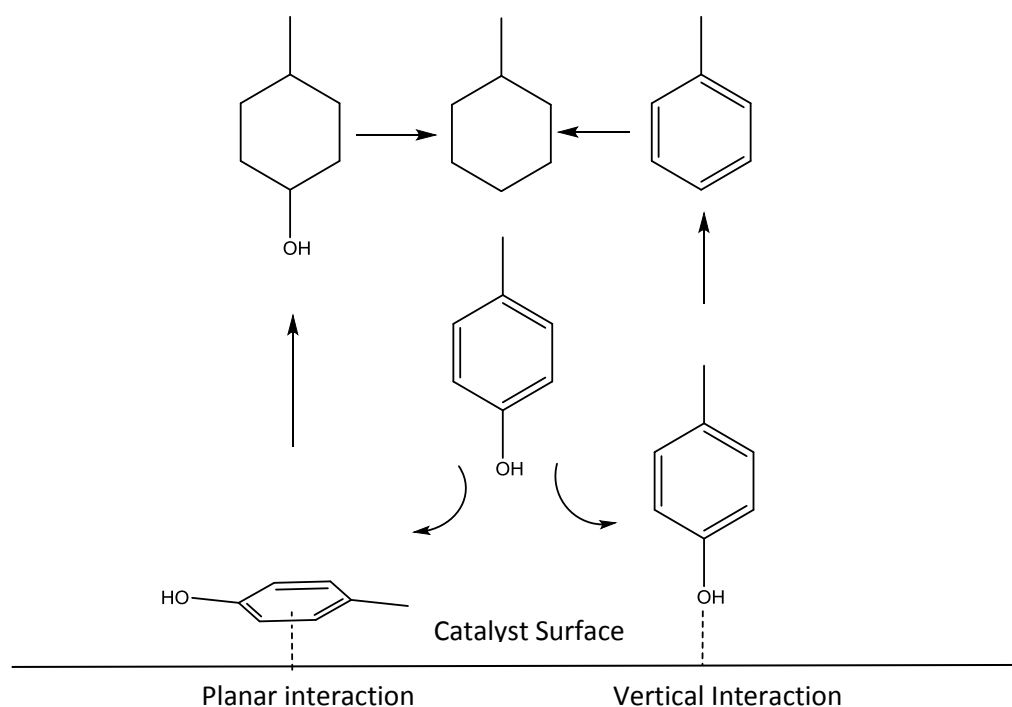


Figure 55: Adsorption behaviour of substituted phenols onto the catalyst surface

### 3.2.3.6 Effect of using Alternative Solvents

There are considerable amounts of research available using ethanol-water as a solvent for lignin conversion, where in general each highlights the ability of ethanol-water to aid the efficient depolymerisation of lignin and yield high monomer production. Ethanol is an

appropriate solvent for biomass conversion because of its low critical temperature and ability to enhance solubility due to its current use in the organosolv isolation process, where it solubilises the lignin fraction from the lignocellulosic biomass. Furthermore, ethanol is also produced from cellulose and hemicellulose fractions of lignocellulose thus promoting its low carbon footprint. However due to the availability of current literature using ethanol, it was important to explore other alternative solvents for lignin depolymerisation. Isopropanol (IPA) was therefore of interest due to its low cost and low environmental impact. Research using isopropanol details the use of IPA during solvent liquefaction, where IPA was used (amongst others) as a solvent with formic acid to convert lignin in air via solvolysis [86]. They found that a high yield of phenolics was obtained after treatment with formic acid and methanol or isopropanol, so the use of IPA here should prove advantageous for effective lignin conversion.

Figure 56 compares the product distribution obtained using methanol-water and IPA-water (50:50 v/v). The experiment using IPA-water yielded 24.3 % of monomeric products in comparison to 16.4 % obtained using the standard MeOH-water mix. The IPA-water experiment also significantly reduced the amount of char formation to 10.7 g/100g as shown in Table 25.

Table 25: The effect of using alternative solvents on char production

<b>Solvent used</b>	<b>Weight (g/100g)</b>
<b>MeOH-water</b>	28.67
<b>IPA-water</b>	10.66

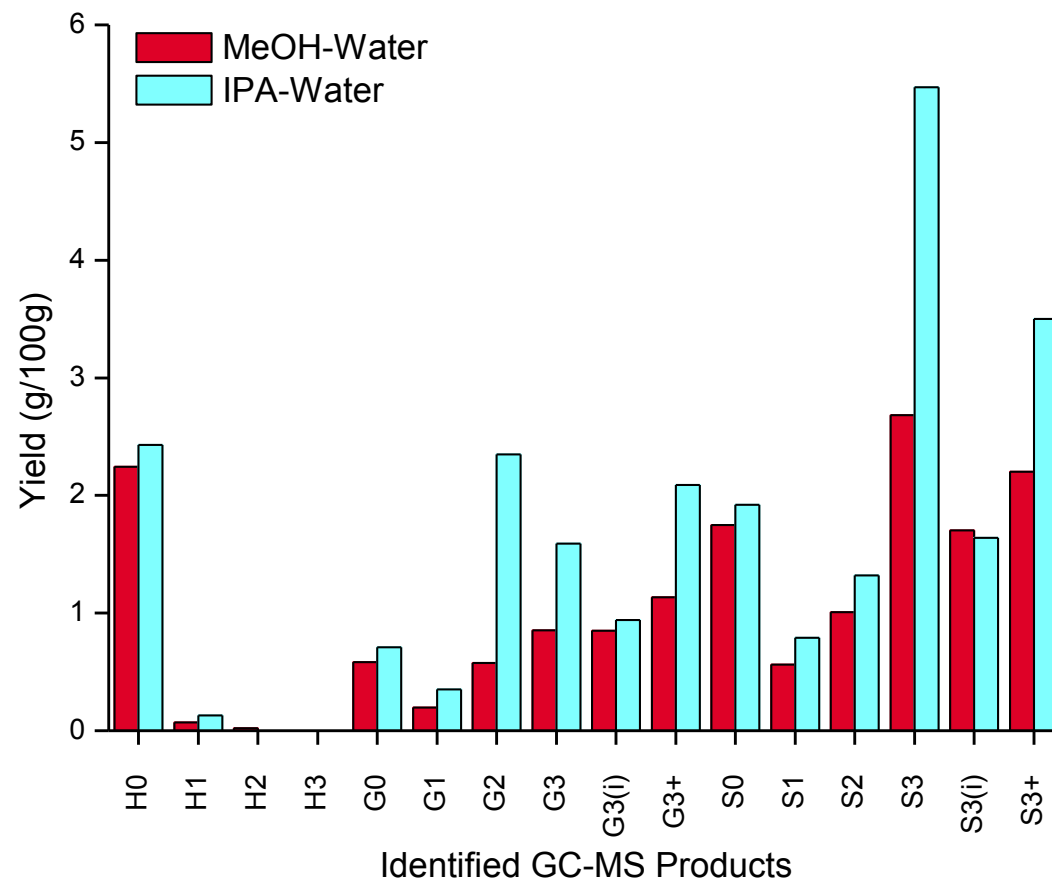


Figure 56: The effect of ammonia depolymerisation with alternative solvents

Isopropanol has a slightly lower critical point (508 K, 57 barg) than methanol so the solution will also have reached its critical point at the reaction temperature of 573 K. This will therefore have aided the depolymerisation reaction in a manner similar to that of methanol. Nevertheless IPA being a better solvent than methanol was slightly surprising given that IPA is less polar, with a lower ability to dissolve lignin and solubilise water. However it is possible that some IPA underwent catalytic dehydrogenation to acetone under the standard conditions to give an IPA-acetone-water mix during the reaction. Acetone has already proven useful for dissolving the lignin and its heavier products as shown during the sample preparation stages in section 2.3.2, so it is possible that this mix promoted dissolution of the lignin and its intermediates. Moreover, IPA is also known to donate hydrogen during its dehydrogenation to acetone. The use of hydrogen donor solvents (HDSs) were first used in coal liquefaction to stabilise free radicals that would otherwise form char [87] so it is likely that this addition of hydrogen reduced repolymerisation of the lignin by stabilising reactive phenols or reaction intermediates, hence resulting in a low char yield. Kim et al compared IPA against tetralin and found that the IPA system showed higher selectivity to alkylated products than the tetralin system due to the higher hydrogen donor capability of IPA. The authors concluded that HDSs were effective in converting lignin [88] and this would be in agreement with the results shown in Figure 56.

### **3.2.3.7 Effect of Changing the Reaction pH**

All reactions were typically carried out in a neutral environment but experiments were also attempted using an acidic and basic medium for comparative work (see Figure 57). In the case of the acidic reaction where HCl was added, the overall yield was 8 % with propylsyringol being the most abundant monomeric product followed by phenol. The char formation in the heavy fraction was 42.7 g/100g (see Table 26) which was significantly higher than that found with the standard run. It was noted during the post-reaction preparation stages that there was a substantial amount of solid material adhered to the bottom of the autoclave which proved difficult to remove and had not been observed with other experiments. This could be a result of phenolic species which were unable to dissolve into the acidic medium and react further, thus leading them to precipitate out of solution. In contrast, when the reaction was carried out in basic conditions using NaOH, the char formation remained low and similar to that obtained for the standard conditions (29.2 g/100g) and the product yield increased to 20.1 % when carried out in basic conditions using NaOH. The S-units (S0, S1 and S2) were the most abundant products but the basic

medium promoted hydrogenation of the propenyl double bond for both the G- and S-units, even when compared to the acidic conditions.

Table 26: The effect of changing pH on char production

<b>pH</b>	<b>Weight (g/100g)</b>
<b>Acidic</b>	42.67
<b>Neutral</b>	28.67
<b>Basic</b>	29.20

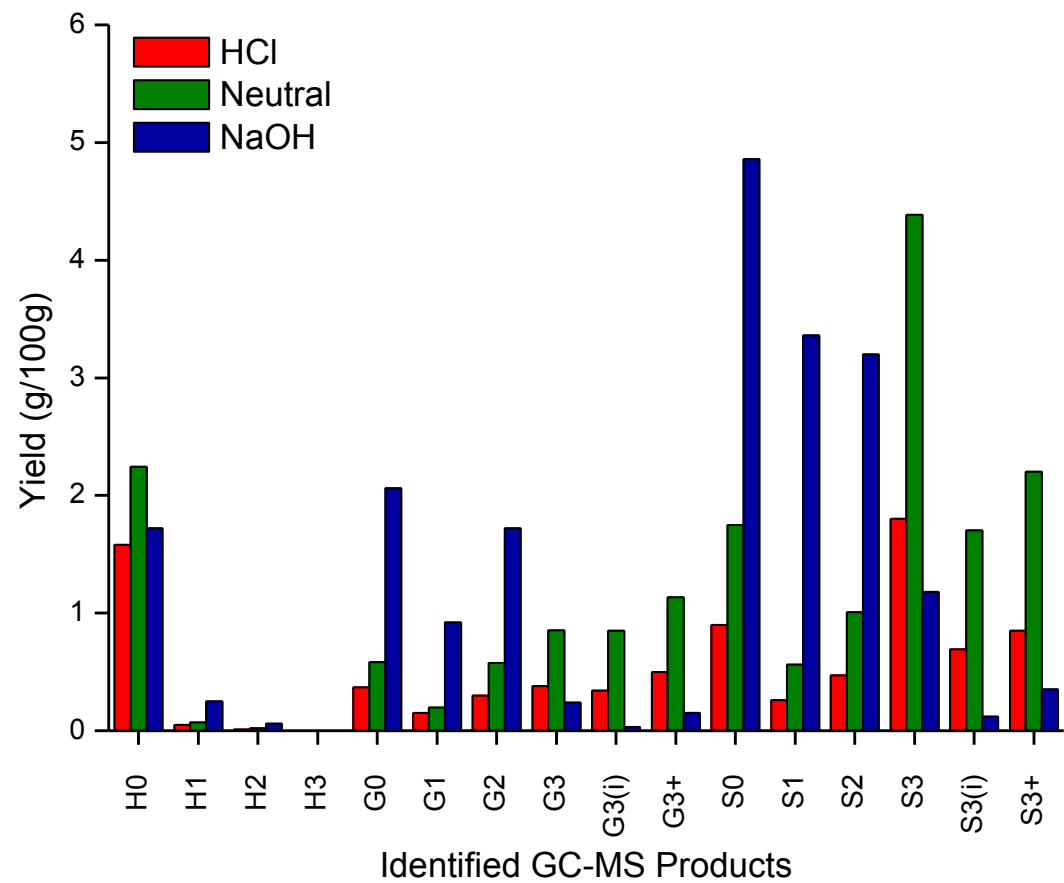


Figure 57: The effect of ammonia depolymerisation using different pH environments

These results showed that by merely changing the pH of the reaction medium, the product distribution could be altered to great effect. In terms of selectivities, the three conditions produced different products with respect to the length of the alkyl chain. All reactions, acidic, neutral and basic favoured products with no alkyl chain (48, 37 and 49 % respectively), and the acidic and neutral conditions created more propyl (25 and 32 %) and propyl + (12 and 16 %) products. The basic reaction in comparison produced little propyl and propyl + monomers, but favoured methyl- and ethyl-type products.

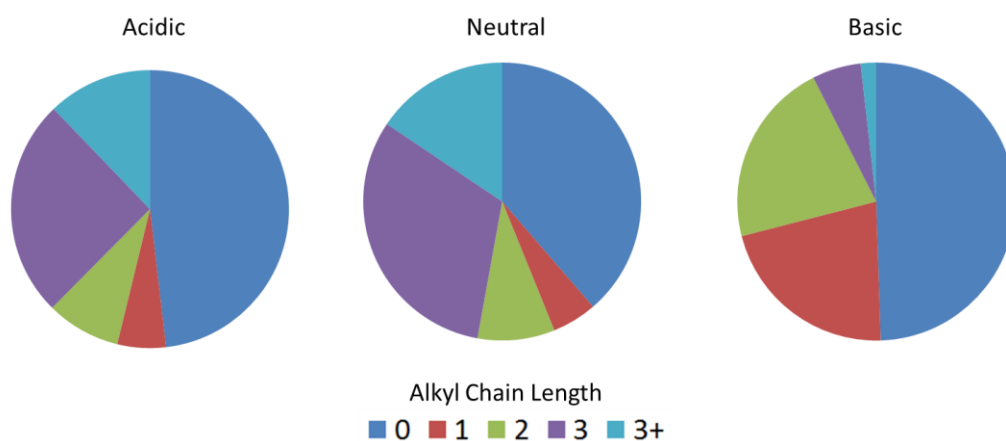


Figure 58: Product selectivities using different pH conditions

Other work also noted the effect of changing pH where the addition of acid or base was referred to as a co-catalyst [48]. They found that the  $H_2SO_4$  co-catalysed reaction with Kraft lignin and Pt/alumina produced mostly guaiacol, followed by ethylcatechol and methanol via acid-catalysed hydrolysis of the aryl-alkyl ether of ethylguaiacol. (This selectivity to guaiacol was due to the high G-unit content in the starting material.) The total amount of monomers obtained in this experiment (17.6 %) was an order of magnitude more than their previous runs and they also found that no solid char was formed. In comparison, their use of Pt/alumina and NaOH resulted in a lower yield of 12.8 % and a different product distribution to that obtained with the  $H_2SO_4$  reaction. Guaiacol was still the main product but they also identified benzyl alcohols which were not observed for the acidic reaction. They concluded that the acidic reactions led to increased C-O bond cleavage via hydrolysis which limited the formation of ethyl ethers and free phenolics, and gave products with intact propyl side-chains, whereas the NaOH-catalysed reaction gave ethyl- and methyl-substituted aromatics. Although the overall yields were opposite to those observed here, the product distribution did follow the same trend with respect the type of products obtained. Interestingly, when the authors carried out same experiments with

organosolv lignin, the overall yields were similar to the results found in our study. Characterisation of the organosolv lignin showed a higher syringyl content than the Kraft lignin which was comparable to the ammonia lignin syringyl content used here. For both pH reactions, syringol-type products were mainly obtained, with the H<sub>2</sub>SO<sub>4</sub>-catalysed reaction giving an overall product yield of 9 % and the NaOH-catalysed reaction giving a larger yield of 11.6 %. These conflicting results ultimately showed that the starting lignin material also had an effect on the product composition when altering the pH and it was decided that neutral conditions were best suited to produce the desired alkylated monomers.

### 3.2.3.8 Effect of Catalyst Mass

The amount of catalyst used in a reaction can affect the reaction rate, the products produced and in commercial applications, the economics of the process. With decreasing lignin to catalyst ratios, it was expected that the monomer yield would increase. 0.05, 0.1 and 0.2 g of catalyst was used under the standard conditions which gave lignin to catalyst ratios of 10, 5 and 2.5. Figure 59 shows that there was variation in the production distribution depending on the amount of catalyst used. The yields obtained were 9.7, 16.4 and 16.85 % for the 0.05, 0.1 and 0.2 g experiments respectively. When the catalyst mass was halved (0.05 g), the depolymerisation yield also halved. This effect was similar to that obtained in the absence of the catalyst where products with no alkyl chain were mainly produced, however there were more alkylated products observed here which was attributed to the presence of the catalyst. Alternatively, when the catalyst concentration doubled, the overall monomeric yield did not double and there was in fact no significant change observed. This would suggest that the overall yield was not able to go above 17 % with respect to the catalyst alone. The selectivities for both reactions did however alter, where the standard run using 0.1 g of catalyst gave a higher selectivity of 16 % to S3 products and lower selectivities to H0 and S3+ (14 and 13 %) respectively, whereas the selectivities when 0.2 g of catalyst was used changed in terms of giving more G3+-type products (22 %) and less propenyl products (GS(i)/S3(i)). Hydrogenation of the double bond on the alkyl chain occurred more favourably due to the higher availability of catalyst and active sites for hydrogenation activity. Table 27 shows that there was a change in the amount of char found in the heavy fraction, where it reduced from 29.6 to 17.3 g/100g with increasing catalyst concentration. This indicated that an increase in catalyst availability suppressed condensation reactions and was deemed a favourable observation.

Table 27: The effect of changing the catalyst mass on char production

<b>Catalyst Mass (g)</b>	<b>Weight (g/100g)</b>
<b>0.05</b>	29.60
<b>0.1</b>	28.67
<b>0.2</b>	17.30

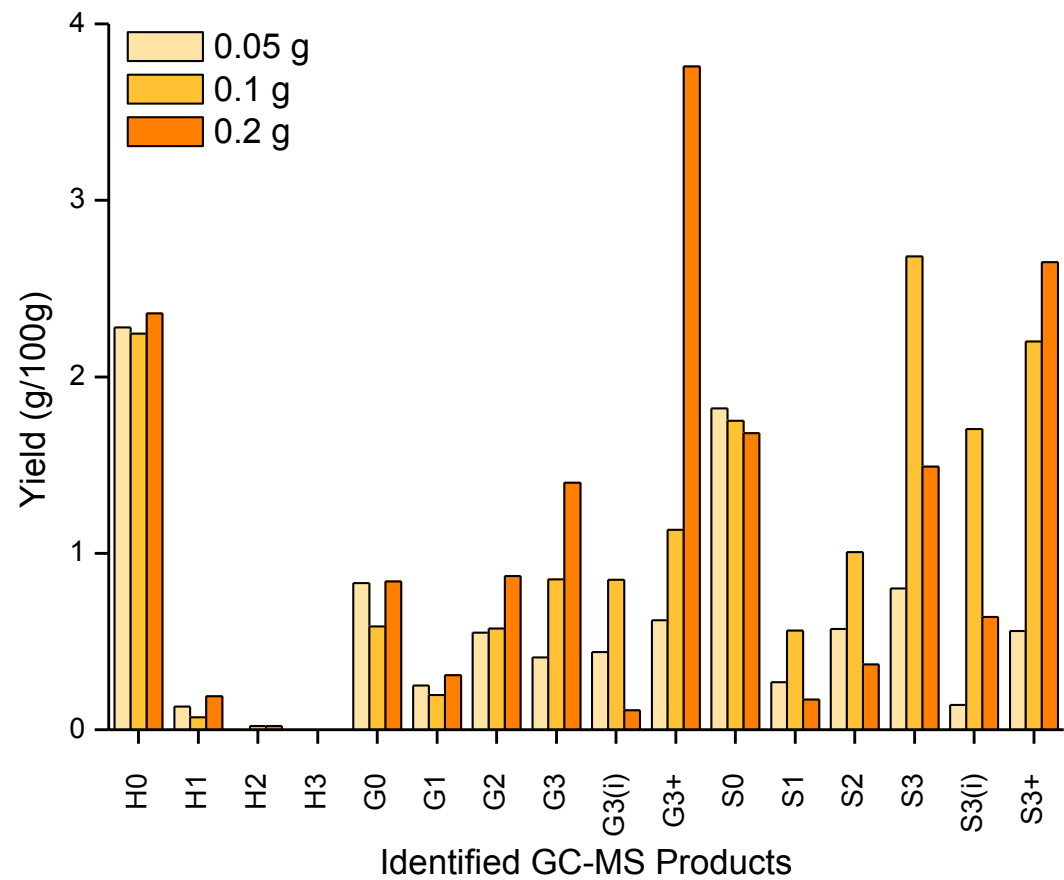


Figure 59: The effect of ammonia depolymerisation using different masses of catalyst

### 3.2.3.9 Effect of Lignin Mass

Effects of the lignin mass on product distributions were also investigated, comparing 0.25 and 0.5 g of lignin under the standard conditions. The lignin to catalyst ratio studied here was 1.25 and 5 respectively. The data in Figure 60 shows that an increased lignin concentration led to a slightly higher product yield which increased from 13.9 to 16.4 %. Work demonstrating a similar effect with increasing lignin concentration found that various substrate concentrations caused little difference to their yields of product [78] but work elsewhere indicated the opposite, with higher lignin concentrations leading to lower product yields [74]. Due to the limited amount of ammonia lignin sample, only a limited number of experiments were possible. It is possible that at higher lignin concentrations, agglomeration could have occurred due to insufficient amounts of solvent being available to dissolve the lignin fully and give a homogeneous solution/ suspension of lignin. Agglomeration would have caused condensation reactions to become more favourable and this would have given a decrease in monomer yield and an increase in char formation. The char residue value here did not change significantly (29.6 and 28.7 g/100g) but it is thought that the char volume would increase with increasing lignin mass.

Table 28: The effect of changing the lignin mass on char production

<b>Lignin Mass (g)</b>	<b>Weight (g/100g)</b>
<b>0.25</b>	29.60
<b>0.5</b>	28.67

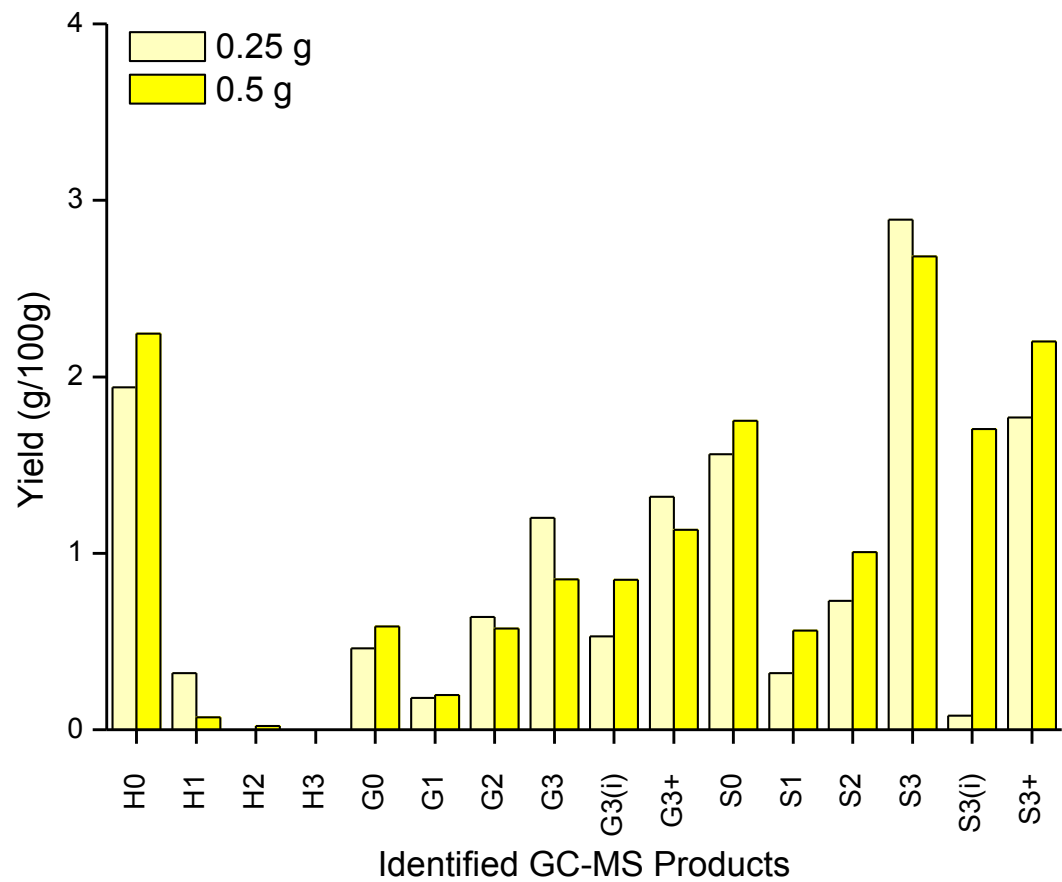


Figure 60: The effect of ammonia depolymerisation using different masses of lignin

### 3.2.3.10 Effect of Alternative Precious Metal Catalysts

Three precious metal catalysts were used in this section to give an initial study on the effects of changing the active metal on the alumina support. The catalysts used were the 1 wt. % Pt/alumina catalyst which was commercially purchased, in comparison to ‘in-house’ catalysts, namely the 1 wt. % Ir/alumina and 1 wt. % Rh/alumina catalysts. Below, the alumina-supported catalysts have been compared, and their depolymerisation activity represented in Figure 61.

Table 29: The effect of changing catalyst on char production

Catalyst Used	Weight (g/100g)
1 wt. % Pt/alumina	28.67
1 wt. % Ir/alumina	38.67
1 wt. % Rh/alumina	29.47

As shown in Figure 61, the product distribution varied considerably with respect to the active metal employed. The overall monomeric yield was 16.4, 9.3 and 19.9 % and the char production was 28.7, 38.7 and 29.5 g/100g for the Pt-, Ir- and Rh/alumina catalyst respectively. This data suggests that the iridium catalyst favoured condensation reaction pathways which will have likely hindered the alkylphenolic production as a result. Its activity in terms of monomer production and char yield was very similar to that observed with the alumina support reaction shown earlier (see section 3.2.2.1) which would imply that the Ir metal did not alter the reaction. The Pt and Rh catalysts gave relatively similar results but the Rh catalyst seemed to favour cleavage of the terminal gamma-group (S3+) which initially suggested that it was more effective at cleaving alkyl-aryl bonds. It is important to note that this benefit could also have been due to a metal loading effect because the Rh catalyst was found to have a higher dispersion value in comparison to the platinum which therefore meant that more metal was available to facilitate the reaction [54]. This phenomenon was observed for some of the product yields as shown in Table 30, where the yields approximately doubled when the Rh/alumina catalyst was used, with the exception of S1.

Table 30: Effect on monomer yield from using Pt and Rh metal

	<b>Pt/alumina</b>	<b>Rh/alumina</b>
	<b>yield</b>	<b>yield</b>
	<b>(g/100g)</b>	<b>(g/100g)</b>
<b>G1</b>	0.2	2.9
<b>G2</b>	0.6	1.2
<b>G3</b>	0.9	1.4
<b>S1</b>	0.6	0.7
<b>S2</b>	1.0	1.9
<b>S3</b>	2.7	4.3

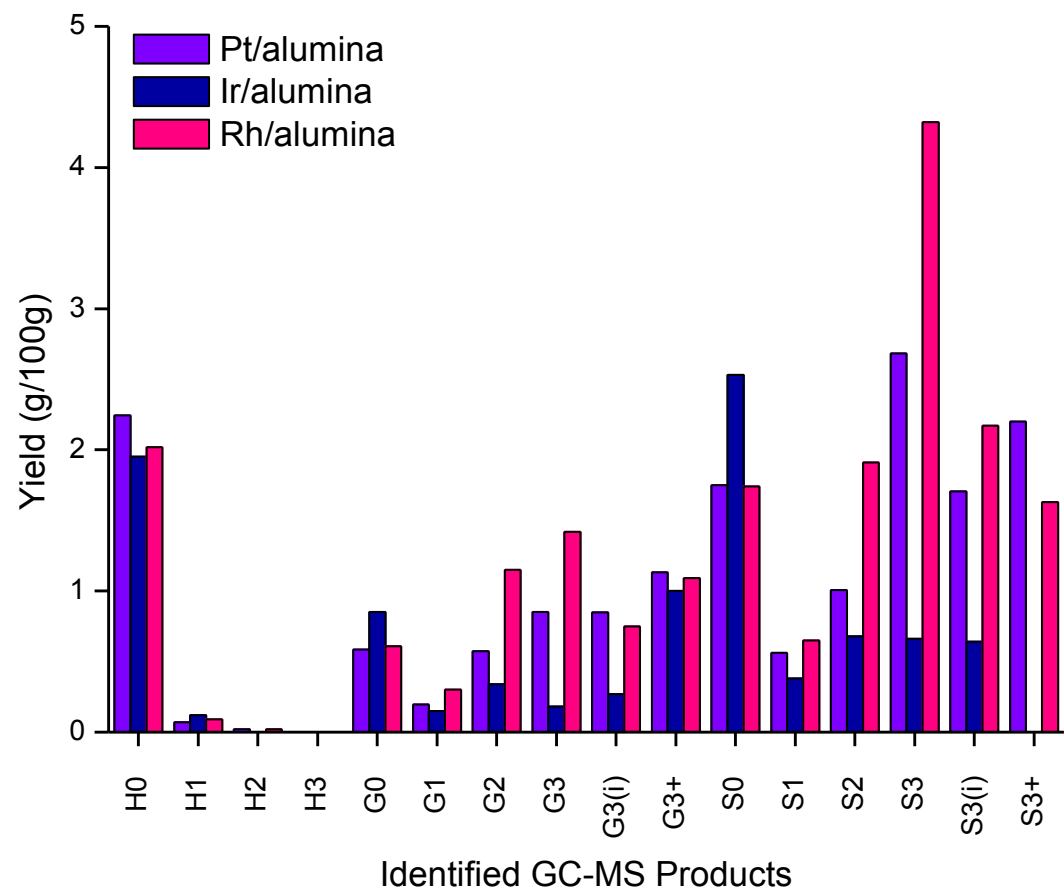


Figure 61: The effect of ammonia depolymerisation using alternative precious metals

With regards to the different product selectivities (see Figure 62), the platinum and rhodium catalysts gave a relatively similar product selectivity overall, where both catalysts selectively favoured the production of S3 products. They did differ slightly with regards to the other products where the platinum catalyst selectively produced S3+ (13 %), H0 (13 %) and S0 (10 %), and the rhodium catalyst selectively formed G3 (11 %) and H0 (10 %). The Pt and Rh catalysts gave a similar ratio of 2.05 and 2.16 with respect to three-chained guaiacyl and syringyl units which was only slightly higher to that value given for the starting ammonia lignin. This is in comparison to the iridium catalyst which gave a very different selectivity plot and favoured non-alkylated products such as syringol (26 %) and phenol (20 %), but produced more three-chained guaiacyl units in comparison to syringyl, with a lower ratio of 1.26.

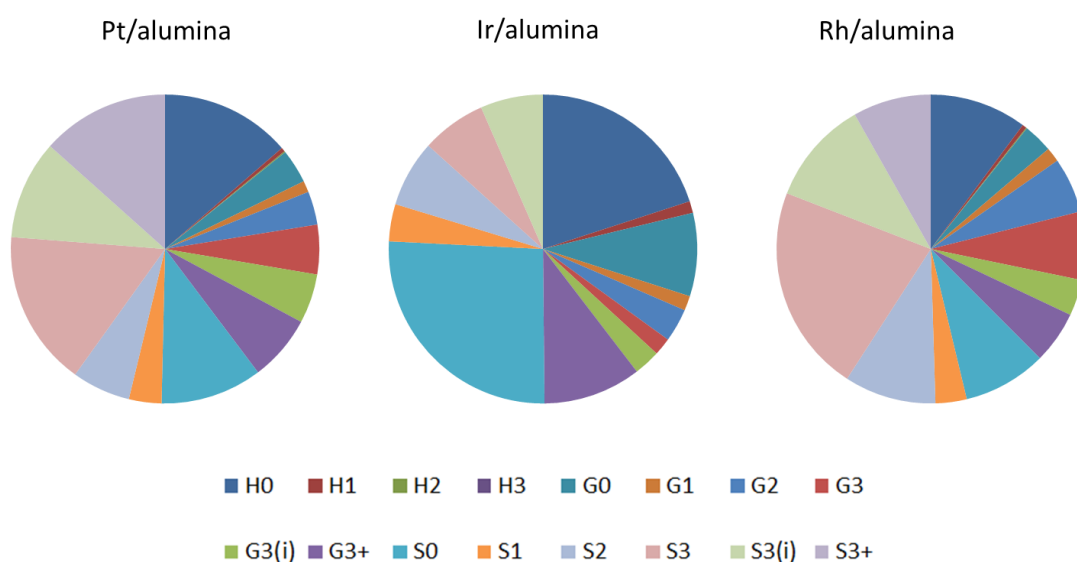


Figure 62: Product selectivity between the three alumina-supported catalysts

Research which compares a range of catalysts under the same reaction conditions generally use model compounds as opposed to the entire lignin molecule [89-92]. Deoxygenation studies using model compounds and different types of catalysts have also generally shown that deoxygenation of the phenolic fraction was sensitive to high hydrogen consumption and high pressure [89, 93]. Demethylation of guaiacol to catechol using Pt catalysts was found to be a fast, favourable reaction during the HDO of guaiacol [90], whilst other authors have shown that coke was also readily formed in the presence of guaiacol and catechol [22]. Double-oxygen containing phenolics have a much higher chance of catalyst

poisoning over single-oxygen phenolics [94]. Coking on the catalyst surface was observed in this work, where the post-catalyst sample was black in colour. This could therefore potentially hinder the reaction fully or partially, or change the product selectivity to give products which maintained their aromaticity. A study aimed at catalysing the HDO reaction of guaiacol and phenol with Pt catalysts have shown that almost no phenol was hydrogenated due to the presence of guaiacol and this was attributed to catalyst deactivation via coking on the surface [91]. The demethoxylation of guaiacol to phenol at high selectivity has been observed using Rh catalysts, with no direct hydrogenation to 2-methoxy-cyclohexanol [91]. This was also recognised as being related to deactivation of the catalyst due to coke formation from the conversion of guaiacol and catechol [91]. Iridium catalysts have rarely been used for hydrogenation of phenols and its derivatives but work investigating the hydrogenation of lignin cresols and xylenols was found to be comparable, and in some cases superior, to platinum in promoting the cleavage of aryl-oxygen via hydrogenolysis [92].

Prior studies have concluded that supported metal hydrogenation catalysts were able to hydrogenate and deoxygenate phenolic compounds via consecutive hydrogenation of the ring and dehydration of the alcohol steps [93]. Although benzene can be favourably formed from the reaction of phenol at higher temperatures, this increase in temperature also led to a decrease in phenol conversion due to a decrease in surface hydrogen and phenol, and a negative activation energy. Hydrogenation also becomes thermodynamically limited at higher temperatures [93]. Foster et al. continued by stating that operating at modest hydrogen pressures could avoid complete hydrogenation of the aromatic ring and that phenolic compounds could be deoxygenated more selectively [93].

Based on this summary, the absence of ring hydrogenation from the standard run could be accredited to the laydown on carbonaceous material from the lignin which will be discussed in section 3.5. This could block active sites from being able to fully hydrogenate the aromatic ring. Furthermore, the added complexity of the system when using the entire lignin molecule will likely cause other reactions to occur before ring hydrogenation, whereas a simple model compound system has limited number of conversion possibilities so therefore has an increased chance of ring hydrogenation.

### 3.2.4 Summary of the Optimisation of Ammonia Lignin

The purpose of this section was to optimise the standard reaction conditions so that a high yield of alkylphenolic product was achievable with low char formation. The best condition found for each parameter change has been summarised in Table 31:

Table 31: Optimised conditions for each parameter change

<b>Parameter Change</b>	<b>Optimum Condition</b>
<b>Temperature</b>	300 °C
<b>Pressure</b>	30 barg
<b>Solvent Composition</b>	100 % methanol
<b>Alternative solvent</b>	IPA-water mix (50:50 v/v)
<b>pH</b>	Neutral
<b>Stirring speed</b>	1000 rpm
<b>Residence time</b>	4 h
<b>Catalyst mass</b>	0.2 g
<b>Lignin mass</b>	0.5 g
<b>Catalyst</b>	1 wt. % Rh/ alumina

Table 32 summarises the results given in this section with regards to alkylphenolic yields and char production from the light and heavy fractions respectively. The autogeneous pressure for each reaction is given, as well as the molecular weight and polydispersity changes observed with each reaction. On average, a 70 % decrease in the molecular weight and a 24 % decrease in the polydispersity value was obtained in comparison to the starting ammonia lignin. These decreases generally conformed to the values obtained for the alkylphenolic and char yields, where for example, an increase in pressure gave higher yields of alkylphenolics and lower yields of char production with an increase in the molecular weight change to lower molecular weights and more uniform polymers. When comparing all experiments carried out in this chapter, it is clear than when 100 % methanol was used as a solvent, with all other parameters remaining as standard, this yielded the highest monomeric fraction of 43.5 %. These conditions also limited char production with a value of 5.6 g/100g.

Table 32: Summary of optimisation results using the ammonia lignin

<b>Parameter Change</b>	<b>Autogeneous Pressure (barg)</b>	<b>Mw (Da)</b>	<b>Mw Decrease (%)</b>	<b>Ip</b>	<b>Ip Decrease (%)</b>	<b>Alkylphenolic Yield (g/100g)</b>	<b>Heavy Yield (g/100g)</b>	<b>Unidentified GC-MS Light Products (~g/100g)</b>	<b>Total Yield (g/100g)</b>
<b>Retest</b>	145	1213	69	1.95	20	14.44	28.67	5.76	48.87
<b>Recycled catalyst</b>	150	1329	66	2.08	13	8.34	26.93	8.37	43.64
<b>Alumina only</b>	140	1087	72	1.79	27	9.21	35.73	1.12	46.06
<b>He with catalyst</b>	100	1371	64	1.91	22	5.38	-	4.16	-
<b>He without catalyst</b>	110	1396	64	1.87	24	4.83	35.33	1.82	41.98
<b>523 K</b>	80	-	-	-	-	10.08	-	2.78	-
<b>0 barg</b>	70	1386	64	1.91	20	5.72	41.87	3.50	51.09
<b>10 barg</b>	115	1201	69	1.84	23	11.84	34.27	3.13	49.24
<b>30 barg</b>	160	1116	71	1.88	23	18.87	23.33	4.86	47.06
<b>0 %</b>	190	1030	73	1.80	27	11.19	47.07	5.92	56.04
<b>25 %</b>	-	-	-	-	-	11.62	38.93	10.43	69.12
<b>75 %</b>	150	1156	70	1.89	23	35.99	5.60	8.70	50.29
<b>100 %</b>	160	918	76	1.91	22	43.51	5.60	12.58	61.69
<b>IPA water</b>	130	1308	66	2.02	18	24.28	10.66	10.46	45.40
<b>Acidic</b>	110	866	78	1.70	29	7.95	42.67	1.30	51.92
<b>Basic</b>	150	737	81	1.57	2935	20.10	29.20	4.27	53.57

(- indicates that no reading was taken or no sample was available for analysis)

Table 31 (continued): Summary of optimisation results using the ammonia lignin

<b>Parameter Change</b>	<b>Autogeneous Pressure (barg)</b>	<b>Mw (Da)</b>	<b>Mw Decrease (%)</b>	<b>Ip</b>	<b>Ip Decrease (%)</b>	<b>Alkylphenolic Yield (g/100g)</b>	<b>Heavy Yield (g/100g)</b>	<b>Unidentified GC-MS Light Products (~g/100g)</b>	<b>Total Yield (g/100g)</b>
<b>500 rpm</b>	135	1054	73	1.75	29	6.70	23.33	6.14	36.17
<b>1500 rpm</b>	135	1164	70	1.79	27	15.93	33.33	10.80	60.06
<b>1 h</b>	120	1160	70	1.78	27	12.51	29.33	7.84	49.68
<b>4 h</b>	140	1077	72	1.86	24	20.06	23.73	7.59	51.38
<b>6 h</b>	160	1069	72	1.83	25	18.56	22.27	8.39	49.22
<b>0.05 g catalyst</b>	140	1137	71	1.79	27	9.66	29.60	9.37	48.63
<b>0.2 g catalyst</b>	150	1247	68	1.85	24	16.85	17.30	11.11	45.26
<b>0.25 g lignin</b>	-	954	75	1.73	29	13.95	29.60	10.67	54.22
<b>Ir/alumina</b>	140	1084	72	1.81	26	9.25	38.67	7.30	55.22
<b>Rh/alumina</b>	140	1057	73	1.85	24	19.94	29.47	6.83	56.24

(- indicates that no reading was taken or no sample was available for analysis)

These results show that the product conversion, in relation to the alkylphenolic products from the light fraction and the char material from the heavy fraction, varied between 32 and 59 % depending on the reaction conditions used which meant that on average 55 % of product was not accounted for. Although the majority of the main peaks were successfully identified, the GC chromatograms did contain other peaks which varied in number (8-25) depending on the conditions used. Peaks between 9 and 32 min (>0.1 % area) were quantified roughly using an average coefficient value (0.85) for the optimisation work only to give an idea of their contribution to the overall product yield. These values are also given in Table 32. Whilst some peaks were small in size, larger peaks were also found that were not identified in this work. This would require further investigation but it is likely that some of these peaks were isomers of the identified products based on their molecular weights or products which contained alkyl groups with hydroxyl groups on different positions or carbonyl groups. Work has been reported where the  $\beta$ -aryl ether bond depolymerises to form aryl-alkyl ketones [95, 96]. As shown in Figure 63 [96], the aryl-alkyl bond in a ketone can undergo a reaction with water to lose the keto substituent and form guaiacol and 2-hydroxyethanoic acid. This would suggest that guaiacol, amongst other products, was not always necessarily a direct result of dealkylation from other products such as ethylguaiacol. It is also highly likely that the light fraction also consisted of higher molecular weights such as dimer, trimers or oligomers which were not GC detectable but again, this would require further investigation.

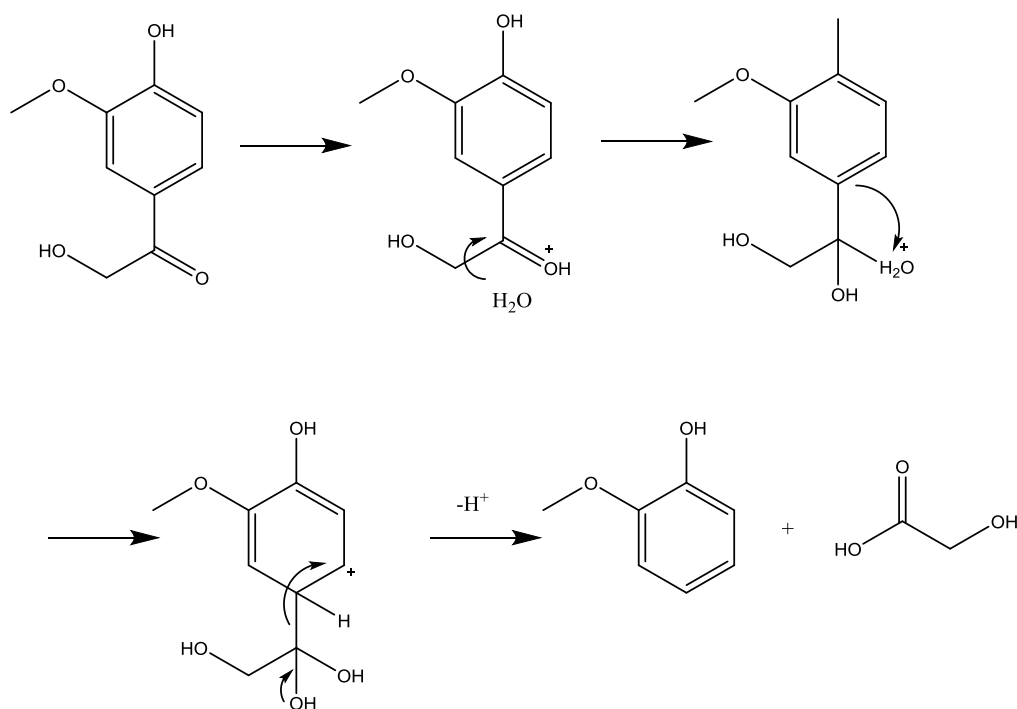


Figure 63: Alternative mechanism to cleave the alkyl chain

Even with these unidentified peaks, the total conversion was 76 % in the best case. In terms of lost product, no significant increase in the catalyst weight was generally observed to suggest that the remaining loss of lignin was due to charred deposits on the catalyst surface. The TGA data presented and discussed in section 3.1.1.4 showed that lignin thermally breaks down to form a variety of gaseous products such as CO<sub>2</sub> and CH<sub>4</sub>. However the reactor set up used in this work meant that these gaseous products could not be identified or quantified. To crudely measure the weight of products lost, the reactor was weighed before and after reaction and it was found that there was a loss of 1.5 g from the overall weight after reaction which corresponded to 30 % of the lignin mass used in standard reactions. This weight loss could be attributed to the release of gaseous products and the cleavage of the alkyl chains from the starting material which could form C1-, C2-, C3-type hydrocarbons or stable allyl cations as shown in Figure 64 [95]. There is also a chance of polymerisation reactions occurring between the allyl cations from species such as G3(i)-type isomers as illustrated in Figure 65 [95, 97]. The methoxy and hydroxyl groups on the lignin alkyl chain could also have hydrolysed to form water molecules, light alcohols such as methanol, or the functional groups could go on to form light gases such as CO<sub>2</sub> and CH<sub>4</sub>. The methanol solvent could also have converted to light hydrocarbons, where formaldehyde or acetaldehyde was also possible.

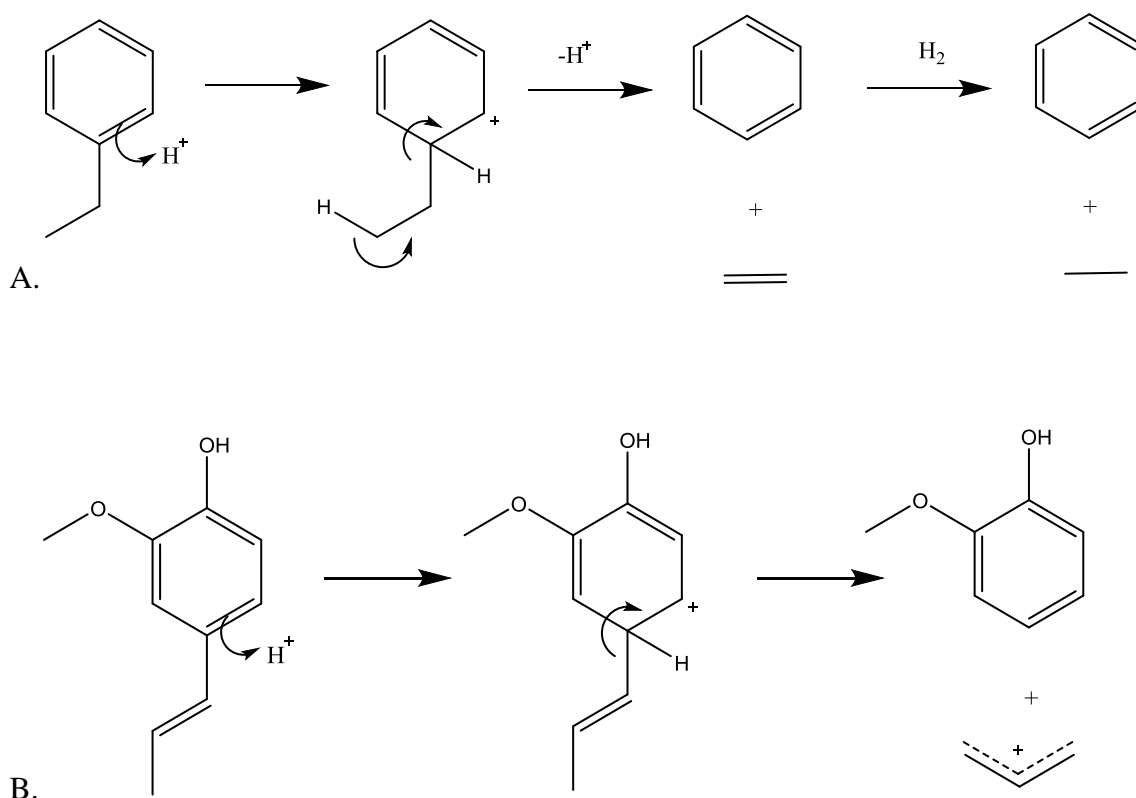


Figure 64: Possible dealkylation mechanisms

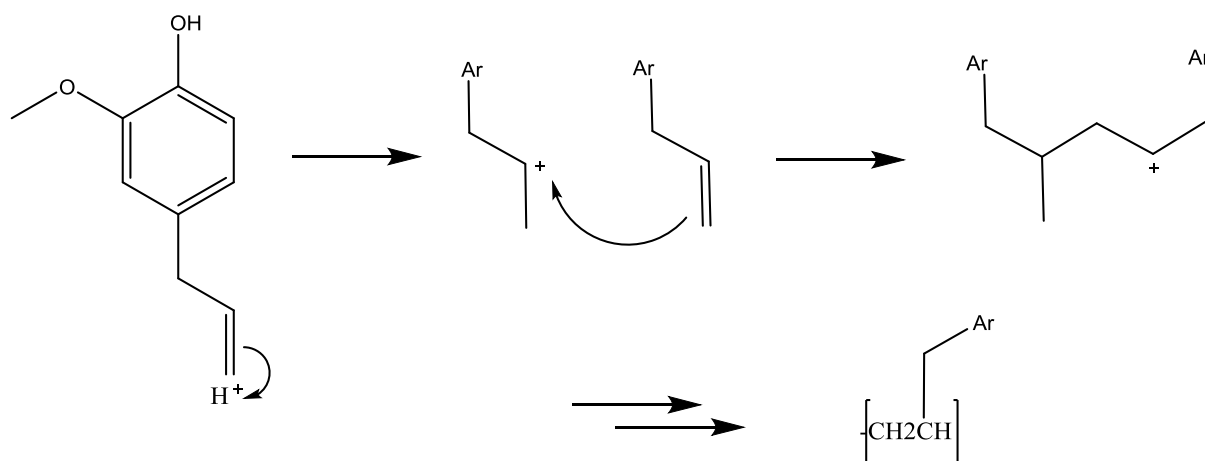


Figure 65: Possible mechanism showing allyl cationic polymerisation

Other factors which could have affected the loss of product include: (1) solid material which had adhered itself to the reactor wall and stirrer; (2) gaseous products such as  $CO_2$  could have dissolved into the solvent which could not be determined; (3) evaporation loss; and (4) water-soluble compounds which could not be extracted fully [74].

This chapter showed that it was possible to optimise the depolymerisation conditions in order to enhance product yields and decrease the char formation depending on the parameter used, and in some cases it also showed the ability to alter the selectivity towards particular sets of products. Whilst the conditions set out in Table 31 were observed to be the best for the ammonia lignin, it should be noted that this may not be the case for other lignins. With that in mind, this study was used as a foundation to build a knowledge base as to how lignin may react under specific conditions in order to tackle more difficult lignins, such as condensed and commercial lignins, or lignins which contain impurities that may cause additional problems during the catalytic reaction. The following section will aim to use the work discussed here as a basis for working with a sulfur-containing Kraft lignin.

### 3.3 Characterisation and Catalytic Depolymerisation Activity of Kraft Lignin using 1 % Pt/alumina

The primary aim of this thesis was to study the depolymerisation of Kraft lignin; a lignin which is readily available as a by-product of the paper and pulp industry but is currently underutilised. Due to the nature of the technique used to isolate the lignin, the Kraft lignin often incorporates sulfur onto its structure from the Kraft pulping process and such impurities could prove detrimental to the catalytic depolymerisation reaction via catalyst poisoning. Sulfur is a recognised catalyst poison [18] so it is therefore imperative that some caution is asserted when working with Kraft lignin. The knowledge ascertained in sections 3.1 and 3.2 has provided a foundation as to how the lignin could react under the conditions used in this thesis. This initial groundwork should also provide some advantage when working with the sulfur-containing lignin.

This section will show characterisation analysis carried out on the Kraft lignin, similar to that shown for the six lignins given in section 3.1.1. This will be followed by standard reaction testing with and without the 1 wt. % Pt/alumina catalyst. Reactions using the optimised conditions set out in section 3.2.4 will also be presented and discussed. In terms of reaction product analysis, GPC was used to give an overview of the mass distribution and GC-MS analysis was used to quantify the identified aromatic monomers.

#### 3.3.1 Characterisation of the Kraft Lignin

The Kraft lignin was characterised using CHN and thioacidolysis analysis, gel permeation chromatography (GPC) and temperature-programmed reduction methods prior to the reaction testing using the Parr autoclave. All experimental methods used are detailed in section 2.4.

##### 3.3.1.1 CHN Analysis

The elemental composition of the Kraft lignin has been tabulated in the following table:

Table 33: Elemental analysis of Kraft lignin

	C %	H %	N %	S %*	O %**	Chemical Formula	O/C Ratio	H/C Ratio
<b>Kraft</b>	62.5	5.7	0.8	3.0	28.0	C <sub>3</sub> H <sub>4</sub> O	0.33	1.33

(\* this value was an estimated value given by Sigma Aldrich

\*\* the oxygen content was calculated as a difference)

The elemental composition of the Kraft lignin is similar to those values found for the six lignins given in Table 6 (see section 3.1.1.1), with the addition of sulfur. The incorporation of sulfur and nitrogen is attributed to the pre-treatment step used to isolate the lignin during the commercial Kraft process. Less oxygen was observed compared to the other lignins which suggested that the Kraft lignin contained less alkyl-aryl linkages.

### 3.3.1.2 Thioacidolysis Analysis

The thioacidolysis experiment estimated the total percentage of  $\beta$ -O-4 bonds found in the Kraft lignin sample, as well as the percentage of each monomer unit (S, G and H) from the total monomer yield generated. This work was carried out by Dr Bouxin and is summarised in Table 34:

Table 34:  $\beta$ -O-4 linkage percentage and monomer ratio of Kraft lignin

	$\beta$ -O-4 %	S:G:H Ratio
<b>Kraft</b>	4.6 (0.1)	0:100:0

(\*standard deviation is in brackets)

The Kraft lignin was found to have a low  $\beta$ -O-4 content and consisted of G-units only, hence the lower oxygen content observed previously with CHN analysis. This lignin sample was obtained from Norway Spruce, a coniferous wood commonly used to produce high-quality paper [98], so the absence of S units was expected. Of the three conventional lignin units, p-hydroxyphenyl (H), guaiacyl (G) and syringyl (S), the third monolignol unit is mainly found in angiosperm species (hardwood) and does not occur in coniferous wood [98]. Although a normal conifer will consist of mainly G units, a smaller proportion of up to 1 % of H units can also be found [98]. No H units were observed with this sample. Additionally, lignins rich in H- or G-units typically contain more carbon-carbon bonds than lignins rich in S units because the C3 or C5 position of the H- or G-unit is free to make another linkage [99]. The low  $\beta$ -O-4 value obtained was comparable to that of the commercial soda lignin and similarly, the harsh conditions of the Kraft pulp likely aided the condensation of the plant material. This data would suggest that the lignin is a condensed lignin and will give a similar reaction profile to that found with the condensed soda lignin when reacted using the standard conditions in the Parr reactor.

### 3.3.1.3 GPC Analysis

Figure 66 shows the separation of the Kraft lignin based on the polymers molecular size as a function of time. The molecular weight, number and polydispersity value was also calculated and can be found in Table 35. The GPC analysis of the Kraft lignin gave a similar molecular weight distribution plot to that of the condensed soda lignin shown in Figure 27 (see section 3.1.1.3), where the main peak centred at ~12 min and a second peak eluted at ~13 min. This GPC profile confirmed that the harsher pretreatment conditions caused partial cleavage of the lignin to give a higher response in the lower molecular weight range. The molecular weight value was found to be higher than the other lignins at 4550 Da, and this was attributed to the fact that softwood lignins (e.g. conifers) generally have a higher weight-average molecular mass than hardwood types (e.g. poplar wood) because softwoods are more cross-linked and lead to larger molecules in the structure [24].

Table 35: GPC data for Kraft lignin

	<b>Molecular Weight (Mw)</b>	<b>Molecular Number (Mn)</b>	<b>Polydispersity (Ip)</b>
<b>Kraft</b>	4550	1363	3.34

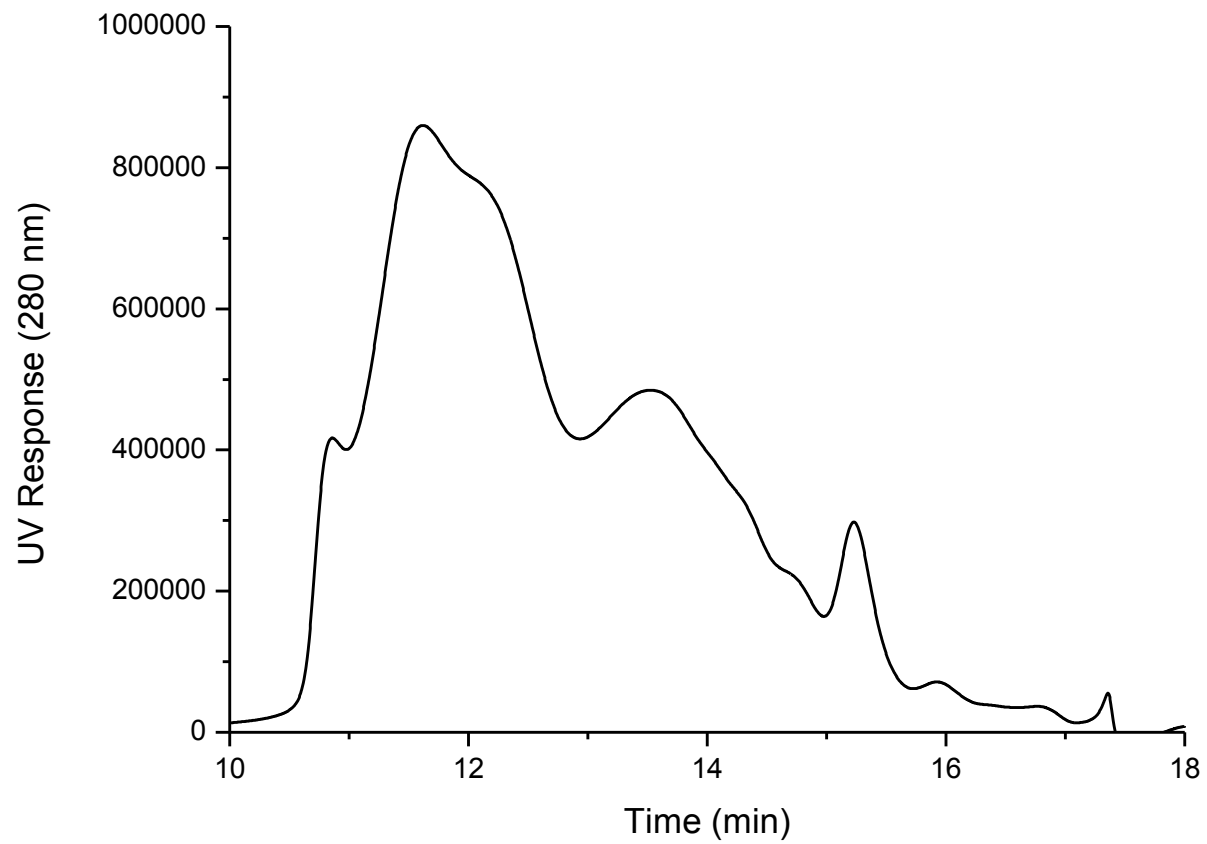


Figure 66: GPC profile of Kraft lignin

#### 3.3.1.4 Temperature-Programmed Reduction (TPR) Analysis

The Kraft lignin was analysed via TPR analysis to envisage its thermal breakdown in a reductive environment. Figure 67 shows a broad temperature range with five breakdown areas, the main of which occurred at ~623 K. The initial step <373 K was attributed to the loss of water via dehydration reactions as illustrated in Figure 68. Similar to the thermal breakdown of the condensed soda lignin (see Figure 28, section 3.1.1.4), the main breakdown peak of Kraft lignin eluted at ~623 K. This breakdown temperature was higher than that observed with the uncondensed lignins. This higher temperature breakdown is likely due to the need to break stronger C-C bonds in the Kraft structure due to its low  $\beta$ -O-4 content, as opposed to the high abundance of aryl ether linkages in uncondensed lignins which will thermally decompose at lower temperatures. The main thermal process occurred between 473-773 K where it is likely that the evolution of hydrocarbons and low molecular phenols such as guaiacol occurred, as well as the formation of gaseous products such as methane, CO, and CO<sub>2</sub> (see Figure 68). Water was also released throughout the main breakdown area as a result of -OH group cleavage. The Kraft lignin was found to lose 66 % of its original weight, which was similar to the weight loss value obtained for the soda lignin (67 %).

With regards to the organically bound sulfur found in the lignin's structure, no H<sub>2</sub>S was observed from the TPR mass spectral data but a minor amount of sulfur dioxide was identified under an oxygen/argon environment. Figure 69 shows the temperature-programmed oxidation (TPO) derivative weight loss diagram for Kraft lignin and the slight evolution of SO<sub>2</sub> between 473-723 K and 723-1073 K.

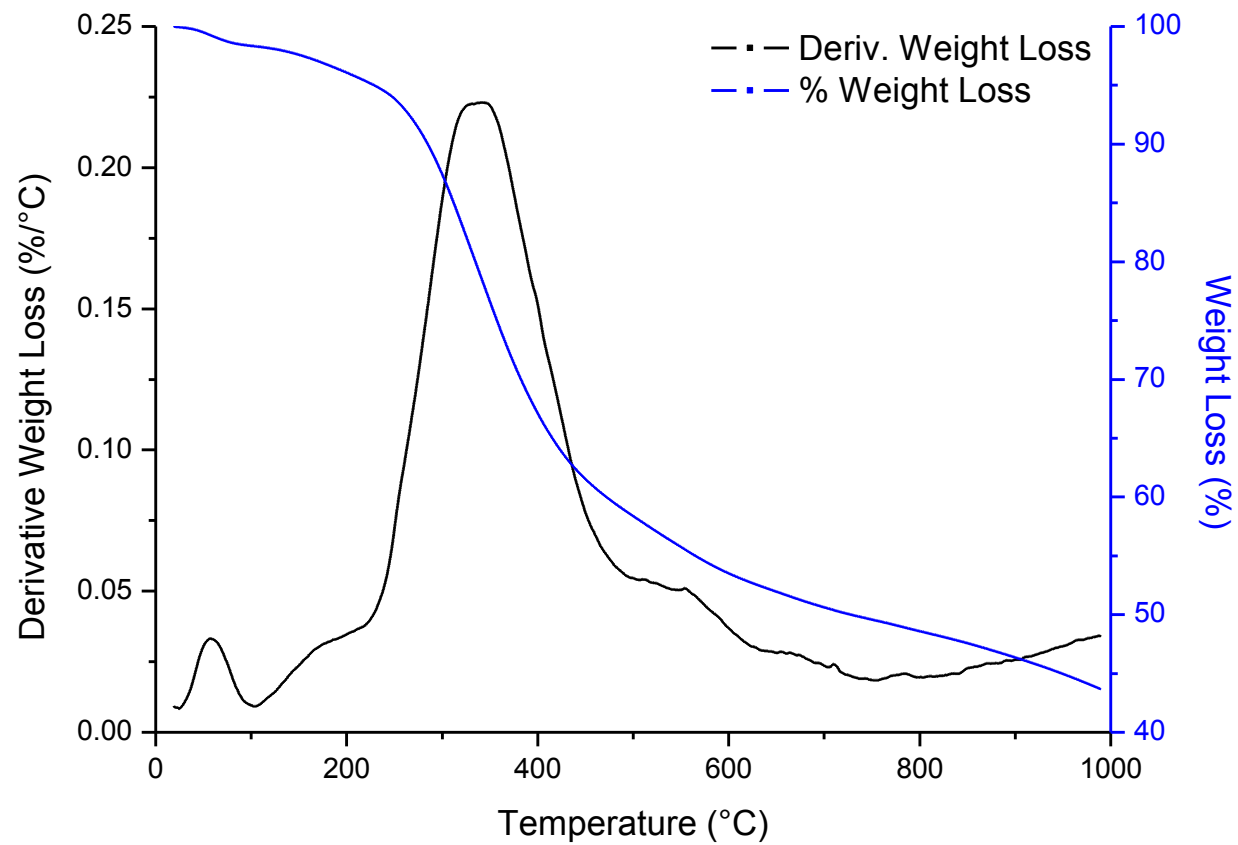


Figure 67: TPR of Kraft lignin

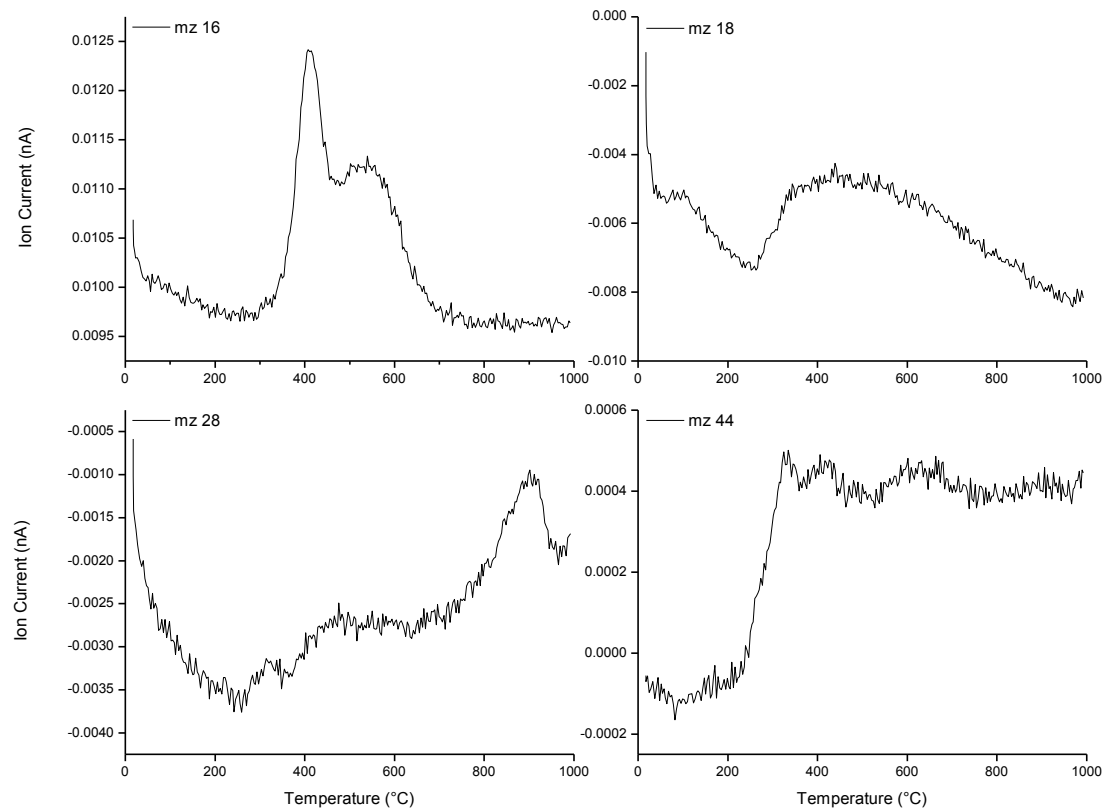


Figure 68: Mass spectra data obtained from TPR of Kraft lignin

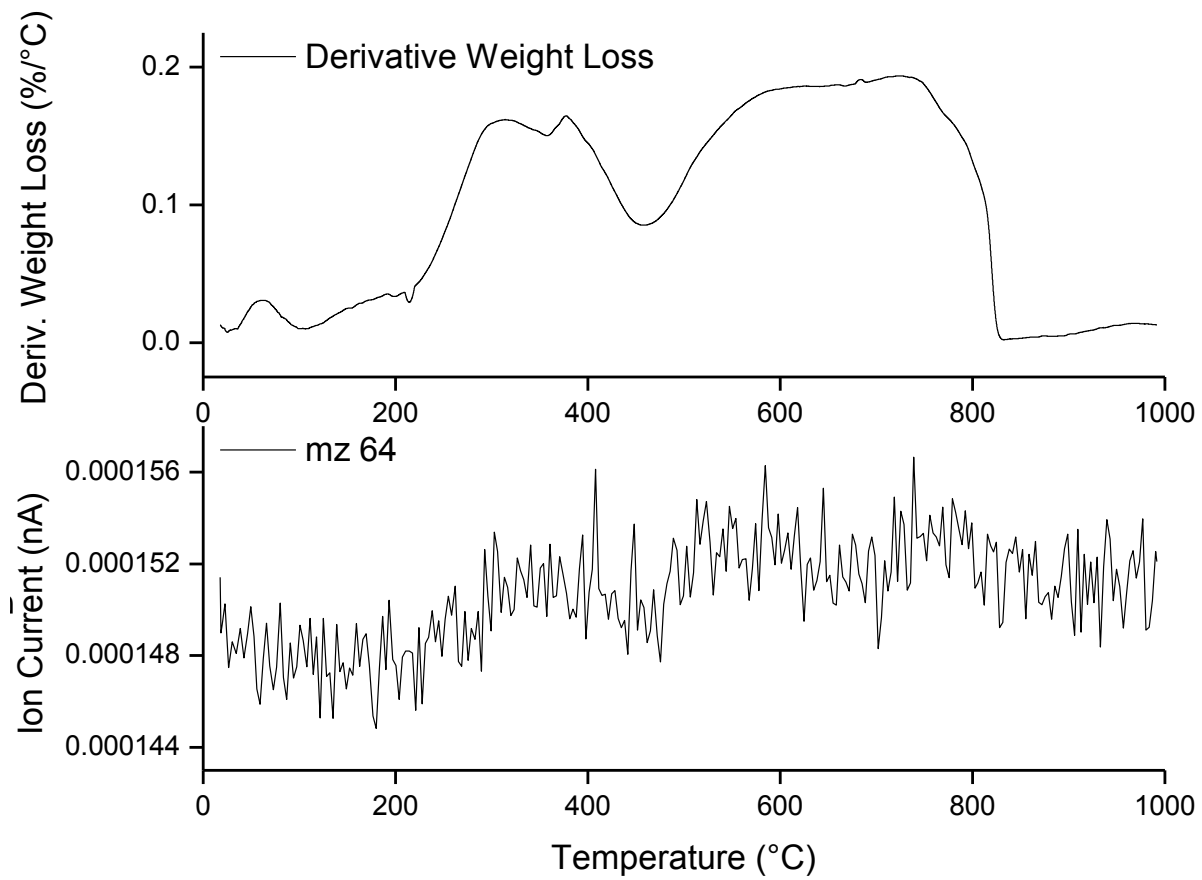


Figure 69: TPO of Kraft lignin showing derivative weight loss and SO<sub>2</sub> evolution

### **3.3.2 Non-Catalytic and Catalytic Standard Reaction Testing**

This section will show product distribution plots for the reactions with Kraft lignin in the presence and absence of the 1 wt. % Pt/alumina catalyst. The standard reaction, as described in section 2.3.2, used 0.5 g of lignin with 0.1 g of 1 wt. % Pt/alumina catalyst in 100 ml of 50:50 v/v methanol-water solution. The reaction was set to 573K, stirred at 1000 rpm and reacted under 20 barg of H<sub>2</sub> pressure for 2 hours (plus 30 min ramp time). The section will then go on to describe the effect observed when the ‘optimised’ conditions for the ammonia lignin were employed with the Kraft lignin instead.

#### **3.3.2.1 Non-Catalytic Reaction Testing**

As shown in previously, some degree of lignin depolymerisation was achievable without the use of a catalyst under the standard conditions. Here, experiments were carried out without the Pt/alumina catalyst in hydrogen and inert helium, as well as in hydrogen with the alumina support. Figure 70 shows that depolymerisation was achieved without the use of a catalyst but the reaction was highly selective towards guaiacol for each experiment (46-55 %). In all three cases, the G2 and G3(OH) product was also favoured. Whilst the run in 4 barg helium yielded 4.7 % of product, the addition of 20 barg H<sub>2</sub> only yielded a further 0.9 % of product (5.6 %) but it did enable slightly higher production of products with some of the alkyl chain intact. The incorporation of hydrogen into the reaction without catalyst also promoted the production of char as shown in Table 36, where it rose from 41.2 to 71.5 g/100g. This was thought to be because hydrogen facilitated the depolymerisation reaction better than helium but simultaneous condensation reactions were also therefore promoted. In comparison to the blank run without catalyst in hydrogen, the alumina support yielded 6.4 % of product and saw an increase in the alkylated products and a decrease in the char production (58.5 g/100g). This suggested that the addition of the alumina support suppressed char formation to some extent as observed with the ammonia lignin reaction (see section 3.2.2.1).

Table 36: Effect of using a catalyst or hydrogen gas on char production

<b>Reaction</b>	<b>Weight (g/100g)</b>
<b>No catalyst in He</b>	41.20
<b>No catalyst in H<sub>2</sub></b>	71.47
<b>Alumina support in H<sub>2</sub></b>	58.53

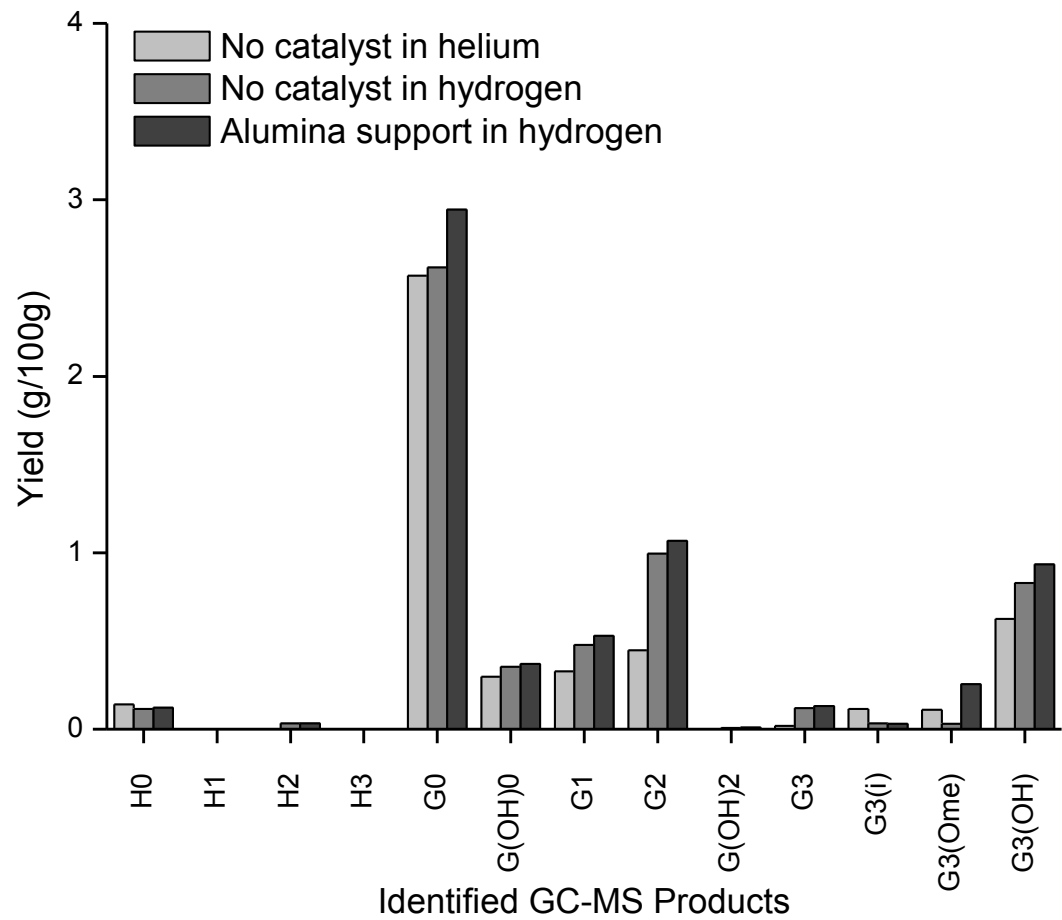


Figure 70: Depolymerisation effect of the catalyst and gas used with Kraft lignin

### 3.3.2.2 Catalytic Standard Reaction Testing

The Kraft lignin was reacted under the standard conditions as stated previously, using the Pt/alumina catalyst. This reaction was then carried out again to ensure its reproducibility as shown in Figure 71. In the same way that the ammonia lignin reproduced runs reacted slightly differently, there was some deviation in the product yields obtained across the two comparative standard runs. The initial standard run gave an overall yield of 9.2 %, in comparison to the reproduced run which gave an overall yield of 7.5 %. The product distribution was fairly similar in terms of the ratio of each product formed but the reproduced run produced slightly less of each monomer. The char weight was also calculated from each of the heavy fractions obtained after reaction was found to be 37.9 and 39.3 g/100g. This difference was also observed with the ammonia lignin standard reactions and shows that more char is produced when less monomeric product is found in the lights fraction.

During the lignin characterisation analysis, Kraft lignin was found to show similar characteristics to the soda lignin. From this, it was expected that the Kraft lignin would react similarly to the soda lignin under the standard conditions, if not worse when the incorporated sulfur was taken into account. The soda lignin yielded a similar amount of alkylphenolic product (7.4 %) in comparison to the Kraft lignin which suggested that the sulfur did not alter the metal catalysis via a poisoning effect. This was also confirmed when compared to the alumina only run in the previous section. If poisoning had been an issue, we would have expected the yields to be similar due to poisoning of the metal but in fact, an increase in yield was observed from 6.4 to 9.2 %. This was deemed a positive observation as it suggested that the sulfur was not as catalytically problematic as first expected.

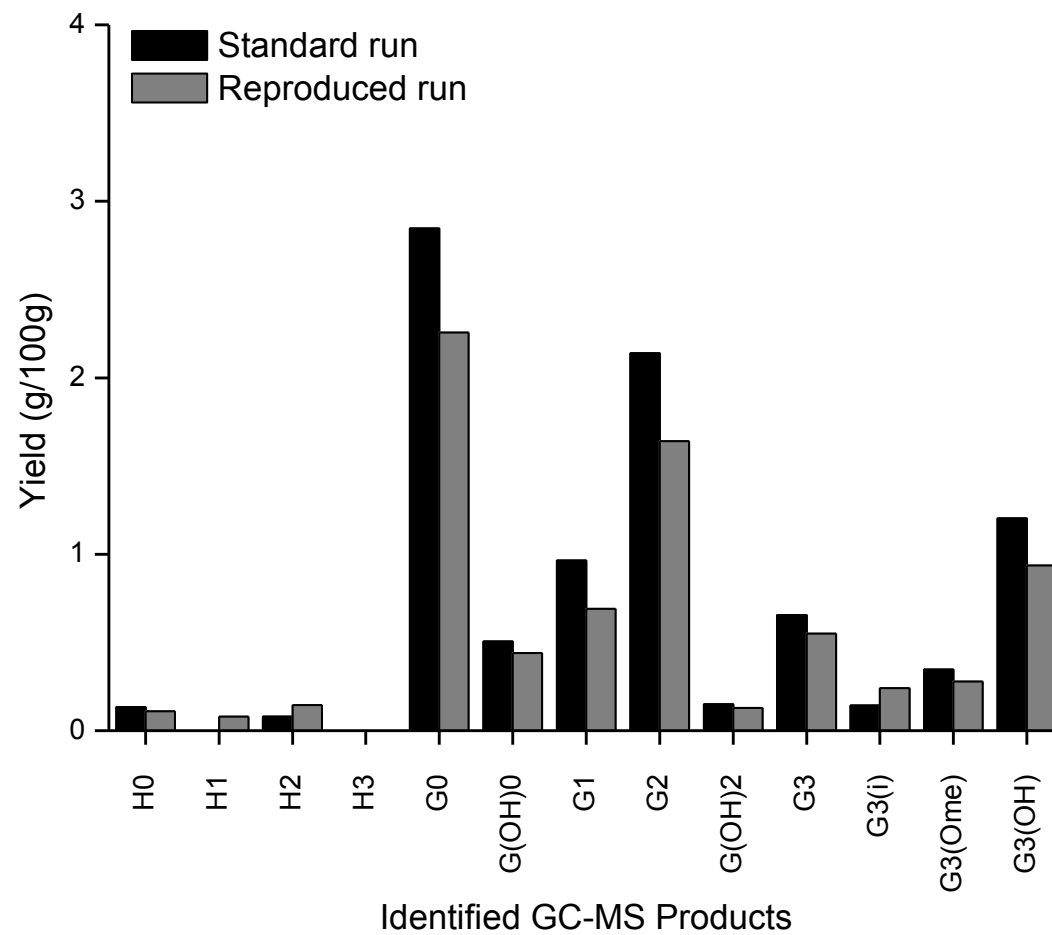


Figure 71: Reproducibility testing of the Pt/alumina catalyst and Kraft lignin

In order to test the recyclability of the catalyst, the catalyst was isolated and collected at the end of the standard run, dried then placed into the clean Parr autoclave with fresh Kraft lignin. As shown in Figure 72, there was a drop in each monomer product. The overall yield decreased from 9.2 % to 7.4 % and the char yield increased from 37.9 to 40.2 g/100g. This reduction in product yield was not as much as that observed for the ammonia lignin recycled run (see section 3.2.1) which demonstrated how differently lignins can react under the same conditions. The slight decrease to 7.4 % is the same value as that observed for the reproduced standard run reaction so it is inconclusive as to whether the run actually deactivated the catalyst or not.

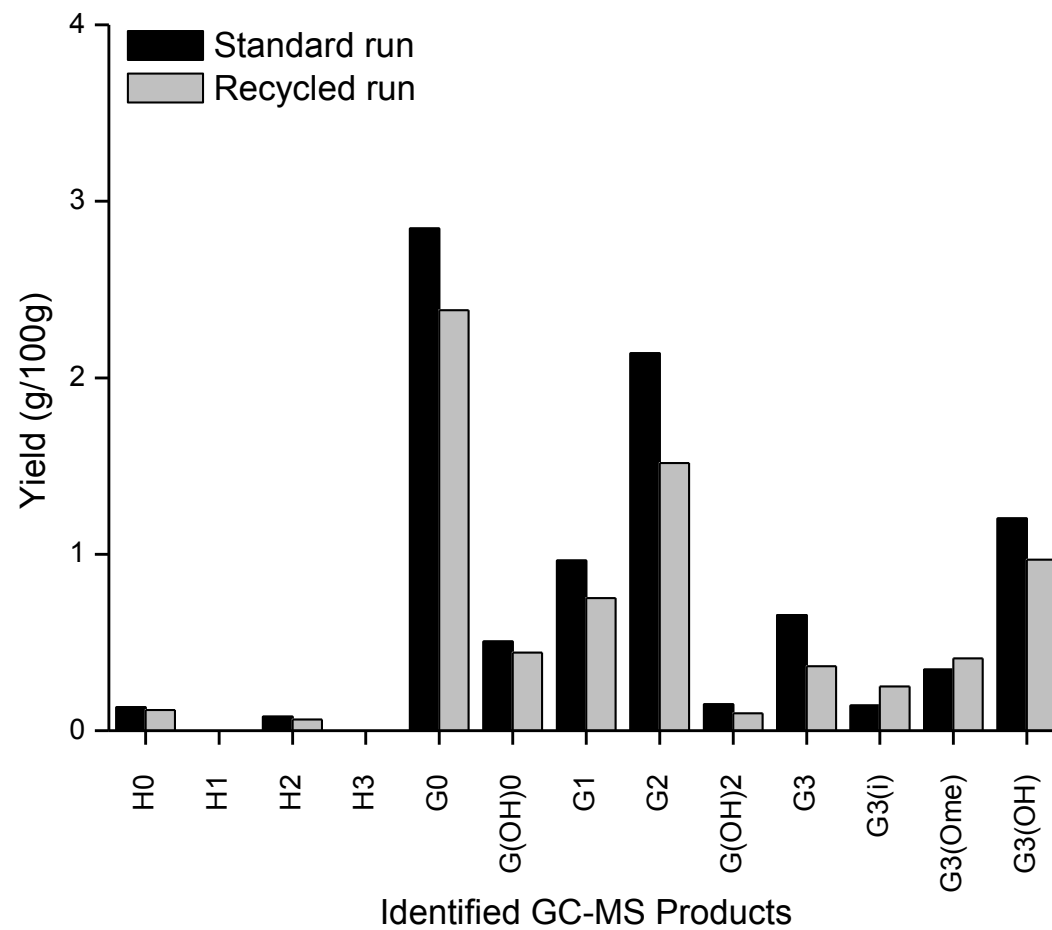


Figure 72: Reproducibility testing of the Pt/alumina catalyst and Kraft lignin

### 3.3.2.3 Optimisation of the Standard Reaction Conditions

The optimised conditions for the depolymerisation of the ammonia lignin was given with respect to the highest monomer yields, lowest char production and best selectivity towards desired products in section 3.2.4. From these results, it was of interest to the project to attempt to use these same ‘optimised’ conditions with the Kraft lignin in hope that they would also increase its product yield and limit char formation. The optimised conditions have been summarised in Table 33 where ‘X’ indicates the reactions carried out in this section. Note that some conditions shown did not differ from those employed in the standard run.

Table 37: Summary of the optimised conditions for ammonia lignin

<b>Parameter Change</b>	<b>Optimum Condition</b>	<b>Required Experiments</b>
<b>Stirring speed</b>	1000 rpm	
<b>Residence time</b>	4 h	X
<b>Temperature</b>	573 K	
<b>Pressure</b>	30 barg	X
<b>Solvent composition</b>	100 % methanol	X
<b>Alternative solvent</b>	IPA-water mix (50:50 v/v)	X
<b>pH</b>	Neutral	
<b>Catalyst mass</b>	0.2 g	X
<b>Lignin mass</b>	0.5 g	
<b>Alternative Catalyst</b>	1 wt. % Rh/ alumina	X

#### 3.3.2.3.1 Effect of Reaction time

As shown previously, the ammonia lignin was found to yield more monomeric product after 4 h reaction time in comparison to the standard 2 h. This was attributed to the longer reaction time being able to break more bonds, chiefly the stronger bonds. It was felt that

the Kraft lignin, which is a particularly recalcitrant lignin, would benefit from a longer reaction period as it would allow time for the Kraft lignin to depolymerise to monomeric products. Evidently from Figure 73, there was an increase in the overall product yield, where the 4 h reaction gave 11.5 % of product compared to the standard run which gave 9.2 %. This value was the highest yield of monomeric product obtained for Kraft lignin depolymerisation and the char formation was also found to decrease slightly to 36.0 from 37.9 g/100g. Although the ammonia lignin did not give higher yields of product when the reaction time was extended to 6 h, the Kraft lignin could benefit from an extended reaction time due to its condensed nature.

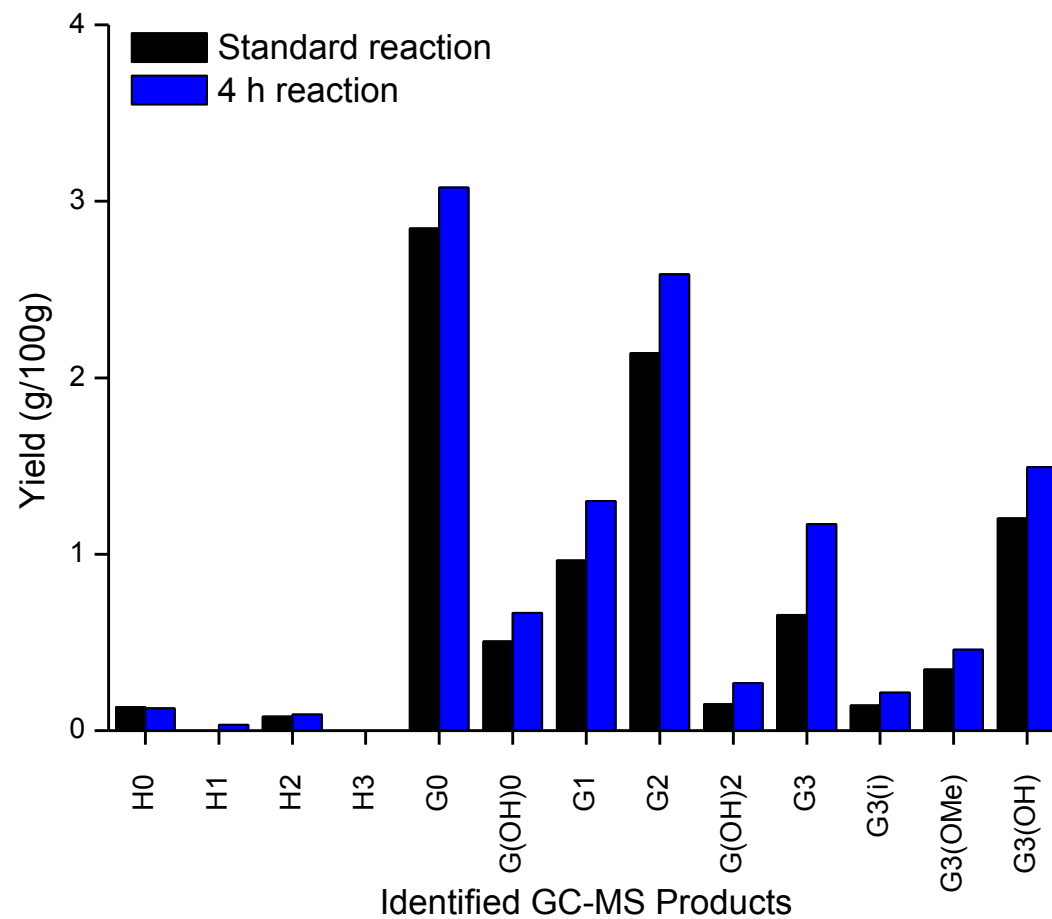


Figure 73: Depolymerisation effect of using a 4 h reaction time with Kraft lignin

Although the literature available on the catalytic conversion of Kraft lignin using precious metal catalysts remains sparse, some studies were found that could be compared to the work presented here to some extent. Zhou recently observed that temperature and time also affected the composition and yield of products obtained when Kraft lignin was converted under hydrothermal conditions at 403, 453 or 503 K for 15 or 60 min in a micro-reactor [100]. The author observed a decrease in the total oil yield with increasing temperature at 15 min (7.4, 6.3 and 5.4 %) because a secondary decomposition of oil to gas had taken place. On the contrary, an increase in total oil yield with increased time (60 min) was observed for each temperature (10.6, 10 and 9.2 %). These values suggest that the conversion of Kraft lignin would not be efficient at higher temperatures as a result of increased condensation reactions, but it would benefit from longer reaction periods.

#### **3.3.2.3.2 Effect of Pressure**

With increased pressure, it was expected that the depolymerisation activity would increase and that monomer yield would also subsequently increase as shown with the ammonia lignin. Figure 74 shows that some difference in the overall yield for each monomer product was achieved when 30 barg hydrogen pressure was employed in comparison to the standard run which used 20 barg pressure, however the overall yield only slightly increased from 9.2 to 9.4 %. A change in product selectivity was observed, where the higher pressure favoured the production of the alkylated products which was a positive observation, however the char formation increased slightly to 40.7 g/100g as well. The residual pressure at room temperature was noted to be 25 barg which was a 5 barg drop from the original starting pressure of 30 barg. This reduction in pressure suggested that the reaction had used the additional 5 barg of hydrogen and therefore needed a higher amount of hydrogen in comparison to the other experiments with reduced back to the original reaction pressure.

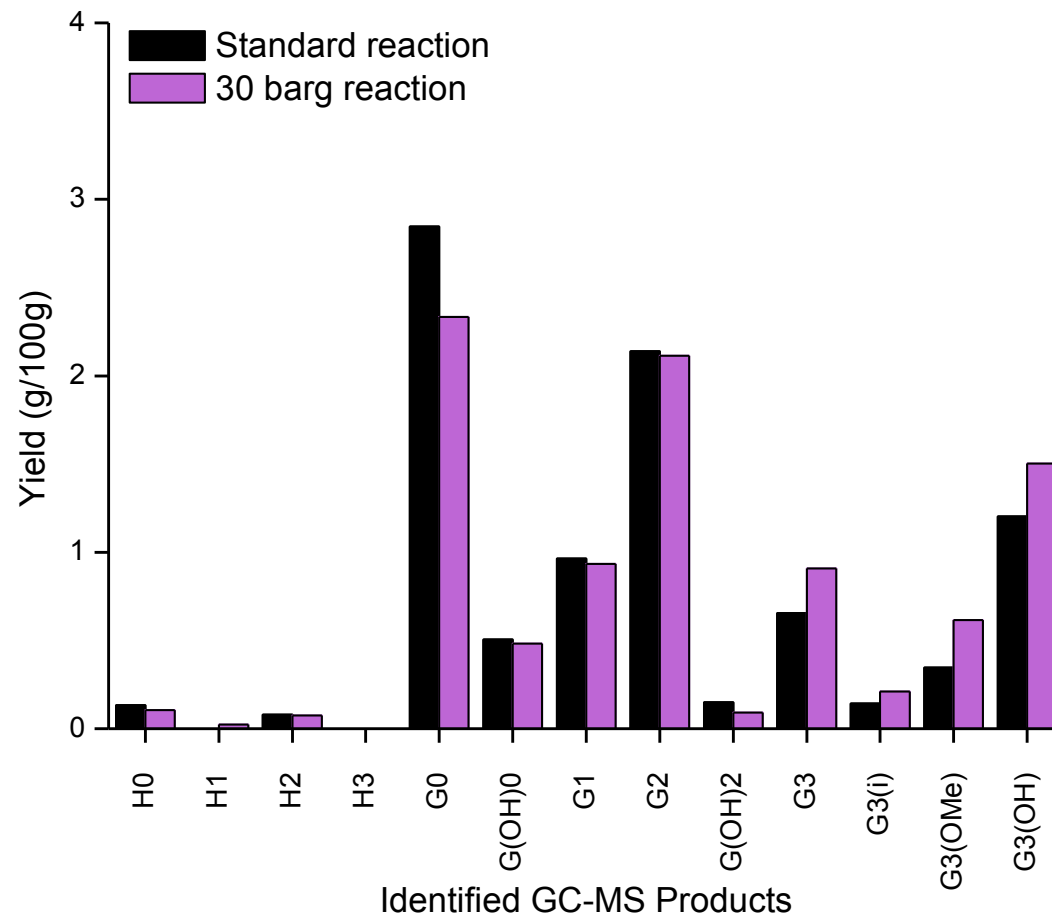


Figure 74: Depolymerisation effect of using 30 barg hydrogen pressure with Kraft lignin

The ammonia lignin experiments showed 0.4 order with respect to hydrogen pressure and a decrease in char formation with increasing hydrogen pressure, whilst the results shown here would suggest that the hydrogen pressure did not influence the depolymerisation activity for the Kraft lignin to the same extent as the ammonia lignin and that it actually promoted char formation. This was also observed earlier, where the inclusion of hydrogen gas in comparison to the helium gas created more char material. From these results, the condensed Kraft lignin clearly does not show a positive hydrogen effect. This could be due to the fact that there are little aryl-alkyl linkages available to cleave via hydrogenolysis reactions so the additional hydrogen would therefore make little difference to the reaction in terms of making monomers. An increase in hydrogen pressure in fact looks to cause the lignin to depolymerise and repolymerise at a faster rate.

Conflicting literature using 30 barg hydrogen was found where the authors carried out hydrogenation reactions with Kraft lignin using Pt/alumina and ethanol under 30 barg H<sub>2</sub> at 473 K and yielded 6.2 % of monomeric product [48]. Although their yield seems reasonably comparable to that shown in this thesis (9.4 %) when the increased temperature of 573 K is taken into account, they stated that propylguaiacol, followed by ethyl-, methyl- and guaiacol were the most abundant products whereas our experiments showed the opposite. Based on the findings presented in this thesis in general, a high production of propylguaiacol units seems unlikely when the starting material is condensed and contains little  $\beta$ -O-4 linkages.

### **3.3.2.3.3 Effect of Solvent**

Similar to the ammonia lignin, it was felt that increasing the methanol composition of the reaction solution would prove advantageous with regards to its increased ability to solubilise lignin and the benefits associated with supercritical methanol as discussed in a previous chapter. However Figure 75 illustrates that this assumption was not the case as the overall yield dropped to 5.6 % when the Kraft lignin was reacted with 100 % methanol as opposed to the standard 50:50 v/v methanol-water solution (9.2 %). Additionally, when the reactor was emptied, a large amount of catalyst and charred lignin material had adhered to the reactor vessel wall and stirrer. This material proved very difficult to remove and was not soluble in acetone. The catalyst and solid material was deemed 'fluffy' in its appearance with respect to its size and shape and it was suggested from these observations that the Kraft lignin had melted during reaction as opposed to dissolving into solution. This melting effect would have caused the material to char severely onto the catalyst and reactor equipment thus reducing the formation of alkylphenolic product. This suggestion would

also imply that water is required for the Kraft lignin to depolymerise effectively, whereas this was not necessarily the case for the ammonia lignin. In order to determine whether this effect was a result of the incorporated sulfur or because of the Kraft lignins condensed nature, the soda lignin was also run under the same conditions with 100 % methanol. Similar to the Kraft lignin, the soda lignin formed a mass of charred lignin and catalyst material at the bottom of the reactor. This mass was also difficult to remove and showed a 101 % weight gain in comparison to the starting catalyst weight. This experiment therefore showed that the solvent effects are dependent upon not only the pre-treatment, but on the type of lignin used as well.

The products that were identified from the lights fraction displayed a change in selectivity with changing solvent composition. Generally, a decrease in each product was observed when 100 % methanol was used, except for the G3(i) and G3(OH) products which increased in their yields. This was likely due to the increased hydrogen content in the reaction medium which favoured the propenyl double bond and terminal gamma carbon hydroxyl group. A drop in the residual pressure was also observed at room temperature (10 barg) which suggested that the 100 % methanol reaction consumed more hydrogen during the reaction in comparison to the standard run.

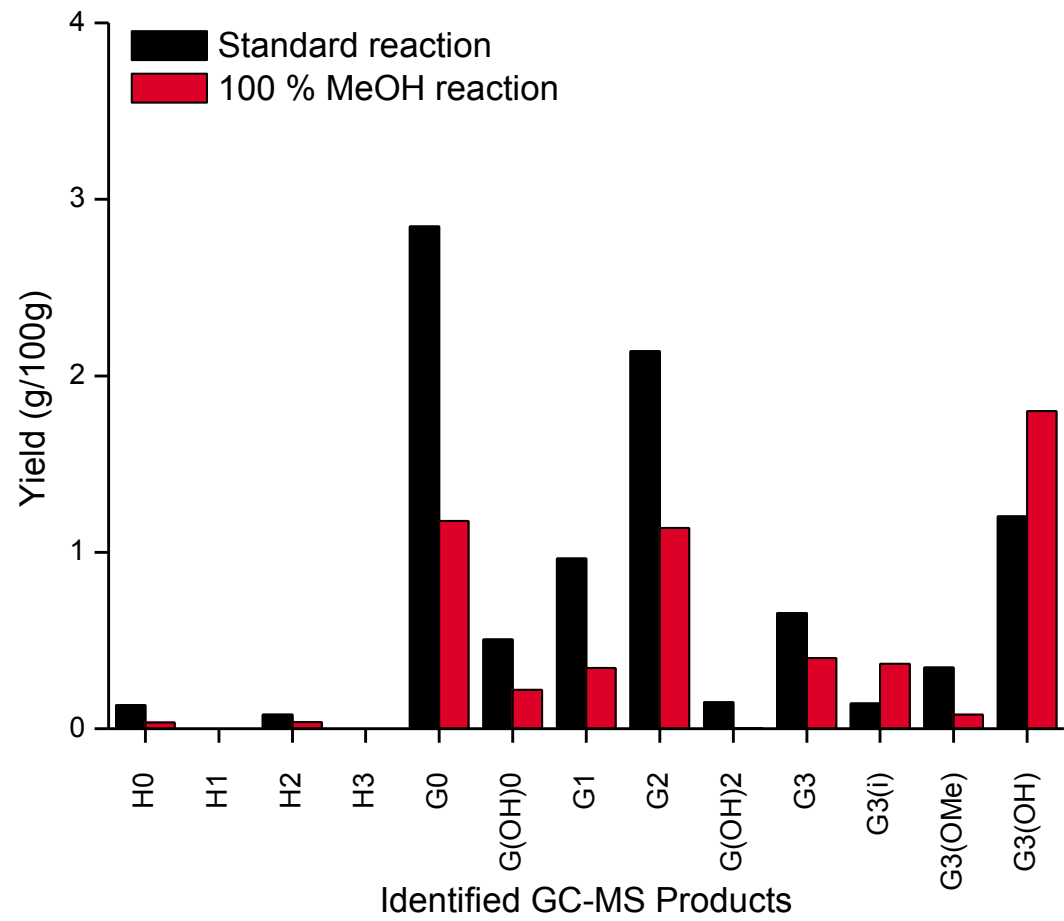


Figure 75: Depolymerisation effect of using 100 % MeOH with Kraft lignin

#### **3.3.2.3.4 Effect of using an Alternative Solvent**

The 50:50 v/v IPA-water mix notably improved the overall yield of the ammonia lignin conversion in the previous chapter. This was attributed to IPA being an excellent hydrogen donor and Figure 76 shows that the Kraft lignin also favoured the IPA-water mix but not to the same extent. The overall yield increased slightly from 9.2 to 9.8 % with an increase in products with propyl chains. The G3 and G3(OH) products increased by approximately 58 % each and a dramatic increase of more than four times its original yield was observed for G3(OMe). The char production significantly decreased from 37.9 to 7.7 g/100g for the IPA-water reaction suggesting that its hydrogen-donating characteristic was particularly favourable with the Kraft lignin in suppressing condensation reactions, possibly via capping mechanisms as discussed in section 3.2.3.6.

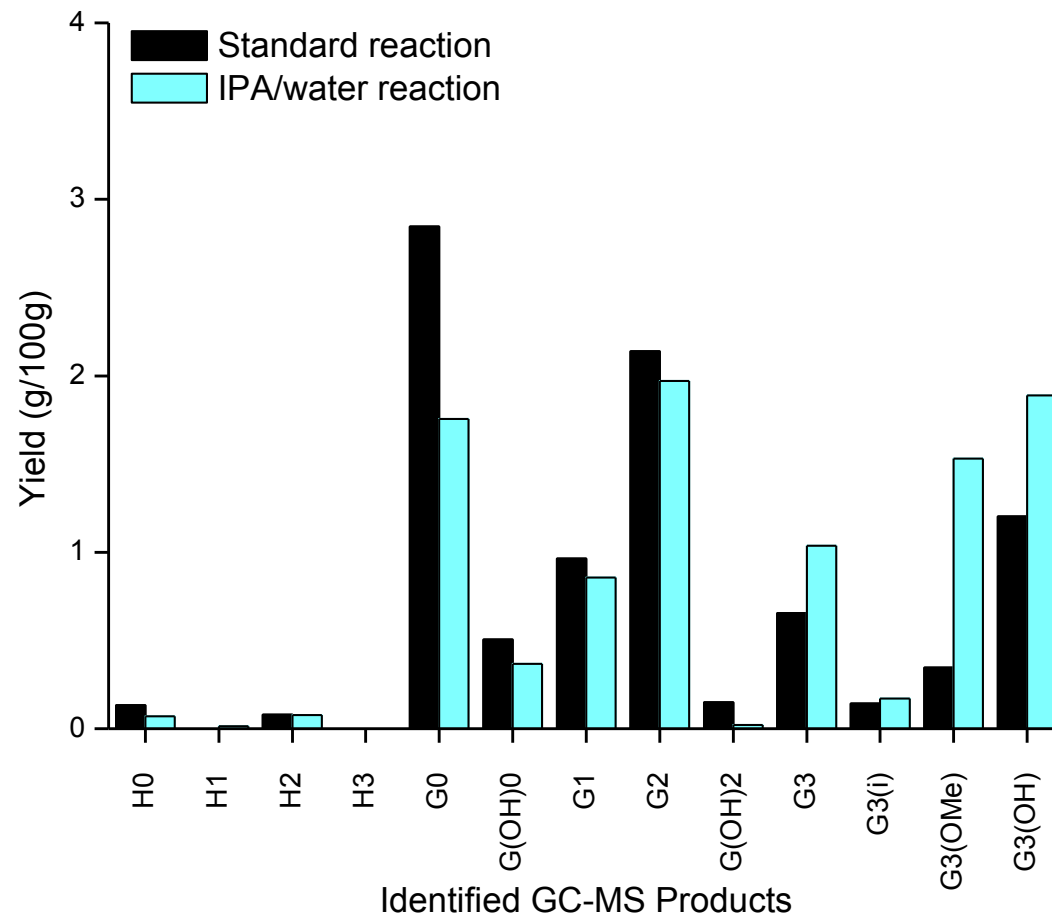


Figure 76: Depolymerisation effect of using IPA/water with Kraft lignin

### **3.3.2.3.5 Effect of Catalyst Mass**

It was expected that an increase in catalyst mass would result in an increase in monomer yield due to increased number of active sites and therefore potential reactions with the active metal. Figure 77 shows that there was a small decrease in the overall yield obtained and that there was a slight change in selectivity where G3 and G3(OH) products were more favourable and the guaiacol formation decreased by almost 30 %. Although the monomer yield decreased from 9.2 to 8.8 %, the char formation was also found to decrease from 37.9 to 29.9 g/100g which showed that the additional catalyst mass aided the suppression of condensation reactions.

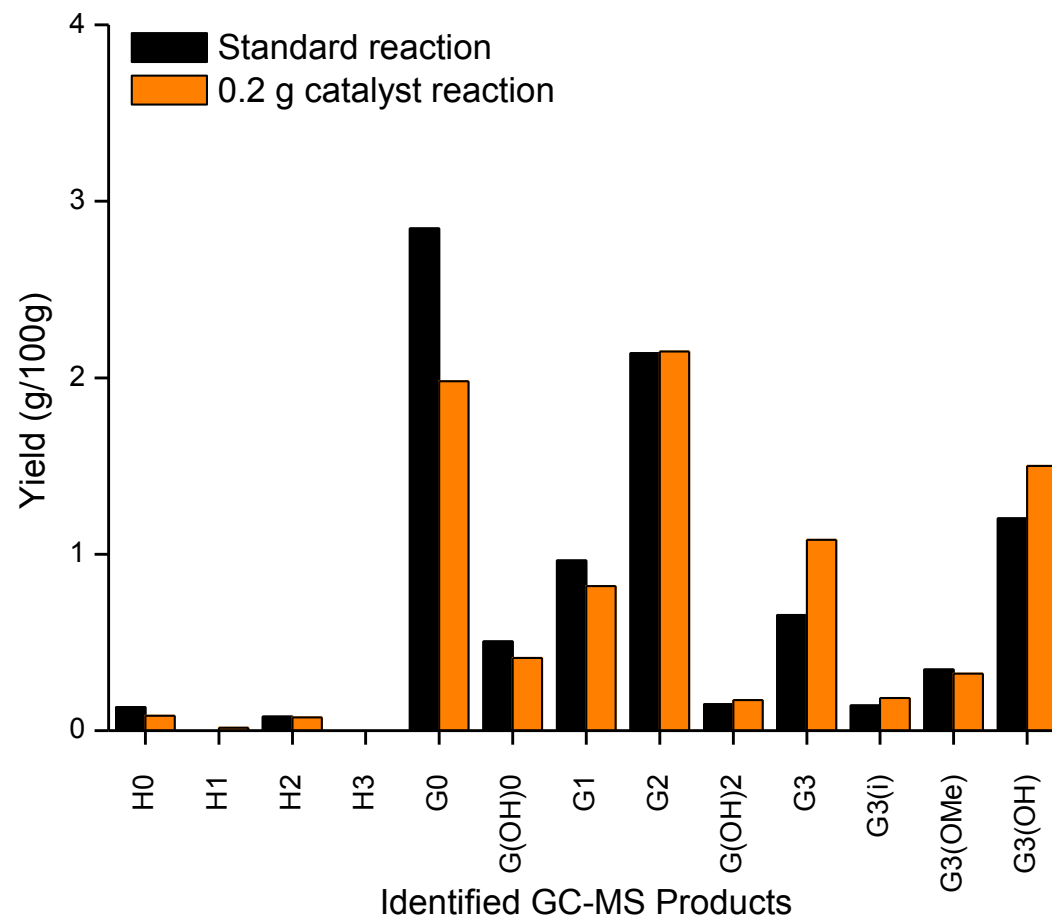


Figure 77: Depolymerisation effect of using 0.2 g of catalyst with Kraft lignin

### **3.3.2.3.6 Effect of using an Alternative Catalyst**

Previously, the 1 wt. % Rh/alumina catalyst was found to give the highest monomeric yield under the standard conditions in comparison to the other precious metal catalysts. Some variation in the product selectivity was also observed, where a lower amount of G3+ products were produced when the rhodium catalyst. These observations were suspected to be in relation to the rhodium catalysts high metal loading and dispersion with respect to Rh atoms so its activity as a lignin conversion catalyst in comparison to the Pt/alumina catalyst was not entirely comparable. Nonetheless, the reaction was carried out and Figure 78 shows that the Rh/alumina catalyst did not yield as much product as the standard Pt/alumina catalyst, where the rhodium catalyst gave 7.9 % product in comparison to the 9.2 % of product achievable with the platinum catalyst. The selectivity did not alter significantly in terms of the ratio of each product to the other, but each product was found in a lower amount. The Rh/alumina experiment also generated slightly higher amounts of char (39.7 g/100g) in comparison to the Pt/alumina experiment. As no significant change was observed for the product selectivity or the char production, these results in comparison to the ammonia lignin results would suggest that the rhodium catalyst was more susceptible to sulfur poisoning, hence the lower yield of monomeric product.

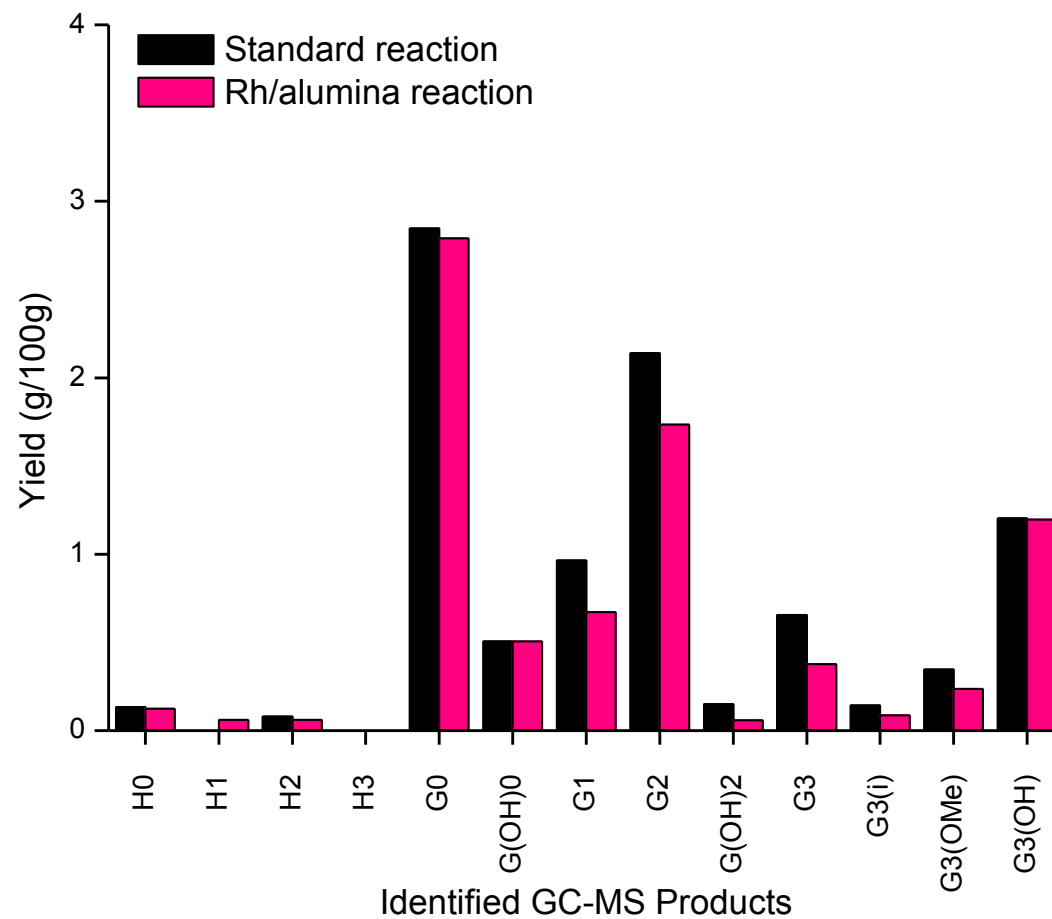


Figure 78: Effect of using 1 wt. % Rh/alumina catalyst with Kraft lignin

### 3.3.3 Summary of the Catalytic Standard Reaction Testing of Kraft Lignin

This work aimed to take the sulfur-containing Kraft lignin and study its depolymerisation activity in comparison to previous lignin conversion studies using other types of lignins. The Kraft lignin was found to be a condensed lignin which consisted of only guaiacyl units with a low abundance of  $\beta$ -O-4 linkages (4.6 %). The TPR data showed that the lignin thermally decomposed at a higher temperature (623 K) than that observed for the uncondensed lignins (573 K), and the GPC data illustrated that lower molecular weights were present in the starting material which was attributed to the severity of the Kraft process. The Kraft lignin in general exhibited similar characteristics to that of the soda lignin so it was believed that they would therefore react similarly under the standard reaction conditions. However due to the Kraft lignin also containing sulfur, it was expected that this impurity would further limit its conversion yield and possibly cause deactivation of the catalyst via sulfur-poisoning of the active sites. The reaction studies found that the inclusion of the Pt/alumina catalyst increased the yield of product in comparison to the experiments without catalyst or with the alumina support only. The results for the standard reaction were comparable to those observed with the soda lignin as originally expected, however the molar fraction ratio of each product showed that the Kraft lignin yielded more of the desired propylphenolics and less of the phenolic products without an alkyl chain than the soda lignin. This has been represented in Figure 79. The difference in product distribution was due to the condensed nature of the starting material, where the soda lignin had less  $\beta$ -O-4 linkages (2.8 %) in comparison to the Kraft lignin (4.6 %). This conforms well to our previous conclusion which stated that the starting structure greatly affects the type and yield of the resultant aromatic products and that catalytic conversion of lignin to fine chemicals is the most promising when the starting lignin is uncondensed in nature. The results found would also suggest that the sulfur present in this particular Kraft lignin sample did not deactivate the metal or alter the reaction mechanism as originally proposed.

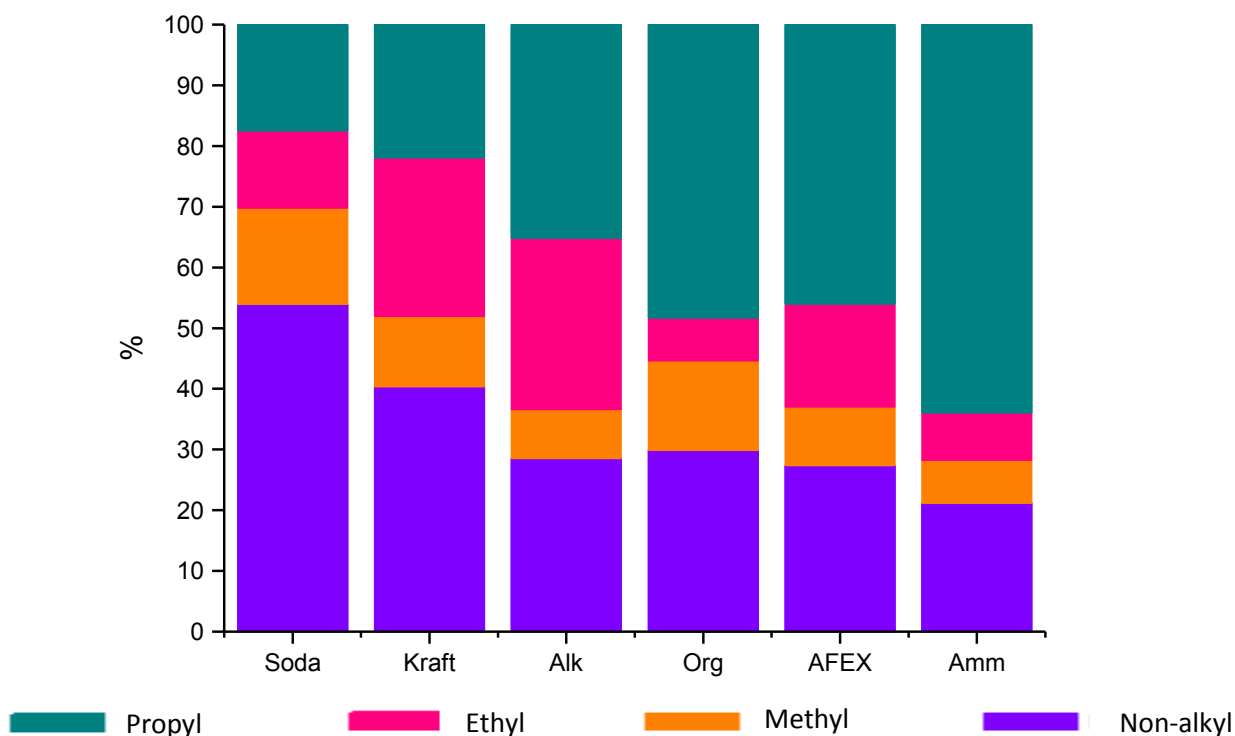


Figure 79: Catalytic depolymerisation products of Kraft lignin compared to the other lignins used

Some optimisation work using the Kraft lignin was also attempted. The optimised conditions found in section 3.2.4 for the effective depolymerisation of the ammonia lignin were used as an initial study to examine whether they had the same positive effect with the Kraft lignin for high alkylphenolic production and low char formation. The results showed that whilst one set of conditions may be efficient for one type of lignin, this was not the case for another. The highest yield of 11.5 % monomeric product was observed when the Kraft lignin was reacted for 4 h but little difference was observed for each of the other optimised reactions. As with the standard reaction with Pt/alumina shown above, the main compound generally observed in the optimisation work from the light fraction was guaiacol, where its selectivity for each reaction ranged from 18-35 % depending on the different conditions used. This work confirmed that no two lignin samples react the same way under the same conditions and that a separate optimisation study would have to be carried out on the Kraft lignin.

Although a change in pH was not carried out for the Kraft lignin reactions, the addition of an acidic or basic co-catalyst was found to be useful in other work. Liquid phase reforming

(LPR) work was also attempted by Zakzeski on the Kraft lignin using ethanol with an acidic co-catalyst ( $\text{H}_2\text{SO}_4$ ) and Pt/alumina under 58 barg He at 498 K. They showed that their main monomeric product was also guaiacol followed by ethylcatechol and methanol, which they attributed to being derived from ethylguaiacol via acid-catalysed hydrolysis of the alkyl-aryl ether bond [48]. Interestingly, they claimed 17.6 % of the lignin's original mass was converted to monomeric products which is almost double that obtained in this work for the best case, and more than three times the yield obtained for the 100 % methanol experiment. They detected  $\text{H}_2$ ,  $\text{CH}_4$  and  $\text{C}_2\text{H}_6$  light gases, as well as  $\text{CO}_2$  which was a result of the LPR conditions favouring the water-gas shift reaction to rid the system of CO. Limited amounts of alkanes resulted from reactions such as Brønsted acid-catalysed dehydration and dealkylation reactions (see section 3.2.4), or alternative reactions such as Fischer Tropsch and methanation of CO,  $\text{H}_2$  and  $\text{CO}_2$  [101]. A combination of Pt/alumina and NaOH was also used and it was found to yield 12.8 % of monomeric product with respect to the starting Kraft lignin mass, with high yields of guaiacol and benzyl alcohol [48].

Due to the condensed nature of the Kraft lignin, the increased formation of char material in the heavy fraction was expected to be similar to that observed for the soda lignin. For the catalytic run using the standard conditions, the Kraft lignin produced the highest amount of char when compared to all other lignins, including the soda lignin, and this significantly increased when no catalyst was employed. The aim of the optimisation work was to limit the char formation as well as increase alkylphenolic conversion but it generally remained much higher than that found with the ammonia lignin. The use of IPA/water solution and more catalyst (0.2 g) did however decrease the char yield obtained whilst maximising the monomeric product so this shows that some optimisation of the system was achievable and that it should be further explored.

All results given in this chapter have been summarised in Table 38 below:

Table 38: Summary of results using Kraft lignin

<b>Parameter Change</b>	<b>Autogeneous Pressure (barg)</b>	<b>Mw (Da)</b>	<b>Mw Decrease (%)</b>	<b>Ip</b>	<b>Ip Decrease (%)</b>	<b>Alkylphenolic Yield (g/100g)</b>	<b>Heavy Yield (g/100g)</b>
<b>He without catalyst</b>	130	1786	61	2.06	38	4.65	41.20
<b>H<sub>2</sub> without catalyst</b>	150	1409	69	1.98	41	5.61	71.47
<b>H<sub>2</sub> with alumina</b>	140	1470	68	1.94	42	6.42	58.53
<b>Standard run</b>	160	942	79	1.66	50	9.17	37.87
<b>Reproduced run</b>	140	1378	79	1.85	45	7.50	39.30
<b>Recycled run</b>	140	1493	67	1.91	43	5.85	40.27
<b>30 barg</b>	155	1170	74	1.85	45	9.39	40.67
<b>100 % methanol</b>	160	726	84	1.95	42	5.60	0.13*
<b>IPA water</b>	130	1874	59	2.23	33	9.76	7.73

Table 39: Summary of results using Kraft lignin (continued)

<b>Parameter Change</b>	<b>Autogeneous Pressure (barg)</b>	<b>Mw (Da)</b>	<b>Mw Decrease (%)</b>	<b>Ip</b>	<b>Ip Decrease (%)</b>	<b>Alkylphenolic Yield (g/100g)</b>	<b>Heavy Yield (g/100g)</b>
<b>4 h reaction</b>	140	1158	75	1.75	48	11.49	36.00
<b>0.2 g catalyst</b>	140	1096	76	1.68	50	8.79	29.87
<b>Rh/alumina</b>	140	1372	70	1.87	44	7.90	39.73

### **3.4 Isotopic Labelling Studies of Lignin**

This section aims to present and describe the results found when deuterium (D) was incorporated into the standard reaction with the benchmark ammonia lignin. This work will then be compared to the deuterium experiments carried out with the sulfur-containing Kraft lignin to investigate whether the two lignins depolymerise in the same way. Standard conditions were used throughout (see section 2.3.2) with either the gas, methanol or water component being substituted for the deuterated equivalent in various combinations. Monomeric yields were determined using GC-MS and kinetic isotope effect values were also calculated. A proposed breakdown mechanism has been given and this was supported by the GC-MS data obtained.

#### **3.4.1 Ammonia Lignin Deuterium Studies**

##### **3.4.1.1 Substitution of the hydrogen gas**

In order to determine the effect of gas on the depolymerisation reaction, the 20 barg hydrogen gas was firstly substituted with 20 barg deuterium gas instead. All other variables remained as standard. No significant change in the monomeric yield was obtained when the H<sub>2</sub> gas was substituted with D<sub>2</sub>. The deuterium gas experiment yielded 16.8 % of product in comparison to 16.4 % when hydrogen gas was used. The yield values obtained are within experimental error so it can be assumed that the gas alone made little difference to the depolymerisation reaction.

##### **3.4.1.2 Substitution of water as the reaction solvent**

It was previously highlighted that the use of water as a solvent caused significant condensation of the lignin so it was of interest to investigate the effect of using deuterium oxide (D<sub>2</sub>O). The incorporation of D<sub>2</sub>O with H<sub>2</sub>, or a fully deuterated system of D<sub>2</sub> and D<sub>2</sub>O, made only a slight difference to the overall yield of product in comparison to the hydrogen equivalent. The H<sub>2</sub>/D<sub>2</sub>O and D<sub>2</sub>/D<sub>2</sub>O reactions yielded 12.2 and 12.1 % of product in comparison to the equivalent H<sub>2</sub>/H<sub>2</sub>O reaction which gave 11.2 %. Little difference was observed for most of the products, although more propenyl and propyl-OMe/OH products were formed during the deuterated reactions.

##### **3.4.1.3 Substitution of methanol as the reaction solvent**

Here the effects of substituting methanol (CH<sub>3</sub>OH) with deuterated methanol (CD<sub>3</sub>OD) are shown. To begin with, the CH<sub>3</sub>OH was substituted with CD<sub>3</sub>OD, where all other variables remained as standard. This is represented by the black and dark grey columns shown in

Figure 80 where a change in the yields obtained was observed. The substituted isotope experiment was found to yield 21 % of monomeric product in comparison to the standard reaction which gave 16.4 %.

A second reaction was carried out to investigate whether using D<sub>2</sub> gas and CD<sub>3</sub>OD together altered the product distribution in any way. Figure 80 shows that there was an increase for most products in general, giving an overall yield of 22.3 %. These combined results would suggest that the methanol and gas worked together during the depolymerisation reaction, and that both were required for increased monomeric yield.

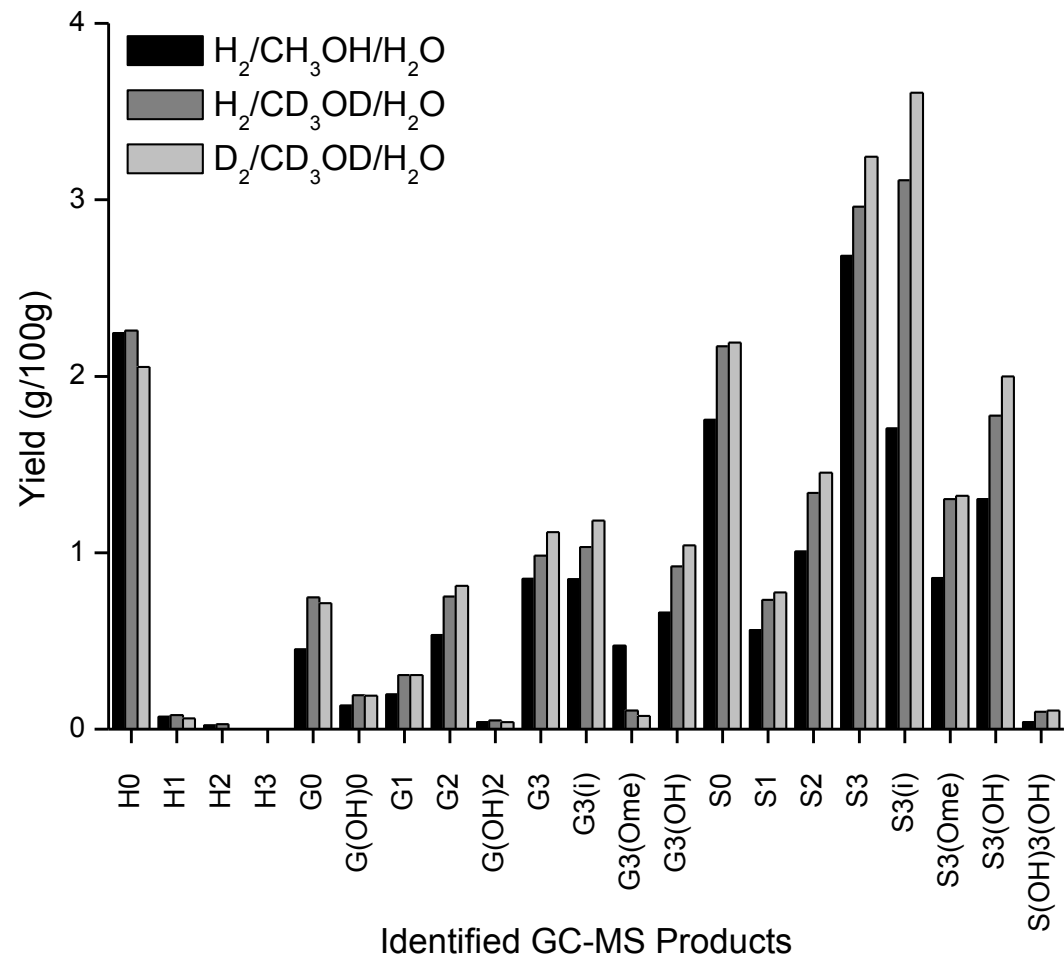


Figure 80: Effect of methanol on the depolymerisation of ammonia lignin

#### 3.4.1.4 Effects of using a fully deuterated system

Lastly, a completely deuterated reaction was carried out to directly compare against the protonated standard reaction. Here, 20 barg of deuterium gas was added to 100 ml of 50:50 v/v deuterated methanol ( $\text{CD}_3\text{OD}$ ) and deuterated water ( $\text{D}_2\text{O}$ ) with 0.5 g of ammonia lignin and 0.1 g of Pt/alumina. Figure 81 shows the distribution plot obtained for the deuterated reaction in comparison to the standard reaction. There was a general increase observed for each of the products with no dramatic change in selectivity for most products, although there was an increase in selectivity towards G3(i) and S3(i) products and a subsequent decrease in G3 and S3 due to the monomers being able to retain the C=C bond when deuterium was added to the reaction. Additionally, G3 and S0 gave a similar yield to the standard reaction which suggested they were not a result of the solvent or gas. Little difference between these results and the  $\text{D}_2/\text{CD}_3\text{OD}/\text{H}_2\text{O}$  experiment (shown in the last section) in terms of the overall yield of each product was noted which would suggest that the methanol had the most influence on the reaction and that it in some way aided efficient depolymerisation of the lignin molecule.

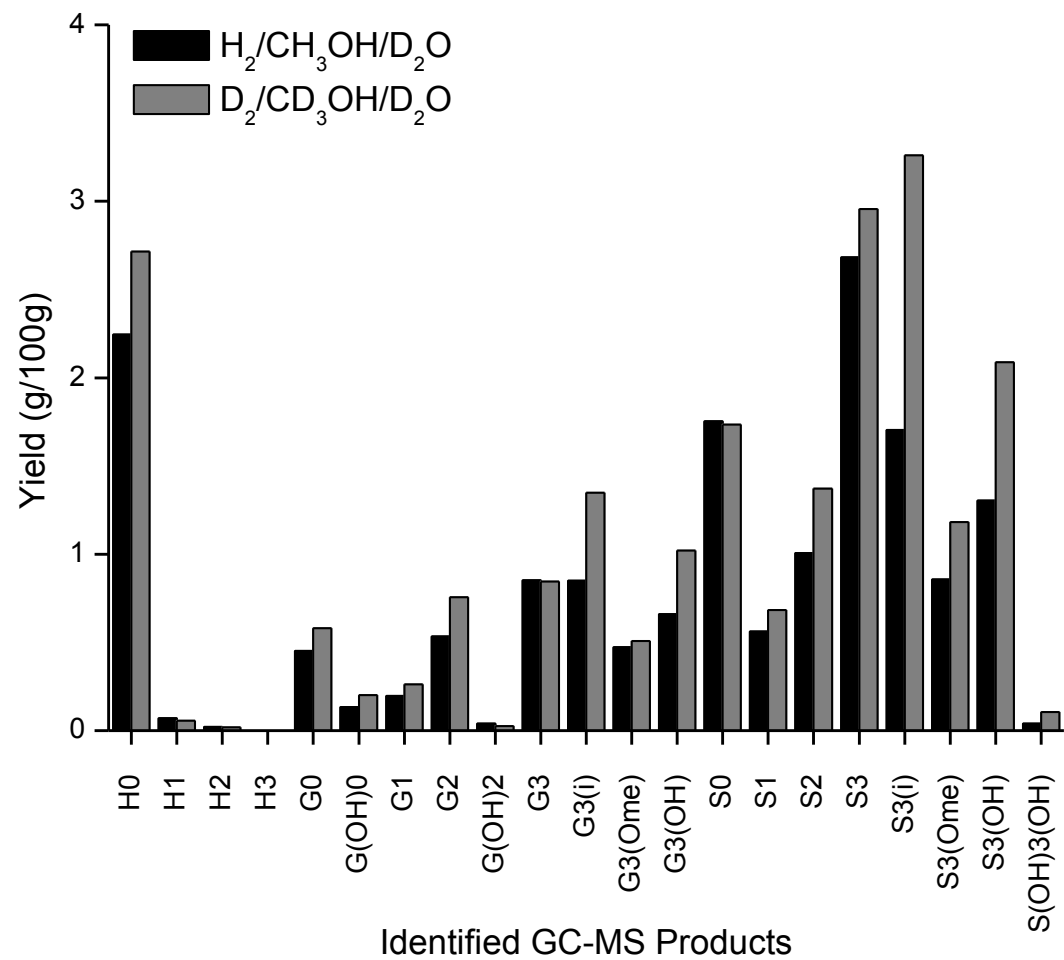


Figure 81: Fully hydrogenated vs. fully deuterated standard reaction with ammonia lignin

### 3.4.1.5 Summary of the Ammonia Lignin Deuterium Results

This section aimed to take the ammonia lignin and study its depolymerisation activity using isotopic labelling experiments. A summary of the reaction products with respect to the alkyl chain length has been illustrated in Figure 82, where it was assumed that the type of product (i.e. H, G or S) did not affect the length of the alkyl chain on that particular unit. When comparing the fully protonated reaction (green) to the fully deuterated reaction (purple), there was a clear increase in the overall yield when the deuterium was added to the reaction thus showing an inverse isotope effect. When the solvents were changed to their deuterated equivalents but the gas remained as hydrogen (pink), the overall monomeric product increased but not to the same extent as the fully deuterated experiment. This confirmed that both the mixed solvent and gas components were required for effective depolymerisation.

It has been proposed throughout this thesis that the methanol was involved in a capping process whereby it reduced the formation of char via condensation reactions by capping free radicals. From the results presented here, the H<sub>2</sub> gas was found to not alter the overall yield of monomeric product when substituted with D<sub>2</sub>, but when combined with methanol it enhanced the overall yield more significantly. The masses of each of the products were found to have increased through H/D exchange or deuteration (see summary section for more detail), where single deuterium atoms incorporated themselves onto the monomeric structure. It was therefore concluded that the proposed capping mechanism occurred via single H/D atoms as opposed to entire methoxy groups. It is plausible that this additional H/D was donated from the methanol and that this was then replaced by the hydrogen gas through an equilibrium reaction, hence the need for both components in the system. Thermodynamically, the transformation of methanol to active hydrogen species is easier than gaseous hydrogen because the bond dissociation energy of the C-H bond in methanol is lower (96.1 kcal mol<sup>-1</sup>) than that of the H-H bond of H<sub>2</sub> (104.2 kcal mol<sup>-1</sup>) [102]. From a dynamics point of view, methanol as a solvent will easily come into contact with the active catalyst sites and therefore generate active hydrogen species, whilst gaseous hydrogen will have to overcome mass transfer limitations from gas to liquid and then to solid in order to be activated [46]. When the standard reaction with ammonia lignin and Pt/alumina was reacted in the autoclave at 573 K, the autogeneous pressure reached 140 barg (see Table 32), which was higher than that found for the heating of methanol-water only to 573 K (110 barg). Although these additional gaseous products could have resulted from the lignin depolymerisation, the methanol could also have been a source of gaseous H<sub>2</sub> after its

transformation on the catalyst surface. Song et al was able to collect effluent gas of decomposed deuterated methanol using a gas bag to study alcohol decomposition. The authors detected CO and CO<sub>2</sub> which led them to conclude that the methanol had decomposed to hydrogen and that this was likely the case during the lignin depolymerisation reaction [46]. From these results it can therefore be assumed that the lignin molecule underwent a solvolysis-type reaction with the methanol-water solvent, where the lignin initially cracked to smaller fragments before further converting to monomer units. In both steps, the methanol was required to first act as a solvolysis molecule and then as a hydrogen source for the formation of monomeric product.

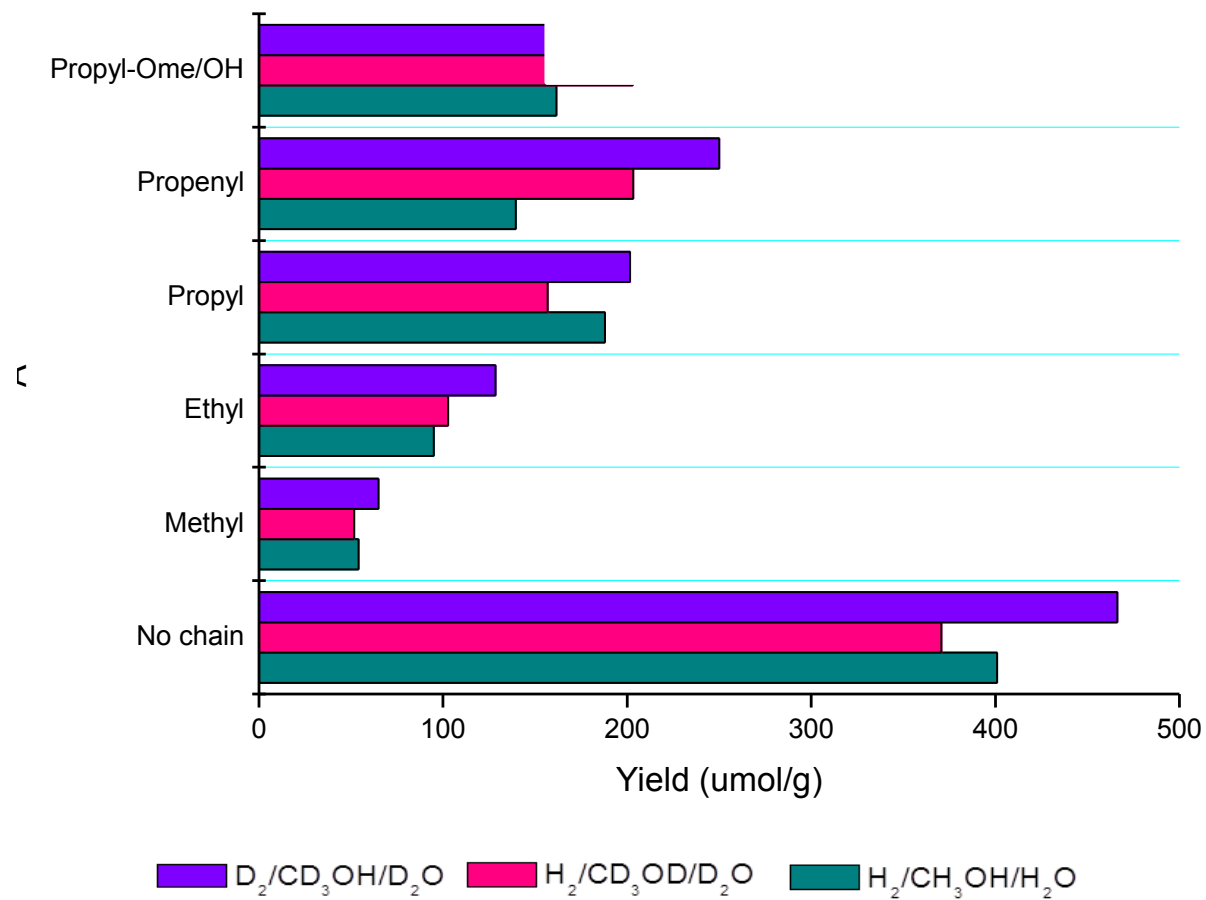


Figure 82: Depolymerisation products of ammonia lignin with respect to alkyl chain length

An inverse kinetic isotope effect was therefore observed for all experiments, where the monomeric yields increased when deuterium was incorporated into the reaction. Isotopic substitution is known to modify the rate of a reaction where, in general, heavier isotopes (i.e. deuterium) lead to lower zero-point energies which require more energy to break the bond. By using deuterium instead of hydrogen, this represented a 100 % increase in the relative mass so it was therefore expected that the rate of reaction using a C-D bond would be much slower than the equivalent C-H bond. This would also result in a higher activation energy being required for C-D bond cleavage, which should in turn lower the rate of reaction or, in this case, the monomeric yield.

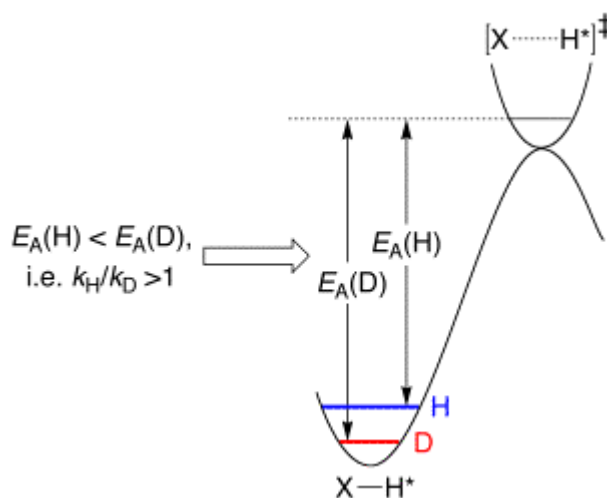


Figure 83: Energy diagram for C-H and C-D bond breakage

In order to determine the activation energies of each reaction, the energy of the vibrational levels of a vibration (i.e. a bond) in a molecule must first be calculated. This is shown by Equation 16 where  $h$  is Planck's constant and  $\nu$  is the frequency of the vibration:

$$E_n = \left(n + \frac{1}{2}\right)h\nu$$

Equation 16: Energy of bond vibrational levels

It is assumed that the molecule is in its ground state so it can be compared to zero-point vibrational energies to give:

$$E_0 = \left(n + \frac{1}{2}\right)h\nu$$

Equation 17: Energy of a bond assuming zero-point vibrational state

By using the harmonic oscillator approximation, the fundamental vibrational frequency can be given as:

$$\nu = \frac{1}{2\pi} \sqrt{\frac{k}{\mu}}$$

Equation 18: Fundamental vibrational frequency equation

Where  $k$  is the force constant of the bond and  $\mu$  is the reduced mass:

$$\mu = \frac{m_1 m_2}{m_1 + m_2}$$

Equation 19: Calculating  $\mu$  for Equation 18

The Arrhenius equation (see Equation 15) can be used to determine the activation energy of a reaction:

$$k_H = A_H e^{-(E_{aH}/RT)}$$

$$k_D = A_D e^{-(E_{aD}/RT)}$$

Equation 20: The Arrhenius equation for both the hydrogen and deuterium systems

Where  $k_H$  and  $k_D$  are the rates constants for each of the reactions, it is assumed that the Arrhenius constants are equal ( $A_H = A_D$ ) because the order of reaction  $s$  for each are assumed to be equal as well. Given that all of the reaction parameters are the same, the monomeric yield can be used to estimate the rate of reaction in this case. This will then give an approximate isotope effect:

$$\frac{k_H}{k_D} = e^{-((E_{aH} - E_{aD})/RT)}$$

Equation 21: Calculating the isotope effect

Activation energy is given by the difference in zero point energies of the reactant and the transition state by substituting Equation 17 in for both C-H and C-D reactions:

$$\text{KIE} = \frac{K_H}{K_D} = e^{-\frac{1}{2}h[(\nu_{H\ddagger} - \nu_{D\ddagger}) - (\nu_{H-H} - \nu_{D-H})]/RT}$$

Equation 22: Activation energy calculation incorporating Equation 17

Thus if the difference in frequencies at the transition state is greater than that of the reactant state, a normal isotope effect takes place ( $k_H/k_D > 1$ ) and deuterium will slow the rate of reaction. However if the opposite occurs and the rate of reaction is increased, an inverse kinetic isotope effect (IKIE) is said to have taken place ( $k_H/k_D < 1$ ) [103]. When the kinetic isotope effect (KIE) of the fully deuterated reaction was calculated using the overall monomeric yield in comparison to the protonated equivalent, it was found to be 0.76 which implied that an inverse kinetic isotope effect had taken place. Table 40 shows the yields obtained for each of the deuterium reactions given in this section, as well as the hydrogen equivalent yields obtained previously. From this, inverse kinetic isotope effect values were calculated for each experiment based on the overall yields obtained as summarised below. The S/G ratio for each reaction was also calculated with respect to the molar quantities of S or G product. The fully deuterated reaction gave a value of 2.0 which matched that of the equivalent hydrogenated system. This shows that the incorporation of deuterium into the reaction did not alter the depolymerisation mechanism or the selectivity to the resultant products, it merely enhanced it. A relationship between the IKIE values and the S/G ratios calculated was also evident, where a high IKIE value led to a high S/G ratio and vice versa.

Table 40: Summary of isotopic labelling results

<b>Reaction</b>	<b>H<sub>2</sub> yield (g/100g)</b>	<b>D<sub>2</sub> yield (g/100g)</b>	<b>KIE (k<sub>H</sub>/k<sub>D</sub>)</b>	<b>S/G Ratio</b>
<b>D<sub>2</sub>/CD<sub>3</sub>OD/D<sub>2</sub>O</b>	16.43	21.72	0.76	2.0
<b>D<sub>2</sub>/CH<sub>3</sub>OH/H<sub>2</sub>O</b>	16.43	16.77	0.97	1.7
<b>H<sub>2</sub>/CD<sub>3</sub>OD/H<sub>2</sub>O</b>	16.43	20.95	0.78	2.2
<b>D<sub>2</sub>/CD<sub>3</sub>OD/H<sub>2</sub>O</b>	16.43	22.28	0.74	2.2
<b>H<sub>2</sub>/D<sub>2</sub>O</b>	11.19	12.15	0.92	1.7
<b>D<sub>2</sub>/D<sub>2</sub>O</b>	11.19	12.06	0.93	1.6

Inverse kinetic isotope effects tend to only occur in secondary KIE systems. For primary KIE, the isotopically substituted bond is broken so that the energy of both bonds in the transition state are equal, but as shown in Equation 18 the frequency is inversely proportional to the square root of mass so the energy of the deuterium atom will be less

than that of the hydrogen atom when in its reactant state. This therefore means that the activation energy of deuterium will be higher; hence a normal KIE will be given. However for secondary KIE, isotopic substitutions occur at a site other than the bond breaking site in the rate determining step of the reaction. These sites can be at the  $\alpha$ ,  $\beta$  or  $\gamma$  position as shown in Figure 84. The energies of secondary KIE transition states are different to primary KIEs because the deuterium bond is retained so the influence of the isotope remains in the transition state as well. If the difference in zero point energy is greater in the transition state than in the reactant state, then this will result in an IKIE. The heavier isotope will concentrate at a site where it is bound strongly to or has a large force constant or frequency, so it will favour the reactant state as opposed to the hydrogen favouring the transition state. Thus the bond with the deuterium atom will be more stable than the bond with the hydrogen; hence why hydrogen systems tend to react faster than deuterium compounds.

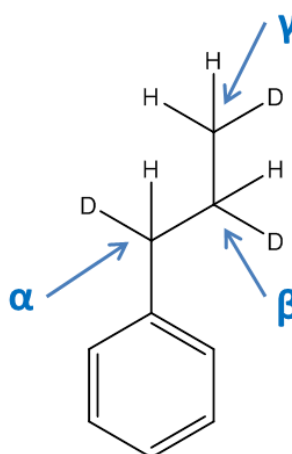


Figure 84: Secondary KIE example

With this information, it could be assumed that the incorporation of deuterium into the reaction medium was favourable to lignin depolymerisation in particular because of the increased bond strength of C-D bonds. As the monomer units are formed, deuterium is incorporated onto the structure and these C-D bonds become more stable than the ordinary C-H bonds. This increased stability, and therefore increased bond strength, reduces condensation by preventing the repolymerisation reactions of free radicals and the monomers themselves. However, assuming that an initial cracking of the lignin molecule occurs, conversion of the fragmented lignin pieces will follow. Hydroxyl groups in native lignin can typically be found on the  $C_\alpha$  and  $C_\gamma$ , whilst the  $C_\beta$  is generally interlinked via C-

O-C linkages. During the reaction, propylguaiacol (S3) for example could be formed from the lignin structure via the cleavage of the ether bond and removal of the hydroxyls from the basic guaiacyl unit. It is possible for the C-OH group to be removed in the form of H<sub>2</sub>O via  $\beta$ -elimination with subsequent hydrogenation of the C=C bond, or via hetero-cleavage on active sites followed by the addition of deuterium, i.e. via hydrogenolysis [46]. The C-O-C linkage can also be cleaved using this hydrogenolysis route. Using this information it can therefore be assumed that a primary KIE is also exhibited as deuterium is incorporated onto the positions where the -OH groups have been removed (C <sub>$\alpha$</sub>  and C <sub>$\gamma$</sub> ), and in place of the oxygen atom of the  $\beta$ -O-4 bond (C <sub>$\gamma$</sub> ). This mechanism has been given in Figure 85, where those highlighted in red have been identified in this work:

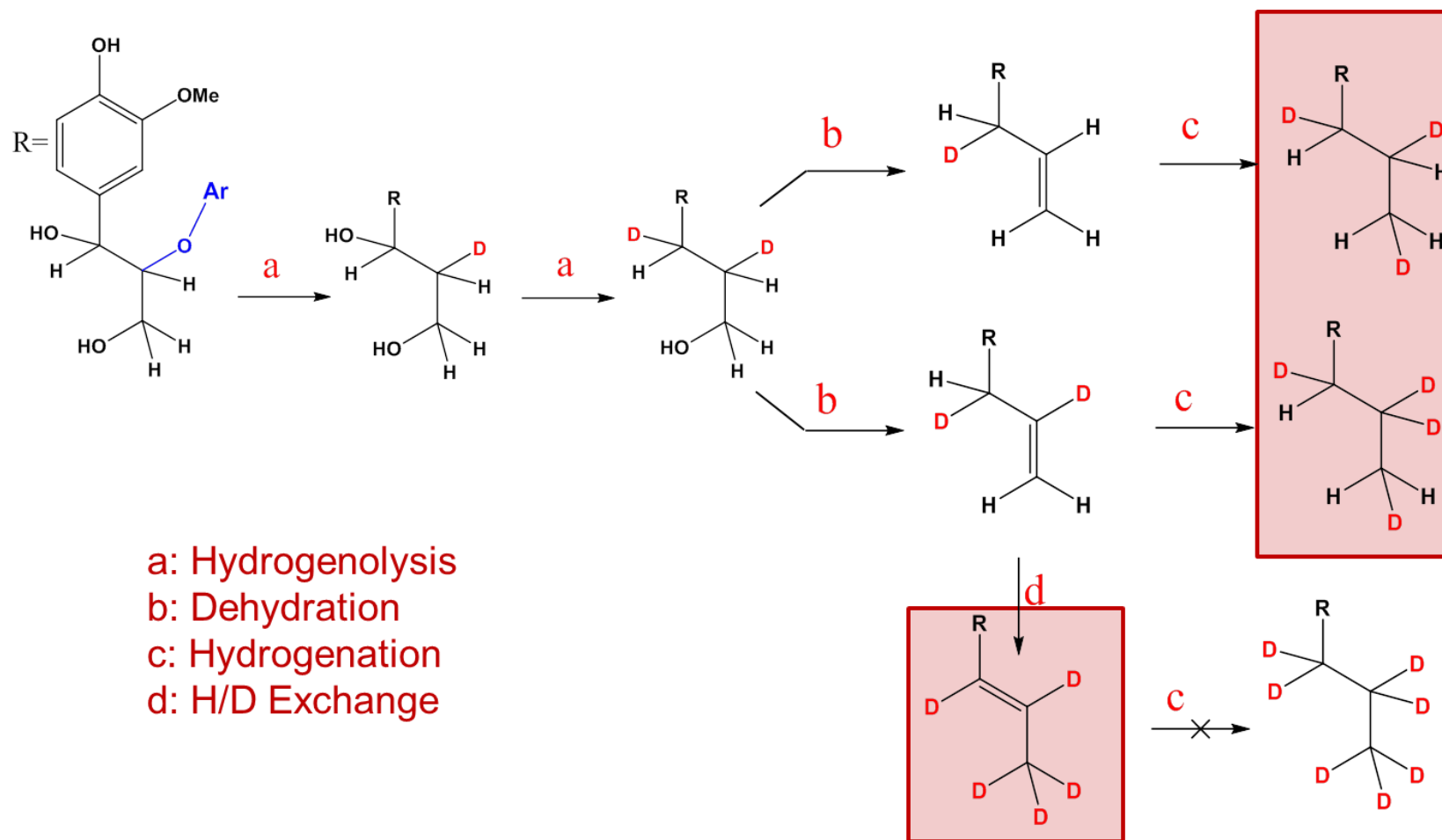


Figure 85: Monomeric product formation from the cracked lignin fragments

Figure 85 illustrates that there are a number of potential reaction steps involved in the formation of monomeric product so secondary KIE is therefore not the only explanation for the IKIE values. It is difficult to ascertain which reaction is the rate-determining step so the overall IKIE was deemed to be an unfair representation of the mechanism as it is clearly dependent on more than one reaction. The kinetic isotope effect for each monomer product for each standard reaction was therefore calculated instead and is given in Table 41. Similar to the conclusions drawn from Figure 82, the KIE values were more positive because the deuterium did not affect the reaction to the same extent as the other experiments. The other experiments gave fairly similar KIE values and the rate-determining step was not evident from this data alone.

Table 41: KIE values for each monomeric product across each standard deuterium reaction

<b>Monomer Product</b>	<b>D<sub>2</sub>/CD<sub>3</sub>OD/D<sub>2</sub>O</b>	<b>D<sub>2</sub>/CH<sub>3</sub>OH/H<sub>2</sub>O</b>	<b>H<sub>2</sub>/CD<sub>3</sub>OD/H<sub>2</sub>O</b>	<b>D<sub>2</sub>/CD<sub>3</sub>OD/H<sub>2</sub>O</b>
<b>H0</b>	0.83	1.21	0.99	1.09
<b>H1</b>	1.24	1.30	0.88	1.17
<b>H2</b>	1.01	0.56	0.73	-
<b>H3</b>	-	-	-	-
<b>G0</b>	0.78	0.77	0.60	0.63
<b>G(OH)0</b>	0.66	1.30	0.69	0.70
<b>G1</b>	0.75	0.80	0.64	0.64
<b>G2</b>	0.71	0.83	0.71	0.66
<b>G(OH)2</b>	1.51	1.80	0.82	1.02
<b>G3</b>	1.01	0.74	0.87	0.76
<b>G3(i)</b>	0.63	1.00	0.82	0.72
<b>G3(OMe)</b>	0.93	0.90	4.51	6.40
<b>G3(OH)</b>	0.65	0.82	0.72	0.63

Table 42: KIE values for each monomeric product across each standard deuterium reaction (continued)

<b>Monomer Product</b>	<b>D<sub>2</sub>/CD<sub>3</sub>OD/D<sub>2</sub>O</b>	<b>D<sub>2</sub>/CH<sub>3</sub>OH/H<sub>2</sub>O</b>	<b>H<sub>2</sub>/CD<sub>3</sub>OD/H<sub>2</sub>O</b>	<b>D<sub>2</sub>/CD<sub>3</sub>OD/H<sub>2</sub>O</b>
<b>S0</b>	1.01	0.95	0.81	0.80
<b>S1</b>	0.82	0.96	0.77	0.72
<b>S2</b>	0.73	1.01	0.75	0.69
<b>S3</b>	0.91	0.93	0.91	0.83
<b>S3(i)</b>	0.52	1.38	0.55	0.47
<b>S3(OMe)</b>	0.73	0.97	0.66	0.65
<b>S3(OH)</b>	0.62	0.93	0.73	0.65
<b>S(OH)3(OH)</b>	0.39	0.56	0.41	0.39

(- indicates no data)

As well as being able to use the GC-MS data to calculate kinetic isotope effects which relate to rate limiting steps and transition states, it could also be used to detect mass changes on the monomer product to support the mechanism proposed in Figure 85. Depending on the conditions used, deuterium atoms were found to have incorporated or exchanged onto the monomer unit in various numbers and this was reflected by the MS data obtained. Table 43 shows the number of deuterium atoms added onto each of the monomer structures for each of the reactions shown previously. The reactions which substituted the gas only, or the gas and methanol only, showed very little deuterium incorporation as opposed to the fully deuterated experiment and the reactions that used deuterium oxide as the reaction solvent.

Table 43: Summary of the H/D exchange onto the monomer products for each reaction

Monomer unit	Monomer mass	Number of incorporated deuterium atoms onto the monomer structure					
		D <sub>2</sub> /CD <sub>3</sub> OD/ D <sub>2</sub> O	D <sub>2</sub> /CH <sub>3</sub> OH/ H <sub>2</sub> O	H <sub>2</sub> /CD <sub>3</sub> OD/ H <sub>2</sub> O	D <sub>2</sub> /CD <sub>3</sub> OD/ H <sub>2</sub> O	H <sub>2</sub> /D <sub>2</sub> O	D <sub>2</sub> /D <sub>2</sub> O
<b>H0</b>	166	3	0	0	1	3	3
<b>H1</b>	180	4	0	1	1	4	4
<b>H2</b>	194	6	0	1	0	6	6
<b>H3</b>	208	-	-	-	-	-	-
<b>G0</b>	196	2	0	0	0	2	2
<b>G(OH)0</b>	254	4	0	1	1	4	4
<b>G1</b>	210	4	0	0	0	5	5
<b>G2</b>	224	5	0	0	1	6	6
<b>G(OH)2</b>	282	7	0	1	1	7	7
<b>G3</b>	238	5	0	0	1	5	5
<b>G3(i)</b>	236	7	0	0	1	7	7
<b>G3(OMe)</b>	268	6	0	0	0	7	9

Table 44: Summary of the H/D exchange onto the monomer products for each reaction (continued)

Monomer unit	Monomer mass	Number of incorporated deuterium atoms onto the monomer structure					
		D <sub>2</sub> /CD <sub>3</sub> OD/ D <sub>2</sub> O	D <sub>2</sub> /CH <sub>3</sub> OH/ H <sub>2</sub> O	H <sub>2</sub> /CD <sub>3</sub> OD/ H <sub>2</sub> O	D <sub>2</sub> /CD <sub>3</sub> OD/ H <sub>2</sub> O	H <sub>2</sub> /D <sub>2</sub> O	D <sub>2</sub> /D <sub>2</sub> O
<b>G3(OH)</b>	326	3	0	0	0	4	4
<b>S0</b>	226	1	0	0	0	3	3
<b>S1</b>	240	5	0	0	0	5	5
<b>S2</b>	254	4	0	0	0	6	6
<b>S3</b>	268	4	0	0	0	6	6
<b>S3(i)</b>	266	6	0	0	1	7	7
<b>S3(OMe)</b>	356	8	0	0	0	8	8
<b>S3(OH)</b>	356	3	0	0	0	4	4
<b>S(OH)3(OH)</b>	414	4	0	0	1	4	4

Using the MS data and Table 43, Figure 86 and Figure 87 confirms that deuterium was added to the C<sub>α</sub> and C<sub>β</sub> positions where hydroxyl groups once occupied. Below, the formation of G2 and S2 from the standard reaction is compared to the fully deuterated reaction (H<sub>2</sub>/CD<sub>3</sub>OD/D<sub>2</sub>O) and the D<sub>2</sub>/D<sub>2</sub>O reaction. The molecular weight of G2 formed in the standard reaction was m/z 224, in contrast to the D<sub>2</sub>/CD<sub>3</sub>OD/D<sub>2</sub>O reaction which gave a molecular weight of m/z 229 and the D<sub>2</sub>/D<sub>2</sub>O experiment which gave m/z 230. Alternatively, the S2 unit had a molecular weight of m/z 254 when produced in the standard reaction, in comparison to m/z 258 and m/z 260 for the D<sub>2</sub>/CD<sub>3</sub>OD/D<sub>2</sub>O and D<sub>2</sub>/D<sub>2</sub>O experiments respectively. These additions to the molecular weights of G2 and S2 show that deuteration or H/D exchange reactions occurred during the course of the monomer formation. The initial mass loss of 30 to m/z 194/199/200 was attributed to the loss of the methoxy group from the aromatic ring, and the second mass loss of 15/18/18 to m/z 179/181/200 was attributed to the cleavage of the C<sub>β</sub> methyl group as illustrated. This incorporation of deuterium onto the alkyl groups reveals that the deuterium must have been added from a hydrogenolysis step as opposed to H/D exchange. That said the remaining deuterium atoms must have been incorporated onto the α-carbon via hydrogenolysis of the hydroxyl on the C<sub>α</sub>, with the remaining weight being a result of H/D exchange onto the ring itself. As shown below, the D<sub>2</sub>/D<sub>2</sub>O reaction had so many extra deuterium atoms remaining that they must therefore have exchanged with hydrogens on the aromatic ring.

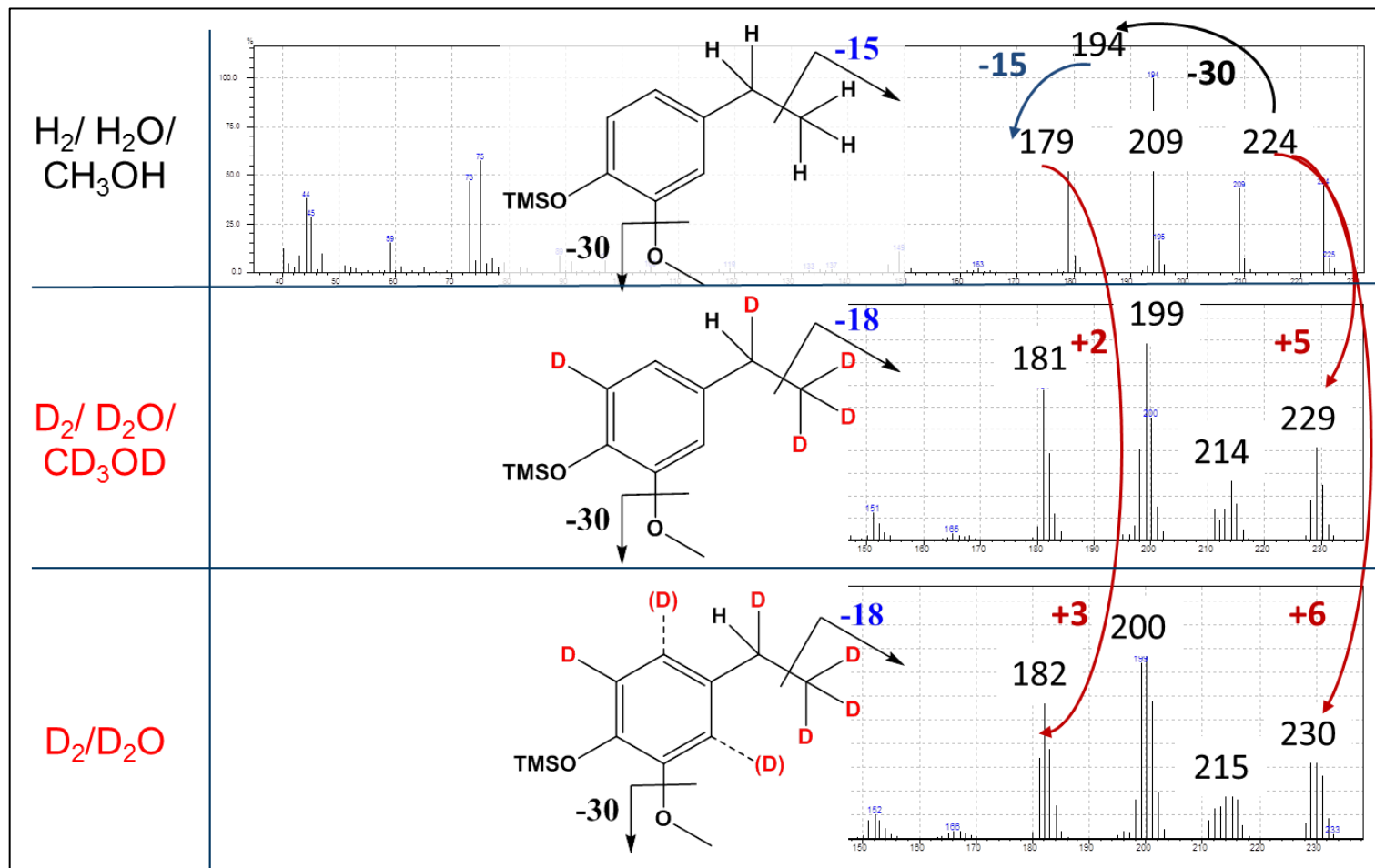


Figure 86: Added deuterium atoms onto G2 product

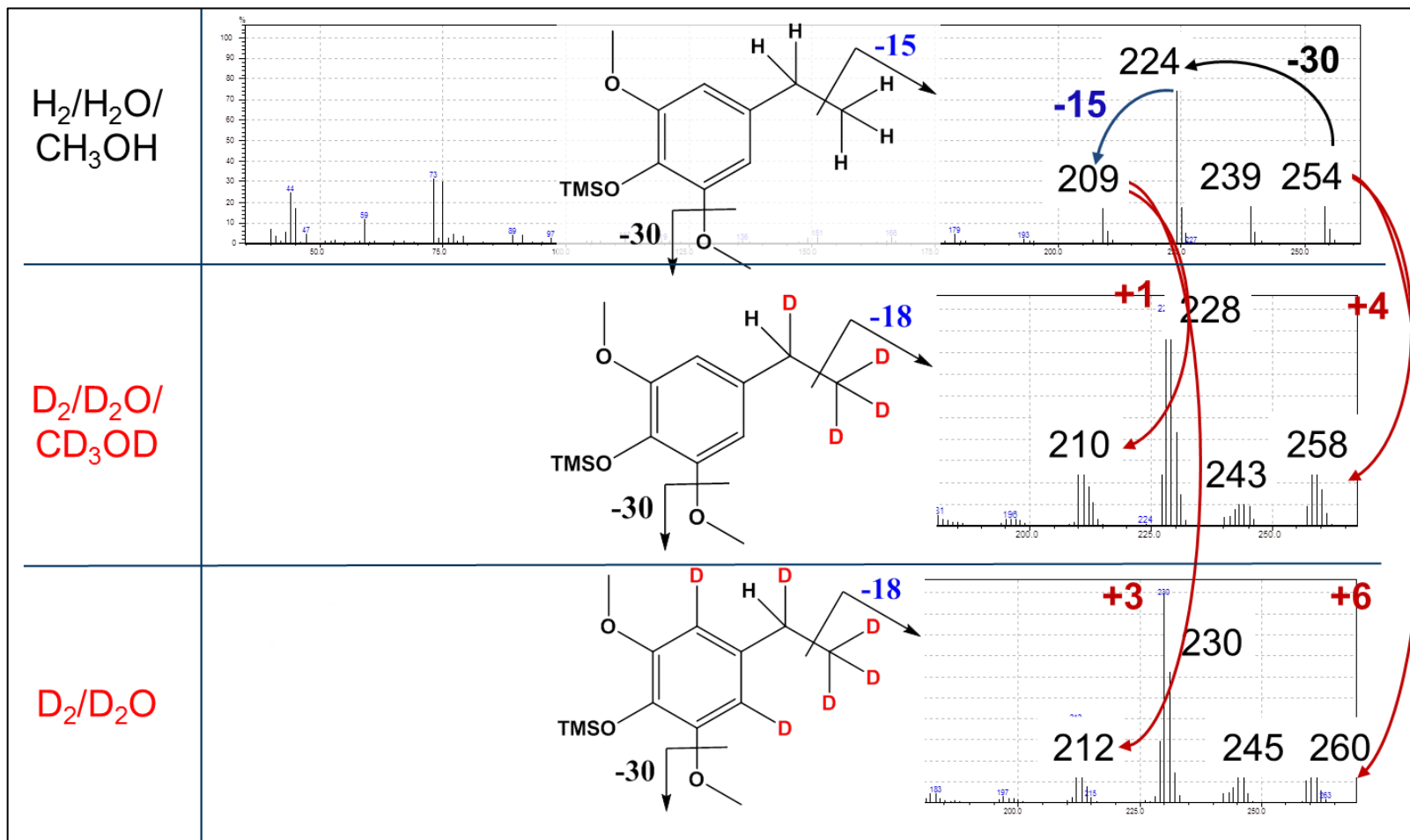


Figure 87: Added deuterium atoms onto S2 product

Figure 88 illustrates the general H/D exchange onto the aromatic ring across the various isotopic substitution reactions. No ring exchange was observed when the hydrogen gas was substituted for deuterium gas, and only one deuterium atom was substituted onto the ortho position of the aromatic ring for the G units during the fully deuterated/deuterated solvent-only experiments. This is in comparison to the water only reactions which exchanged two deuterium atoms onto the ring, one of which exchanged on the ortho position and either of the meta positions. This higher number of deuterium atoms found with the H<sub>2</sub>O/D<sub>2</sub>O experiments was thought to have been a result of hydration of the alumina support as illustrated in Figure 89. It was thought that when 100 % water was used as the reaction solvent, the water hydrated the alumina to give hydroxyls which were subsequently exchanged with deuterium during the D<sub>2</sub>O reactions, therefore increasing the chance of H/D exchange onto the monomer unit. In comparison, the methanol will have methoxylated the alumina support so the standard methanol-water mix was assumed to have not hydrated the alumina to the same extent as the water only reaction, if at all.

Note that the H<sub>2</sub>/CD<sub>3</sub>OD/D<sub>2</sub>O reaction was not discussed in this chapter but the overall yield slightly increased to 17.5 % in comparison to the standard reaction thus giving an inverse kinetic isotope effect of 0.94. The number of incorporated deuterium atoms was similar to that of the fully deuterated system.

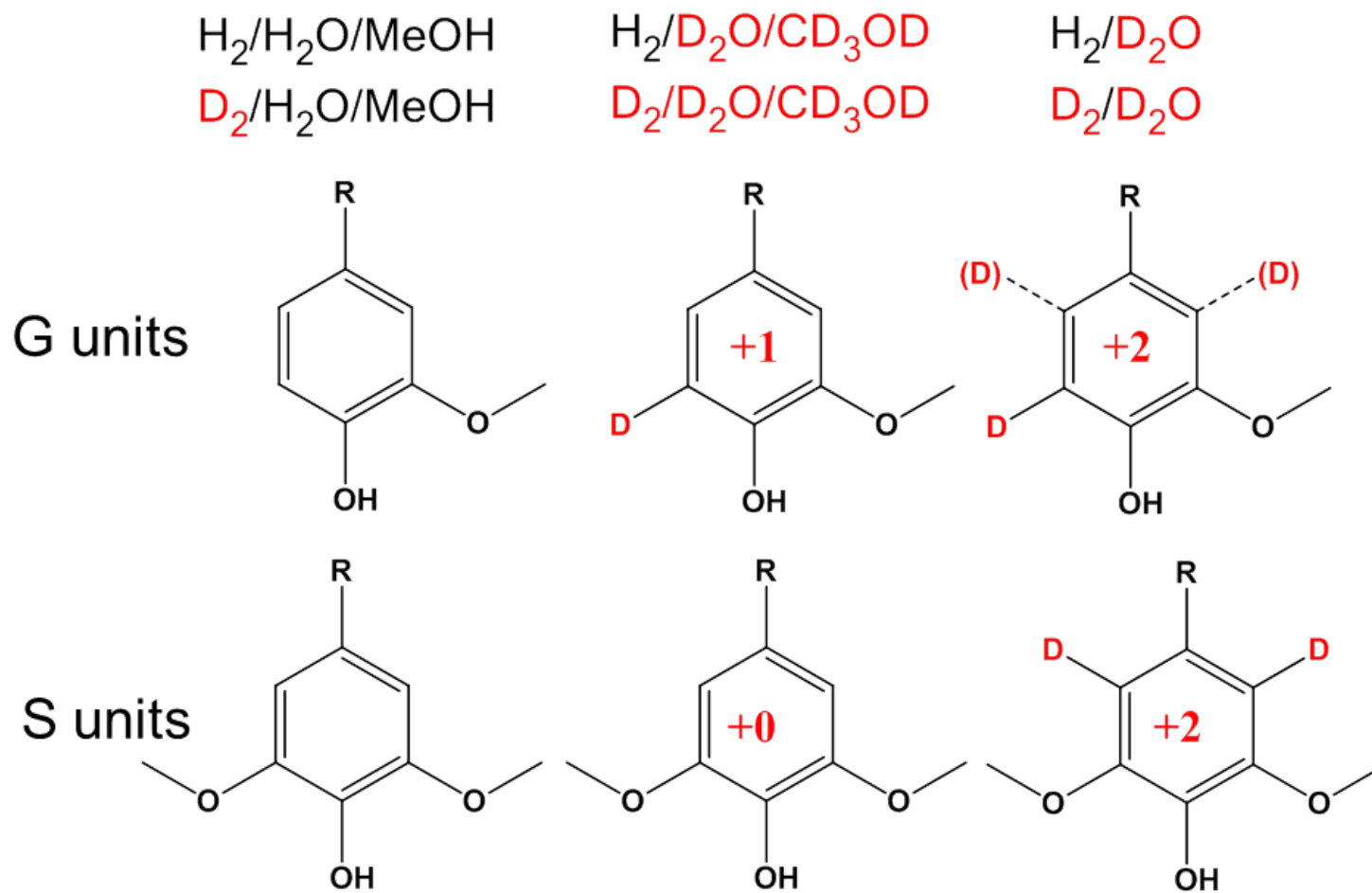


Figure 88: H/D exchange on the aromatic ring

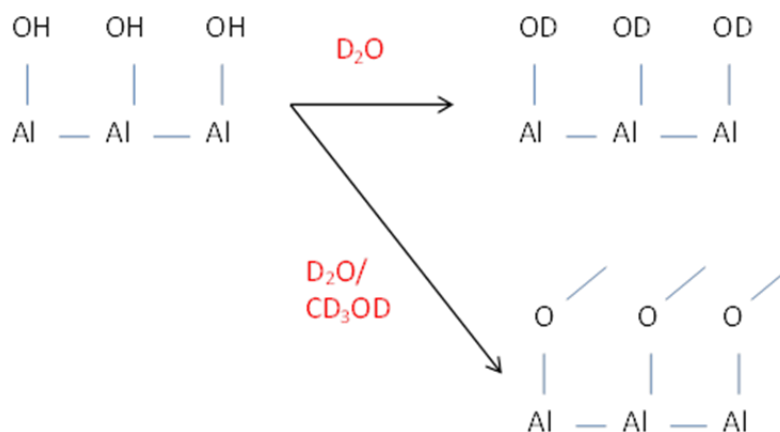


Figure 89: Deuterium exchange onto the alumina support via hydration depending on the reaction solvent used

### 3.4.2 Kraft Lignin Deuterium Studies

Based on the ammonia deuterium studies, it was of interest to the project to investigate whether the addition of deuterium also showed an inverse kinetic isotope effect during Kraft lignin depolymerisation. Figure 90 compares the product distributions obtained under the standard reaction conditions with hydrogen to that obtained under the deuterated equivalent reaction. Figure 90 shows that the Kraft lignin also showed a clear increase in product formation when deuterium was added to the reaction, where it produced 20.8 % of product in comparison to 9.2 %. The increase in monomeric yield was considerably higher for Kraft lignin than it was for the ammonia lignin, and the selectivity to the individual products also changed with the addition of deuterium. An increase in selectivity towards G3(i) and G3(OH) was noted and attributed to increased bond stability via deuteration and/or H/D exchange onto the alkyl chain, with a subsequent decrease in G0 and G3 products as a result. This has been summarised in Table 45.

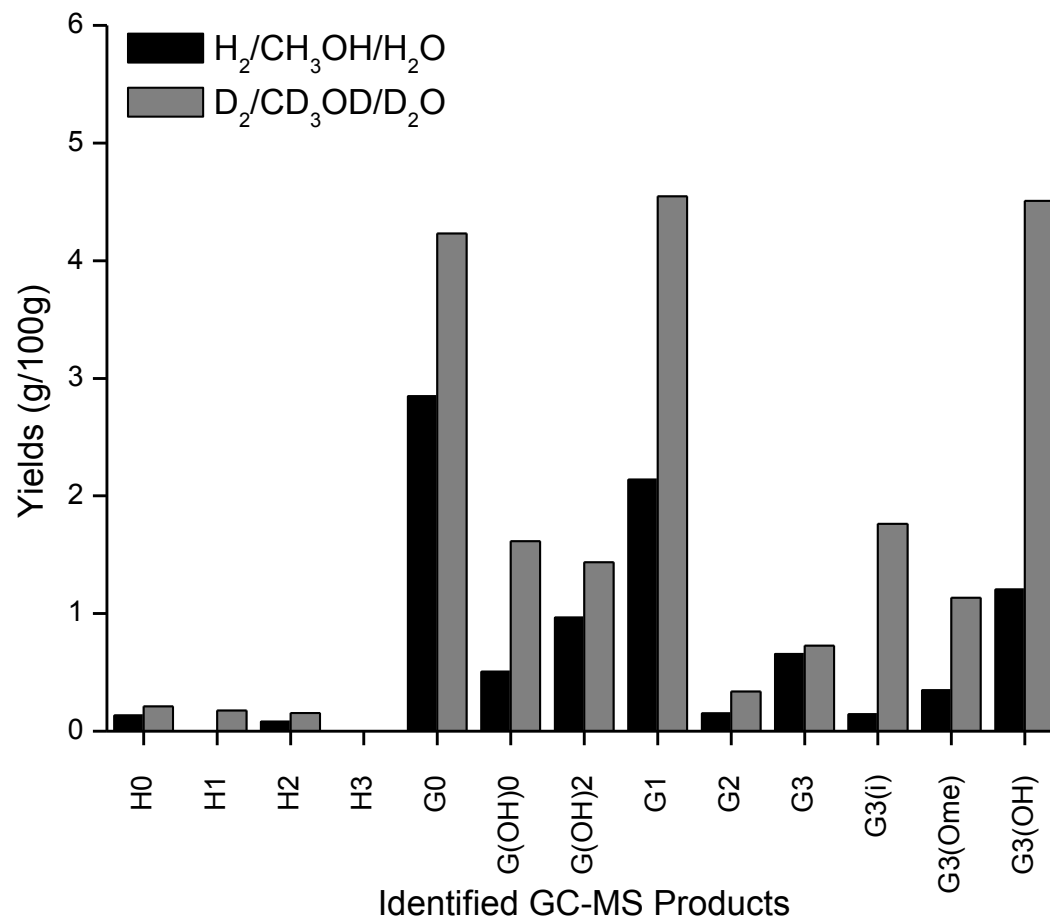


Figure 90: Fully hydrogenated vs. fully deuterated standard reaction with Kraft lignin

Table 45: Product selectivities obtained between the protonated and deuterated standard reactions

<b>Monomer</b>	<b>H<sub>2</sub>/CH<sub>3</sub>OH/H<sub>2</sub>O</b>	<b>D<sub>2</sub>/CD<sub>3</sub>OD/D<sub>2</sub>O</b>
<b>Product</b>		
<b>H0</b>	1.46	1.00
<b>H1</b>	0.00	0.84
<b>H2</b>	0.88	0.74
<b>H3</b>	0.00	0.00
<b>G0</b>	31.04	20.31
<b>G(OH)0</b>	5.51	7.75
<b>G(OH)2</b>	10.52	6.89
<b>G1</b>	23.33	21.82
<b>G2</b>	1.64	1.62
<b>G3</b>	7.16	3.49
<b>G3(i)</b>	1.56	8.46
<b>G3(OMe)</b>	3.78	5.44
<b>G3(OH)</b>	13.13	21.63

With respect to the general behaviour of the Kraft lignin across a range of deuterated experiments, it exhibited the same behaviour as the ammonia lignin where exchanging the H<sub>2</sub> gas with D<sub>2</sub> made little difference to the overall reaction yield. Whilst the use of D<sub>2</sub>O aided the reaction slightly, the use of CD<sub>3</sub>OD aided the depolymerisation to a better extent. The highest yield was obtained when a fully deuterated reaction was used as shown previously. In terms of the number of deuterium atoms incorporated onto the Kraft lignin monomer products, the masses were also found to be the same as that found with the ammonia lignin products, with the exception of G3, G3(i) and G3(OH) as shown in

Table 46. This difference with the 3-chained alkylphenolics was likely due to the Kraft lignins condensed nature and therefore lack of hydroxyls and ether linkages on the chain available for cleavage via hydrogenolysis and subsequent deuteration. These results would lead to the conclusion that the Kraft lignin also depolymerised in a similar manner to the ammonia lignin, where it initially fragmented to smaller lignin pieces followed by monomer formation.

Similar to the ammonia lignin, the Kraft lignin also showed an overall inverse kinetic isotope effect (0.44) based on the total monomeric yield obtained, but this was also reflected with each of the monomeric products as well. The IKIE values were much higher than those found for the ammonia lignin which showed that the deuterium affected the depolymerisation of Kraft lignin more significantly. Again, this was likely due to the Kraft lignins condensed nature, where the deuterium stabilised the monomers as they were formed thus reducing the repolymerisation and condensation of the molecules.

Table 46: Comparison of the H/D exchange for the ammonia and Kraft lignins

Monomer unit	Monomer mass	No. of incorporated D atoms		KIE values
		Ammonia	Kraft	Kraft
H0	166	3	3	0.64
H1	180	4	n/d	0.00
H2	194	6	6	0.52
H3	208	-	-	-
G0	196	2	2	0.67
G(OH)0	254	4	4	0.31
G1	210	4	4	0.67
G2	224	5	5	0.47
G(OH)2	282	7	7	0.44
G3	238	5	4	0.90
G3(i)	236	7	6	0.08
G3(OMe)	268	6	4	0.31
G3(OH)	326	3	1	0.27

### 3.4.3 Summary of the Isotopic Labelling Studies of Lignin

In summary, although conventional isotopic labelling studies are typically used to investigate the mechanistics of a reaction and to determine the rate-determining step, the inclusion of deuterium into the depolymerisation of lignin gave alternative, yet interesting results. It was found that the deuterium increased the rate of reaction to give higher monomeric yields and this was accredited to increased stability of the C-D bond in comparison to the usual C-H bonds which were plagued with repolymerisation and

condensation issues. With the increasing monomeric yield, it was important to note that the addition of deuterium did not alter the product selectivity significantly for the uncondensed ammonia lignin in comparison to the equivalent protonated reaction, but it did have a dramatic effect on the condensed Kraft lignin. This again highlighted the difference in reaction possibilities between lignin types and showed that the Kraft lignin was capable of producing monomeric product in a yield equivalent to that of the ammonia lignin when the condensation problems were addressed. Inverse kinetic isotope values were also determined for each of the monomeric products as it was assumed that overall IKIE values were not a fair representation of the lignin depolymerisation reaction. The rate-determining step in the reaction was not determined from this work and it was concluded that a more thorough study would be required. In terms of the reaction mechanism, it was proposed that the lignin underwent an initial fragmentation step followed by a number of other steps, including hydrogenolysis, dehydration and hydrogenation, to form monomeric products. This was confirmed through mass spectral data analysis which showed the incorporation of deuterium onto the monomeric structure with the cleavage of the ether bond and the removal of the hydroxyl groups from the alkyl chain. It was also found that additional H/D exchange occurred on the ring due to hydration of the alumina support when water was used as the reactant solvent. This work emphasised the catalyst-lignin interactions during the reaction, although it would be beneficial to also study the deuterium exchange from the solvent as suggested by the capping mechanism.

### 3.5 Post-Reaction Catalyst Characterisation

This final section aims to analyse the spent catalyst taken from various reactions studied in this thesis and investigate any property changes that may have occurred to the catalyst during the catalytic depolymerisation reaction. As mentioned in previous sections, it was assumed that the lignin deposited and charred onto the catalyst surface during the reaction, but it was also possible that some of the higher molecular weight product species deposited on to the surface as well. In order to characterise the nature of this carbonaceous material, the post-reaction samples were analysed using temperature-programmed oxidation, BET, XRD, elemental analysis, and Raman spectroscopy as described in section 2.4.

#### 3.5.1 Analysis of the Post-Reaction Catalyst Samples from the Standard Reactions with the Seven Lignins

This section will look specifically at the post-reaction catalyst samples used after the standard reaction with each of the lignins used in this thesis. This will include the catalyst samples used with the poplar lignins (ammonia and organosolv), the wheat straw lignins (alkali, AFEX, Fr-AFEX and soda), and finally the Kraft lignin from Norway spruce.

Figure 91 shows the thermal breakdown of the spent Pt/alumina catalyst taken from the standard reaction with poplar lignins, namely the ammonia and organosolv lignins. Both catalyst samples showed an initial loss of water from the sample, followed by the main breakdown loss between ~423-873 K and whilst the ammonia lignin catalyst sample only displayed two main breakdown areas, the catalyst used with the organosolv lignin displayed six areas of loss which would suggest it consisted of different surface species to the ammonia catalyst. It was however found that the major derivative weight loss for both samples corresponded to the evolution of CO<sub>2</sub> (mz 44) as detected by the online mass spectrometer (see Figure 91). This was an exothermic process as expected, with an uptake of oxygen. The loss of CO<sub>2</sub> indicated the burn-off of carbonaceous material, highlighting the hydrocarbon-like nature of the deposit on the catalyst surface. The absence of a water signal during the main weight loss area would suggest that the lignin polymer was strongly absorbed onto the catalyst surface [104]. A loss of mz 30 and 46 was also observed for both catalyst samples between 473-873 K and this was attributed to a loss of nitrogen from the surface. The evolution of nitrogen was assumed to have come from the nitrogen which was found to have been incorporated into the lignin structure (see Table 6) and confirmed that the lignin had deposited onto the catalyst surface during the reaction. Literature reports that disordered carbon combusts at lower temperatures than highly ordered graphitic sheets

[105] suggesting that the carbon on the ammonia lignin catalyst was more disordered in nature, whilst the organosolv lignin catalyst exhibited a weight loss >873 K which would suggest more ordered graphitic carbon. However it should also be noted that coke combustion is known to readily combust in the presence of Pt particles where Pt catalyses the reaction but additional analysis would be required [105].

Similar to the catalysts used with the poplar lignins, the catalysts used during the depolymerisation of the wheat straw lignins exhibited similar behaviour, where an initial weight loss of water was followed by a broad thermal breakdown loss between 423-873 K. This loss corresponded to the loss of CO<sub>2</sub> (mz 44) as shown in Figure 92 and a loss of nitrogen from the surface was also evident for each of the samples. Again, this correlated well to the presence of nitrogen in the lignin samples.

The TPO data from the catalyst sample used during the Kraft lignin standard reaction showed a derivative weight loss between 423-873 K, with an initial weight loss of physisorbed water and the evolution of CO<sub>2</sub> throughout the main breakdown area as indicated by Figure 93. This loss of CO<sub>2</sub> also represented the oxidation of carbonaceous material on the catalyst surface. No loss of nitrogen was apparent from the MS data and there was also an absence of signals corresponding to the loss of sulfur from the lignin sample. It was thought that the sulfur from the lignin structure may have reacted with the hydrogen during the depolymerisation reaction to form hydrogen sulfide (H<sub>2</sub>S) therefore explaining its absence from the TPO MS data.

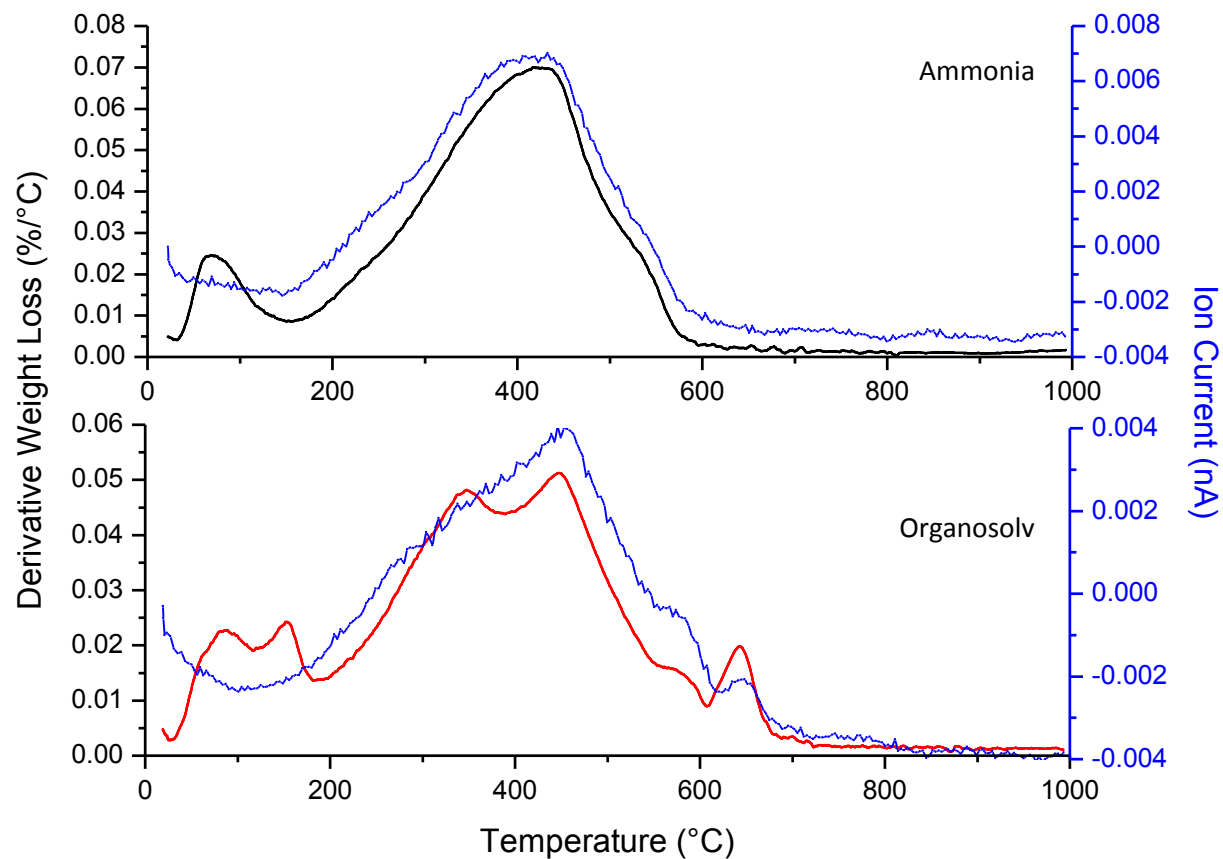


Figure 91: TPO of spent Pt/alumina catalyst after standard reaction with the poplar lignins showing derivative weight loss (black and red) and m/z 44 evolution (blue)

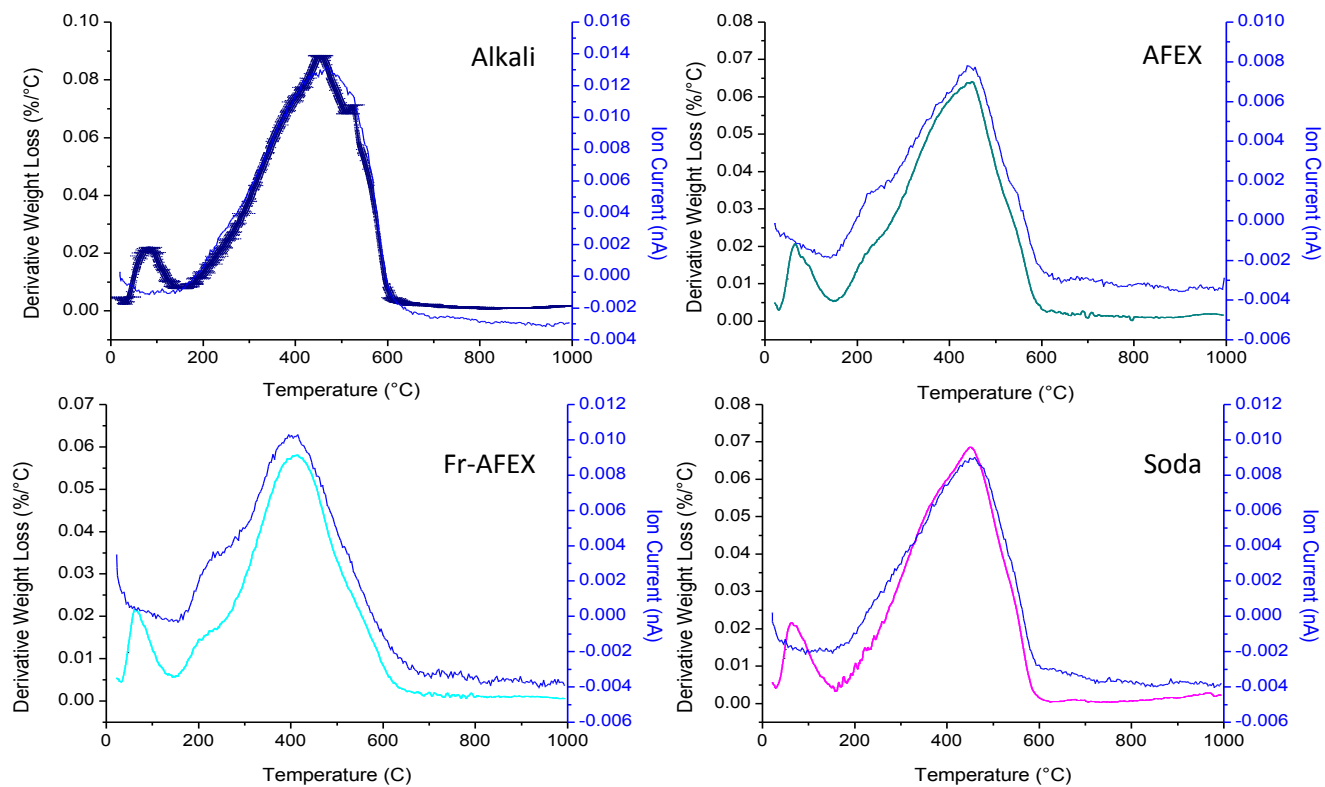


Figure 92: TPO of spent Pt/alumina catalyst after standard reaction with the wheat straw lignins showing derivative weight loss (various colours) and m/z 44 evolution (blue)

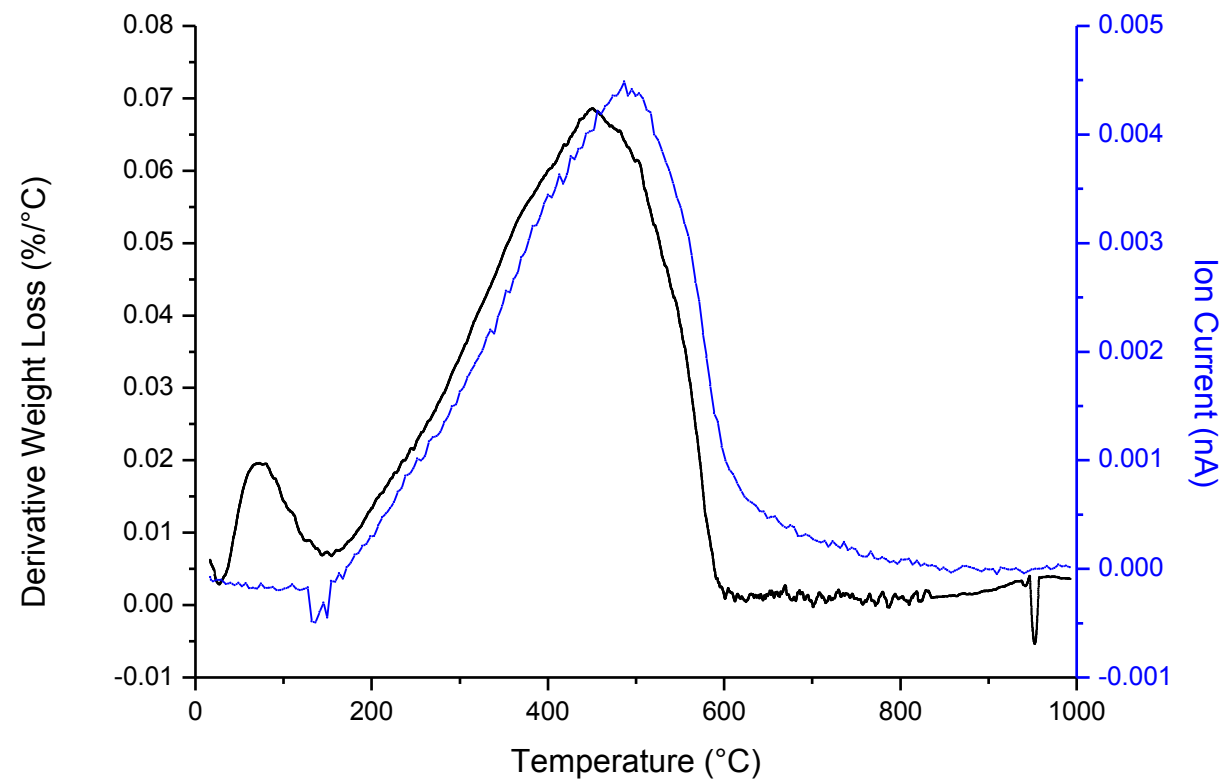


Figure 93: TPO of spent Pt/alumina catalyst after standard reaction with the Kraft lignin showing derivative weight loss (black) and m/z 44 evolution (blue)

The total weight loss calculated during the TPO across the temperature programme has been reported in Table 47. These values were much higher than that of the TPO weight loss observed for the catalyst pre-reaction which was found to be ~4 wt.% thus confirming that material had been deposited onto the catalyst surface during reaction. The values ranged between 16-24 wt.% and showed no obvious trend with respect to the lignin starting material. This increase in weight loss correlated well to the carbon content of each of the post-reaction samples as determined by elemental analysis and as expected, the carbon content of the sample increased with the weight loss of the sample.

Table 47: Weight loss observed for each catalyst used in the standard reaction of each lignin

<b>Lignin used in the standard reaction</b>	<b>TPO weight loss (wt. %)</b>	<b>Carbon (%)</b>
<b>Ammonia</b>	18.6	9.9
<b>Organosolv</b>	17.9	6.6
<b>Alkali</b>	24.0	12.7
<b>AFEX</b>	17.5	9.1
<b>Fr-AFEX</b>	16.1	8.6
<b>Soda</b>	17.9	10.1
<b>Kraft</b>	19.7	11.6

BET analysis of the post-reaction sample was compared to the starting catalyst material. As stated in section 2.2.1, the Pt/alumina had an original surface area of  $102 \text{ m}^2 \cdot \text{g}^{-1}$  and a pore volume of  $0.51 \text{ cm}^3 \cdot \text{g}^{-1}$ . Table 48 shows that the surface area generally increased for each sample whilst the pore volume decreased after the catalyst was exposed to the standard reaction with each of the lignins. The decrease in pore volume suggests that the carbonaceous material was deposited into the pores of the catalyst, hence the increase in surface area. It is possible that this blockage and filling of pores also contributed to the lower depolymerisation activity observed with the recycled catalyst experiments presented in sections 3.2.1 and 3.3.2.2 via a deactivation mechanism. No obvious relationship

between the type of lignin used in the reaction and the changes in surface area and pore volume was observed.

Table 48: Surface area and pore volume data for each catalyst used in the standard reaction of each lignin

<b>Lignin used in the standard reaction</b>	<b>Surface Area (m<sup>2</sup>.g<sup>-1</sup>)</b>	<b>Pore Volume (cm<sup>3</sup>.g<sup>-1</sup>)</b>
<b>Ammonia</b>	125	0.35
<b>Organosolv</b>	134	0.43
<b>Alkali</b>	124	0.34
<b>AFEX</b>	129	0.38
<b>Fr-AFEX</b>	115	0.39
<b>Soda</b>	133	0.37
<b>Kraft</b>	122	0.39

In order to determine the nature of the carbonaceous material, the post-reaction catalyst samples were run at room temperature using XRD as described in section 2.4.2. The samples were then compared to the starting catalyst diffraction pattern pre-reaction as shown in Figure 94. Although hydration of the alumina was originally a concern as discussed in section 3.2.2.1, no significant changes in the XRD patterns was observed for any of the post-reaction samples. The pre-reaction catalyst exhibited main characteristic  $\theta$ -alumina peaks at  $2\theta = 17.5, 20, 31, 33, 37, 39, 45, 60, 62$  and  $67.5$  [53], and these remained for each of the post-reaction samples. Although some broadening on the post-reaction peaks was noted, this was attributed to the lignin deposits on the surface which are known to be amorphous in nature. No graphite peak in the area of  $2\theta = 26$  was observed.

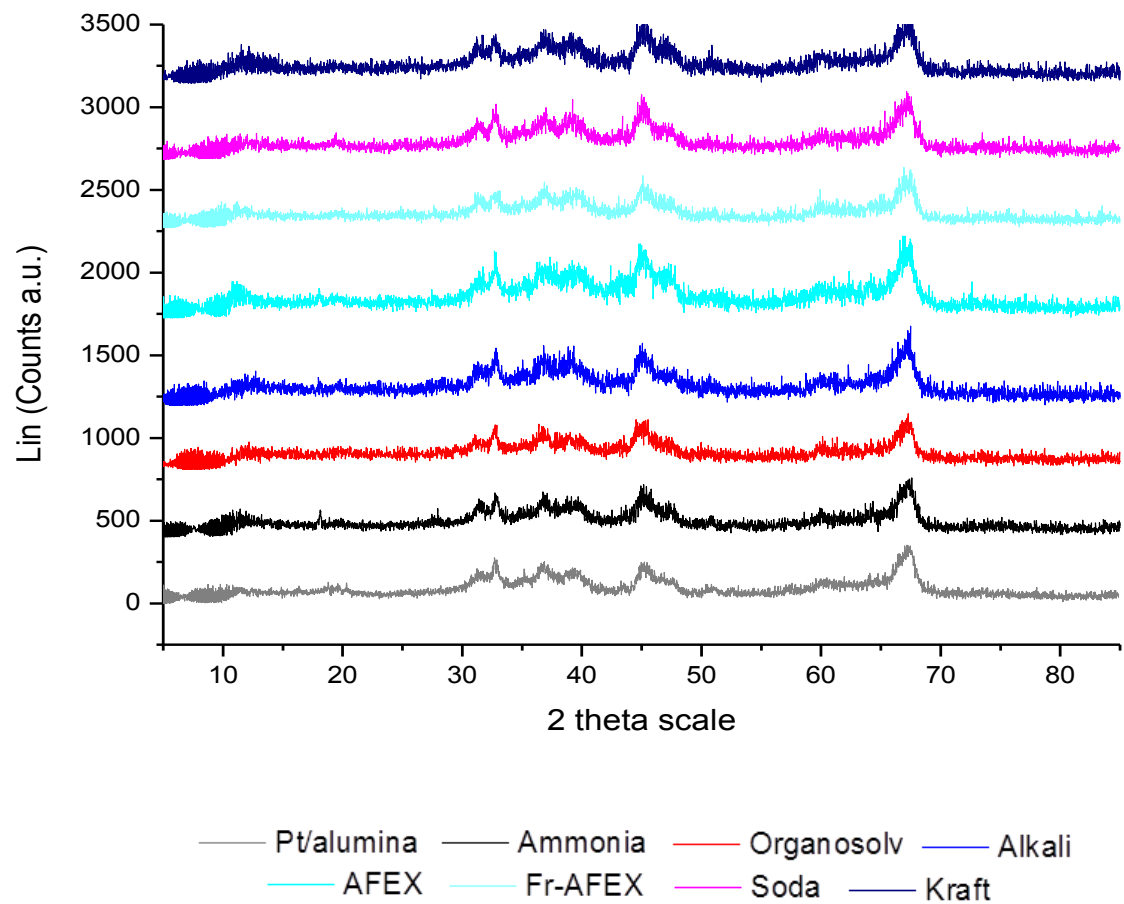


Figure 94: XRD diffraction patterns of the catalyst pre-reaction compared to the post-reaction samples

In order to analyse the surface carbon, Figure 95 shows the Raman spectra obtained for the post-reaction catalyst sample used in the standard reactions of the ammonia and alkali lignins. These are given as a representation of the seven Raman spectra obtained and show the catalyst samples which displayed the largest and smallest difference between the two bands present. Each spectra showed two overlapping bands with peak maxima at  $\sim 1380\text{ cm}^{-1}$  and  $\sim 1600\text{ cm}^{-1}$  which corresponded to D and G bands respectively. These bands are typical for coke deposits [105], where the G ('graphite') band at  $\sim 1600\text{ cm}^{-1}$  corresponds to an ideal graphitic lattice vibration mode and the D ('defect') band at  $1380\text{ cm}^{-1}$  is known to be characteristic of disordered graphite [106]. Disordered graphite is known to grow in intensity relative to the G band with increasing degree of disorder in the graphitic structure. The ratio of the D and G bands intensities are given in Table 49. These values show that there was little difference observed between the seven samples, although the higher values would indicate a slight increase in the amount of defects in the graphitic lattice or a slight decrease in the size of the graphitic crystallites [105]. No overtone band in the region of  $2700\text{ cm}^{-1}$  indicative of a particularly ordered carbonaceous matrix was detected for any of the samples. Notably, the low intensity shown in Figure 95 could have been a result of carbon absorbing the UV light [105], whilst the noise may have been a result of the fluorescence caused by the deposited lignin.

Table 49: D:G ratios determined from the Raman analysis for each catalyst used in the standard reaction of each lignin

<b>Lignin used in the standard reaction</b>	<b>D:G Ratio</b>
<b>Ammonia</b>	0.88
<b>Organosolv</b>	0.82
<b>Alkali</b>	0.74
<b>AFEX</b>	0.84
<b>Fr-AFEX</b>	0.81
<b>Soda</b>	0.81
<b>Kraft</b>	0.77

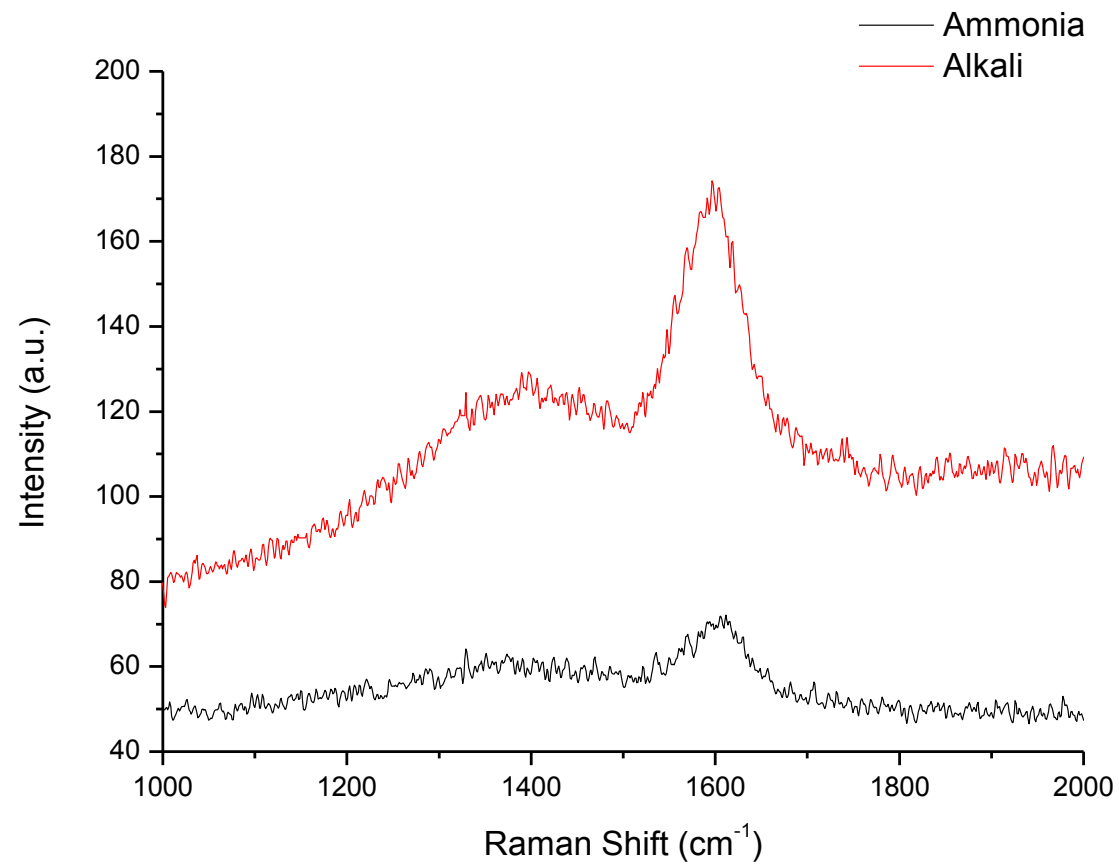


Figure 95: Raman spectra obtained for the post-reaction catalyst used in the standard reaction with the ammonia and alkali lignin

### 3.5.2 Analysis of the Post-Reaction Catalyst Samples from the Optimisation Studies

During the optimisation studies of the ammonia and Kraft lignin, the catalyst for each standard reaction was recycled in order to investigate its stability. Each of the post-reaction samples were analysed under TPO conditions and are given in Figure 96. The two samples displayed very different characteristics, where the peak maxima for the ammonia lignin occurred at 703 K with an additional sharp peak at 808 K and the Kraft lignin peak maxima occurred at 728 K with a continued broad weight loss.

The ammonia lignin thermal breakdown of the recycled catalyst was slightly broader than that observed with the original run (see Figure 91) as it occurred between 423-923 K. The initial weight loss of water was observed and the main weight loss peak matched that of CO<sub>2</sub> evolution as shown in Figure 96, although mass losses for m/z 16, 18, 28, 30 and 46 corresponding to CH<sub>4</sub>, H<sub>2</sub>O, CO, NO and NO<sub>2</sub> were also detected which had not been visible for the single standard reaction. This was likely due to the fact that additional layers of material had been able to deposit onto the surface with the additional reaction, hence more was released from the sample during oxidation. Furthermore, the formation of water in the same region as the release of CO<sub>2</sub> is indicative that the adsorbed lignin consisted of a high oxygen content [49], whereas no loss of water in this region was detected for the single standard reaction. It should also be noted that although the sharp peak at 808 K originally looked to be an anomaly, it was found to match the CO<sub>2</sub> signal so was also deemed carbonaceous in nature.

It was expected that the additional use of the catalyst would allow for more lignin, and therefore carbon, to deposit onto the surface so it was therefore unsurprising that the thermal breakdown required higher temperatures. This was reflected by the larger percentage weight loss value of 29.7 wt.% in comparison to the single standard run sample which lost 18.6 wt.%. Consequently, the carbon content of the sample was also higher (15.1 %) as determined by elemental analysis and BET analysis showed that the pore volume was smaller than that of the single reaction, and the surface area was subsequently larger. Compared to the single standard run, the catalyst sample appeared to be more graphitic in nature as indicated by the slight increase in the decomposition temperature above 873 K, and the Raman analysis which displayed a more intense G band resulting in a lower D:G ratio. XRD analysis exhibited a similar diffraction pattern to the single standard sample, with no graphitic carbon peak. The values given here have been summarised in Table 50.

The TPO data obtained for the breakdown of the recycled catalyst used with Kraft lignin has been given in Figure 96 and occurred between 423-1073 K. Compared to the single use catalyst, the decomposition of the surface carbon occurred over a much broader temperature range and at temperatures >873 K which are typical of ordered graphitic carbon. The major derivative weight loss between 423 and 1073 K corresponded to an evolution of CO<sub>2</sub> (mz 44) and uptake of oxygen, but signals consistent with those noted for the ammonia lignin were also found. The evolution of CH<sub>4</sub> (mz 16) was found to occur at peak maximas of 673 K and 1073 K respectively, whilst water (mz 18), CO (mz 28) and NO (mz 30) corresponded to two main peaks between 328-733 K and 733-1273 K. Low intensity signals relating to the loss of benzene (mz 78) and phenol (mz 94) were also acquired which had not been noted for any of the samples taken after the standard reaction. This could have been a result of the lignin deposits on the surface or possibly due to the deposition of reaction products. This would require further investigation to give conclusive results.

Table 50 shows that the overall percentage weight loss and the carbon content of both samples was fairly similar, although the Kraft recycled catalyst carbon content was slightly higher (17.9 wt.%) which conformed to the TPO data. The pore volume of both recycled catalysts unsurprisingly decreased more than that noted for the single use samples, although the Kraft almost halved in value (0.23 cm<sup>3</sup>.g<sup>-1</sup>). Whilst the ammonia lignin catalyst exhibited the same behaviour as the single use catalysts where the surface area increased, the Kraft lignin catalyst resulted in a lower surface area (94 m<sup>2</sup>.g<sup>-1</sup>) in comparison to the starting catalyst pre-reaction. This difference would suggest that a different species, such as the higher molecular weight reaction products, filled the pores of the catalyst with this reaction. The XRD data was similar to that of the single use sample but the D:G ratio of the recycled catalyst was calculated as being 0.61 which is indicative of an ordered graphitic sample as suggested by the thermal breakdown between 873-1073 K. It is therefore expected that the XRD pattern would have displayed broadening of the  $\theta$ -alumina peaks as a result of the deposited alumina, with the possibility of graphite peaks. These results, in relation to the lower monomeric yields obtained in comparison to the initial reaction suggest that the catalyst sites may have been inhibited by the coke deposits, although sintering could also have been an issue. This would require further investigation to give conclusive results.

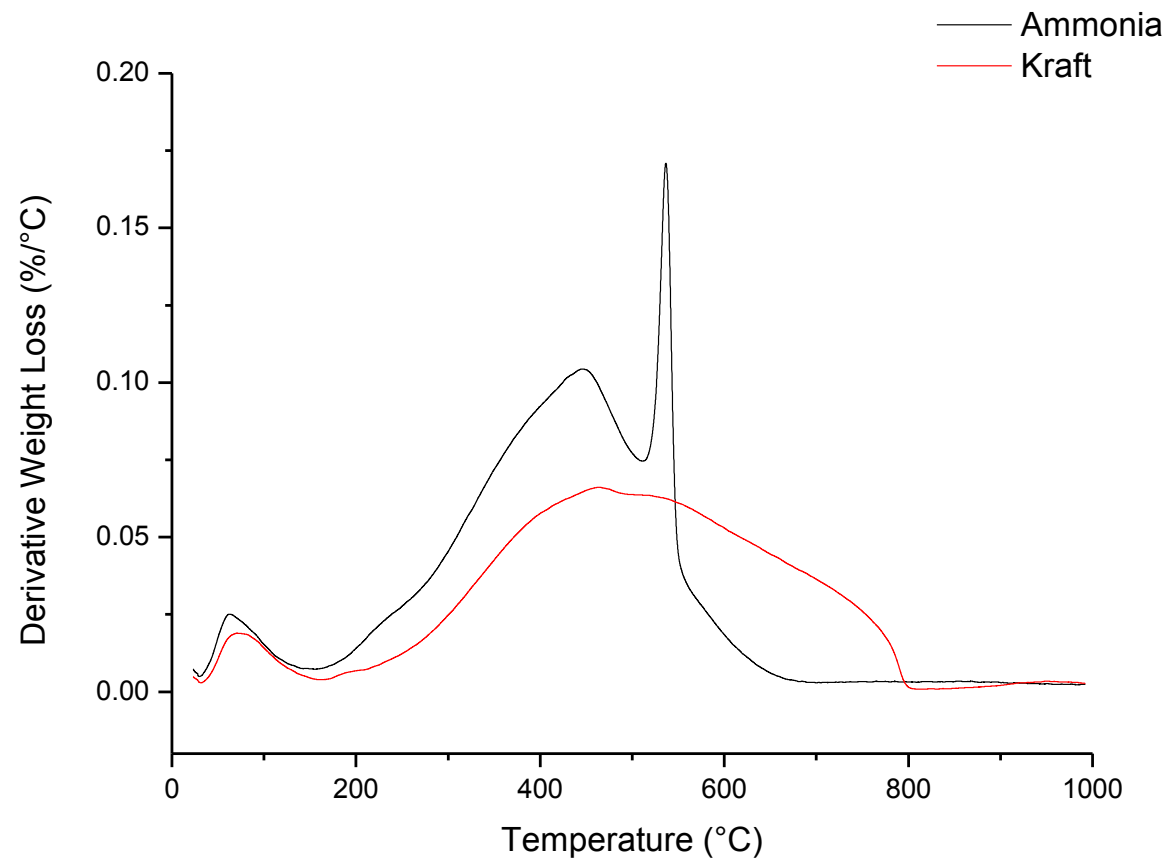


Figure 96: Derivative weight loss profiles of the spent Pt/alumina catalysts after recyclability testing with the ammonia and Kraft lignin

Table 50: Characterisation of the recycled catalysts used with the ammonia and Kraft lignins

<b>Lignin used in the recycled reaction</b>	<b>TPO weight loss (wt.%)</b>	<b>Carbon (%)</b>	<b>Surface Area (m<sup>2</sup>.g<sup>-1</sup>)</b>	<b>Pore Volume (cm<sup>3</sup>.g<sup>-1</sup>)</b>	<b>D:G Ratio</b>
<b>Ammonia</b>	29.7	15.1	130	0.30	0.63
<b>Kraft</b>	26.9	17.9	94	0.23	0.61

From the optimisation studies using the ammonia lignin, it was concluded that the standard reaction which used 100 % methanol instead of the 50:50 (v/v) methanol-water mix yielded the best results in terms of maximising alkylphenolic production and limiting char formation, whilst the use of 100 % water caused significant condensation of the lignin and yielded poor monomeric production. It was expected that the spent catalyst taken from the 100 % water experiment would consist of more carbonaceous material due to the additional condensation reactions so it was therefore of interest to compare the two post-reaction catalyst samples to note any visible differences.

Figure 97 exhibits the derivative weight loss profiles of both catalyst samples under oxidative conditions, where the two plots differed with respect to the upper temperatures with the catalyst from the 100 % water reaction continuing to lose weight up to 973 K. The catalyst from the 100 % MeOH reaction produced a similar derivative weight loss plot to that given for the standard reaction using the methanol-water mix, although the decomposition continued slightly after 873 K and the main peak was sharper in appearance. The MS data showed that water was released <473 K and the main thermal breakdown area corresponded to the loss of CO<sub>2</sub> with an uptake of oxygen. The release of nitrogen from the sample was also evident.

The derivative weight loss of the spent catalyst taken from the 100 % water experiment occurred between 423-973 K which would suggest that more graphitic carbon had deposited onto the surface of the catalyst. As with the other samples, CO<sub>2</sub> evolution matched that of the main weight loss area with an initial loss of water, but similar to the recycled catalysts, the evolution of m/z 16, 18, 28, 30 and 46 also occurred. Methane, water and CO were released between 573-873 K, whilst nitrogen was released between 673-973 K. Small signals for benzene and phenol were also detected.

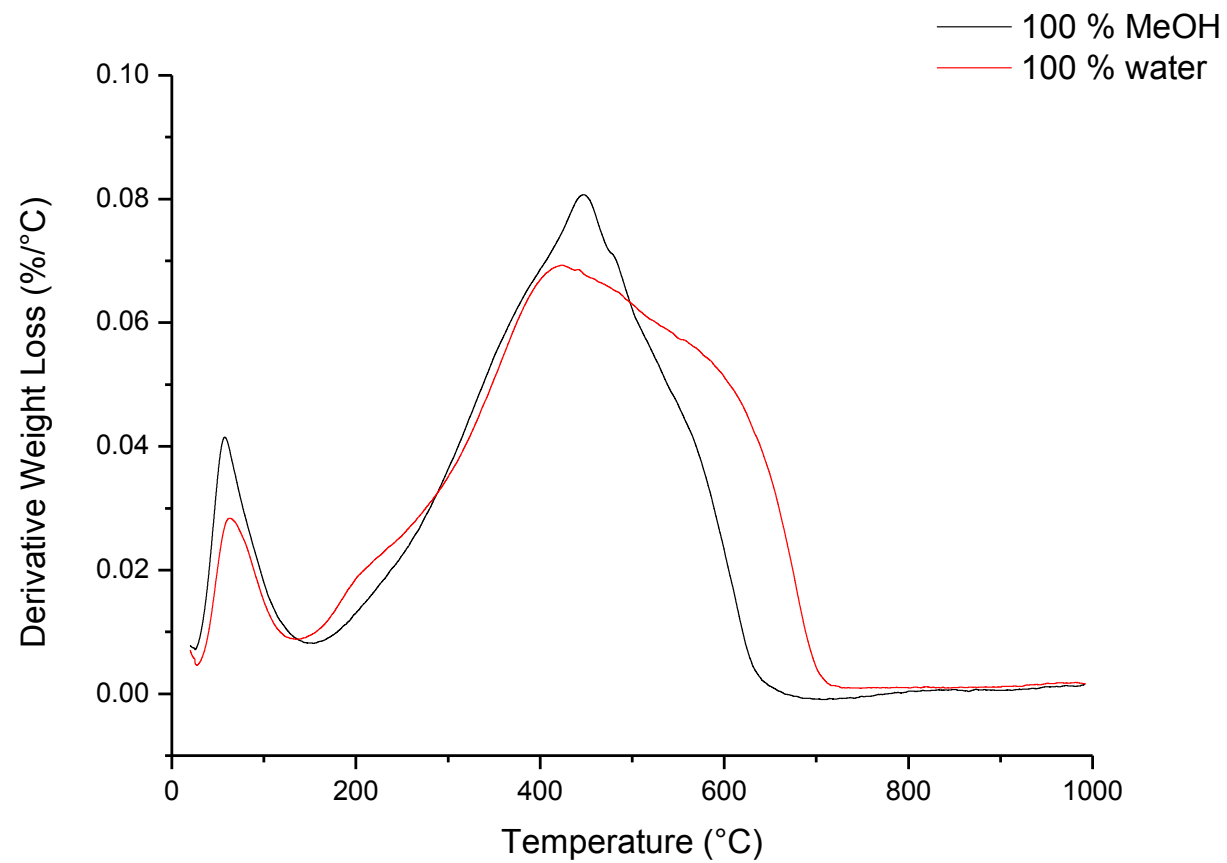


Figure 97: Derivative weight loss profiles of the spent Pt/alumina catalysts after solvent optimisation testing using the ammonia lignin

As suggested by the TPO data, a larger weight loss was observed for the 100 % water experiment than for the 100 % methanol experiment, and this correlated well with the carbon percentage as detected by elemental composition. No significant change in the catalyst surface areas were observed, and the pore volumes were found to decrease for both which suggested that the pores had been blocked with the carbonaceous material. No difference between both reactions was noted with respect to the XRD data and Raman spectra obtained, however the ratios for both was found to be much lower in comparison to the catalyst from the standard reaction. This information has been summarised in Table 51:

Table 51: Characterisation of the solvent optimisation catalysts used with the ammonia lignin

<b>Lignin used in the solvent optimisation reaction</b>	<b>TPO weight loss (wt.%)</b>	<b>Carbon (%)</b>	<b>Surface Area (<math>\text{m}^2\cdot\text{g}^{-1}</math>)</b>	<b>Pore Volume (<math>\text{cm}^3\cdot\text{g}^{-1}</math>)</b>	<b>D:G Ratio</b>
<b>100 % MeOH</b>	23.2	13.1	110	0.35	0.65
<b>100 % water</b>	26.4	17.8	110	0.28	0.63

### 3.5.3 Analysis of the Post-Reaction Catalyst Samples from the Isotopic Labelling Studies

Experiments incorporating deuterium into the standard reaction were also carried out for both the ammonia and Kraft lignins, where the gas and solvent was substituted with the deuterated equivalent. It was found that the fully deuterated experiments yielded the highest amount of monomeric product for both lignins so it was therefore of interest to investigate the coke deposits on the surface of the catalysts used. Figure 98 shows that the catalyst sample used with the ammonia lignin displayed very little change in comparison to the catalyst taken from the equivalent protonated reaction, whilst the catalyst used with the Kraft lignin exhibited a broader thermal weight loss than the protonated equivalent reaction. No MS data was collected for these particular samples but it was expected that, in relation to the previous data obtained, that the derivative weight loss will have matched that of  $\text{CO}_2$  burn-off.

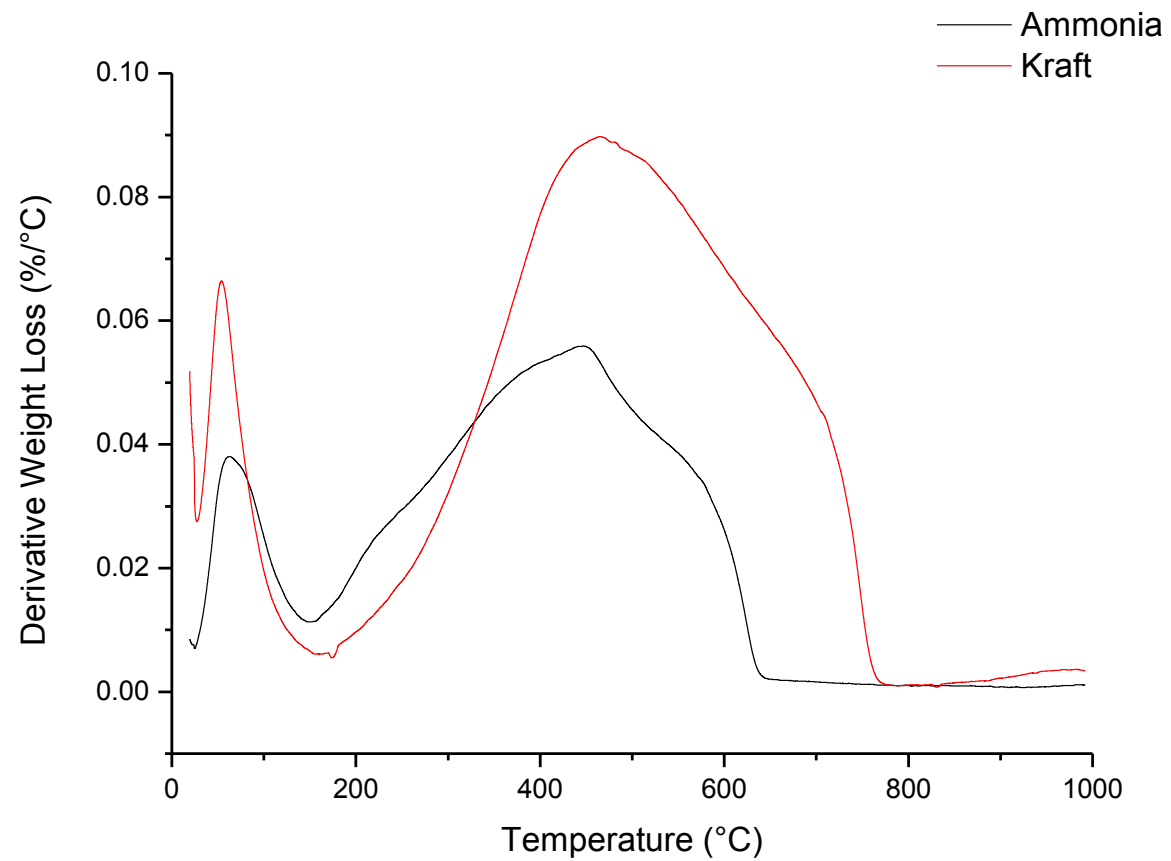


Figure 98: Derivative weight loss profiles of the spent Pt/alumina catalysts after the isotopic labelling testing using the ammonia and Kraft lignins

The data given in Table 52 for the ammonia lignin catalyst sample shows that the data obtained for the deuterated equivalent was very similar to that obtained for the protonated reaction, however the Kraft lignin catalyst gave similar characteristics to those given for the recycled catalyst (see Table 50) rather than the standard protonated reaction. With respect to the Raman spectrum obtained for the Kraft catalyst sample, the narrowing of the bands observed is indicative of a higher ordered carbon structure with fewer defects on the catalyst surface. The ratio of the D and G bands (0.56) would additionally suggest a carbon that is ordered in nature. These results imply that although the monomeric yield more than doubled with the inclusion of the deuterium, the formation of carbonaceous material on the catalyst was still unavoidable and was likely simultaneously enhanced by the inverse kinetic isotope effect.

Table 52: Characterisation of the isotopic labelling catalysts used with the ammonia and Kraft lignins

<b>Lignin used in the solvent optimisation reaction</b>	<b>TPO weight loss (wt.%)</b>	<b>Carbon (%)</b>	<b>Surface Area (<math>\text{m}^2 \cdot \text{g}^{-1}</math>)</b>	<b>Pore Volume (<math>\text{cm}^3 \cdot \text{g}^{-1}</math>)</b>	<b>D:G Ratio</b>
<b>Ammonia</b>	21.3	10.2	126	0.39	0.85
<b>Kraft</b>	36.4	21.2	94	0.22	0.56

### 3.5.4 Summary of the Post-Reaction Catalyst Characterisation

This work aimed to do an initial investigation involving the characterisation of a selection of post-reaction catalyst samples taken from the depolymerisation reactions in this thesis. Catalyst deactivation is a common problem during many industrial catalytic reactions and the laydown of carbon deposits is believed to be one of the major causes of catalyst deactivation. This coking can either occur on the acidic sites of the alumina support or on the active metal nanoparticles and although this coke formation cannot be prevented completely, it is possible for the catalyst to be regenerated by burning the carbon deposits and adding an additional reduction step to return the metal oxide to its metallic phase. However these steps can also aid sintering which can decrease the activity of the catalyst. Initial analysis was employed to envisage the type of carbon on the catalyst surface and to

determine whether or not there was any relationship between the type of carbon and the type of lignin or experiment used.

The catalysts typically displayed thermal breakdown behaviour between 423-873 K which corresponded to the decomposition of carbonaceous material on the catalyst surface. This was supported by the evolution of CO<sub>2</sub> with an uptake of oxygen. The evolution of nitrogen was attributed to the nitrogen present in the lignin samples so this therefore confirmed that the lignin had deposited onto the catalyst surface and subsequently condensed during the reaction. The thermal decomposition behaviour was found to alter and occur at higher temperatures when the catalyst was recycled, when water was used as the reaction solvent or when deuterium was substituted in the Kraft lignin standard reaction, but no obvious relationship between the carbon deposits and the type of lignin used was established. The carbon content of the catalyst samples was consistent with the TPO total weight loss, and BET analysis was found to fluctuate depending on the reaction conditions. No change in the support diffraction pattern was observed for the standard reaction samples using XRD analysis so Raman spectroscopy was employed to further characterise the surface carbon. Disordered (D) and graphitic (G) bands were evident for each of the catalyst samples and their ratios were found to change depending on the reaction conditions.

## 4 Project Conclusions

Lignin as one of the few natural aromatic resources available in abundance holds huge potential to be used as a key feedstock for future fuel and chemical applications. The paper and pulp industry produces approximately 50 million tonnes of residual lignin per year worldwide in the form of a by-product, of which only 2 % is commercially used at present [9], and although the lignin streams produced during this process are currently utilised in the paper mills as a source of heat and energy, it is typically viewed as industrial waste with little or no commercial value beyond this application. To exploit lignin to its full potential, one of the key challenges of lignin conversion lies with successfully recovering the lignin from the process streams of the paper and pulp industry effectively, as well as developing a catalytic technology capable of performing the required depolymerisation step to monomeric product. If it was possible to selectively rupture C-C and C-O bonds within the lignin polymer, there would be enormous potential for the formation of monomeric aromatic compounds which could be used as platform molecules. These platform molecules could then undergo transformations to value-added products using existing technology and subsequently incorporated into current petrochemical or pharmaceutical processes.

The primary aim of this thesis was to study the depolymerisation of Kraft lignin to functional aromatic monomers using heterogeneous catalysis and in line with the project aims set out in section 1.6, the following conclusions were made:

- Under the standard conditions, it was found that the ammonia lignin achieved the highest overall yield of monomeric product (16.4 %), and that the soda lignin yielded the lowest amount in comparison (7.4 %). These results, in line with the other lignins used, showed that the starting structure of lignin greatly affected the type and yield of the resultant monomeric aromatic products. The catalytic conversion of lignin to fine chemicals was therefore found to be the most promising when the starting lignin was uncondensed in nature, like the ammonia lignin, with a high  $\beta$ -O-4 content.
- Condensation of the lignin during the catalytic step was found to be one of the greatest issues associated with its conversion abilities. This highlighted the need for optimisation studies and showed that different lignins had different charring abilities depending on their starting structure and that this would have to be addressed accordingly.

- Optimisation of the standard reaction conditions was required to give a high yield of alkylphenolic product, with low char formation, and the ammonia lignin was used as the benchmark lignin due to its efficiency during the standard reaction testing. Each of the parameters set out in the standard reaction was altered and it was found that the use of 100 % methanol gave the highest monomeric yield (43.5 %), whilst the use of 100 % water gave the highest char formation (47.1 %).
- 100 % carbon mass balance was not obtainable and this was attributed to factors such as: (1) solid material adhering itself to the reactor wall and stirrer; (2) gaseous products such as CO<sub>2</sub> dissolving into the solvent which could not be identified or quantified; (3) evaporation loss; and (4) water-soluble compounds which could not be extracted fully. Adaptation of the reaction methodology and set-up would be useful in any further work.
- The standard reaction using the Kraft lignin produced results comparable to those observed with the soda lignin. This was expected after characterisation of the samples proved to be similar however the Kraft lignin yielded more of the desired propylphenolics and less of the phenolic products without an alkyl chain compared to the soda lignin. This result fell in nicely with a previous conclusion which stated that the starting structure and  $\beta$ -O-4 content directly affected the type and yield of resultant monomeric products. The sulfur content did not prove to be as detrimental as first assumed, but further investigation with respect to quantifying the sulfur content or using other sulfur-containing lignins is required to confirm this.
- The results obtained from the optimisation of the Kraft lignin depolymerisation reaction showed that whilst one set of conditions may be efficient for one type of lignin, this may not be the case for another. In order for lignin conversion to be viable, each type of lignin would therefore require a different conversion approach. The conversion of highly uncondensed lignins, such as the ammonia or AFEX lignins, will require more gentle and carefully optimised conditions to achieve selective cleavage of the C-O bonds to generate high yields of fine aromatic chemicals, whilst the more condensed lignins such as the Kraft, soda or organosolv lignins will require harsher conditions and possibly different types of catalysts to crack the material efficiently
- During the isotopic labelling studies, it was found that the inclusion of deuterium into the reaction system increased the rate of reaction to give higher monomeric yields. This was accredited to increased stability of the C-D bond in comparison to the usual C-H bonds which were plagued with repolymerisation and condensation

issues. With the increasing monomeric yield, it was important to note that the addition of deuterium did not alter the product selectivity significantly for the uncondensed ammonia lignin in comparison to the equivalent protonated reaction, but it did have a dramatic effect on the condensed Kraft lignin. This again highlighted the difference in reaction possibilities between lignin types and showed that the Kraft lignin was capable of producing monomeric product in a yield equivalent to that of the ammonia lignin when the condensation problems were addressed.

- In terms of the reaction mechanism, it was proposed that the lignin underwent an initial fragmentation step followed by a number of other steps, including hydrogenolysis, dehydration and hydrogenation, to form monomeric products. This was confirmed using the GC-MS data during the isotopic labelling studies.
- Finally, analysis of the post-catalyst samples identified the presence of carbon deposits on the catalyst surface, but no obvious trend was observed with respect to the lignin sample used during the reaction.

## 5 Recommendations for Future Work

As an initial study and starting project there is plenty of scope for ways to take this work forward. Unfortunately due to limited sample availability, most experiments were only carried out once so the project would clearly benefit from a larger sample volume so that each experiment could be conducted 2-3 times each to ensure that relative experimental errors are within an appropriate level. A larger reference library could be investigated in order to identify the unidentified GC-MS peaks and the analysis methodology could be further established to enable the detection of BTX and cyclo-products should they arise. The autoclave reactor set-up would benefit from modifications such as an online GC-TCD which would enable the researcher to take samples throughout the reaction to carry out a thorough kinetic study and determine gaseous products such as CO, CH<sub>4</sub> and C<sub>2</sub>-C<sub>3</sub>. Furthermore, due to the sheer abundance of products produced from this reaction, methods to separate out the products could be considered. Distillation of the post-reaction mix seems to be the best option, where products could be separated based on their boiling points to reduce the amount of product in one mix. Realistically, lignin conversion will never produce one or even close to one product so separation methods post-reaction look to be the best way of providing a group of similar platform monomers. Additionally, two-step processes could be explored where the initial cracking step of the lignin into smaller fragments would precede valorisation to functional monomers, and the use of different catalysts suitable for each of the steps could be investigated.

Moreover, this study aimed at looking at how the lignin behaved under catalytic conditions but there was little focus on the actual catalytic chemistry being carried out. There are an abundance of experiments which could focus on how different types of catalysts could be used to change the lignin reaction pathway and a study concentrating on finding the best lignin depolymerisation catalyst would also prove interesting. Studies looking at altering the metal, metal loading and support could be further investigated, with detailed emphasis on the catalyst characterisation in terms of acid-site analysis, dispersion, and surface chemistry etc. Up-scaling of the reaction using 'real' lignin samples would also increase the knowledge base and show how this reaction could be taken forward and used commercially.

Further analysis of the starting Kraft material could be carried out in order to determine the forms of sulfur present, as well as the amount of each respective form found. Literature suggests that the sulfur may be present as inorganic sulfur, mainly sulfate ions (SO<sub>4</sub><sup>2-</sup>), as

elemental sulfur ( $S_0$ ), as adsorbed polysulfide ( $S_nS^{2-}$ ), and as organically bound sulfur: thiol (-SH), sulfide bonds (-S-) and disulfide bonds (-S-S-) [16]. Ion chromatography and inductively coupled plasma techniques could be used to quantify the different forms of sulfur as set out by Svensson [16]. Investigations into lowering the Kraft lignins sulfur content prior to catalytic reaction could also be explored.

Although Kraft lignin has huge potential for producing biofuels and chemicals due to its structure and sheer abundance, the resultant char was found to be generally much higher with Kraft lignin compared to the ammonia lignin so alternative uses for it could be explored. As with all chars produced in this work, its high carbon content makes it an ideal candidate for preparing activated carbon. Activated carbons are porous materials with large surface areas and pore volume, which contain various oxygen containing functional groups on the surface and are commonly used as catalyst supports [107]. Activated carbons are also used to remove organic and inorganic pollutants from water and waste water streams, and the demand for them as a water-purifying agent has significantly increased as the need to reduce environmental impacts caused by water pollution has become more vital than ever [108]. Additionally, coal is the current main source for the production of activated carbons [107] so there it is essential that other alternatives are explored. Activated carbons can be prepared in two steps: the carbonisation of the raw carbonaceous material (the char) in an inert atmosphere followed by activation of the product [109]. Literature on the production of char from lignin is available as a foundation and shows that it is possible to make activated carbon via physical or chemical activation methods [110], where the chemical activation method using KOH in particular is generally more positive [107, 109]. Additionally, some researchers also consider these char residues as low value soil amendment materials [111] and attention towards bio-based polyols [112] and lignin-polyols [113] has also risen due to rising petroleum prices and sustainability concerns from the current source. Studies into the use of char in other applications would make use of the waste by-product from catalytic conversion and provide an opportunity to increase the potential profit available from lignin valorisation.

## 6 References

1. F.P. Bouxin, A. McVeigh, F. Tran, N.J. Westwood, M.C. Jarvis, and S.D. Jackson, *Catalytic depolymerisation of isolated lignins to fine chemicals using a Pt/ alumina catalyst: Part 1 - Impact of the lignin structure*. Green Chemistry, 2015. **17**: p. 1235-1242.
2. M. Finley *The oil market to 2030 - Implications for investment and policy*. Economics of Energy & Environmental Policy, 2012. **1**.
3. *Short-term energy outlook*. 2015 [cited August 2015; [http://www.eia.gov/forecasts/steo/pdf/steo\\_full.pdf](http://www.eia.gov/forecasts/steo/pdf/steo_full.pdf)].
4. B.N. Kuznetsov, N.V. Chesnokov, O.V. Yatsenkova, and V.I. Sharypov, *New methods of heterogeneous catalysis for lignocellulosic biomass conversion to chemicals*. Russian Chemical Bulletin, International Edition, 2013. **62**: p. 1493-1502.
5. Y. Lin and G.W. Huber, *The critical role of heterogeneous catalysis in lignocellulosic biomass conversion*. Energy and Environmental Science, 2009. **2**: p. 68-80.
6. D.Y.C. Leung, X.L. Yin, and C.Z. Wu, *A review on the development and commercialization of biomass gasification technologies in China*. Renewable Sustainable Energy Reviews, 2004. **8**: p. 565-580.
7. A. Brandt, J. Grasvik, J.P. Hallett, and T. Welton, *Deconstruction of lignocellulosic biomass with ionic liquids*. Green Chemistry, 2013. **15**: p. 550-583.
8. S.K. Ritter, *Lignocellulose: A complex biomaterial*. Chemical & Engineering News, 2008. **86**: p. 15.
9. F.S. Chakar and A.J. Ragauskas, *Review of current and future softwood kraft lignin process chemistry*. Industrial Crops and Products, 2004. **20**: p. 131-141.
10. C. Lapierre, B. Pollet, and C. Rolando. *Structural investigation of hardwood lignins by chemical degradative methods*. in *The 8th International Symposium on Wood and Pulping Chemistry*. 1995. Helsinki, Finland.
11. *New and future developments in catalysis: Catalytic biomass conversion*, S.L. Suib, Editor 2013, Elsevier.
12. A.J. Ragauskas, M. Nagy, D.H. Kim, C.A. Eckert, J.P. Hallett, and C.L. Liotta, *From wood to fuels: Integrating biofuels and pulp production*. Industrial Biotechnology, 2006. **2**: p. 55-65.
13. P.T. Patil, U. Armbruster, M. Richter, and A. Martin, *Heterogeneously catalyzed hydroprocessing of organosolv lignin in sub- and supercritical solvents*. Energy & Fuels, 2011. **25**: p. 4713-4722.
14. S. Yang, H. El-Ensashy, and N. Thongchul, *Bioprocessing technologies in biorefinery for sustainable production of fuels, chemicals and polymers*, 2013, John Wiley & Sons.
15. J.H. Lora and W.G. Glasser, *Recent industrial applications of lignin: A sustainable alternative to nonrenewable materials*. Journal of Polymers and the Environment, 2002. **10**: p. 39-48.
16. S. Svensson, *Minimizing the sulfur content in Kraft lignin*, in *School of sustainable development of society and technology 2008*, STFI-Packforsk: Stockholm.
17. C.N. Satterfield, *Heterogeneous Catalysis in Industrial Practice*, 1996, Krieger Publishing Company.
18. C.H. Bartholomew, *Mechanisms of catalyst deactivation*. Applied Catalysis A: General, 2001. **212**: p. 17-60.

19. E. Dorrestijn, L.J.J. Laarhoven, I.W.C.E. Aends, and P. Mulder, *The occurrence and reactivity of phenoxyl linkages in lignin and low rank coal*. Journal of Analytical and Applied Pyrolysis, 2000. **54**: p. 153-192.
20. M. Brebu and C. Vasile, *Thermal degradation of lignin -A review*. Cellulose Chemistry and Technology, 2009. **44**: p. 353-363.
21. I. Brodin, E. Sjöholm, and G. Gellerstedt, *The behaviour of kraft lignin during thermal treatment*. Journal of Analytical and Applied Pyrolysis, 2010. **87**: p. 70-77.
22. E. Furimsky, *Catalytic hydrodeoxygenation* Applied Catalysis A: General, 2000. **199**: p. 147-190.
23. A. Centeno, E. Laurent, and B. Delmon, *Influence of the support of CoMo sulfide catalysts and of the addition of potassium and platinum on the catalytic performances for the hydrodeoxygenation of carbonyl, carboxyl, and guaiacol-type molecules*. Journal of Catalysis, 1995. **154**: p. 288-298.
24. E. Sjöström, *Lignin*. Wood Chemistry, Fundamentals and Applications Edition 1993, San Diego: Academic Press.
25. J.C. Duchet, E.M.v. Oers, V.H.J.d. Beer, and R. Prins, *Carbon-supported sulfide catalysts*. Journal of Catalysis, 1983. **80**: p. 386-402.
26. J.P.R. Vissers, T.J. Lensing, V.H.J.d. Beer, and R. Prins, *Carbon black composites as carrier materials for sulfide catalysts*. Applied Catalysis, 1987. **30**: p. 21-31.
27. J.P.R. Vissers, F.P.M. Mercx, S.M.A.M. Bouwens, V.H.J.d. Beer, and R. Prins, *Carbon-covered alumina as a support for sulfide catalysts*. Journal of Catalysis, 1988. **114**: p. 291-302.
28. G. Muralidhar, F.E. Massoth, and J. Shabtai, *Catalytic functionalities of supported sulfides: I. Effect of support and additives on the CoMo catalyst*. Journal of Catalysis, 1984. **85**: p. 44-62.
29. V.L. Parola, G. Daganello, and A.M. Venezia, *CoMo catalysts supported on alumina silicates: Synergy between support and sodium effects*. Applied Catalysis: A General, 2004. **260**: p. 237-247.
30. E. Laurent and B. Delmon, *Study of hydrodeoxygenation of carbonyl, carboxylic and guaiacyl groups over sulfided CoMo/ $\gamma$ -Al<sub>2</sub>O<sub>3</sub> and NiMo/ $\gamma$ -Al<sub>2</sub>O<sub>3</sub> catalysts: Catalytic reaction schemes*. Applied Catalysis A: General, 1994. **109**: p. 77-96.
31. V.N. Bui, D. Laurenti, P. Afanasiev, and C. Geantet, *Hydrodeoxygenation of guaiacol with CoMo catalysts. Part I: Promoting effect of cobalt on HDO selectivity and activity*. Applied Catalysis B: Environmental, 2011. **101**: p. 239-245.
32. V.N. Bui, D. Laurenti, P. Delichere, and C. Geantet, *Hydrodeoxygenation of guaiacol: Part II: Support effect for CoMoS catalysts on HDO activity and selectivity*. Applied Catalysis B: Environmental, 2011. **101**: p. 246-255.
33. A.L. Jongorius, R. Jastrzebski, P.C.A. Bruijninx, and B.M. Weckhuysen, *CoMo sulfide-catalyzed hydrodeoxygenation of lignin model compounds: An extended reaction network for the conversion of monomeric and dimeric substrates*. Journal of Catalysis, 2012. **285**: p. 315-323.
34. A. Tejado, C. Pena, J. Lbidi, J.M. Echeverria, and I. Mondragon, *Physico-chemical characterization of lignins from different sources for use in phenol-formaldehyde resin synthesis*. Bioresource Technology, 2007. **98**: p. 1655-1663.
35. A. Gutierrez, R.K. Kaila, M.L. Honkela, R. Slioor, and A.O.I. Krause, *Hydrodeoxygenation of guaiacol on noble metal catalysts*. Catalysis Today, 2009. **147**: p. 239-246.
36. H. Ohta, H. Kobayashi, K. Hara, and A. Fukuoka, *Hydrodeoxygenation of phenols as lignin models under acid-free conditions with carbon-supported platinum catalysts*. Chemical Communications, 2011. **47**: p. 12209-12211.

37. C. Lui, Z. Shao, Z. Xiao, and C. Liang, *Hydrodeoxygenation of benzofuran over activated carbon supported Pt, Pd, and Pt-Pd catalysis*. Reaction Kinetics, Mechanisms and Catalysis, 2012. **107**: p. 393-404.
38. T. Nimmanwudipong, C. Aydin, J. Lu, R.C. Runnebaum, K.C. Brodwater, N.D. Browning, D.E. Block, and B.C. Gates, *Selective hydrodeoxygenation of guaiacol catalyzed by platinum supported on magnesium oxide*. Catalysis Letters, 2012. **142**: p. 1190-1196.
39. R.C. Runnebaum, T. Nimmanwudipong, D.E. Block, and B.C. Gates, *Catalytic conversion of anisole: Evidence of oxygen removal in reactions with hydrogen*. Catalysis Letters, 2011. **141**: p. 817-820.
40. A. Oasmaa and R. Alen, *Catalytic hydrotreatment of some technical lignins*. Bioresource Technology, 1993. **45**: p. 189-194.
41. R. Singh, A. Prakash, S.K. Dhiman, B. Balagurumurthy, A.K. Arora, S.K. Puri, and T. Bhaskar, *Hydrothermal conversion of lignin to substituted phenols and aromatic ethers*. Bioresource Technology, 2014. **165**: p. 319-322.
42. R. Beauchet, F. Monteil-Rivera, and J.M. Lavoie, *Conversion of lignin to aromatic-based chemicals (L-chems) and biofuels (L-fuels)*. Bioresource Technology, 2012. **121**: p. 328-334.
43. R.J.A. Gosselink, W. Teunissen, J.E.G.v. Dam, E.d. Jong, G. Gellerstedt, E.L. Scott, and J.P.M. Sanders, *Lignin depolymerisation in supercritical carbon dioxide/acetone/water fluid for the production of aromatic chemicals*. Bioresource Technology, 2012. **118**: p. 648-651.
44. A.L. Jongerijs, *Catalytic conversion of lignin for the production of aromatics*, in *Faculty of Science 2013*, University of Utrecht: Utrecht, Netherlands.
45. Z. Yuan, S. Cheng, M. Leitch, and C. Xu, *Hydrolytic degradation of alkaline lignin in hot-compressed water and ethanol*. Bioresource Technology, 2010. **101**: p. 9308-9313.
46. Q. Song, F. Wang, J. Cai, Y. Wang, J. Zhang, W. Yu, and J. Xu, *Lignin depolymerization (LDP) in alcohol over nickel-based catalysts via a fragmentation-hydrogenolysis process*. Energy and Environmental Science, 2013. **6**: p. 994-1007.
47. J. Zakzeski and B.M. Weckhuysen, *Lignin solubilization and aqueous phase reforming for the production of aromatic chemicals and hydrogen*. ChemSusChem, 2011. **4**: p. 369-378.
48. J. Zakzeski, A.L. Jongerijs, P.C.A. Bruijninx, and B.M. Weckhuysen, *Catalytic lignin valorization process for the production of aromatic chemicals and hydrogen*. ChemSusChem, 2012. **5**: p. 1602-1609.
49. A.L. Jongerijs, J.R. Copeland, G.S. Foo, J.P. Hofmann, P.C.A. Bruijninx, C. Sievers, and B.M. Weckhuysen, *Stability of Pt/ $\gamma$ -Al<sub>2</sub>O<sub>3</sub> catalysts in lignin and lignin model compound solutions under liquid phase reforming reaction conditions*. ACS Catalysis, 2013. **3**: p. 464-473.
50. R.M. Ravenelle, J.R. Copeland, A.H.V. Pelt, J.C. Crittenden, and C. Sievers, *Stability of Pt/ $\gamma$ -Al<sub>2</sub>O<sub>3</sub> catalysts in model biomass solutions*. Topics in Catalysis, 2012. **55**: p. 162-174.
51. F.P. Bouxin, S.D. Jackson, and M.C. Jarvis, *Organosolv pretreatment of Sitka spruce wood: conversion of hemicelluloses to ethyl glycosides*. Bioresource Technology, 2014. **151**: p. 441-444.
52. F.P. Bouxin, S.D. Jackson, and M.C. Jarvis, *Isolation of high quality lignin as a by-product from ammonia percolation pretreatment of poplar wood*. Bioresource Technology, 2014. **162**: p. 236-242.
53. *ICDD's PDF-4 database*, 2006: International Center for Diffraction Data: Newton Square, USA.

54. C. Gillan, *Deactivation of Precious Metal Steam Reforming Catalysts*, in *Department of Chemistry* 2009, The University of Glasgow: Glasgow, Scotland.
55. S. Wilson and S.D. Jackson, *Unpublished results*.
56. A. Tolbert, H. Akinosho, R. Khunsupat, A.K. Naskar, and A.J. Ragauskas, *Characterization and analysis of the molecular weight of lignin for biorefining studies*. *Biofuels, Bioproducts and Biorefining*, 2014. **8**(6): p. 836-856.
57. G. Brunow, *Methods to reveal the structure of lignin*, 2005, *Biopolymers Online*. p. 89-99.
58. F. Tran, C.S. Lancefield, P.C.J. Kamer, T. Lebl, and N.J. Westwood, *Selective modification of the  $\beta$ - $\beta$  linkage in DDQ-treated Kraft lignin analysed by 2D NMR spectroscopy*. *Green Chemistry*, 2015. **17**(1): p. 244-249.
59. J.C.D. Rio, J. Rencoret, P. Prinsen, A.n.T. Martinez, J. Ralph, and A. Gutierrez, *Structural characterization of wheat straw lignin as revealed by analytical pyrolysis, 2D-NMR, and reductive cleavage methods*. *Journal of Agricultural and Food Chemistry*, 2012. **60**: p. 5922-5935.
60. R. Alen, E. Kuoppala, and P. Oesch, *Formation of the main degradation compound groups from wood and its components during pyrolysis*. *Journal of Analytical and Applied Pyrolysis*, 1996. **36**: p. 137-148.
61. J. Rodrigues, J. Garca, and H. Pereira, *Influence of tree eccentric growth on syringyl/ guaiacyl ratio in Eucalyptus globulus wood lignin assessed by analytical pyrolysis*. *Journal of Analytical and Applied Pyrolysis*, 2001. **58-59**: p. 481-489.
62. E. Avni, R.W. Coughlin, P.R. Soloman, and H.H. King, *Mathematical modelling of biomass pyrolysis phenomena*. *Fuel*, 1985. **64**: p. 1495-1501.
63. M.P. Pandey and C.S. Kim, *Lignin Depolymerization and Conversion: A Review of Thermochemical Methods*. *Chemical Engineering Technology*, 2011. **34**(1): p. 29-41.
64. A.I. Afifi, J.P. Hindermann, E. Chornet, and R.P. Overend, *The cleavage of the aryl-O-CH<sub>3</sub> bond using anisole as a model compound*. *Fuel*, 1989. **68**: p. 498-504.
65. D. Ferdous, A.K. Dalai, S.K. Bej, and R.W. Thring, *Pyrolysis of Lignins: Experimental and Kinetics Studies*. *Energy Fuels*, 2002. **16**: p. 1405-1412.
66. M.S. Jahan and B.S.P. Mun, *Characteristics of dioxane lignins isolated at different ages of Nalita wood*. *Journal of Wood Chemistry and Technology*, 2007. **27**: p. 83-99.
67. S. Bauer, H. Sorek, V.D. Mitchell, A.B. Ibanez, and D.E. Wemmer, *Characterization of Miscanthus giganteus lignin isolated by ethanol organosolv process under reflux condition*. *Journal of Agricultural and Food Chemistry*, 2012. **60**: p. 8203-8212.
68. M. Saidi, F. Samimi, D. Karimipourfard, T. Nimmanwudipong, B.C. Gates, and M.R. Rahimpour, *Upgrading of lignin-derived bio-oils by catalytic hydrodeoxygenation*. *Energy and Environmental Science*, 2014. **7**: p. 103-129.
69. R.M. Ravenelle, J.R. Copeland, W. Kim, J.C. Crittenden, and C. Sievers, *Structural changes of  $\gamma$ -Al<sub>2</sub>O<sub>3</sub>-supported catalysts in hot liquid water*. *ACS Catalysis*, 2011. **1**: p. 552-561.
70. A.F. Holleman and E. Wiberg, *Inorganic Chemistry*. Vol. 34. 2001, New York: Academic Press.
71. P.S. Santos, H.S. Santos, and S.P. Toleda, *Standard transtion aluminas. Electron Microscopy studies*. *Materials Research*, 2000. **3**: p. 104-114.
72. R.D. Cortright, R.R. Davda, and J.A. Dumesic, *Hydrogen from catalytic reforming of biomass-derived hydrocarbons in liquid water*. *Nature*, 2002. **418**: p. 964-967.
73. T.M. Liitia, S.L. Mauni, B. Hortling, M. Toikka, and I. Kilpelainen, *Analysis of technical lignins by two- and three-dimensional NMR spectroscopy*. *Journal of Agricultural and Food Chemistry*, 2003. **51**: p. 2136-2143.

74. Y. Ye, Y. Zhang, J. Fan, and J. Chang, *Novel method for the production of phenolics by combining lignin extraction with lignin depolymerization in aqueous ethanol*. Industrial & Chemical Engineering Research, 2012. **51**: p. 103-110.
75. S. Cheng, C. Wilks, Z. Yuan, M. Leitch, and C. Xu, *Hydrothermal degradation of alkali lignin to bio-phenolic compounds in sub/supercritical ethanol and water-ethanol co-solvent*. Polymer Degradation Stability, 2012. **97**: p. 839-848.
76. W.S. Mok and M.J. Antal, *Uncatalyzed solvolysis of whole biomass hemicelluloses by hot compressed liquid water*. Industrial & Chemical Engineering Research, 1992. **31**: p. 1157-1161.
77. H. Wan, R.V. Chaudhari, and B. Subramaniam, *Catalytic hydroprocessing of p-cresol: Metal, solvent and mass-transfer effects*. Topics in Catalysis, 2012. **55**: p. 129-139.
78. N. Mahmood, Z. Yuan, J. Schmidt, and C. Xu, *Production of poyols via direct hydrolysis of kraft lignin: Effect of process parameters*. Bioresource Technology, 2013. **139**: p. 13-20.
79. D. Wen, H. Jiang, and K. Zhang, *Supercritical fluids technology for clean biofuel production*. Progress in Natural Science, 2009. **19**: p. 273-284.
80. B. Joffres, D. Laurenti, N. Charon, A. Daudin, A. Quignard, and C. Geantet, *Thermochemical conversion of lignin for fuels and chemicals: A review*. Oil & Gas Science and Technology, 2013. **68**: p. 753-763.
81. S.E. Hunter and P.E. Savage, *Recent advances in acid- and base-catalyzed organic synthesis in high-temperature liquid water*. Chemical Engineering Science, 2004. **59**: p. 4903-4909.
82. M. Saisu, T. Sato, M. Watanabe, T. Adschiri, and K. Arai, *Conversion of lignin with supercritical water-phenol mixtures*. Energy Fuels, 2003. **17**: p. 922-928.
83. S. Kang, X. Li, J. Fan, and J. Chang, *Hydrothermal conversion of lignin: A review*. Renewable Sustainable Energy Reviews, 2013. **27**: p. 546-558.
84. B. Zhang, H.J. Huang, and S. Ramaswamy, *Reaction kinetics of the hydrothermal treatment of lignin*. Applied Biochemistry and Biotechnology, 2008. **147**: p. 119-131.
85. Y. Ye, Y. Zhang, J. Fan, and J. Chang, *Selective production of 4-ethylphenolics from lignin via mild hydrogenolysis*. Bioresource Technology, 2012. **118**: p. 648-651.
86. M. Kalabova, S. Suty, T. Lauko, M. Jablonsky, A. Haz, A. Sladkova, and I. Surina, *Conversion of lignin to liquid compounds*, in *5th International Scientific Conference Renewable Energy Sources 2014*: Slovak Republic.
87. N.P. Vasilakos and D.M. Austgen, *Hydrogen-donor solvents in biomass liquefaction*. Industrial & Engineering Chemistry Process Design and Development, 1985. **24**: p. 304-311.
88. K.H. Kim, R.C. Brown, M. Kieffer, and X. Bai, *Hydrogen-donor-assisted solvent liquefaction of lignin to short-chain alkylphenols using a micro reactor/gas chromatography system*. Energy Fuels, 2014. **28**: p. 6429-6437.
89. M.S. Zanuttini, C.D. Lago, C.A. Querini, and M.A. Peralta, *Deoxygenation of m-cresol on Pt/ $\gamma$ -Al<sub>2</sub>O<sub>3</sub> catalysts*. Catalysis Today, 2013. **213**: p. 9-17.
90. R.C. Runnebaum, T. Nimmanwudipong, D.E. Block, and B.C. Gates, *Catalytic conversion of compounds representative of lignin-derived bio-oils: a reaction network for guaiacol, anisole, 4-methylanisole, and cyclohexanone conversion catalysed by Pt/[ $\gamma$ ]-Al<sub>2</sub>O<sub>3</sub>*. Catalysis Science Technology, 2012. **2**: p. 113-118.
91. W. Mu, H. Ben, X. Du, X. Zhang, F. Hu, W. liu, A.J. Ragauskas, and Y. Deng, *Noble metal catalysed aqueous phase hydrogenation and hydrodeoxygenation of*

- lignin-derived pyrolysis oil and related model compounds*. Bioresource Technology, 2014. **173**: p. 6-10.
92. P.N. Rylander, *Catalytic hydrogenation over platinum metals* 1967, New York and London: Academic Press.
  93. A.J. Foster, P.T.M. Do, and R.F. Lobo, *The synergy of the support acid function and the metal function in the catalytic hydrodeoxygenation of m-cresol*. Topics in Catalysis, 2012. **55**: p. 118-128.
  94. A. Popov, E. Kondratieva, J.M. Goupil, L. Mariey, P. Bazin, J. Gilson, A. Travert, and F. Mauge, *Bio-oils hydrodeoxygenation: Adsorption of phenolic molecules on oxidic catalyst supports*. Journal of Physical Chemistry C, 2010. **114**: p. 15661-15670.
  95. J.B. Binder, M.J. Gray, J.F. White, Z.C. Zhang, and J.E. Holladay, *Reactions of lignin model compounds in ionic liquids*. Biomass and Bioenergy, 2009. **33**: p. 1122-1130.
  96. T.J. McDonough, *The chemistry of organosolv delignification*. Tappi Journal, 1993. **76**(186-193).
  97. J.P. Kennedy, *Cationic isomerization polymerization of  $\beta$ -methylstyrene and allylbenzene*. Journal of Polymer Science, 1964. **2**: p. 171-176.
  98. J. Wadenback, *Lignin studies of transgenic Norway Spruce*, in *Department of Plant Biology and Forest Genetics* 2006, Swedish University of Agricultural Sciences: Uppsala, Sweden.
  99. C. Halpin, *Investigating and manipulating lignin biosynthesis in the postgenomic era*. Avances in Botanical Research, 2004. **41**: p. 63-106.
  100. X.F. Zhou, *Conversion of kraft lignin under hydrothermal conditions*. Bioresource Technology, 2014. **170**: p. 583-586.
  101. R.R. Davda, J.W. Shabaker, G.W. Huber, R.D. Cortright, and J.A. Dumesic, *A review of catalytic issues and process conditions for renewable hydrogen and alkanes by aqueous-phase reforming of oxygenated hydrocarbons over supported metal catalysts*. Applied Catalysis B: Environmental, 2005. **56**: p. 171-186.
  102. S.J. Blanksby and G.B. Ellison, *Bond dissociation energies of organic molecules*. Accounts of Chemical Research, 2003. **36**: p. 255-263.
  103. P. Agarwal, M.S. Deenadayalan, and R. Mukherjee, *Inverse kinetic isotope effect*, Indian Institute of Science Education and Research.
  104. J.J. Delgado, J.A. Perez-Omil, J.M. Rodriguez-Izquierdo, and M.A. Cauqui, *The role of the carbonaceous deposits in the Catalytic Wet Oxidation (CWO) of phenol*. Catalysis Communication, 2006. **7**: p. 639-643.
  105. J.J.H.B. Sattler, A.M. Beale, and B.M. Weckhuysen, *Operando Raman spectroscopy study on the deactivation of Pt/Al<sub>2</sub>O<sub>3</sub> and Pt-Sn/Al<sub>2</sub>O<sub>3</sub> propane dehydrogenation catalysts*. Physical Chemistry Chemical Physics, 2013. **15**: p. 12095-12103.
  106. A. Sadezky, H. Muckenhuber, H. Grothe, R. Niessner, and U. Poschl, *Raman microspectroscopy of soot and related carbonaceous materials: Spectral analysis and structural information*. Carbon, 2005. **43**: p. 1731-1742.
  107. X. Li, Q. Xu, Y. Fu, and Q. Guo, *Preparation and characterization of activated carbon from Kraft lignin via KOH activation*. American Institute of Chemical Engineers, 2013. **33**: p. 519-526.
  108. R.A. Khalkhali and R. Omidvari, *Adsorption of mercuric ion from aqueous solutions using activated carbon*. Polish Journal of Environmental Studies, 2005. **14**: p. 185-188.
  109. J. Sahira, A. Mandira, P.B. Prasad, and P.R. Ram, *Effects of activating agents on the activated carbons prepared from Lapsi seed stone*. Research Journal of Chemical Sciences, 2013. **3**: p. 19-24.

110. K.R. Jena, *Studies on the removal of Pb(II) from wastewater by activated carbon developed from neem wood activated with sulfuric acid*. International Journal of Engineering and Science Research, 2012. **2**: p. 382-394.
111. J. Lehmann and S. Joseph, *Biochar for environmental management: an introduction* Biochar for Environmental Management: Science and Technology. Vol. London. 2009: Earthscan. 1-12.
112. C. Bueno-Ferrer, E. Hablot, M.D.C. Garrigos, S. Bocchini, L. Averous, and A. Jimenez, *Relationship between morphology, properties and degradation parameters of novativebiobased thermoplastic polyurethanes obtained from dimer fatty acids*. Polymer Degradation Stability, 2012. **97**: p. 1964-1969.
113. E.A.B.d. Silva, M. Zabkova, J.D. Araujo, C.A. Cateto, M.F. Barreiro, M.N. Belgacem, and A.E. Rodrigues, *An integrated process to produce vanillin and lignin-based polyurethanes from Kraft lignin*. Chemical Engineering Reseach and Design, 2009. **87**: p. 1276-1292.

## 7 Glossary

### Lignins

Kraft	Kraft
Soda	Soda
Ammonia Fibre Expanded	AFEX
Fermented Ammonia Fibre Expanded	Fr-AFEX
Acid Organosolv	Org
Ammonia	Amm
Alkali	Alk

### Catalyst metals

Platinum	Pt
Rhodium	Rh
Iridium	Ir

### Gases, Compounds and Solvents etc.

Hydrogen	H <sub>2</sub>
Nitrogen	N <sub>2</sub>
Oxygen	O <sub>2</sub>
Argon	Ar
Helium	He
Methane	CH <sub>4</sub>
Water	H <sub>2</sub> O

Carbon Monoxide	CO
Carbon Dioxide	CO <sub>2</sub>
Dichloromethane	DCM
Hydrochloric acid	HCl
Hexadecane	C16
Tetrahydrofuran	THF
Polystyrene	PS
Trimethylsilyl	TMS
Benzene, toluene, xylene	BTX

### **Analysis Methods**

Brunauer, Emmett and Teller	BET
X-ray Diffraction	XRD
Thermogravimetric Analysis	TGA
Temperature-Programmed Reduction	TPR
Carbon, Nitrogen and Hydrogen (analysis)	CHN
Fourier Transform Infrared	FT-IR
2D Nuclear Magnetic Resonance	2D NMR
Gel Permeation Chromatography	GPC
Gas Chromatography	GC
Mass Spectroscopy	MS

### **Other Terms**

Hydrodeoxygenation	HDO
--------------------	-----

Hydrodesulfurisation	HDS
Molecular Weight	Mw
Molecular Number	Mn
Polydispersity	Ip
Total Ion Chromatogram	TIC
Intensity of Reference	IRef
Intensity of Internal Standard	IIS
Mass of Reference	MRef
Mass of Internal Standard	MIS

### **Reaction Products**

H	hydroxyphenyl
G	guaiacyl
S	syringyl
H0	phenol
H1	methylphenol ( <i>p</i> -cresol)
H2	ethylphenol
H3	propylphenol
G0	2-methoxyphenol (guaiacol)
G(OH)0	1,2-dihydroxybenzene (catechol)
G1	2-methoxy-4-methylphenol
G2	4-ethyl-2-methoxyphenol
G(OH)2	4-ethylbenzene-1,2-diol
G3	2-methoxy-4-propylphenol

G3(i)	2-methoxy-4-propenylphenol
G3(OMe)	2-methoxy-4-(3-methoxypropyl)phenol
G3(OH)	4-(3-hydroxypropyl)-2-methoxyphenol
S0	2,6-dimethoxyphenol (syringol)
S1	2,6-dimethoxy-4-methylphenol
S2	4-ethyl-2,6-dimethoxyphenol
S3	2,6-dimethoxy-4-propylphenol
S3(i)	2,6-dimethoxy-4-propenylphenol
S3(OMe)	2,6-dimethoxy-4-(3-methoxypropyl)phenol
S3(OH)	4-(3-hydroxypropyl)-2,6-dimethoxyphenol
S(OH)3(OH)	5-(3-hydroxypropyl)-3-methoxybenzene-1,2-diol